An *in vivo* and *ex vivo* investigation of the cellular effects of the heavy metals cadmium and chromium alone and in combination

By

Chantelle Venter

Submitted in partial fulfilment of the requirements for the degree of

DOCTOR OF PHILOSOPHY

(PhD)

In the Faculty of Health Sciences
Department of Anatomy
University of Pretoria
South Africa

Supervisor: **Dr HM Oberholzer**
Co-supervisor: **Prof MJ Bester**

Department of Anatomy
Faculty of Health Sciences
2017

An *in vivo* and *ex vivo* investigation of the cellular effects of the heavy metals cadmium and chromium alone and in combination

By

CHANTELLE VENTER

Supervisor: Dr HM Oberholzer

Co-supervisor: Prof MJ Bester

Department: Anatomy

Degree: PhD (Anatomy with specialization in Human Cell Biology)

Abstract

The growth in the industrial sector has caused some unfavourable environmental effects. Heavy metals have become synonymous with industrial pollution due to their toxicological and physiological effects on the ecosystem. This is especially true in South Africa, a country that has a thriving industrial sector and not always the means to correctly dispose of toxic materials, like heavy metals, which then enters the air and water supplies. People living in the areas near the polluted air and/or water are the most affected and not only by one metal at a time, but most likely to a combination of metals. Thus the aim of the current study was to investigate the cellular effects of the heavy metals cadmium (Cd) and chromium (Cr) alone and in combination on liver, pancreas and kidney tissue and human blood by implementing *in vivo and ex vivo* models, respectively.

The *in vivo* model was implemented successfully over a period of 28 days where male Sprague-Dawley rats received daily dosages of Cd and Cr alone and in combination at a 1000 times that of the World Health Organization's acceptable water limits. The liver, pancreas and kidney tissue as well as blood was collected from the animals and analysed for histological and ultrastructural alterations, with electron energy-loss spectroscopy. In addition, the blood was evaluated for blood plasma and chemistry levels and ultrastructural analysis with scanning electron microscopy. The blood plasma levels confirmed the presence of the metals in the blood and the blood chemistry levels revealed that the levels of certain liver and kidney tests decreased, indicating that the function of these organs were altered. The histological analysis showed major alterations in the liver and kidney, with minor changes seen in the pancreas, with no fibrosis seen overall. The ultrastructural analysis of

the tissue revealed that the metals had some effects on the organelles, as well as bio-accumulated in the organelles investigated. Ultrastructural analysis was also completed on the coagulation system of the animals using scanning electron microscopy, with the erythrocytes, platelets and fibrin networks showing some ultrastructural alterations in all the metal exposed groups.

In the *ex vivo* model, the ultrastructural, confocal and viscoelastic characteristics of human blood after exposure to Cd and Cr alone and in combination was evaluated. The heavy metals affected all the components of the coagulation system, which included an increase in eryptosis, Annexin-V positive signal, platelet activation and spreading as well as significant increase in fibrin fibre thickness. The thromboelastography® analysis, although not statistically significant, indicated that the final clot will probably result in a fragile, less-stable clot, due to changes mainly to the platelets and fibrin networks.

In conclusion, Cd and Cr alone and in combination had an effect on the blood enzymes and proteins levels, morphology and ultrastructure of the tissue, thus influencing the function of the liver and kidneys and to a lesser extent the pancreas. The heavy metals also influenced the coagulation system, as it led to fragile, less-stable clots which might lead to diverse cardiovascular diseases.

Keywords: Heavy metals, cadmium, chromium, ultrastructure, microscopy, liver, pancreas, kidney, coagulation system, electron energy-loss spectroscopy.

Declaration

I, Chantelle Venter declare that this thesis entitled:

"An *in vivo* and *ex vivo* investigation of the cellular effects of the heavy metals cadmium and chromium alone and in combination"

which I herewith submit to the University of Pretoria for the Degree Doctor of Philosophy in Anatomy with specialization in Human Cell Biology and Histology, is my own original work and has never been submitted for any academic award to any other tertiary institution for any degree.

_____   _____

 C Venter   **Date**

Department of Anatomy, Faculty of Health Sciences,
University of Pretoria
Pretoria
South Africa

Ethical clearance

Animal ethical clearance

UNIVERSITEIT VAN PRETORIA
UNIVERSITY OF PRETORIA
YUNIBESITHI YA PRETORIA

Animal Ethics Committee

PROJECT TITLE	An *in vivo* and *ex vivo* investigation of the cellular effects of the heavy metals cadmium and chromium alone and in combination
PROJECT NUMBER	H009-15
RESEARCHER/PRINCIPAL INVESTIGATOR	C Venter

STUDENT NUMBER (where applicable)	29227454
DISSERTATION/THESIS SUBMITTED FOR	PhD

ANIMAL SPECIES	Rats	
NUMBER OF ANIMALS	48	
Approval period to use animals for research/testing purposes		1 July 2015 – 30 June 2016
SUPERVISOR	Dr. HM Oberholzer	

KINDLY NOTE:

Should there be a change in the species or number of animal/s required, or the experimental procedure/s - please submit an amendment form to the UP Animal Ethics Committee for approval before commencing with the experiment

APPROVED	Date	17 August 2017
CHAIRMAN: UP Animal Ethics Committee	Signature	

S4285-15

The Research Ethics Committee, Faculty Health Sciences, University of Pretoria complies with ICH-GCP guidelines and has US Federal wide Assurance.
- FWA 00002567, Approved dd 22 May 2002 and Expires 03/20/2022.
- IRB 0000 2235 IORG0001762 Approved dd 22/04/2014 and Expires 03/14/2020.

UNIVERSITEIT VAN PRETORIA
UNIVERSITY OF PRETORIA
YUNIBESITHI YA PRETORIA

Faculty of Health Sciences Research Ethics Committee

9/11/2017

Approval Certificate
Amendment
(to be read in conjunction with the main approval certificate)

Ethics Reference No: 111/2016

Title: An in vivo and ex vivo investigation of the cellular effects of the heavy metals cadmium and chromium alone and in combination

Dear Ms Chantelle C Venter

The **Amendment** as described in your documents specified in your cover letter dated 26/10/2017 received on 1/11/2017 was approved by the Faculty of Health Sciences Research Ethics Committee on its quorate meeting of 8/11/2017.

Please note the following about your ethics amendment:
- Please remember to use your protocol number (**111/2016**) on any documents or correspondence with the Research Ethics Committee regarding your research.
- Please note that the Research Ethics Committe may ask further questions, seek additional information, require further modification, or monitor the conduct of your research.

Ethics amendment is subject to the following:
- The ethics approval is conditional on the receipt of **6 monthly written Progress Reports**, and
- The ethics approval is conditional on the research being conducted as stipulated by the details of all documents submitted to the Committee. In the event that a further need arises to change who the investigators are, the methods or any other aspect, such changes must be submitted as an Amendment for approval by the Committee.

We wish you the best with your research.

Yours sincerely

Dr R Sommers; MBChB; MMed (Int); MPharMed; PhD
Deputy Chairperson of the Faculty of Health Sciences Research Ethics Committee, University of Pretoria

___

The Faculty of Health Sciences Research Ethics Committee complies with the SA National Act 61 of 2003 as it pertains to health research and the United States Code of Federal Regulations Title 45 and 46. This committee abides by the ethical norms and principles for research, established by the Declaration of Helsinki, the South African Medical Research Council Guidelines as well as the Guidelines for Ethical Research: Principles Structures and Processes, Second Edition 2015 (Department of Health).

___

☎ 012 356 3084   📠 deepeka.behari@up.ac.za / fhsethics@up.ac.za   🖱 http://www.up.ac.za/healthethics
✉ Private Bag X323, Arcadia, 0007 - Tswelopele Building, Level 4, Room 60, Gezina, Pretoria

Acknowledgments

"For I can do everything through Christ, who gives me strength"
Philippians 4:13

Firstly, I want to thank God almighty, for His guidance, wisdom and love He provided me throughout this study.

To my supervisor, Dr Nanette Oberholzer, thanks for your guidance, motivation, knowledge and most of all your patience throughout this study. Without your guidance this thesis would not have been possible. Your guidance has encouraged me to grow into the researcher I am today.

Thank you to my co-supervisor, Professor Megan Bester, for your advice and guidance throughout this study. Thank you for always being available to share your end-less knowledge.

I would like to offer my special thanks to the staff of the Laboratory for Microscopy and Microanalysis of the University of Pretoria, for the use of their microscopes and their support throughout this study.

To my colleagues at the Division of Cell Biology, Histology and Embryology of the Department of Anatomy, thank you June Serem, Dr Helena Taute and Sandra Arbi for your assistance, guidance and patience throughout this study.

A special thanks to all the staff and students of the Division of Cell Biology, Histology and Embryology of the Department of Anatomy for their assistance during the termination of the animal study.

Professor Resia Pretorius of the Department of Physiology of the University of Pretoria for the use of their thromboelastograph and to Dr Janette Bester, Dr Albé Swanepoel and Dr Mia van Rooy, also from the Department of Physiology of the University of Pretoria, for their assistance and support in acquiring and the analysis of the TEG® results.

To all the phlebotomists of the Department of Physiology at the University of Pretoria, thank you for helping me with the drawing of blood and to all the volunteers that generously donated blood required for this study.

Articles published

Venter C, Oberholzer HM, Taute H, Cummings FR and Bester MJ. 2015. An *in ovo* investigation into the hepatotoxicity of cadmium and chromium evaluated with light- and transmission electron microscopy and electron energy-loss spectroscopy. Journal of Environmental Science and Health, Part A: Toxic/Hazardous Substances and Environmental Engineering, 50: 830-838.

Venter C, Oberholzer HM, Cummings FR and Bester MJ. 2017. Effects of metals cadmium and chromium alone and in combination on the liver and kidney tissue of male Spraque-Dawley rats: An ultrastructural and electron-energy-loss spectroscopy investigation. Microscopy Research and Techniques, 80: 878-888.
***Image was selected for Cover Page of the Journal.**

Venter C, Oberholzer HM, Bester J, Van Rooy M-J and Bester MJ. 2017. Ultrastructural, confocal and viscoelastic characteristics of whole blood and plasma after exposure to cadmium and chromium alone and in combination: An *ex vivo* study. Cellular Pathology and Biochemistry, 43: 1288-1300.

Arbi S, Oberholzer HM, Van Rooy MJ, **Venter C** and Bester MJ. 2017. Effects of chronic exposure to mercury and cadmium alone and in combination on the coagulation system of Sprague-Dawley rats. Ultrastructural Pathology, 41: 275-283.

MICROSCOPY
RESEARCH&TECHNIQUE

x
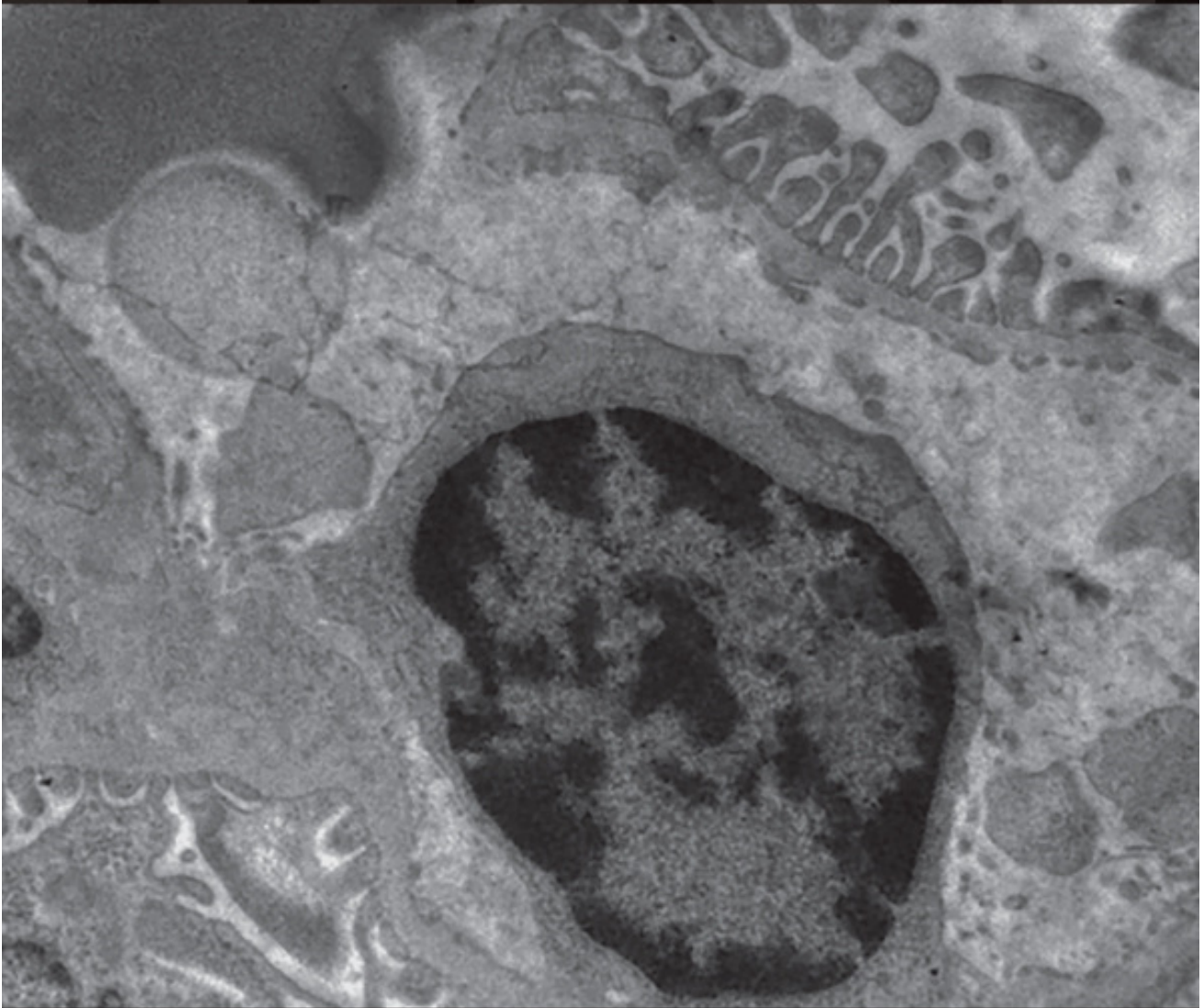
Conferences attended

51th Microscopy Society of Southern Africa, Farm Inn, Pretoria, Gauteng, South Africa, December 2013.

Oral presentation: <u>Venter C</u>, Van der Merwe CF and Oberholzer HM. An *in ovo* model for testing the cellular effects of cadmium toxicity.

Department of Science and Technology and National Research Foundation internship, Research presentation day, Midrand Conference Centre, Midrand, Gauteng, South Africa, Febuary 2014.

Poster presentation: <u>Venter C</u>, Oberholzer HM, Taute H, Bester MJ and Van der Merwe CF. An *in ovo* investigation of the ultrastructural effects of the heavy metals cadmium and chromium on liver tissue.

*Award: 2nd Prize for research poster.

Health Sciences Faculty Day of University of Pretoria, Pretoria, Gauteng, South Africa, August 2014.

Poster presentation: <u>Venter C</u>, Oberholzer HM, Taute H, Bester MJ and Van der Merwe CF. An *in ovo* investigation of the ultrastructural effects of the heavy metals cadmium and chromium on liver tissue.

Microscopy and Microanalysis congress, Hartford, Connecticut, USA, August 2014 (invited).

Oral presentation: <u>Venter C</u>, Oberholzer HM, Taute H, Bester MJ and Van der Merwe CF. An *in ovo* investigation of the ultrastructural effects of the heavy metals cadmium and chromium on liver tissue.

*Award: Castaing Award for Best Student Paper at the Microscopy and Microanalysis congress held in Hartford, Connecticut, USA in August 2014

14th European Microbeam Analysis Society (EMAS), Portorož, Slovenia, May 2015 (invited).

Oral presentation: <u>Venter C</u>, Oberholzer HM, Taute H, Bester MJ and Van der Merwe CF. An *in ovo* investigation of the ultrastructural effects of the heavy metals cadmium and chromium on liver tissue.

Health Sciences Faculty Day of University of Pretoria, Pretoria, Gauteng, South Africa, August 2016.

Poster presentation: <u>Arbi S</u>, Oberholzer HM, Van Rooy MJ, Venter C and Bester MJ. Effect of heavy metals on the coagulation system: An ultrastructural study with focus on cadmium and mercury alone and in combination.

54th Microscopy Society of Southern Africa, Boardwalk Convention Centre, Port Elizabeth, South Africa, December 2016.

Oral presentation: <u>Venter C</u>, Oberholzer HM, Cummings FR and Bester MJ. Investigating heavy metal toxicity on liver, pancreas and kidney tissue: An ultrastructural and EELS study.

*Award: Carl Zeiss Prize for Best presentation or poster that uses microscopy to address an industry related problem.

Table of contents

Appendix A: Published articles

1. **Venter C**, Oberholzer HM, Taute H, Cummings FR and Bester MJ. 2015. An *in ovo* investigation into the hepatotoxicity of cadmium and chromium evaluated with light- and transmission electron microscopy and electron energy-loss spectroscopy. Journal of Environmental Science and Health, Part A: Toxic/Hazardous Substances and Environmental Engineering, 50: 830–838.

2. **Venter C**, Oberholzer HM, Cummings FR and Bester MJ. 2017. Effects of metals cadmium and chromium alone and in combination on the liver and kidney tissue of male Spraque-Dawley rats: An ultrastructural and electron-energy-loss spectroscopy investigation. Microscopy Research and Techniques. 80: 878-888.

   *Image was selected for Cover Page of the Journal.

3. **Venter C**, Oberholzer HM, Bester J, Van Rooy MJ and Bester MJ. 2017. Ultrastructural, confocal and viscoelastic characteristics of whole blood and plasma after exposure to cadmium and chromium alone and in combination: An *ex vivo* study. Cellular Pathology and Biochemistry. Cellular Physiology and Biochemistry, 43: 1288-1300.

4. Arbi S, Oberholzer HM, Van Rooy MJ, **Venter C** and Bester MJ. 2017. Effects of chronic exposure to mercury and cadmium alone and in combination on the coagulation system of Sprague-Dawley rats. Ultrastructural Pathology, 41: 275–283.

List of figures, tables and diagrams

CHAPTER 6:

List of abbreviations, symbols, chemical formulae and SI units

α	Alpha
ADP	Adenosine diphosphate
AEC	Animal Ethics Committee
ALP	Alkaline phosphate
ALT	Alanine transaminase
ANOVA	Analysis of variance
As	Arsenic
AST	Aspartate transaminase
ATF-2	Activating transcription factor 2
ATP	Adenosine triphosphate
β	Beta
Ca^{2+}	Calcium (ion)
Cd	Cadmium
$CdCl_2$	Cadmium chloride
Cl^-	Chloride
CLSM	Confocal Laser Scanning Microscopy(e)
Cr	Chromium
Cr(III)	Trivalent chromium
Cr(VI)	Hexavalent chromium
Cu	Copper
δ	Delta
DCT	Distal convolutes tubules
ddH_2O	Double distilled water
DNA	Deoxyribonucleic acid
ECM	Extracellular matrix
EELS	Electron energy-loss spectroscopy
EFTEM	Energy filtered transmission electron microscopy
ER	Endoplasmic reticulum
FA	Formaldehyde
FII	Prothrombin
FIIa	Thrombin
FV	Factor V
FVa	Activated factor V
FVII	Factor VII
FVIIa	Activated factor VII
FVIII	Factor VIII
FVIIIa	Activated factor VIII
FIX	Factor IX
FIXa	Activated factor IX
FX	Factor X

FXa	Activated factor X
FXI	Factor XI
FXIa	Activated factor XI
GSH	Glutathione
GA	Glutaraldehyde
H&E	Haematoxylin and Eosin
Hg	Mercury
HMDS	Hexamethyldisilazane
H$_2$O	Water
H$_2$O$_2$	Hydrogen peroxide
HSPs	Heat shock proteins
ICP-MS	Inductively coupled plasma mass spectrometry
I-κB	Inhibitor of NF-κB
***iso*PBS**	Isotonic phosphate buffered saline
JNK	c-jun N-terminal kinase
K	Kinetics
K$^+$	Potassium (ion)
KCl	Potassium chloride
K$_2$Cr$_2$O$_7$	Potassium dichromate
MA	Maximal Amplitude
MAPK	Mitogen-activated protein kinase
MMP	Mitochondrial membrane potential
MRTG	Maximum rate of thrombus generation
MT	Metallothionein
Na$^+$	Sodium ion
Ni	Nickel
NF-κB	Nuclear factor kappa B
•OH	Hydroxyl radicals
O$_2$•$^-$	Superoxide anion
OsO$_4$	Osmium tetroxide
PAI-1	Plasminogen activator inhibitor-1
PARP	Poly (ADP-ribosome) polymerase
PCT	Proximal convoluted tubule
Pb	Lead
PBS	Phosphate buffer saline
pH	Measure of the acidity and basicity
PO$_4$	Phosphate
PP	Pancreatic polypeptide
PR	Picrosirius red

PRP	Platelet-rich plasma
PRP+T	Platelet rich plasma with thrombin
PS	Phosphatidylserine
R	Reaction time
RBC(s)	Red blood cell(s)
rER	Rough endoplasmic reticulum
RNA	Ribonucleic acid
rRNA	Ribosomal ribonucleic acid
ROS	Reactive oxygen species
SA	South Africa
SD	Standard deviation
SEM	Scanning electron microscopy(e)
sER	Smooth endoplasmic reticulum
SOD	Superoxide dismutase
TAFI	Thrombin activatable factor inhibitor
TB	Total bilirubin
TBA	*tert*-Butyl alcohol
TEG®	Thromboelastography®
TEM	Transmission electron microscopy(e)
TF	Tissue factor
TMRTG	Time to maximum rate of thrombus generation
tPA	Tissue plasminogen activator
TP	Total protein
TTG	Total thrombus generation
UN	Urea nitrogen
UPBRC	University of Pretoria Biomedical Research Centre
V-curve	Velocity curve
vWF	von Willebrand factor
WB	Whole blood
WB+T	Whole blood with thrombin
WHO	World Health Organization
Zn	Zinc

SI Units

ºC	Degree Celsius
eV	Electron volts
g	Gram
g/ℓ	Gram per litre
g/µℓ	Grams per microliter
KeV	Kiloelectron volts

kg	Kilogram
µg/kg	Microgram per kilogram
µg/ℓ	Microgram per litre
µg/mℓ	Microgram per millilitre
µg	Microgram
mg/ℓ	Milligram per litre
mmol/ℓ	Millimoles per litre
µℓ	Microlitre
µm	Micrometer
µM	Micromolar
µmol/ℓ	Micromoles per litre
mℓ	Millilitre
M	Molar
nm	Nanometer
%	Percent
±	Plus or minus
x	Times
xg	Times gravity
U/ℓ	Units per litre
U/mℓ	Unite per millilitre

Chapter 1

General introduction

No clear definition exists of what a heavy metal is, but density is mostly used as the defining factor, thus a heavy metal has a density of more than $5g/cm^3$ (Järup, 2003). Many heavy metals are essential for human biological functions as the metals may be structural elements, stabilizers of biological structures, components of control mechanisms like nerves and muscles, and of redox systems (Nordberg, *et al.*, 2007). However, some of these metals, especially at high concentrations, can have toxic, carcinogenic and/or teratogenic effects in humans. Sources of heavy metal pollution include geogenic, industries, agriculture, pharmaceutical, domestic effluence and atmospheric. Most heavy metals, for example arsenic (As), cadmium (Cd), chromium (Cr), lead (Pb), and mercury (Hg), occur naturally in the earth's crust, but the main environmental and human exposure occurs from anthropogenic activities, such as mines, foundries, smelters and other metal-based industrial operations (Al-Attar, 2011; Tchounwou, *et al.*, 2012). In South Africa (SA), with the fifth largest mining sector in the world, the waste from mines easily enters the water sources (Kearney, 2012). In 2013, Bester reported that the As and beryllium found in the Marico-Bosveld, Roodekopjes and Vaalkop dams in the North West province of SA may cause a health risk for people that consume the fish from those dams (Bester, 2013). Another study examined the Pb, zinc (Zn), copper (Cu), As, and nickel (Ni) concentrations in the ground water and soil associated with an old copper mine near Musina, SA. Although levels in the ground water and soil was below the World Health Organization's (WHO) limit, recommendations were that this water should be regularly monitored. The soil was found to be a health threat and immediate remedial action was recommended (Singo, 2013). Accumulation of these metals in water sources hold a high risk for people using this water, whether for drinking, washing, cooking and/or irrigation. Heavy metals can be absorbed through the skin, orally and/or through inhalation (Awofolu, *et al.*, 2005). The degree of heavy metal toxicity depends on dose, duration, route of administration and other physiological factors, especially nutrition (Al-Attar, 2011; Chowdhury, 2009).

This study focussed on the effects of two heavy metals Cd and Cr alone and in combination. These two metals were selected based on the likelihood of being exposed to them in SA. Cd was chosen based on the high levels that were found in certain rivers and dams in the Eastern Cape Province of SA, that can not only affect the aquatic ecosystem but also the people using this water in the rural communities (Fatoki and Awofolu, 2003). Hexavalent chromium [Cr(VI)] was chosen based on the high levels of Cr(VI) found in wastewater, due to mining in the Brits area in the North West Province of SA as well as the high levels of

Cr(VI) in the air in the eMalahleni (Witbank) and Mpumalanga region of SA (Molokwane, *et al.*, 2008; Tempelhoff, 2013). These two heavy metals are thus very relevant to SA specifically, but also worldwide.

In addition, exposure is often not limited to a single heavy metal but to a mixture of different metals such as a combination of Cd and Cr, as was used in this study. Also, exposure often occurs at different concentrations of the metals which might be higher than the approved WHO safety limits, therefore a 1000-fold higher concentrations than the WHO water limits were used. Toxicity is a function of absorption, distribution, metabolism and excretion. Organs and cells involved in these processes are often the primary targets of toxicity. Therefore the aim of this study was to determine the effects of Cd and Cr alone and in combination on the functioning and cellular structure of the liver, pancreas and kidney tissue, as well as the blood. The liver, pancreas and kidney were evaluated as the organs are susceptible to toxicity (Sharma, *et al.*, 2014; Solis-Heredia, *et al.*, 2000; Venter, *et al.*, 2017). Studies on the rat and human blood was also undertaken to determine the risk for thrombosis as well as to identify possible markers of cellular damage or function so that markers of tissue damage as a result of exposure can be identified and eventually can be used in population-based screening and risk assessment.

Chapter 2

Literature review

2.1 <u>Introduction</u>

The growth in the industrial sector has provided many benefits since its establishment, but has come with some unfavourable environmental effects. Heavy metals have become synonymous with industrial pollution due to their toxicological and physiological effects on the ecosystem, especially those found high on the World Health Organization (WHO) list of toxic heavy metals (Al-Othman*, et al.*, 2012; W.H.O., 2010). Most of the heavy metal pollution can be linked to anthropogenic activities, such as mines, foundries, smelters and other metal-based industrial operations (Al-Attar, 2011; Tchounwou*, et al.*, 2012), with cigarette smoking being the main non-occupational source of heavy metal pollution (Langárd and Costa, 2007; Prozialeck and Edwards, 2012). The increase in heavy metal levels in the water sources directly affects the people in the specific areas that are using the water for consumption, preparing food, and bathing, as well as the irrigation of crops. Heavy metals can be absorbed through the skin, orally or through inhalation (Awofolu*, et al.*, 2005; Venter*, et al.*, 2015). In addition, exposure is not limited to a single heavy metal but a mixture of different types such as a combination of lead (Pb), cadmium (Cd), chromium (Cr), manganese (Mn), mercury (Hg) and/or copper (Cu) (Binning and Baird, 2001; Venter, 2015).

In this thesis *in vivo and ex vivo* models were implemented to test the effects of the heavy metals Cd and Cr alone and in combination. The effects of Cd and Cr will be discussed according to several different parameters including the effects on the normal histology and ultrastructure of the liver, pancreas and kidney tissue and whether the metals bio-accumulate in these organs. The effects of the metals on the ultrastructural and viscoelasticity of the clot will also be evaluated. The liver, pancreas and kidney tissue were chosen as they play a major role in the absorption, distribution and excretion of toxic compounds, like Cd and Cr (Timbrell, 1999). In the liver, pancreas and kidneys, Cd and Cr are metabolized differently, but induce similar effects namely oxidative stress that leads to lipid peroxidation, protein and deoxyribonucleic acid (DNA) damage and apoptosis. These effects may lead to functional and ultrastructural changes to the tissue and cellular components of the liver, pancreas and kidney (Timbrell, 1999; Venter, 2015). Alterations to the carefully controlled coagulation system, which may lead to for example stroke (Zhang*, et al.*, 2015), will be evaluated as any changes to the ultrastructure and viscoelasticity of clots can induce major problems.

5

Therefore, this chapter includes the sources and physiological effects of Cd and Cr alone and in combination, in conjunction with the specific effects the metals have on the liver, pancreas and kidney tissue. This chapter is concluded with the specific aims and objectives of this study.

2.2 <u>Cadmium</u>

2.2.1 <u>Sources and bio-accumulation of cadmium</u>

Cd is a transition metal that is found in group IIb of the periodic table of elements (Cullinane, et al., 2009). Cd is found in the earth's crust and generally exists in a divalent cation, for example $CdCl_2$, and is not biodegradable and will persist in the environment. Cd is usually found as an impurity in zinc (Zn) and lead (Pb) deposits and is a by-product in the process of Zn and Pb melting (Bernhoft, 2013; Jomova and Valko, 2011; Prozialeck and Edwards, 2012). Cd is also commercially used in television screens, lasers, batteries, paint pigments, cosmetics, etc. (Bernhoft, 2013). Humans are typically exposed to Cd either in their workplace or through contaminated food and water, with cigarette smoking being the major non-occupational source of Cd exposure (Prozialeck and Edwards, 2012). Depending on the dose, route of administration and duration of Cd exposure, various organs including the lungs, liver, kidney and bone can be damaged (Prozialeck and Edwards, 2012). The main organ that is affected by Cd toxicity is the kidney and will cause generalized dysfunction of the proximal tubule, which include polyuria, increased urinary excretion of glucose, amino acids, electrolytes [sodium (Na^+), potassium (K^+) and calcium (Ca^{2+})] and low molecular weight proteins (Jomova and Valko, 2011; Prozialeck and Edwards, 2012). After Cd exposure via inhalation and/or ingestion, it will bind to albumin in the blood and will be transported to the liver (Fig. 2.1) (Nordberg, 2009).

As the Cd-albumin complex enters the liver, it is separated and the Cd can cause toxicity (Fig. 2.1). A small amount of Cd is excreted into the bile bound to glutathione (GSH) (Fig. 2.1). The presence of Cd in the liver induces metallothionein (MT) production by hepatocytes and this causes a gradual increase in the proportion of Cd bound to MT in the liver (Nordberg, et al., 2007). The binding of Cd to MT buffers hepatocytes from the toxic effect of Cd. When a hepatocyte contains a considerable amount of the Cd-MT complex, it will be released into the bloodstream and filter through the renal glomeruli and absorbed in the proximal renal tubules of the kidney via endocytosis (Fig. 2.1) (Nordberg, 2009; Nordberg, et al., 2007; Prozialeck and Edwards, 2012). This process is mediated by the ZIP8 transporter.

After the absorption of Cd into the proximal renal cells, Cd enters the lysosomes and is released from MT (Nordberg, 2009). The free Cd ions can then cause damage in the absence of MT. When the renal cells are exposed to Cd for a long period, the unbound Cd will stimulate new MT production that will bind to Cd and protect the cells (Fig. 2.1) (Nordberg, 2009). When the Cd concentration increases above the protective ability of the renal cells, toxic effects are observed (Fig. 2.1).
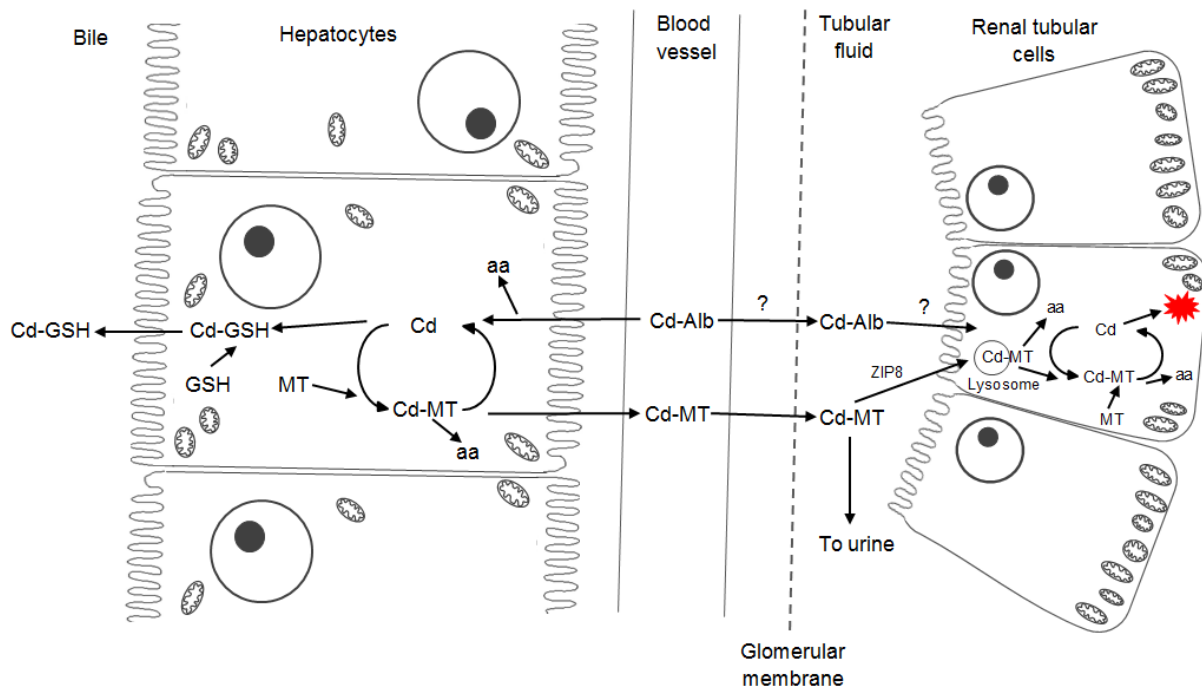
Figure 2.1: Basic flow diagram of Cd as it is transported through the body. **Key:** aa: amino acids; Alb: albumin; : Damage (Modified from: Nordberg, 2009; Venter, 2015).

Recently, Chang, *et al*. and Edwards and Prozialeck concluded that β-cell injury in the pancreas may lead to suppression of insulin release and possibly play a role in causing diabetes (Chang*, et al*., 2013; Edwards and Prozialeck, 2009). The process in which Cd causes β-cell injury is summarized in figure 2.2. Cd induces β-cell death through the mitochondrial-dependent apoptosis pathway, where mitochondrial dysfunction (loss of mitochondrial membrane potential (MMP), increase in cytochrome *c* release, and decrease in *Bcl-2* and increase in *p53* expression), increased poly (adenosine diphosphate (ADP)-ribosome) polymerase (PARP) cleavage and activation of caspase-3, -7 and -9 plays a crucial role in causing apoptosis (Chang*, et al*., 2013). Chang and his colleagues also showed that c-jun N-terminal kinase (JNK), part of the mitogen-activated protein kinase (MAPK) family and plays a role in sequential transduction of biological signals from the cell membrane to the nucleus, is activated by oxidative stress, which is an important signalling event in Cd-induced pancreatic β-cell apoptosis (Fig. 2.2) (Chang*, et al*., 2013).
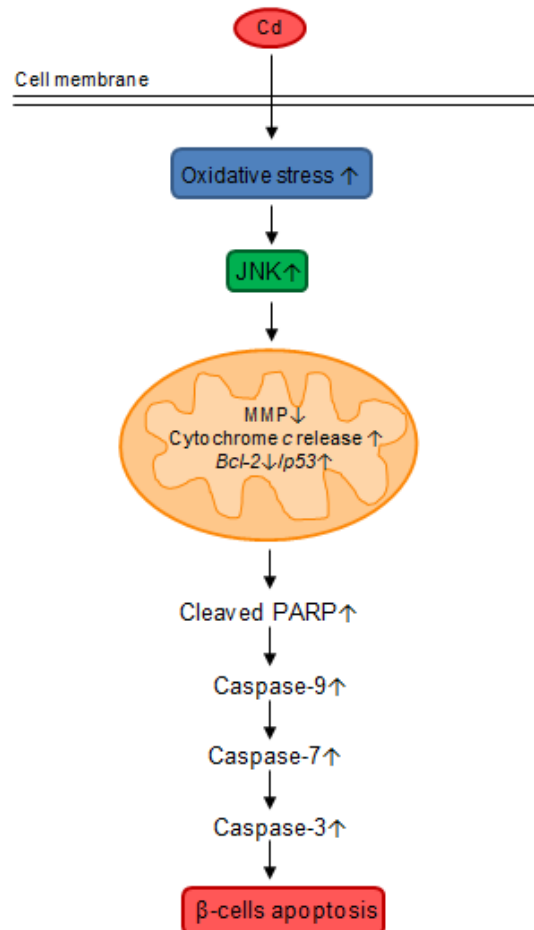
Figure 2.2: Signalling pathways involved in Cd-induced pancreatic β-cell apoptosis (Modified from: Chang*, et al.*, 2013).

Cd toxicity induces oxidative stress by means of indirect processes, as it is not a Fenton metal and therefore does not undergo redox cycling. Cd binds intracellular thiols, like GSH and/or interferes with the actions of various enzymes that protect the cells against oxidative stress (Prozialeck and Edwards, 2012). These indirect processes are comprised of the decrease of cellular antioxidants and the production of reactive oxygen species (ROS) by the mitochondria (Fig. 2.3). Cd toxicity thus increases hydrogen peroxide (H_2O_2), superoxide anion ($O_2\bullet^-$) and hydroxyl radical ($\bullet OH$) production and thus increases oxidative stress in the cell (Fig. 2.3) (Bertin and Averbeck, 2006; Jomova and Valko, 2011). The oxidative stress caused by Cd toxicity has many effects on the cells, for example damage to proteins and thus an increase in production of heat shock proteins (HSPs). The HSPs are chaperone proteins that are activated by hyperthermia and several environmental stresses that include Cd toxicity. Cd toxicity causes overexpression of certain HSPs, which helps with the repair of misfolded proteins or eliminates aggregated proteins by the ubiquitin-proteasome system (Fig. 2.3) (Bertin and Averbeck, 2006).

Cd-induced oxidative stress also causes DNA damage. DNA is important for normal cellular functions that include replication, gene expression and protein synthesis. When DNA is damaged, it can induce cell cycle arrest, mutagenesis, genome instability, cancer and apoptosis (Fig. 2.3) (Bertin and Averbeck, 2006). Another effect of Cd-induced oxidative stress is the peroxidation of lipids (Fig. 2.3). Lipid peroxidation may cause cross-linking and polymerization of membrane components and therefore cause cell membrane modification in their lipid composition and will thus affect the function and integrity of membranes such as the mitochondrial membranes (Bertin and Averbeck, 2006).
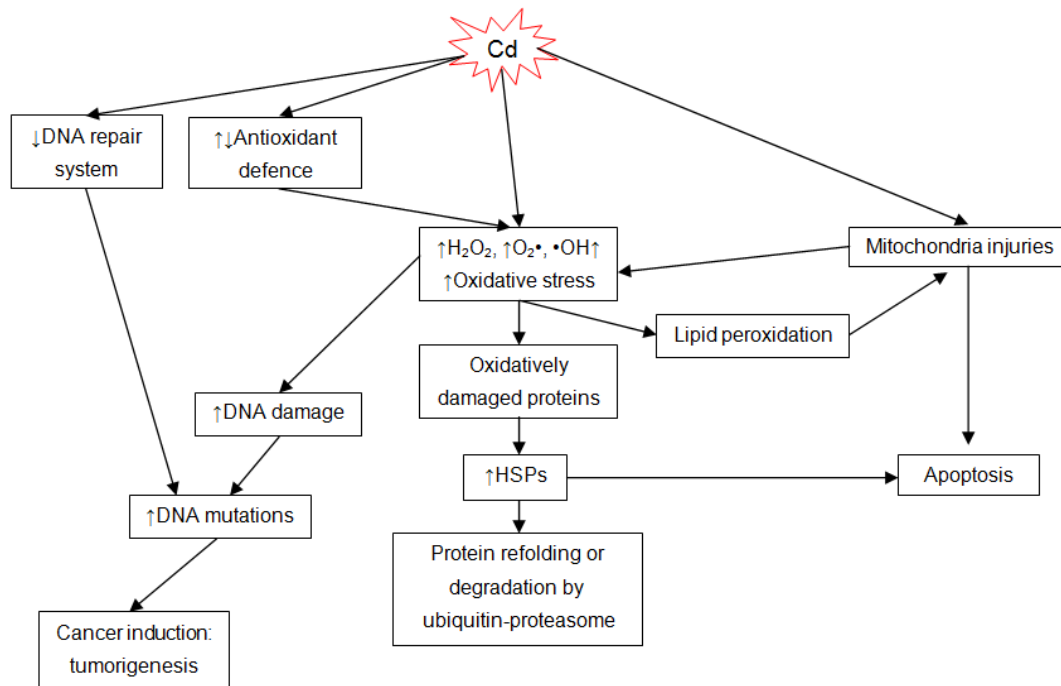
Figure 2.3: The biological pathway of Cd toxicity in cells (Venter, 2015).

No mechanism exists to excrete Cd and thus it accumulates in the body, with the largest amount deposited in the kidneys, liver, pancreas and lungs. Cd has a half-life of 25 years in the tissue and persists for approximately 75-128 days in erythrocytes. Vitamin C and Vitamin E supplementation have been shown to reduce the toxic effects of Cd (Bernhoft, 2013; Jomova and Valko, 2011).

2.3 Chromium

2.3.1 Sources and bio-accumulation of chromium

Cr is one of the most common elements that can be found on earth and exists in a variety of oxidation states that range from Cr(II) to Cr(VI) (Jomova and Valko, 2011; Patlolla, *et al.*, 2009; Yoon, *et al.*, 2007), where only the trivalent [Cr(III)] and hexavalent [Cr(VI)] forms are

important in human health (Dayan and Paine, 2001; Langárd and Costa, 2007). Human Cr exposure occurs mainly due to inadequate disposal of waste from industrial companies involved in processes like, electroplating, steel manufacturing, leather tanning and wood preservation (Balakrishnan, *et al.*, 2013). Cr is also present in cigarettes and about 0.246mg/kg–14.6mg/kg gets inhaled when smoking (Langárd and Costa, 2007). Cr(III) is an essential dietary mineral for glucose and lipid metabolism (Quinteros, *et al.*, 2007; Song, *et al.*, 2012; Valko, *et al.*, 2006). When Cr(III) becomes deficient in the body, it has been shown that it can contribute to cardiovascular diseases, metabolic diseases like diabetes, and infertility. Cr(III) can be found in small quantities in most fresh food, including bread, meat, vegetables and drinking water. In the human body, Cr(III) is unable to cross cell membranes, as it is not part of the cellular anion transport system and thus is the reason it is less toxic than Cr(VI) (Jomova and Valko, 2011).

Cr(VI) is highly toxic and carcinogenic at high dosages. Cr(VI) can enter the body via all three routes of exposure, namely: inhalation, ingestion and/or absorption through the skin. Humans are exposed to Cr(VI) mainly through occupational exposure, where the airways and skin are mostly affected, resulting in cellular damage, tumour formation, allergic dermatitis and skin ulcers, respectively (Jomova and Valko, 2011; Myers, 2012; Quinteros, *et al.*, 2007). Other effects found in both occupational and non-occupational exposure include gastrointestinal problems, hypertension, and hepatic and renal failure. Cr(VI)'s high toxicity and carcinogenic incidence is due to its tetrahedral co-orientation that emulates biological phosphates and sulphides. This allows Cr(VI) to be readily taken up through channels for the transfer of the isoelectric and isostructural anions into the cells (Jomova and Valko, 2011).

After oral exposure to Cr(VI), it is effectively detoxified by the saliva, gastric juices and intestinal bacteria. If the Cr(VI) reaches the intestines, it will be reduced by the blood and subsequently the liver. This pathway of exposure will only account for low genotoxicity and carcinogenicity, except when the Cr(VI) exposure occurs over a long period of time and at high dosages (Jomova and Valko, 2011). In the cells, the reduction of Cr(VI) reduces the potentially carcinogenic metal ion (Fig. 2.4). In the erythrocytes, Cr(VI) is depleted to lower oxidation states, whereafter it forms protein complexes and is unable to leave the cells. The reduction of Cr(VI) to its lower oxidative states are not without risk, because during the process various free radicals are formed (Jomova and Valko, 2011). Ascorbate has shown to be the most effective biological reductant of Cr(VI) in cells as it plays a dual role in Cr(VI) toxicity. Outside the cells it plays a protective-antioxidant role and inside the cells a pro-oxidative role (Fig. 2.4). The intracellular reduction of Cr(VI) generates high levels of Cr-DNA

adducts and mutations that leads to DNA damage (Fig. 2.4). The reduction of Cr(VI) to Cr(III) can also be accomplished by non-enzymatic reactions with cysteine and GSH (Fig. 2.5) (Jomova and Valko, 2011).
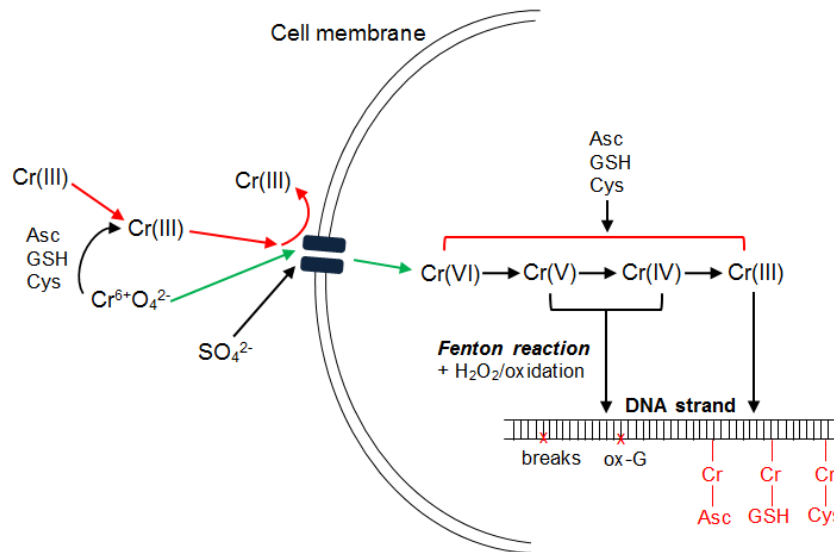
Figure 2.4: Intracellular uptake and DNA damage due to Cr(VI) toxicity. **Key:** Asc: Ascorbate; GSH: Glutathione; Cys: Cysteine (Modified from: Jomova and Valko, 2011).

The intermediate oxidative states of Cr, Cr(IV) and Cr(V), also play a part in Cr genotoxicity and carcinogenicity, either directly or through the Fenton reaction to produce ROS (Fig. 2.5). In the reduction of Cr(VI) ROS, like H_2O_2, singlet oxygen and $O_2^{\bullet-}$ are produced. The hydrogen peroxide that is formed in the cells is able to react with DNA bases and cause DNA damage (Jomova and Valko, 2011). Cr toxicity is also linked to single strand DNA breaks, DNA-DNA interstrand crosslinks, DNA-protein crosslinks, Cr-DNA adducts, oxidative nucleotide changes and chromosomal changes.
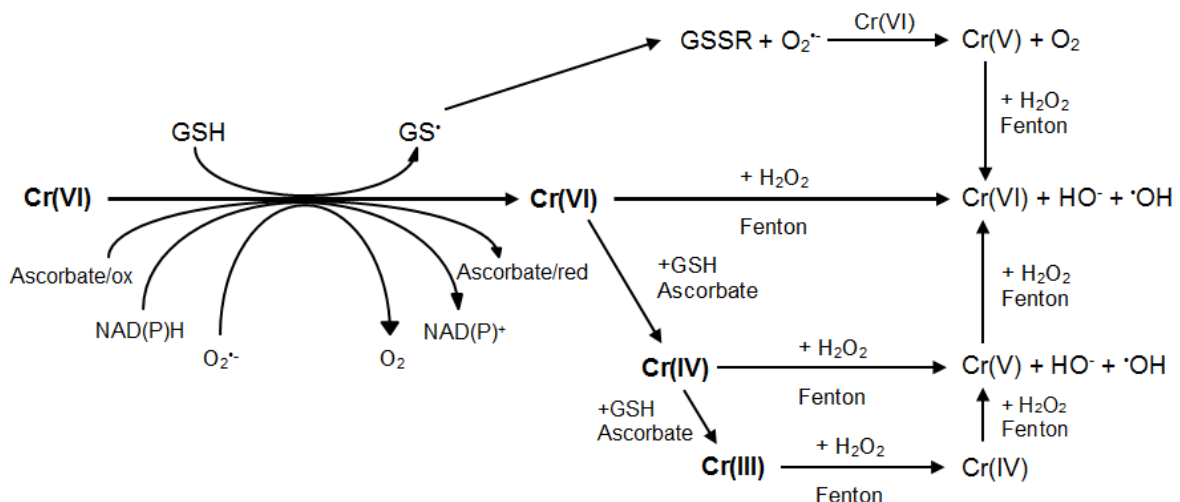
Figure 2.5: The reduction reactions of Cr(VI) by GSH (Jomova and Valko, 2011).

Cr toxicity is also involved in the MAPK signal transduction pathway, where nuclear factor kappa B (NF-κB), activating transcription factor 2 (ATF-2) and *p53* play a role in regulating cellular processes, including apoptosis (Jomova and Valko, 2011).

Cr is excreted from the body in the form of Cr(III) and is detected in the urine and faeces. It is only when the liver cells are compromised that Cr(VI) may be excreted in the bile. The excretion rate of Cr depends on the valence state of the Cr and thus excretion can occur after a few hours to a few days (Langárd and Costa, 2007; Wilbur, *et al.*, 2011).

2.4 <u>Metal combinations</u>

Although Cd and Cr affect the cells through different biochemical pathways, similar end results are observed. As described above, Cd will deplete protein-bound sulfhydryl groups and increase the production of ROS such as H_2O_2, $O_2\bullet^-$ and $\bullet OH$ (Bertin and Averbeck, 2006; Stohs and Bagchi, 1995). In the case of Cr, it will enter the redox cycle and will also increase the production of ROS. The increase in ROS will cause certain alterations, which include lipid peroxidation, DNA and membrane damage, altered gene expression and apoptosis or necrosis (Stohs and Bagchi, 1995).

Although limited information is available in the literature on the combined effects of these metals specifically on the liver, pancreas and kidneys, Jin and colleagues concluded that Cd and Cr alone and in combination have the ability to induce apoptosis via oxidative and endoplasmic reticulum (ER) stress (Jin, *et al.*, 2014). These changes are due to the disturbance in the balance of ROS and antioxidant enzymes; the transcriptional status of genes related to oxidative- and ER-stress and the activities of caspase-9 and caspase-3 in liver tissue (Jin, *et al.*, 2014). Histological and ultrastructural evaluations of liver and kidney tissue revealed that acute Cd and Cr exposure does not cause any major damage, but was hypothesised that the combination might have the potential to cause functional alterations when chronically exposed (Venter, 2015). According to this literature, it is still unclear if Cd and Cr, in combination, will have an antagonistic, additive or synergistic effect on the liver, pancreas and kidney.

2.5   Specific organs targeted by heavy metal toxicity

Toxic compounds can cause direct and/or indirect damage to tissue that can lead to cell death and functional changes. These alterations caused by toxic compounds may be reversible or irreversible. The ability of the organ or tissue to resist toxicity depends on many factors including the degree of specialization, reserve functional capacity and ability to repair the damage (Timbrell, 1999). Thus any organ can be a target for toxic compounds, but there are many factors that play a role in the targeting of an organ. These factors include: the blood supply of the specific organ, the presence of a particular enzyme or biochemical compound, function and/or location of an organ, vulnerability to disruption or degree of specialization, ability to repair damage, specific uptake systems, ability to metabolize the toxic compound, balance between toxicity and detoxification systems, and binding to particular macromolecules (Timbrell, 1999). Thus, factors that influence the absorption, distribution and excretion of toxic compounds and the physicochemical characteristics of those compounds can all affect the toxicity to particular target organs (Timbrell, 1999).

2.5.1   The liver as a target of heavy metal toxicity

Normal structure and function of the liver

When observing normal liver histology, the liver mainly consists of hexagonal areas that constitute the hepatic lobules. In a transverse section of the liver, each lobule consists of hepatocytes arranged in thin plates that anastomose with one another and form a network (Singh, 2011). The thin plates are separated by fine vascular sinusoids, the walls of which consist of fenestrated endothelium and Kupffer cells (Coetzee, *et al.*, 2009b; Kierszenbaum and Tres, 2012; Singh, 2011; Young, *et al.*, 2006). The sinusoids drain into the central veins found in the centre of each lobule, which drains into the portal vein that removes the blood from the liver. Together with the portal vein, a hepatic artery and interlobular bile duct can be found that forms the portal triad (Singh, 2011).

The hepatocytes are cuboidal in shape, with a round nucleus in the centre of the cell. Rough ER (rER) and smooth ER (sER), Golgi complex, mitochondria, lysosomes, lipid droplets and glycogen granules can be found in the cytoplasm of the hepatocyte (Singh, 2011; Young, *et al.*, 2006). The sinusoidal space allows for absorption of nutrients from digestion as well as secretion of products into the blood (Young, *et al.*, 2006). Between the sinusoid and hepatocyte, the space of Disse can be found and is filled with blood plasma that leaked through the endothelial pores. The microvilli found on the surface of the hepatocytes, extend

into this space and thus increase the liver cell surface (Coetzee, *et al.*, 2009b; Singh, 2011). Reticular fibres and lipid forming cells are also found in the space of Disse, with the lipid storing cells responsible for the production of the reticular fibres in the area (Coetzee, *et al.*, 2009b). The liver has a variety of functions that includes uptake and distribution of substances, metabolism of carbohydrates, proteins and lipids, storage of various substances including glycogen, lipids, vitamins and iron, and detoxification of toxic substances (Coetzee, *et al.*, 2009b; Moini, 2016b; Singh, 2011).

Liver toxicity

The liver is one of the organs that are the most vulnerable to toxicity due to the following factors: its rich blood supply and position in the body; large and diverse metabolic capacity, its extensive role in intermediary metabolism and synthesis and consequently interference with endogenous metabolic pathways, and the secretion of bile (Timbrell, 1999). The detection of the alterations to the liver can be determined by enzymes such as alanine transaminase (ALT), aspartate transaminase (AST) and bilirubin in plasma. When a biopsy is taken, the histological and ultrastructural alterations can be detected (Timbrell, 1999).

2.5.2 <u>The pancreas as a target of heavy metal toxicity</u>

Normal structure and function of the pancreas

The pancreas consists of two types of glandular tissue namely the exocrine and endocrine components. The exocrine pancreas makes up the largest part of the organ with the endocrine pancreas, found as islets, embedded in the exocrine component. The exocrine pancreas is the largest part of the pancreas and consists of compound tubulo-alveolar glands with acinus secretory units (Coetzee, *et al.*, 2009b; Singh, 2011). The glandular cells of the acini are pyramidal-shaped with two zones. The first is found on the basal area of the cells, and is known as the basal zone. In this zone well-developed rER can be found with flattened cisternae. The zymogenic zone is the second zone that can be found in the glandular cells of the acini. The zymogenic zone contains acidophilic zymogen granules that are the largest secretory granules. The Golgi complex can be found in the supranuclear part of the cell (Coetzee, *et al.*, 2009b; Singh, 2011). The secretory glands of the exocrine pancreas produce two types of secretions. The one type is watery and rich in bicarbonate, which neutralizes the acid contents entering the duodenum from the stomach. The other type of secretion is thicker and contains many enzymes, including trypsinogen, chymotrypsinogen, amylase, lipase and the production of these enzymes starts when the cholecystokinin hormone is released by the endocrine cells of the duodenal mucosa (Singh,

2011). The secretions will be released from the acinar cells into the intercalated ducts via the centro-acinar cells. The centro-acinar cells are flattened cells that line the luminal surface of the acini. From the intercalated ducts the secretions are released into the interlobular ducts, lined with simple columnar epithelium, and then pass into the duodenum through the main pancreatic duct and accessory pancreatic duct (Coetzee*, et al.*, 2009b; Singh, 2011).

The endocrine tissue contains the islets of Langerhans that are scattered in between the exocrine component as groups of glandular cells. The glandular cells are arranged in cords of small groups with capillaries which run in between them. The glandular cells can be divided into three different types of cells, namely the alpha (α)-, beta (β)-, delta (δ)- and pancreatic polypeptide (PP) cells, each with their distinct morphology and function (Coetzee*, et al.*, 2009b; Rana, 2014; Singh, 2011). The α-cells secrete the hormone glucagon, with the β-cells, constituting the largest number in the endocrine pancreas, secreting insulin. The δ-cells secrete gastrin and somatostatin. The somatostatin inhibits the secretion of glucagon by the α-cells (Coetzee*, et al.*, 2009b; Singh, 2011). The PP cells secrete a 36-amino-acid linear polypeptide of unknown function (Rana, 2014). The granules of the islets of Langerhans are membrane bound. The α-cell granules are round or oval with high electron density. The granules of the β-cells are fewer, larger and less electron dense then those of the α-cells. The δ-cells also have round or oval granules, similar to those of the α-cells, but have a lower electron density (Singh, 2011).

Pancreas toxicity

In recent years the β-cells and thus insulin production and secretion has been studied in the field of toxicology (Chang*, et al.*, 2013; Lei*, et al.*, 2007; Rana, 2014). When the β-cells of the pancreas are affected by toxic compounds, it may induce diabetes mellitus. This may be due to the mitochondria of the β-cells being highly vulnerable to oxidative damage (Chang*, et al.*, 2013). Studies on the toxicity of Cd have shown that Cd accumulates in the pancreas, and this influences the production of insulin and may lead to diabetes (Rana, 2014).

2.5.3 <u>The kidney as a target of heavy metal toxicity</u>

Normal structure and function of the kidney

The kidney is a bean-shaped organ that is responsible for urine formation. When a coronal section is made through the kidney, two distinct areas can be observed, the outer area termed the cortex and the inner area, the medulla (Moini, 2016c; Singh, 2011). Both the cortex and medulla contains the functional units of the kidney, the nephrons. The nephron

can be divided into the renal capsule and proximal and distal convoluted tubules (PCT and DCT) which are connected by the loop of Henle (Kierszenbaum and Tres, 2012; Singh, 2011). The renal capsule consists mainly of the oval shaped double-walled Bowman's capsule that surrounds the anastomosing capillaries of the glomerulus. Bowman's capsule consists of two layers: the visceral and parietal layers. The parietal layer, associated with the connecting tissue stroma, is covered with basal lamina and supported by simple squamous epithelium that is continuous with the simple cuboidal cells of the PCT (Singh, 2011). The visceral layer is attached with the glomerular capillaries and is lined with podocytes (Kierszenbaum and Tres, 2012; Singh, 2011). Between the glomerulus and Bowman's capsule, the urinary space or Bowman's space can be found and is continuous with the PCT (Kierszenbaum and Tres, 2012; Singh, 2011).

The glomerular capillaries are fenestrated and are surrounded by a thick basal lamina. The blood enters the glomerulus through the afferent arterioles and exits through the efferent arterioles and forms the vascular pole of the renal capsule (Kierszenbaum and Tres, 2012; Singh, 2011). In this region, three types of specialized cells can be found as the ascending DCT come into contact with the arterioles, and is known as the juxtaglomerular apparatus. These three cells, juxtaglomerular cells, macula densa and extraglomerular mesangial cells regulate filtration formation rates and systemic blood pressure (Kierszenbaum and Tres, 2012; Moini, 2016c). The juxtaglomerular cells are modified muscle cells, which secretes renin necessary for increase in blood pressure. The macula densa is a thickening in the wall of the DCT, as it comes into contact with the arterioles and acts as chemoreceptors. This area regulates the sodium chloride content of the filtrate as it enters the DCT (Moini, 2016c; Singh, 2011). The extraglomerular mesangial cells are found in between the arterioles and tubule cells and the function of these cells are unknown. It has been speculated that these cells might be involved in passing signals from the macula densa cells to the juxtaglomerular cells (Kierszenbaum and Tres, 2012; Moini, 2016c).

The PCT and DCT consist of distinctive cuboidal cells. The nuclei of the cuboidal cells of the PCT are situated near the base of the cell with a well-developed brush border on the luminal surface (Kierszenbaum and Tres, 2012; Moini, 2016c). The DCT cuboidal cells are smaller than the PCT cells, with a minimal amount of microvilli present at the brush border on the luminal surface of the DCT. The loop of Henle connects the PCT and DCT, and is a U-shaped tubule that extends into the medulla and returns to the renal cortex and empties into the collecting duct (Kierszenbaum and Tres, 2012; Moini, 2016c).

Kidney toxicity

The main function of the kidney is to filter waste products and toxins out of the blood while conserving essential substances like glucose, amino acids and ions (Timbrell, 1999). Kidney damage occurs due to a variety of reasons. Firstly, the kidneys are target organs for toxicity due to the high volume of blood that filters through them. Although it only represents 1% of the body mass, 25% of the cardiac output passes through the kidneys. The reabsorption capacity of the kidneys, allows for concentrated amounts of foreign compounds in the tubular fluid that can cause renal tubular necrosis (Timbrell, 1999). The active transport of compounds by the tubular cells can cause damage to the proximal tubular cells, as the toxic compounds may accumulate in the cells. Kidney damage can also occur when certain compounds involved in metabolism is activated and collected in the kidney (Timbrell, 1999).

2.6   Cellular alterations due to metal toxicity

The effects that heavy metals have on cells, translate not only to functional changes, but also histological and ultrastructural changes. These changes can be divided into three events namely, primary, secondary and tertiary. In the primary event, the toxic compound may cause lipid peroxidation, covalent binding to macromolecules, changes in thiol status, enzyme inhibition and ischaemia (Timbrell, 1999). The toxic compounds may cause several of these primary events or only one. The secondary events follow on the primary events and describe the biochemical and structural changes that may occur in the cells after exposure. Major secondary events include changes in membrane structure and permeability, alterations in the cytoskeleton, mitochondrial damage, inhibition of mitochondrial function, depletion of adenosine triphosphate (ATP) and other cofactors, changes in Ca^{2+} concentration, DNA damage, lysosomal destabilization, stimulation of apoptosis and alterations to the endoplasmic reticulum (Timbrell, 1999). These events may also feature as a primary event. Tertiary events are the final, observable changes after exposure to toxic compounds. Tertiary events include steatosis/fatty change, oedema degradation, blebbing, apoptosis and necrosis (Timbrell, 1999).

The primary effects of Cd and Cr includes the depletion of GSH, inhibition of antioxidant enzymes, DNA damage and increase in ROS formation (see Figures 2.1-2.5) (Bertin and Averbeck, 2006; Jomova and Valko, 2011; Venter, *et al.*, 2017). Major effects of ROS include lipid peroxidation and oxidative damage, thus one of the first targets of ROS is the plasma membrane. The plasma membrane which is involved in the movement of substances in and out of the cell allows for selective communication between intracellular and extracellular compartments and provides structure and protection to the cells (Coetzee, *et*

al., 2009c; Moini, 2016a). The membrane consists of a double layer of phospholipid molecules and protein molecules that are scattered throughout the membrane, with cholesterol molecules to stabilize the membrane (Moini, 2016a). Based on the composition of the plasma membrane and its direct contact with plasma and blood in the liver, pancreas and kidney, the plasma membrane is vulnerable to the effects of ROS.

Besides the plasma membrane, Cd and Cr also have the ability to cause alterations in the mitochondria and nucleus. The mitochondrion is a highly compartmentalized organelle, the main function of which is the production of ATP. The mitochondrion consists of an outer and inner mitochondrial membrane and between the two membranes, an intermembrane space can be found. The inner mitochondrial membrane has a series of folds known as cristae, which encloses the fluid filled matrix. The mitochondria contain DNA, ribonucleic acid (RNA) and some ribosomes (Kierszenbaum and Tres, 2012; Moini, 2016a). Each cell contains several hundred mitochondria usually localised in the cytoplasm below the plasma membrane. The mitochondria produce ROS that is essential for the functioning of several pathways including cytochrome *b*5 reductase, monoamine oxidases, dihydroorotate dehydrogenase, dehydrogenase of α-glycerophosphate, succinate dehydrogenase, aconitase and α-ketoglutarate dehydrogenase complex. Excessive production of ROS causes membrane damage, changes to membrane permeability and function (Andreyev*, et al.*, 2005).

The nucleus is the largest organelle in the cell and serves as the control centre for the cell. The nucleus consists of three components, the nuclear envelope, chromatin and nucleolus (Kierszenbaum and Tres, 2012; Moini, 2016a). The nuclear envelope also consists of two phospholipid membranes that aid in communication and transport between the nucleus and cytosol of the cell. The chromatin consists of the DNA and protein fibers that will coil up to form chromosomes during mitosis. The nucleolus is mostly made up of RNA and proteins and is not surrounded by a membrane. Ribosomes are produced in the nucleolus (Kierszenbaum and Tres, 2012; Moini, 2016a). Not only are the nuclear membrane, DNA and protein found in the nucleus sensitive to the effects of ROS, excessive ROS can lead to irregular chromatin condensation and via apoptosis leads to cell death (Venter, 2015).

2.7   The coagulation system and heavy metal toxicity

The one system that connects all the organs of the body and might also be affected by the heavy metals is the cardiovascular system. The major cell type found in the blood is the erythrocytes which are round, biconcave-shaped cells, with no nucleus and other organelles.

Erythrocytes only consist of a plasma membrane, with its underlining cytoskeleton, haemoglobin and glycolytic enzymes (Coetzee, *et al.*, 2009a; Kierszenbaum and Tres, 2012).

The erythrocyte plasma membrane is a lipid bilayer and consists of cholesterol and phospholipids. There are four major phospholipids found in the membrane, namely phosphatidylcholine and sphingomyelin, found on the outer membrane, while phosphatidylethanolamine, phosphatidylserine (PS) and the minor phosphoinositide constituents, are found in the inner membrane layer (Mohandas and Gallagher, 2008). Several energy-dependent and -independent phospholipid transport proteins have been identified to generate and maintain phospholipid asymmetry. Flippase moves phospholipids from the outer to the inner membrane leaflet; floppase does the opposite against the concentration gradient and is energy-dependant; and scramblase moves lipids in a bi-directional manner from both the inner and outer membranes and is also energy-dependant (Mohandas and Gallagher, 2008; Pretorius, *et al.*, 2016b). Other plasma membrane proteins involved in the maintenance of the structural integrity of the membrane include two macromolecular complexes, namely ankyrin-based and protein 4.1 R-based. With the ankyrin complex band 3 and RhAG proteins (found in the lipid bilayer) connect the lipid bilayer with the cytoskeleton via their cytoplasmic domains with ankyrin. Glycophorin, XK, Rh and Duffy proteins does the same by connecting the protein 4.1 R with the cytoskeleton (Mohandas and Gallagher, 2008).

Disruption of the erythrocyte plasma membrane symmetry, in particular the externalisation of PS, has several functional implications (Mohandas and Gallagher, 2008; Pretorius, *et al.*, 2016b). The exposure of PS in the outer leaflet of the membrane serves as a signal of eryptosis and can lead to membrane vesicle formation, microparticle shedding, with pathological shape changes of the erythrocytes (Pretorius, *et al.*, 2016b). During eryptosis, the increase in cytosolic Ca^{2+} activates the Ca^{2+}-sensitive K^+ channels that causes the exit of potassium chloride (KCl) and result in cell shrinkage (Pretorius, *et al.*, 2016a). Ca^{2+} cytosolic levels can be increased due to oxidative stress generated as described above. The increase of Ca^{2+} can also stimulate sphingomyelinase to form ceramide. Ca^{2+} and ceramide then causes activation of scramblase, which inhibits flippase and causes floppase to translocate PS to the outer membrane, resulting in externalization of PS (Pretorius, *et al.*, 2016a). The increase in Ca^{2+} also activates calpain, which degrades the ankyrin R-complex of the cytoskeleton. This will cause cell shrinkage and cell membrane scrambling and finally initialise clearing from circulation through removal by macrophages (Pretorius, *et al.*, 2016a; Pretorius, *et al.*, 2016b).

Other essential components of the coagulation system include the platelets and fibrin networks. Generated ROS can also cause the activation of platelets which are cytoplasmic discoid fragments derived from the megakaryocyte. Platelets also contain no nuclei, but have a few mitochondria, glycogen and granules (Kierszenbaum and Tres, 2012; Swanepoel, et al., 2015). There are three types of granules found in the platelet cytoplasm, namely α-granules, dense granules and lysosomes, each containing their own distinct constituents that is important for the coagulation cascade (Swanepoel, et al., 2015). Fibrinogen and fibrin are involved in the last steps in the coagulation pathway. Fibrinogen has a centrosymmetric, trinodular, s-shaped structure. Fibrinogen is cleaved by thrombin, during the coagulation, at two N-terminal peptides from the Aα- and Bβ-chains that results in the formation of protofibrils and fibrin fibres (Kell and Pretorius, 2016; Swanepoel, et al., 2015).

As the coagulation system is constantly and tightly regulated, any erythrocyte, platelet and fibrin fibre alterations can influence the coagulation system (Pretorius, et al., 2013; Van Rooy, et al., 2015). The coagulation system is important as it is responsible for preventing blood loss (Smith, 2009). Under normal conditions, the balance between prothrombotic (pro-coagulation) and antithrombotic (anti-coagulation) factors needs to be tightly monitored, as an imbalance can lead to pathological thrombi or haemorrhage (Van Rooy, 2015). The classic coagulation pathway introduced in 1964 focused on the role of the coagulation factors in thrombus formation and ignored the role of cellular elements in the activation of the coagulation system. For this reason a new model has been introduced that includes platelets and tissue factor (TF) - expressing cells. This model is known as the cell-based model of coagulation and consists of three phases, namely initiation, amplification and propagation phases that will be explained in detail below (Pérez-Gómez and Bover, 2007; Smith, 2009; Van Rooy, 2015). In the initiation phase, after the rupture of dysfunction of the vascular endothelium and the exposure or release of TF (Van Rooy, 2015), on the TF-bearing cell, activated factor VII (FVIIa) binds to the exposed TF. The TF-FVIIa complex can then activate additional factor VII (FVII) to FVIIa to produce more TF-FVIIa complexes and a small amount of factor IX (FIX) and factor X (FX) (Figure 2.6 A ①). TF-FVIIa converts FX to activated FX (FXa) and together with activated factor V (FVa) and forms a prothrombinase complex, which cleaves prothrombin (II) and produces a small amount of thrombin (IIa) (Figure 2.6 A ② and ③) (Smith, 2009; Swanepoel, et al., 2015).

During the second phase, amplification phase, the small amount of thrombin, generated in the initiation phase, causes the activation of platelets that have migrated to the injury site (Figure 2.6 B ①). The activation of platelets causes extreme changes to the platelet

membrane that leads to shape changes, shuffling of membrane phospholipids, and causes the release of granular content. Additionally, thrombin cleaves factor XI (FXI) to activated FXI (FXIa) and in the presence of calcium, cleaves factor V (FV) to activated FV (FVa) on the platelet surface (Figure 2.6 B ① and ②) (Smith, 2009; Swanepoel, *et al.*, 2015). Thrombin also cleaves one of the plasma proteins, von Willebrand factor (vWF), of factor VIII (FVIII) and subsequently activates FVIII to activated FVIII (FVIIIa). The free vWF can mediate platelet adhesion and aggregation (Figure 2.6 B ③) (Smith, 2009).

In the final stage, propagation phase, the last amount of thrombin is generated. This final stage takes place on the surface of the activated platelet that will cause cell-cell interactions and aggregation of platelets. This phase starts through the activated platelet that releases its granular content to recruit more platelets to the injury site (Figure 2.6 C ①). FIX is converted to FIXa via FXIa that was generated during the amplification phase (Figure 2.6 C ②). FIXa binds to FVIIIa to convert FX to FXa on the platelet surface (Figure 2.6 C ③) (Smith, 2009; Swanepoel, *et al.*, 2015). FXa rapidly binds to FVa and cleaves prothrombin (FII) to thrombin (FIIa) (Figure 2.6 C ④) that leads to the cleavage of fibrinopeptide A from fibrinogen. The production of thrombin will generate fibrin that will spontaneously polymerize into fibrin strands, resulting in a complex or meshwork of fibrin fibres (Kell and Pretorius, 2016; Smith, 2009; Swanepoel, *et al.*, 2015).

An equally important process during the coagulation process is fibrinolysis or the breakdown of the clot through proteolysis (Van Rooy, 2015). The breakdown is achieved by a number of enzymes of which plasmin plays a major role. Plasmin is formed when plasminogen is activated via tissue plasminogen activator (tPA). Plasmin is involved in the breakdown of the fibrin fibres that results in the breakdown of the clot (Van Rooy, 2015). Fibrinolysis is also controlled by plasminogen activator inhibitor-I (PAI-1) that prevents the premature activation of plasminogen and thus premature fibrinolysis. Other proteins like α2-antiplasmin and thrombin activatable factor inhibitor (TAFI) also regulate fibrinolysis (Van Rooy, 2015).
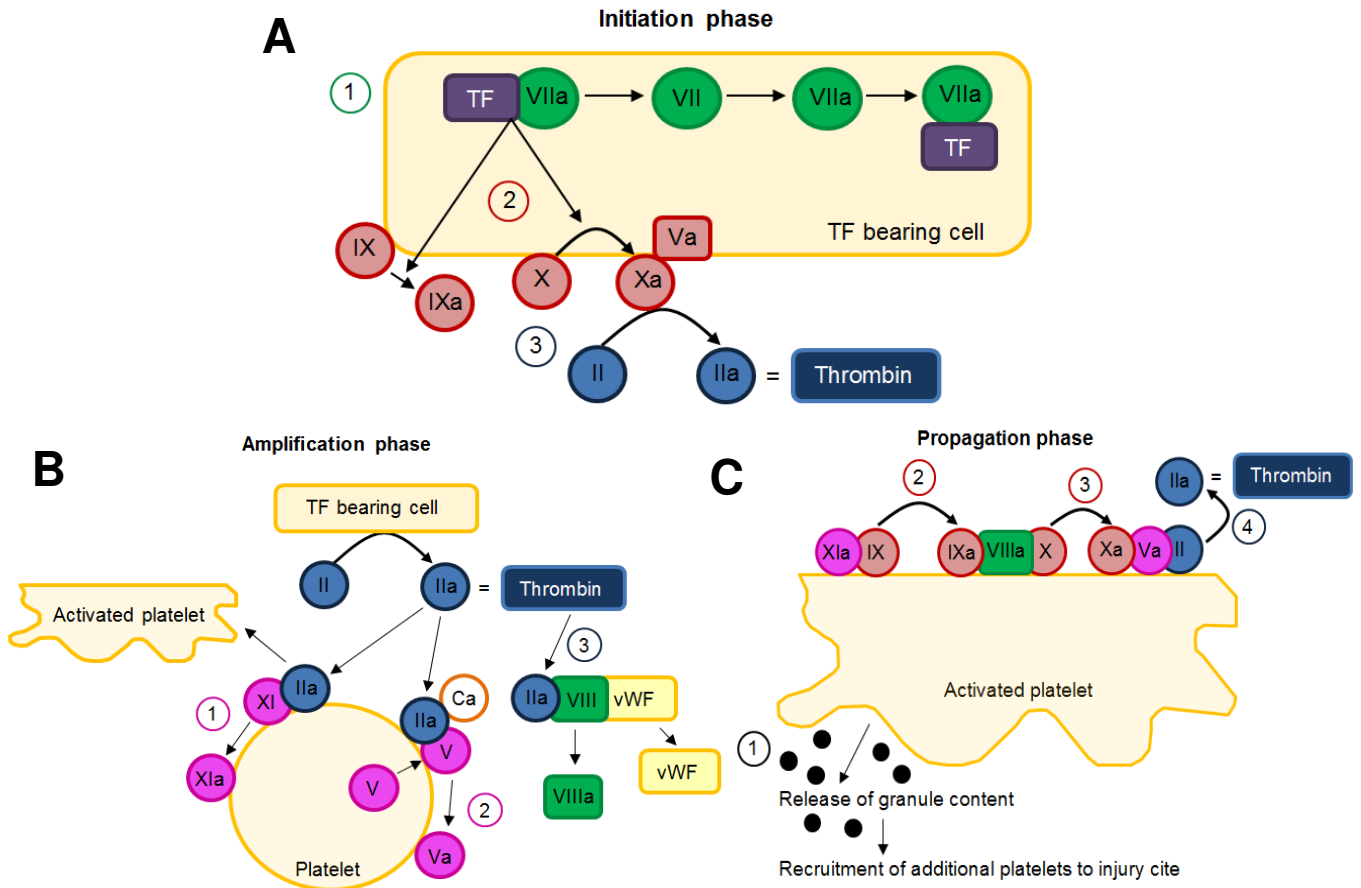
Figure 2.6: Summary of cell-based model for coagulation pathway (see text for more detail and abbreviations) (Modified from: Smith, 2009; Swanepoel, *et al.*, 2015).

The coagulation system might be influenced by heavy metals such as Cd and Cr, as in previous studies completed on the coagulation system and in smokers. It was found that smokers have a higher risk of cardiovascular problems, including being hypocoagulable, i.e., an increase in blood clot formation and thrombi formation (Kell and Pretorius, 2015; Pretorius, *et al.*, 2013; Pretorius, *et al.*, 2010). Cd and Cr are some of the elements found in cigarettes and might play a role in the altered cardiovascular system through their production of oxidative stress and inflammation (Dallüge, *et al.*, 2002; Fresquez, *et al.*, 2013; Lang and Lang, 2015; Lupescu, *et al.*, 2012; Pretorius, *et al.*, 2016b; Pretorius, *et al.*, 2014; Sopjani, *et al.*, 2008). This highlights the possible adverse effects of Cd and Cr on the coagulation system.

2.8   <u>Aim and objectives</u>

The aim of this study was to investigate the histological and ultrastructural effects as well as the cellular bioaccumulation of Cd and Cr alone and in combination on the liver, pancreas and kidney tissue using a male Sprague-Dawley rat animal model. Furthermore the aim was to evaluate the effects of these metals on the coagulation system by implementing an *ex vivo* blood coagulation model.

Objectives:

1. Implementing the Sprague-Dawley rat animal model exposed to Cd and Cr alone and in combination over a 28-day experimental period.
2. To determine if exposure to Cd and Cr alone and in combination causes changes in the weight, plasma levels of Cd and Cr and blood markers of tissue function and toxicity.
3. To determine if Cd and Cr alone and in combination causes changes in the histology of the liver, pancreas and kidney and/or induces fibrosis.
4. To evaluate the ultrastructural effects of Cd and Cr alone and in combination on the cellular morphology of the liver, pancreas and kidney.
5. Determine the possible bio-accumulation of Cd and Cr using electron energy-loss spectrometry.
6. Using an *ex vivo* model to determine the effect of Cd and Cr alone and in combination on erythrocytes, platelets and fibrin network morphology, erythrocyte Annexin-V positive expression and viscoelastic parameters of clot formation.

Chapter 3

Establishment of the Sprague-Dawley rat *in vivo* model

3.1 <u>Introduction</u>

Animal models are used in various fields of study that include medicine, pharmacology, genetics and biochemistry (www.understandinganimalresearch.org.uk; Badyal and Desai, 2014). Animal testing has ensured many advances in the field of medicine such as the discovery and isolation of insulin in 1921 (Gorden, 1997), the antibiotic treatment and vaccines for leprosy (Badyal and Desai, 2014) and more recently in the initial stages in the search for a vaccine for the Ebola virus (Sullivan*, et al.*, 2000). Animal testing is based on the principles of the 3 R's of animals research, namely replacement, reduction and refinement (Badyal and Desai, 2014). Replacement, to ensure that animals are not used where a substitute laboratory-based test could have been used; reduction, to ensure that the minimal amount of animals are used to still obtain statistically significant results; and refinement, to make sure that the study will cause as little as possible stress and/or discomfort to the animals (Vitale*, et al.*, 2015). The choice of animal used is dependent on many factors such as similarities to humans regarding disease, development, metabolism and genetics, and includes rats, mice, guinea pigs, hamsters, fish, cats, dogs and monkeys (Badyal and Desai, 2014).

Humans are continuously exposed to heavy metals as complex mixtures of several metals, present at different concentrations often in combination with other toxic compounds. The type, concentration and duration of exposure to these metals can vary. To study these effects, animal models fulfil an important role, as they are genetically homogenous, of the same age and maturity and the study is conducted under controlled experimental conditions, which makes it an ideal model to study these effects of heavy metals alone and in combination.

In this study the Sprague-Dawley rat animal model was implemented as this model has been widely used to study toxicity including the effects of heavy metal exposure (Khalil*, et al.*, 2013; Lee*, et al.*, 2014; Van Der Schoor, 2014) and these include the nephrotoxicity in male Sprague-Dawley rats after Cd exposure (Lee*, et al.*, 2014) and the ability of extra-virgin olive oil to reduce Cr-induced toxicity of the spleen (Khalil*, et al.*, 2013). The aim of the research presented in this chapter is the establishment of a male Sprague-Dawley rat model. The effects of exposure on rat weight, plasma levels and blood chemistry levels were also determined.

3.2 **Materials and methods**

3.2.1 Sprague-Dawley rat model

Six week old male Sprague-Dawley rats (200-250g) were obtained from the University of Pretoria Biomedical Research Centre (UPBRC). The animals were housed in conventional cages complying with the sizes laid down in the SANS 10386:2008 recommendations (South Africa national standard, 2008). A room temperature of 22°C (±2°C); relative humidity of 50% (±20%) and a 12 hour light/dark cycle were maintained during the entire study. A total of 24 rats were used. The rats were housed separately in cages with autoclaved pinewood shavings as bedding material. White facial tissue paper was added for enrichment according to standard procedures at the UPBRC. All experimental protocols complied with the requirements of the University of Pretoria Animal Ethics Committee (AEC) (Animal ethics number: h009-15). The rats were randomly divided into four groups, as indicated in Table 3.1. A summary of the exposure and analytic techniques used are illustrated in Figure 3.1. The animals were allowed to acclimatise for 7 days prior to when the project started, that ran for 28 days after acclimatisation and thus the rats were housed for a total of 35 days

Table 3.1: *In vivo* experimental design

Groups	Number of rats per group
Control	6
Cd	6
Cr	6
Cd and Cr	6
TOTAL	24

3.2.2 *Metal administration* Cadmium chloride ($CdCl_2$) [Merck (Pty) Ltd, SA] and potassium dichromate ($K_2Cr_2O_7$) [Merck (Pty) Ltd, SA] were dissolved in sterile water and was administered to the rats daily via oral gavage. The control rats only received 0.9% sodium chloride saline solution that was also administered daily. The rats were exposed to the metals as indicated in Table 3.2. These concentrations where chosen based on the World Health Organization's (WHO) acceptable water limits (mg/ℓ) for Cd and Cr times 1000 (W.H.O, 2011). The period that the rats were exposed to the heavy metals can be correlated to a human chronic metal exposure. Rats were weighed daily to monitor any weight loss during the experimental period and this data was statistically analysed.

Table 3.2: *In vivo* control and metal dosages

Groups	Dosages	Days
Control	0.5mℓ Saline	28
Cd	0.854mg/kg body weight	28
Cr	14.22mg/kg body weight	28
Cd and Cr	0.854mg/kg and 14.22mg/kg body weight	28

3.2.3 Termination and sample collection

The rats were terminated via isoflurane overdose, according to standard methods employed by the UPBRC. On the day of termination (day 28), 5–10mℓ of blood was collected via cardiac puncture under isoflurane anaesthesia. Blood was collected in heparin tubes to measure the plasma levels of Cd and Cr in all of the experimental groups, as well as to determine the levels of the following blood proteins and molecules: total protein (TP), alanine aminotransferase (ALT), alkaline phosphatase (ALP), aspartate aminotransferase (AST), urea nitrogen (UN), creatinine, total bilirubin (TB) and glucose. The Cd and Cr levels in the blood samples were quantified with inductively coupled plasma mass spectrometry (ICP-MS).

Blood was also collected in citrate tubes for scanning electron microscopy analysis. The liver, pancreas and kidney tissue was harvested and prepared for light- and transmission electron microscopy, as indicated in Figure 3.1.

3.2.4 Statistical analysis

Statistical analysis on the levels of heavy metals in the blood and blood chemistry analysis were performed on GraphPad Prism Version 6.01 using 1-way analysis of variance (ANOVA) and Tukey's multiple comparisons test, where a *p*-value of ≤0.05 was considered significant.
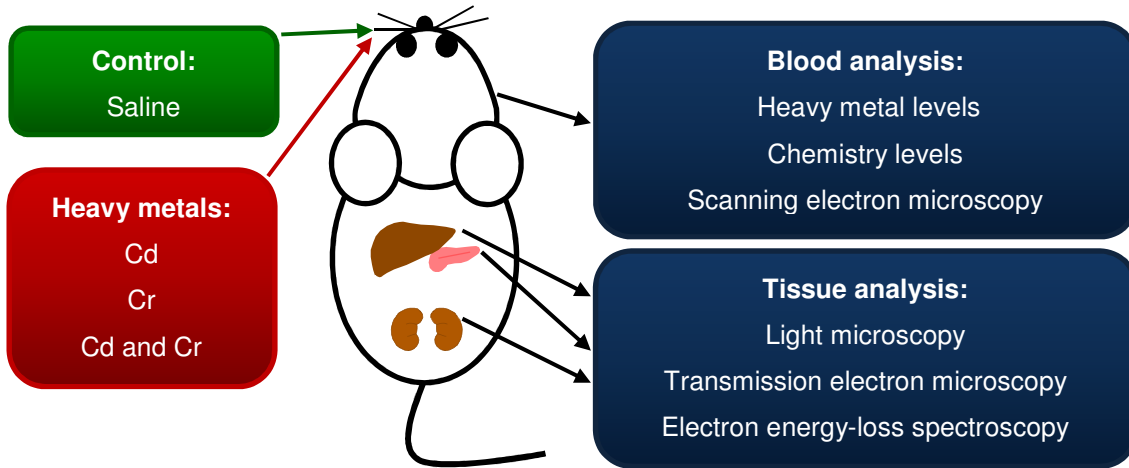
Figure 3.1: Summary of *in vivo* model and techniques used in this study.

3.3   Results

3.3.1 Analysis of weight

During the experimental period, the rats were weighed daily. As shown Figure 3.2, there were no significant changes in weight between the control and metal-exposed animals (Figures 3.2 and 3.3).
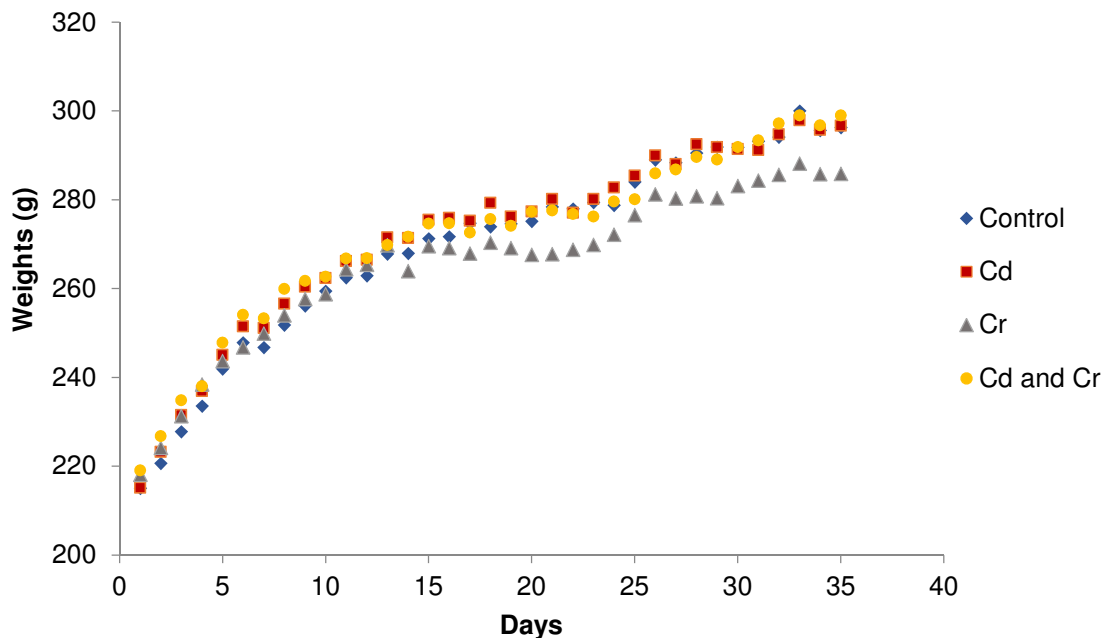
Figure 3.2: Daily rat weight gain from the first day until day 28 of the experiment. Significant differences between groups were evaluated at *p*-value: ≤0.05
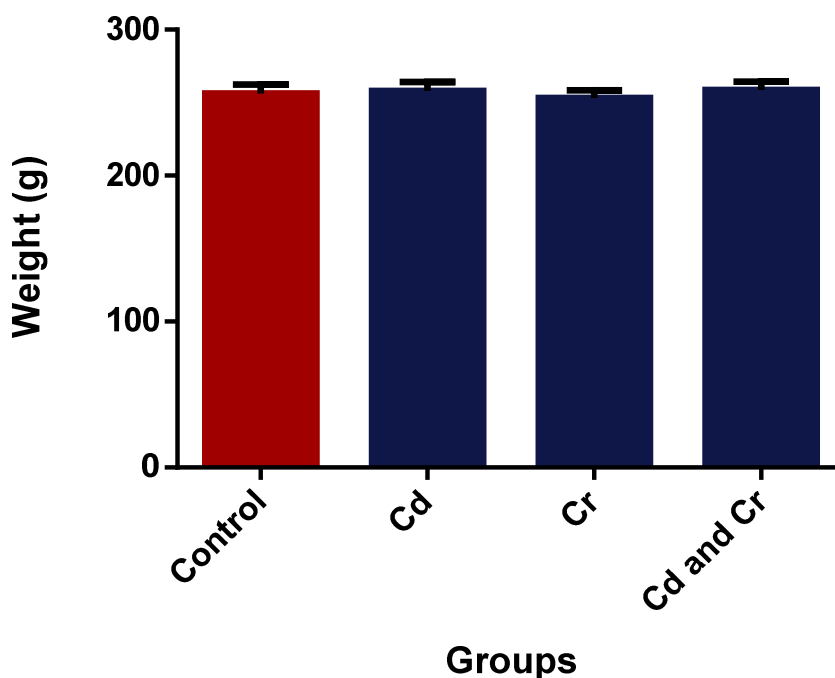
Figure 3.3: Total average weight of Sprague-Dawley rats exposed to Cd and Cr alone and in combination. Each group consists of 6 rats exposed for 28 days. Significant differences between groups were evaluated at *p*-value: ≤0.05.

3.3.2 Plasma levels of heavy metals

Plasma levels indicate that the heavy metals Cd and Cr were absorbed (Table 3.3) and consequently organ exposure has occurred and also confirms that the *in vivo* model was successfully implemented. An increase in Cd plasma levels can also be seen in the combination group compared with the individual metal exposure.

Table 3.3: Administered dosages and blood levels of metals

Group	Administered dose (µg/kg)	Plasma concentrations (µg/ℓ)	Plasma concentrations (µM)
		Mean ± SD	Mean ± SD
Cd	696.01	1.872 ± 0.37	0.010 ± 0.002
Cr	20619.00	1054.52 ± 864.59	3.55 ± 2.91
Cd and Cr	696.01 and 20619.00	3.6 ± 0.82 and 1015.46 ± 513.97	0.020 ± 0.0045 and 3.42 ± 1.73

SD: standard deviation

3.3.3 Blood chemistry analysis

Several identified blood parameters indicating organ damage were measured. The TP levels in the combination group were significantly lower than that of the group exposed to Cd alone. Also ALP and creatinine levels in the combination group were significantly lower than the

control group. Evaluation of the other blood markers for liver damage revealed that although not statistically significant, TB levels were slightly increased in the exposed groups, compared to the control. Compared to the control group no increase in ALT, AP, AST levels was observed (Table 3.4). Levels for markers of pancreatic damage compared to the control were unchanged.

Table 3.4: Organ specific blood chemistry analysis

	TP (g/ℓ)		UN (mmol/ℓ)		Creatinine (µmol/ℓ)	
	Range	Mean ± SD	Range	Mean ± SD	Range	Mean ± SD
Control	53.9–62.7	58.30 ± 3.65	7.0–8.0	7.55 ± 0.41	24.0–30.0	27.17 ± 2.23
Cd	58.3–61.6	60.18 ± 1.29	5.9–7.9	7.03 ± 0.78	23.0–26.0	24.17 ± 1.17
Cr	54.2–58.5	56.28 ± 1.63	6.0–9.1	7.68 ± 1.05	22.0–28.0	25.33 ± 2.34
Cd + Cr	52.0–61.3	54.30** ± 3.54	6.4–7.6	6.95 ± 0.42	21.0–25.0	23.17* ± 1.83
	ALT (U/ℓ)		ALP (U/ℓ)		AST (U/ℓ)	
	Range	Mean ± SD	Range	Mean ± SD	Range	Mean ± SD
Control	55–69	61.50 ± 5.58	163–245	201.67 ± 30.43	82–140	94.67 ± 24.90
Cd	50–66	57.17 ± 6.37	156–198	183.33 ± 14.79	73–80	77.60 ± 2.88
Cr	42–64	56.33 ± 9.03	121–223	165.33 ± 38.47	79–245	130.17 ± 58.54
Cd + Cr	52–65	57.67 ± 5.50	122–165	146.33* ± 18.45	75–138	110.67± 26.69
		TB (µmol/ℓ)		Glucose (mmol/ℓ)		
		Range	Mean ± SD	Range	Mean ± SD	
	Control	0.3–1.1	0.70 ± 0.30	5.6–8.4	6.85 ± 1.06	
	Cd	0.6–1.4	0.93 ± 0.28	5.7–7.5	6.43 ± 0.77	
	Cr	0.7–1.6	0.97 ± 0.33	5.1–8.1	6.38 ± 1.10	
	Cd + Cr	0.7–1.3	1.02 ± 0.21	5.4–8.2	6.77 ± 0.99	

*statistical significance compared to control.

**statistical significance compared to Cd: *p*-value of ≤0.05.

SD: Standard deviation

3.4 Discussion

The Sprague-Dawley rat model was utilized in this study as it is an excellent, reliable and reproducible model for long-term exposure studies (Van Der Schoor, 2014). Rats aged six weeks at study initiation were used, as at this age the rats are sexually-matured and represent the beginning of adolescence, where during the period of the study the rats enter adulthood (Sengupta, 2013). The concentrations chosen for this study was based on the

WHO acceptable water limits for Cd and Cr times 1000 (W.H.O, 2011) and the period the rats were exposed to the metals can be correlated to a human chronic metal exposure.

There were no significant changes in the weights of all exposed rat groups throughout the duration of the study. There was a steady increase in weight comparable to that of the controls. The blood plasma levels indicate that the study was implemented successfully and it seems that Cd in combination with the Cr, is processed at a different rate than when administered alone. Similar results were seen by Arbi and colleagues, where the Cd blood plasma level was increased in the combination group compared to the individual exposure to the metal (Arbi, *et al.*, 2017). The blood chemistry markers of the liver, pancreas and kidney only showed significant changes in a few of the markers. TP, ALP and creatinine levels were lowered but were only significant for the Cd and Cr combination group compared to the control. A reduction in ALP levels have been reported for rats treated with $CdCl_2$ (El-Demerdash, *et al.*, 2001; Rana, *et al.*, 1996). Cd can influence zinc (Zn) either through replacing membrane associated Zn or by inhibiting the apoptosis and necrosis prevention properties of Zn (El-Demerdash, *et al.*, 2004; Jacquillet, *et al.*, 2006). Zn is a cofactor essential for ALP function and with Zn displacement, ALP synthesis and function is compromised (Suzuki, *et al.*, 2005).

Compared to the control, creatinine levels were significantly lower in the metal combination group and may indicate renal tubular and glomerular dysfunction, as seen after Cd exposure, also observed by Asagba and Obi and Babaknejad, *et al.* (Asagba and Obi, 2004; Babaknejad, *et al.*, 2015). Several researchers have also reported lower ALP and creatinine levels after exposure to Cr (Kumar and Kumar, 2013; Kumar, *et al.*, 1984). The TP and bilirubin levels (although the latter was not significant) were altered and may suggest early changes in liver and kidney function. Similar results were obtained in the studies of Lakshimi, *et al.* and Kumar, *et al.* whereafter exposure to Cd and Cr, the TP and bilirubin levels were decreased and increased respectively (Kumar and Kumar, 2013; Lakshmi, *et al.*, 2012). The blood chemistry results showed no major damage to the liver, pancreas and kidneys, however, small reductions in TP, creatinine and ALP indicates that some changes has occurred in the biochemical functioning of the tissue (Venter, *et al.*, 2017) .

3.5   Conclusion

In this study, the *in vivo* model was established over a period of 28 days and was a highly reliable model for toxicological analysis throughout the experimental procedure. Exposure to

Cd and Cr alone and in combination did not result in any significant weight loss and normal weight gain was seen during the experimental period. Blood levels of each metal were increased and ALT, AST, UN, TB and glucose levels were unchanged. The significant changes in the TP, ALP and creatinine levels indicated liver and kidney dysfunction. These results will be further evaluated with the histological and ultrastructural evaluation of the liver, pancreas and kidney tissue in the chapters to follow.

Chapter 4

Histological changes in liver, pancreas and kidney tissue of Sprague-Dawley rats exposed to Cd and Cr alone and in combination

4.1 Introduction

In this chapter the effects of the heavy metals cadmium (Cd) and chromium (Cr) alone and in combination on the liver, pancreas and kidney tissue of male Sprague-Dawley rats were evaluated. The liver, pancreas and kidney tissue was used, as they each play a major role in the detoxification of foreign toxins in the body and consequently are vulnerable to the effects of toxins especially if the detoxification pathways are depleted (Coetzee, *et al.*, 2009d; Nordberg, 2009; Venter, 2015).

The liver, due to its high blood supply and its diverse metabolic capacity including the detoxification pathways and the secretion of bile, is prone to cellular damage, which compromises organ function (Timbrell, 1999). The liver consists mainly of hepatocytes that are arranged in plates, separated by sinusoidal spaces that extend to the central vein (Kierszenbaum and Tres, 2012). The endothelium is incomplete and consequently the hepatocytes are in direct contact with the blood. Metals such as Cd and Cr can induce the formation of reactive oxygen species (ROS) via various mechanisms and this can cause cellular damage leading to cell death such as necrosis (Cuypers, *et al.*, 2010; Park, *et al.*, 2013; Venter, *et al.*, 2015). Characteristic cellular features of necrosis is cell swelling, vacuolation, karyolysis and loss of cellular content (Venter, 2015). ROS can cause lipid peroxidation and activation of Kupffer cells with the release of specific inflammatory and cytotoxic mediators (Koyu, *et al.*, 2006). Likewise the kidney is also involved in detoxification and both the collecting ducts and the functional unit, the nephron, are targets of toxicity. The urine blood barrier of the glomeruli and the epithelium of the proximal convoluted tubule (PCT) are specific targets of toxicity as both play a major role in the filtration system of the kidneys (Kierszenbaum and Tres, 2012). Not only can ROS induce oxidative damage, but the ability of metals such as Cd and Cr to inhibit enzyme activity and disrupt functioning of the urine blood barrier can cause kidney damage (Venter, *et al.*, 2017).

Although the pancreas is not a specific organ associated with detoxification, especially the endocrine component of the pancreas, it is still sensitive to the effects of toxins. The pancreas is affected by Cd and Cr reduction of zinc levels in the pancreas and thus altering the function of the pancreas (El Muayed, *et al.*, 2012; Solis-Heredia, *et al.*, 2000). The pancreas is divided into two parts, the exocrine and endocrine components. The exocrine

pancreas consists of pancreatic acinar cells. These cells have a pyramidal shape and contain zymogen granules, Golgi complexes, rough endoplasmic reticulum (rER), mitochondria and nuclei (Kierszenbaum and Tres, 2012). The zymogen granules can contain up to 20 different pancreatic enzymes, depending on the diet, and regulates various functions that include the release of water and bicarbonate ions (Kierszenbaum and Tres, 2012). The endocrine pancreas is mainly involved in insulin production, but also produces glucagon, gastrin, somatostatin and pancreatic polypeptide. The cells that produce these enzymes include the α- (glucagon), β- (insulin), δ- (gastrin and somatostatin) and PP cells (pancreatic polypeptide). They are collectively known as the Islets of Langerhans, that makes-up only about 2% of the pancreas mass (Liu*, et al.*, 2010; Nachnani*, et al.*, 2010).

In addition to direct cellular injury, fibrosis associated with an excessive accumulation of extracellular matrix (ECM) proteins, including collagen can also occur (Bataller and Brenner, 2005; Wynn, 2008). The ECM is a non-cellular component of tissue that provides both an essential physical scaffolding to all cellular components and initiates crucial biochemical and biomechanical signals that are needed for tissue morphogenesis, differentiation and homeostasis (Frantz*, et al.*, 2010). The hardening or stiffening of the microenvironment will cause disruption of the basal membrane, which compromises tissue integrity and destabilizes cell-cell adhesions (Frantz*, et al.*, 2010). Fibrosis can be initiated in all the organs and ROS has been implicated in the mechanism of fibrosis (Bataller and Brenner, 2005; Ha and Lee, 2003; Liu, 2006).

In this chapter, the effects of Cd and Cr alone and in combination on the histology of the liver, pancreas and kidneys were evaluated. Furthermore, picrosirius red (PR) staining was used to evaluate the presence of possible fibrosis in the tissues by using polarised light.

4.2 **Materials and methods**

4.2.1 *Histological analysis*
Liver, pancreas and kidney tissue were collected as described in Chapter 3.

4.2.2 *Sample processing*
The liver, pancreas and kidney tissue were fixed in 2.5% glutaraldehyde (GA)/formaldehyde (FA) (1mℓ of 25% GA, 1mℓ of 25% FA, 5mℓ 0.15M phosphate buffer, pH 7.4, and 3mℓ ddH$_2$O) for an hour and was then rinsed three times in 0.075M phosphate buffer, pH 7.4, for 15 minutes each before the tissue samples were dehydrated in 30%, 50%, 70%, 90% and three

changes of 100% ethanol. The tissue samples were then left overnight in 100% ethanol. The next day the liver, pancreas and kidney samples were placed in *tert*-Butyl alcohol (TBA) for two days, renewing the TBA three times a day. Subsequently, wax pellets were added to create a 50:50 mixture. The samples were then placed in an oven at 60ºC for two days, renewing the TBA-wax mixture three times a day. The TBA-wax mixture was followed by a 100% wax solution for 24 hours at 60ºC, whereafter the samples were placed in a steel mould, filled with wax, and a marked grid was placed on top. The moulds with the marked grids were then placed on a cooling plate to allow the wax to cool and harden. Sections of 3-5µm were made with a Leica RM 2255 wax microtome (Leica Microsystems, Wetzlar, Germany).

4.2.3 *General morphology: Haematoxylin and eosin staining*

General tissue morphology was evaluated with haematoxylin and eosin (H&E) staining. Haematoxylin stains the cell nucleus, ribonucleic acid (RNA)-rich structures present in the cytoplasm such as the ribosomes and rER (Jacobs*, et al.*, 2006). Eosin, which binds positively charged protein and collagen, is used as a counter-stain and both the cytoplasm and collagen stain pink (Coetzee*, et al.*, 2009c).

To evaluate general tissue morphology, slides with the sections were cleared in xylene twice for ten minutes to remove the paraffin wax. The slides were then placed in a series of descending ethanol concentrations to rehydrate the tissue. The series started with placing the slide twice in 100% ethanol for two minutes, then the slides were placed in 90% ethanol for a minute and then in 70% ethanol for another minute. Before the slides were placed in the haematoxylin for fifteen minutes they were rinsed in ddH$_2$O for a minute. After the haematoxylin staining, the slides were then placed into the Scott's blue buffer solution for eight minutes, this changes the reddish-purple colour of the haematoxylin into a purple-bluish colour (Ernst*, et al.*, 2011). The tissue was then rinsed with ddH$_2$O, whereafter it was counterstained by dipping it in eosin for five times for approximately two seconds each. After the eosin, the tissue was dipped in a series of ascending ethanol concentrations (70%, 90% and 100% ethanol) to dehydrate the tissue and ensure that the excess dye is removed. Finally the slides were dipped in xylene before the coverslip was mounted using Entellan[®] mounting medium. The slides were viewed with a Nikon Optiphod transmitted light microscope (Nikon Instruments Inc., Amsterdam, Netherlands) and Olympus BX63 light microscope (Olympus, Tokyo, Japan).

The haematoxylin dye solution was prepared by dissolving 1g haematoxylin in 1ℓ ddH$_2$O to a final concentration of 0.1%, whereafter 0.2g sodium iodate and 50g potassium aluminium

sulphate were added and dissolved. Lastly, 1g citric acid and 50g chloral hydrate were added to the solution and dissolved. To prepare the eosin stain, 2g of eosin powder was dissolved in 200mℓ of ddH$_2$O. The Scott's blue buffer solution was prepared by dissolving 2g potassium-bicarbonate and 20g magnesium-sulphate in 1ℓ ddH$_2$O.

4.2.4 *Fibrosis: Picrosirius red*

To determine if the metals induced fibrosis, PR staining of the sections was undertaken. For this, 0.5g of sirius red dye was dissolved in 500mℓ of a saturated aqueous solution of picric acid. Acidified water was used for washing, made by adding 5mℓ of glacial acetic acid to 1ℓ of ddH$_2$O. Firstly, the excess paraffin wax was removed, by putting the slides in xylene twice for 10 minute intervals. The slides were then placed in a series of descending ethanol concentrations to rehydrate the tissue. The series started with placing the slide in 100% ethanol twice for two minutes, then the slides were placed in 90% ethanol for a minute and then in 70% ethanol for another minute. The slides were then rinsed ddH$_2$O for a minute. The tissue was then stained in haematoxylin, prepared as described above, for fifteen minutes and then placed into the Scott's blue buffer solution for eight minutes. The PR solution was applied for one hour and then the slides were washed twice with acidified water. The tissue was then dehydrated twice in 100% ethanol and cleared with xylene before mounting with Entellan® mounting medium (Mitra*, et al.*, 2012). The slides were viewed with a Nikon Optiphod transmitted light microscope (Nikon Instruments Inc., Amsterdam, Netherlands) and Olympus BX63 light microscope (Olympus, Tokyo, Japan), using polarizing light to detect fibrosis.

4.2.5 *Analysis of morphological alterations*

The degree of damage of the liver, pancreas and kidney was classified according to Table 4.1.

Table 4.1: Morphological alterations criteria (Modified from Brzoska, *et al.*, 2003)

Value	Description of damage
-	Normal/No alterations
+	Minor alterations
++	Mild alterations
+++	Severe alterations

4.3 <u>Results</u>

4.3.1 *General morphology: Liver*
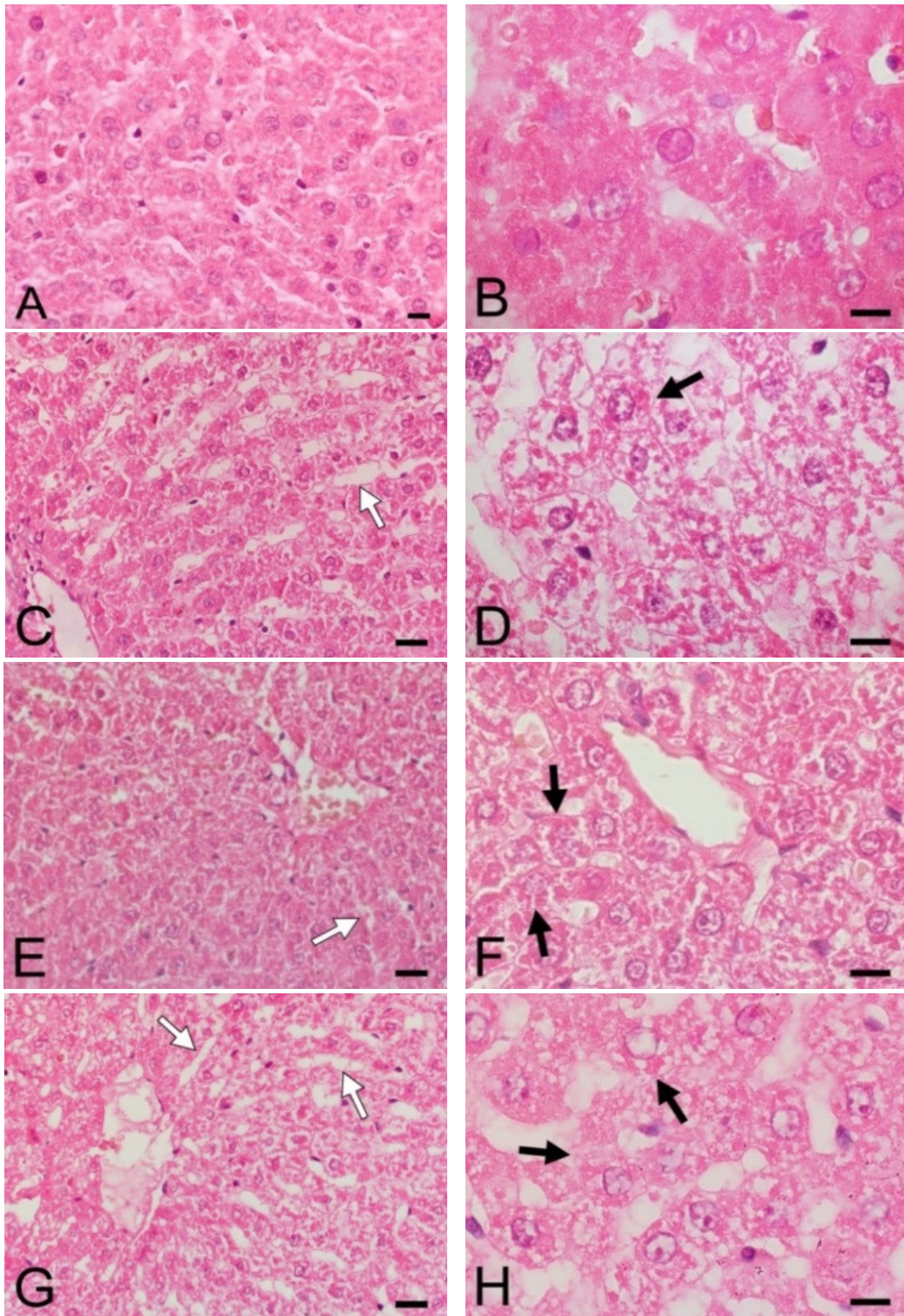
Figure 4.1: Representative light micrographs of control (A and B), Cd (C and D), Cr (E and F) and Cd and Cr (G and H) exposed liver tissue. **Key:** White arrows: Sinusoidal dilation; Black arrows: Necrosis (Scale bars: A, B, D, F and H: 10µm; C, E and G: 20µm). H&E staining.

In the liver tissue, necrosis and sinusoidal dilation were evaluated. In the control group, the normal morphology of the liver was seen with the hepatocytes neatly arranged in plates, with minor to no sinusoidal dilation present (Fig. 4.1 A and B). In the metal exposed groups, the incidence of necrosis was prominent [Fig. 4.1 D, F and H (black arrows)] with also an increase in the sinusoidal spaces in all the metal exposed groups [Fig. 4.1 C, E and G (white arrows)]. Table 4.2 summarizes these histological changes seen in the liver. Liver exposed to Cd alone and in combination with Cr showed the greatest degree of damage with both necrosis and sinusoidal dilation.

Table 4.2: Summary of histological changes in the liver tissue

Group	Necrosis	Sinusoidal dilation
Control	+	+
Cd	++	++
Cr	++	+
Cd and Cr	++	++

-, none; +, minor, ++, mild, +++, severe.

4.3.2 *Pancreas*
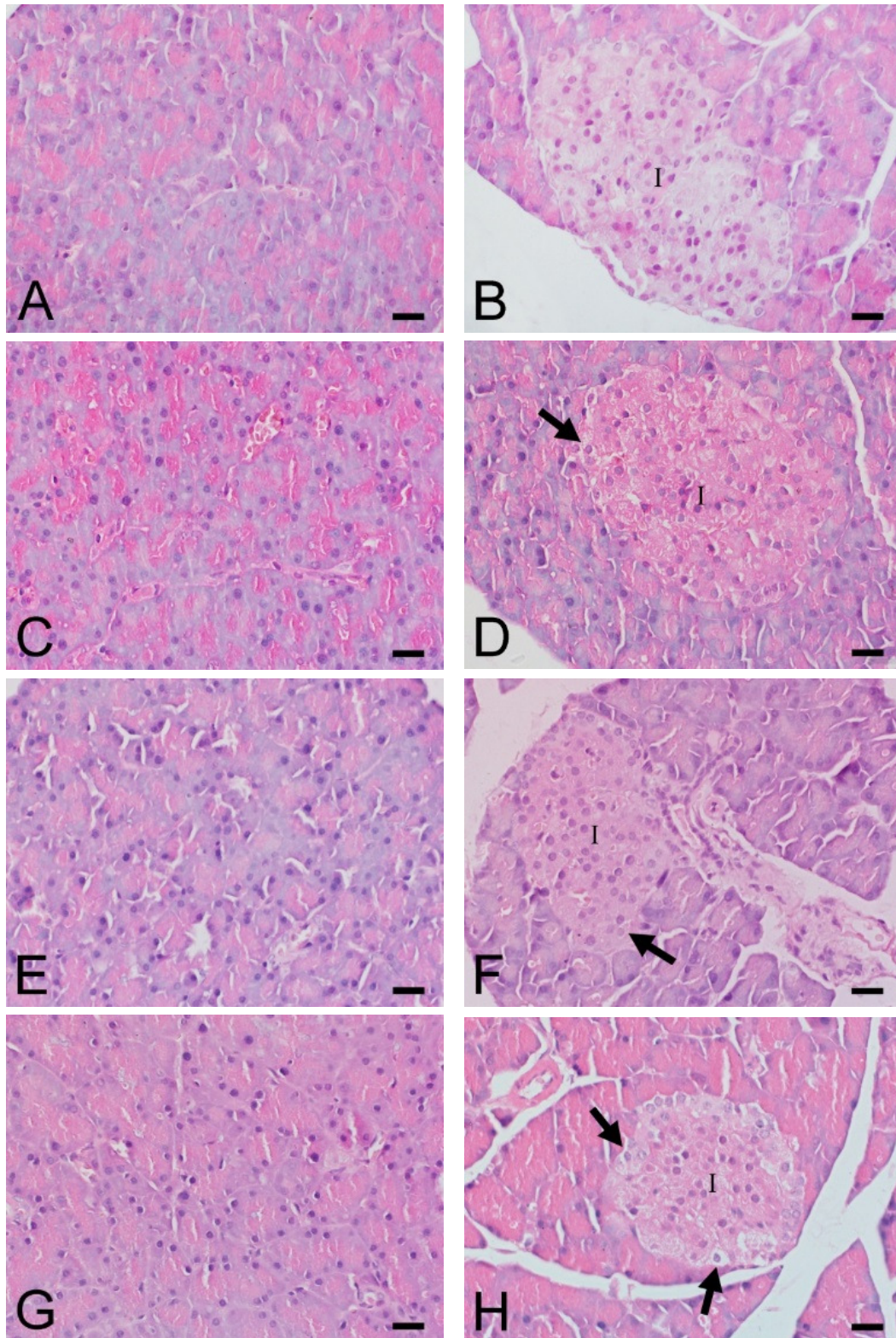
Figure 4.2: Representative light micrographs of the exocrine (A, C, E and G) and endocrine pancreas (B, D, F and H) of control (A and B), Cd (C and D), Cr (E and F) and Cd and Cr (G and H) exposed pancreatic tissue. **Key:** Black arrows: Necrosis; I: Islet of Langerhans (Scale bars: A–H: 20µm). H&E staining.

The morphology of the exocrine and the endocrine components of the pancreas were evaluated. The morphology and arrangement of the acinar cells of the exocrine pancreas and that of the Islets of Langerhans were evaluated. The exocrine pancreas exhibited no major morphological alterations of the acinar cells, with only minor necrosis being observed in the Cd and Cr groups (Fig. 4.2 C and E). In the endocrine pancreas, minor to mild necrosis were seen in the Cd and Cr and combination groups, respectively [Fig. 4.2 D, F and H (black arrows)]. It was also noticed that the necrosis seen in the metal combination group was mainly observed at the periphery of the Islets of Langerhans, which is typically where the α-cells are located [Fig. 4.2 H (black arrows)]. A summary of these effects are presented in Table 4.3.

Table 4.3: Summary of histological changes in the pancreas tissue

Group	Exocrine pancreas			Endocrine pancreas	
	Necrosis	**Acinar pyramidal shape**	**Patency of acinar lumen**	**Necrosis**	**Vacuoles**
Control	-	-	-	-	-
Cd	+	-	-	+	-
Cr	+	-	-	+	-
Cd and Cr	-	-	-	++	-

-, none; +, minor, ++, mild, +++, severe.

4.3.3 *Kidney*
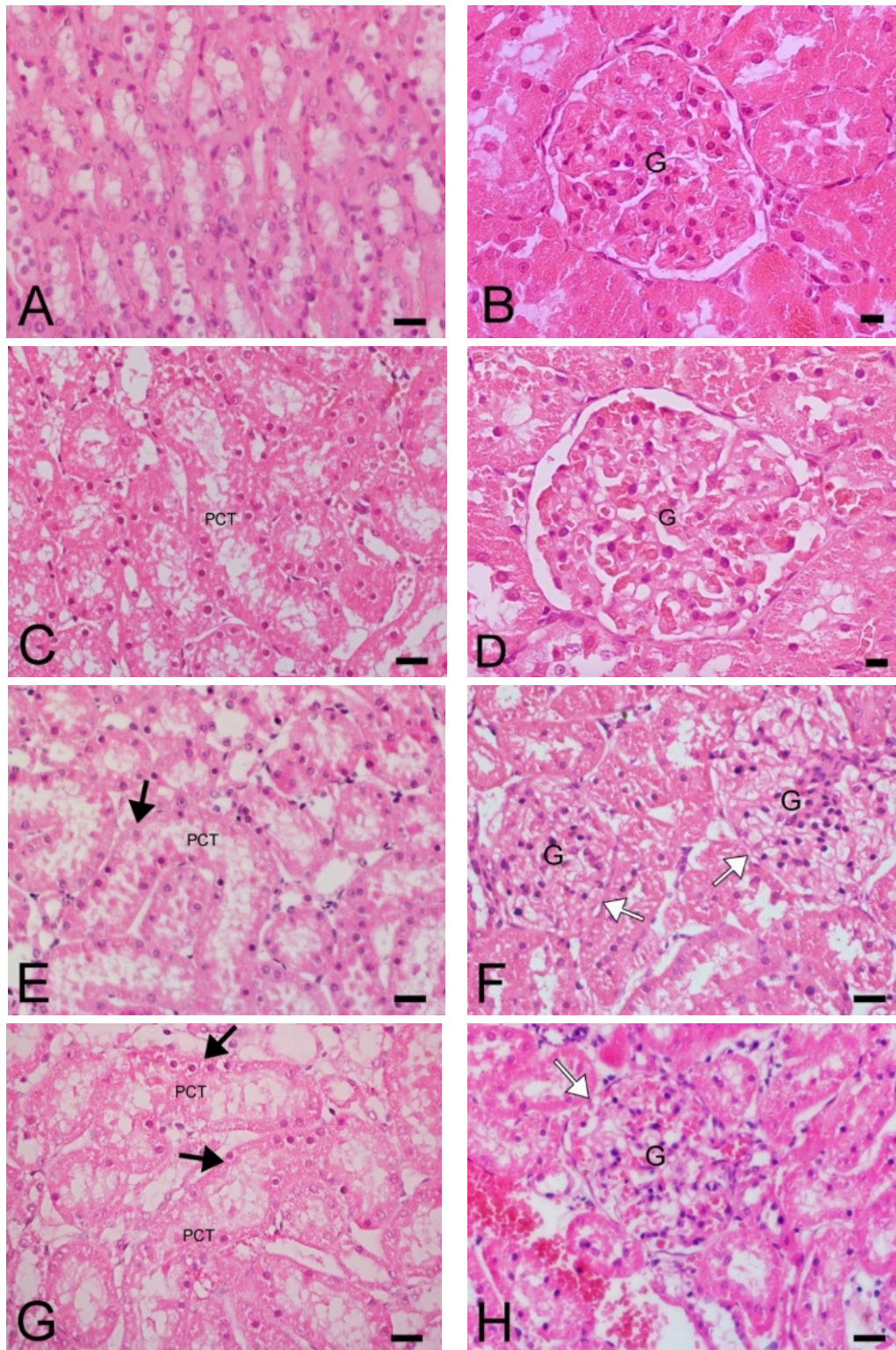
Figure 4.3: Light micrographs of renal tubules (A, C, E and G) and glomeruli (B, D, F and H) of control (A and B), Cd (C and D), Cr (E and F) and Cd and Cr (G and H) exposed kidney tissue. **Key:** Black arrows: Necrosis; White arrows: Diluted glomeruli; G: Glomeruli; PCT: Proximal convoluted tubule (Scale bars: B and D: 10µm; A, C, E–H: 20µm). H&E staining.

In the kidney tissue, due to the important role of these structures the morphology of the renal tubules and glomeruli were evaluated (Coetzee*, et al.*, 2009d; Nordberg, 2009; Venter, 2015). In figure 4.3 the effects of the heavy metals Cd and Cr alone and in combination on the PCT (Fig. 4.3 A, C, E and G) and glomeruli can be seen (Fig. 4.3 B, D, F and H). Renal tubule necrosis was present in the Cd and Cr groups alone [Fig. 4.5 C and D (black arrow)], with more severe necrosis seen in the combination group [Fig. 4.3 G (black arrows)]. Evaluation of the glomeruli in the control group showed some alterations although overall morphology was normal (Fig. 4.3 B). The Cd group showed the same trend as seen in the control group, with only some dilation visible in the glomeruli in the Cr, and Cd and Cr combination groups respectively [Fig. 4.3 F and H (white arrows), respectively]. In Table 4.4 the effects of the metals on the kidney tissue are summarized.

Table 4.4: Summary of histological changes in the kidney tissue

Group	Proximal convoluted tubules	Glomeruli		
	Necrosis	Necrosis	Dilation	Contraction
Control	+	-	+	+
Cd	++	-	+	+
Cr	++	-	++	+
Cd and Cr	+++	-	++	+

-, none; +, minor, ++, mild, +++, severe.

4.3.4 *Fibrosis: Liver, pancreas and kidney*
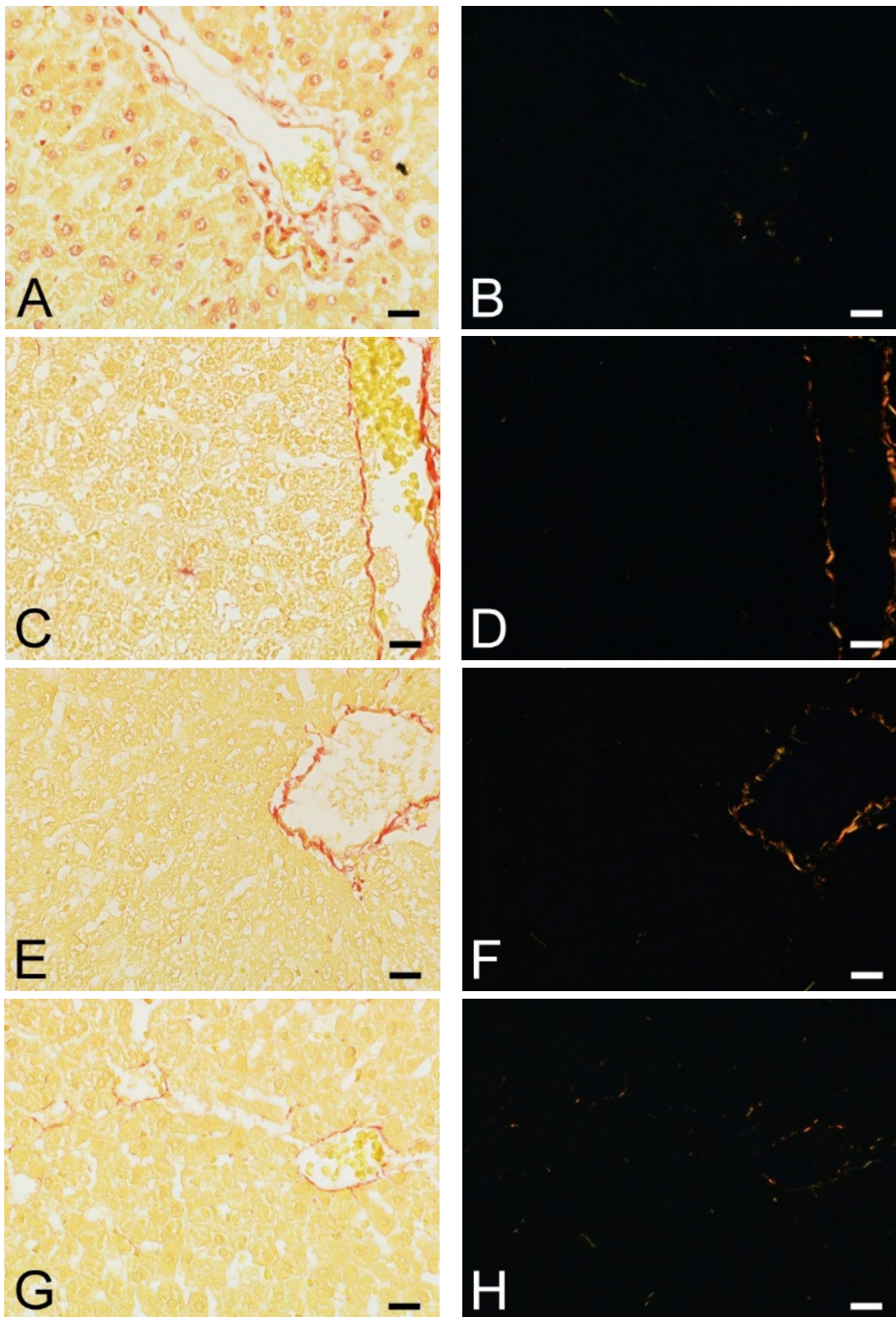
Figure 4.4: Light micrographs of liver tissue of the control (A and B), Cd (C and D), Cr (E and F) and Cd and Cr (G and H) groups, where no fibrosis was observed in the metal exposed groups (D, F and H). Figures A, C, E and G are the bright field micrographs and B, D, F and H are the polarized micrographs (Scale bars: A–H: 20µm). PR staining.
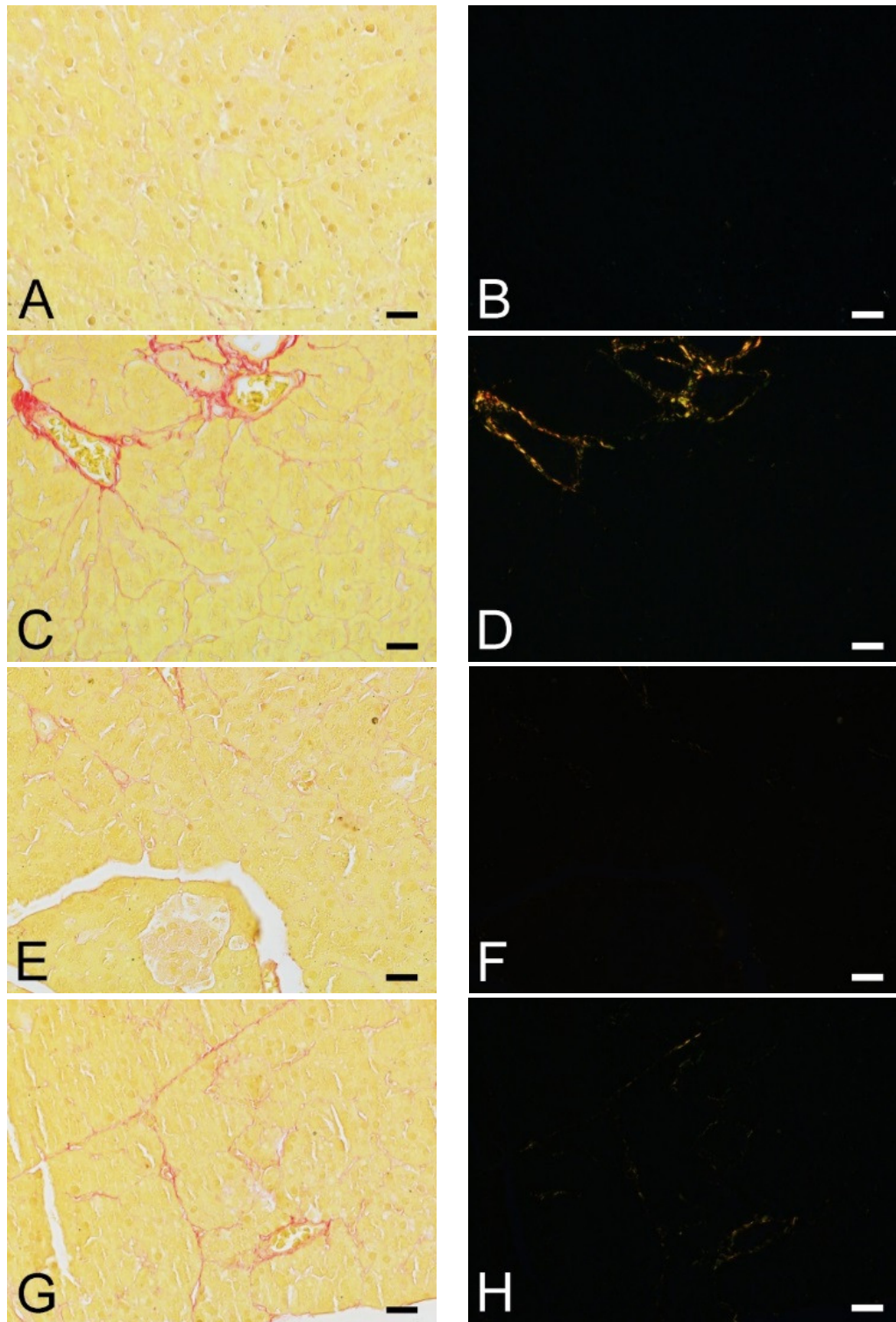
Figure 4.5: Light micrographs of the exocrine pancreas of the control (A and B), Cd (C and D), Cr (E and F) and Cd and Cr (G and H) groups, where no fibrosis was seen in the metal exposed groups (D, F and H). Figures A, C, E and G are the bright field micrographs and B, D, F and H are the polarized micrographs (Scale bars: A–H: 20μm). PR staining.
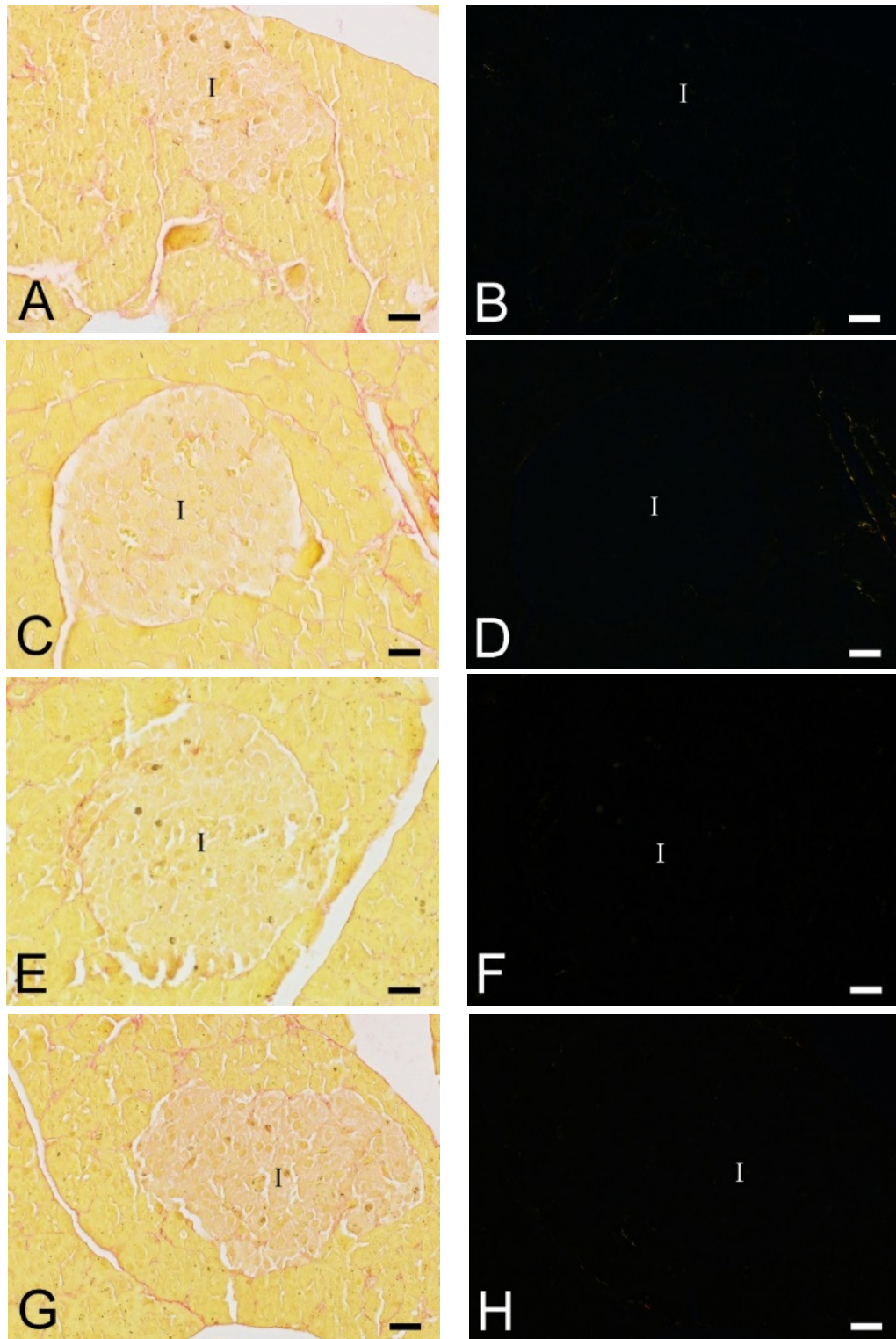
Figure 4.6: Light micrographs of the endocrine pancreas of the control (A and B), Cd (C and D), Cr (E and F) and Cd and Cr (G and H) groups, with no fibrosis were seen in the metal exposed groups (D, F and H). Figures A, C, E and G are the bright field micrographs and B, D, F and H are the polarized micrographs. **Key:** I: Islet of Langerhans (Scale bars: A–H: 20µm). PR staining.
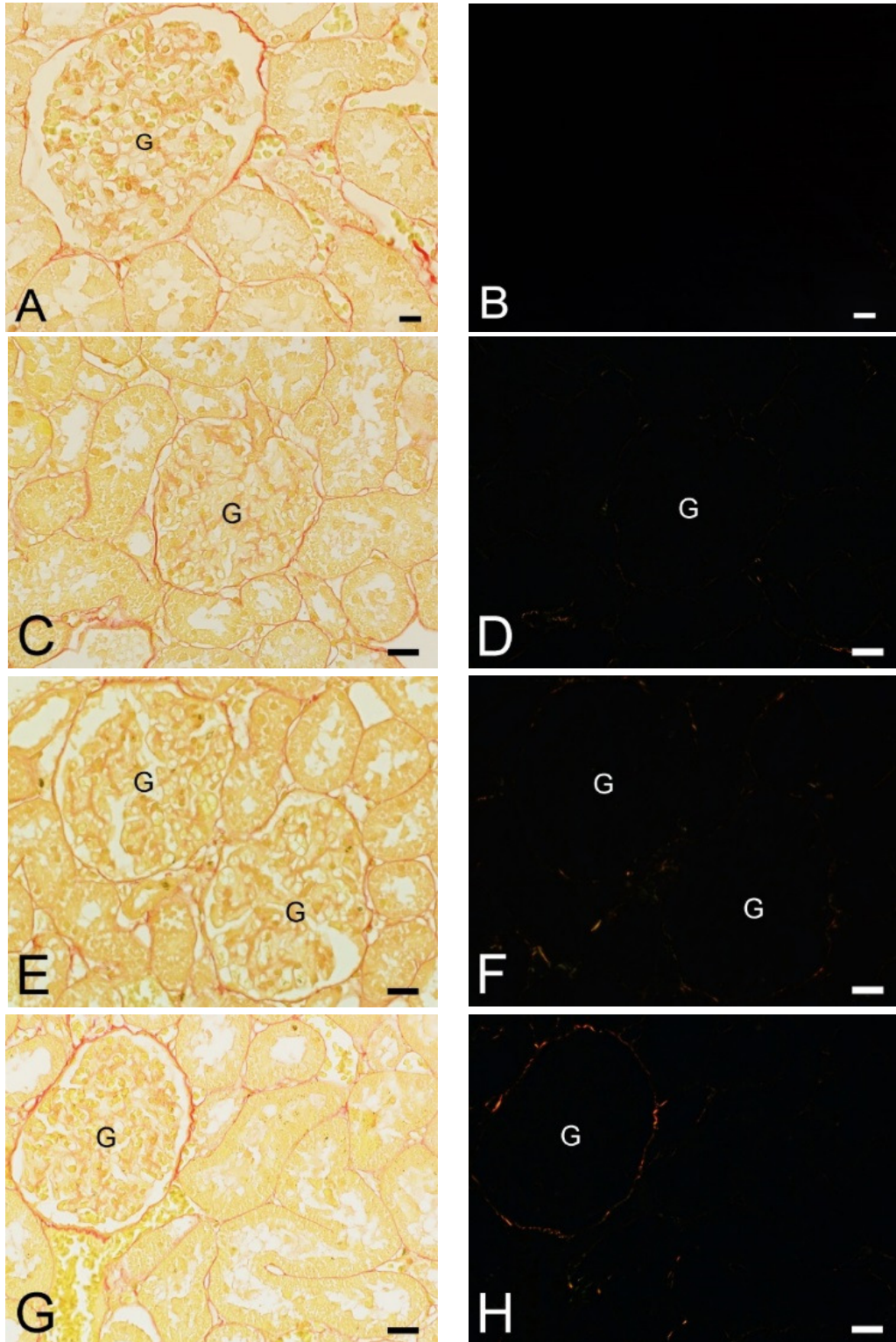
Figure 4.7: Light micrographs of the kidney tissue, incorporating both the renal tubules and glomeruli, of the control (A and B), Cd (C and D), Cr (E and F) and Cd and Cr (G and H) groups, with no fibrosis seen in the metal exposed groups (D, F and H). Figures A, C, E and G are the bright field micrographs and B, D, F and H are the polarized micrographs. **Key:** G: Glomeruli (Scale bars: A and B: 10µm; C–H: 20µm). PR staining.

Excessive ROS formation has been well studied in increasing the deposition of ECM (Ha and Lee, 2003). PR stains the ECM red and with polarisation it either has an orange-red or green-yellow birefringence that indicates the thickness of the collagen fibres present in the ECM (Arbi, 2015; Rich and Whittaker, 2005). Evaluation of the possible presence of fibrosis in the liver, pancreas and kidney tissue revealed that after exposure to Cd and Cr alone and in combination, no increase in fibrosis was observed in any of the tissue sections evaluated (Fig. 4.4 – 4.7).

4.4 Discussion

The current chapter evaluated the possible changes caused by Cd and Cr heavy metal toxicity on the morphology of the liver, pancreas and kidney tissue by using light microscopy. Upon evaluation of the liver control tissue, almost unnoticeable changes were seen and morphology typical of control liver tissue was observed (Fig. 4.1 A and B). In contrast to the control group, in the metal exposed groups the occurrence of mild necrosis (black arrows) and an increase in the sinusoidal spaces (white arrows) (Fig. 4.1 B–H) was observed. These findings are similar to previously described studies where an increase in necrosis and sinusoidal dilation after exposure to Cd and Cr alone and in combination were observed (Mishra and Mohanty, 2008; Venter, 2015; Venter*, et al.*, 2015). In the liver tissue, no induction of fibrosis was observed (Fig. 4.4). These findings also support, in part, the results obtained from the blood chemistry analysis (Chapter 3), where significant differences of the alkaline phosphatase (ALP) levels were seen in only the combination group, that will decrease the liver functions, as ALP plays a role in the transport of metabolites across cell membranes in the liver (Giannini*, et al.*, 2005; Venter*, et al.*, 2017). The loss in plasma membrane function, due to Cd and Cr exposure, also contributes to the reduction in ALP levels (El-Demerdash*, et al.*, 2004; Kumar and Kumar, 2013; Venter*, et al.*, 2017). The absence of changes in the other blood markers tested does not reflect the observed histological effects. Therefore the markers usually used are poor indicators of tissue damage, and therefore in population based studies changes in liver function enzymes will not be observed and the conclusion that will be made is that no liver damage has occurred.

In the exocrine pancreas the control group had normal acinar cells, with basally located round nuclei, and zymogen granules that were found at the apical portion of the pancreatic acinar cells (Fig. 4.2 A). Only the Cd and Cr groups showed minor necrosis of the acinar cells. This is similar to the findings of Edwards and Prozialeck, where the acinar cells of the exocrine pancreas showed irregular appearance after exposure to Cd (Edwards and

Prozialeck, 2009). In contrast, Liu, *et al.* reported no changes in the morphology of exocrine cells following exposure to Cr. This can be due to the low levels of Cr (0.5mg/kg/day) given to the mice in that study, compared to Cr levels used in the current study (14.22mg/kg/day) (Liu*, et al.*, 2010). The endocrine pancreas showed an increase in necrosis in the metal exposed groups (Fig. 4.2 D, F and H) compared to the control (Fig. 4.2 B). As for the liver, Cd and Cr alone and in combination did not induce fibrosis. In a study using streptozotocin-induced diabetic pregnant rats, exposure to Cd (0.49mg/kg/day) caused changes to the morphology of the pancreas by causing degeneration, necrosis, and weak degranulation of the β-cells of the pancreatic islets (Kanter*, et al.*, 2003). In contrast to a study by Liu, *et al.*, no changes were observed in the Islets of Langerhans after exposure to Cr (0.5mg/kg/day) (Liu*, et al.*, 2010), however this may be due to the low dosages used in that study, compared to Cr levels used in the current study (14.22mg/kg/day). Disruption of the functioning of the endocrine component of the pancreas can lead to an increase in glucose levels in the blood. Related to glucose levels found in Chapter 3, no changes in glucose levels were found, which is in contradiction to the levels of histological damage observed. Minimal literature exists regarding the effects of Cd and Cr alone on pancreatic tissue (Shimada*, et al.*, 2000) and, to our knowledge, no literature exists on the effects of Cd and Cr in combination. The results of the present study showed an increase in damage due to the additive necrotic effect of Cd and Cr on the Islets of Langerhans. No effect on the exocrine acinar cells was observed [Fig. 4.2 G and H (black arrows)]. No fibrotic changes were observed in either the exocrine or endocrine components of the pancreas (Fig. 4.5 and 4.6).

The alterations seen in the kidney tissue showed that there is an increase in necrotic PCT cells in all the exposed groups [Fig. 4.3 C, E and G (black arrows)]. In terms of the glomeruli, the Cr and combination groups showed a decrease in the urinary spaces of the renal corpuscles [Fig. 4.3 F and H (white arrows)], with the control and Cd groups showing some altered glomeruli, but had overall normal glomerular morphology (Fig. 4.3 B and D). No fibrotic changes in the kidney tissue were observed (Fig. 4.7). These results correlate with our previous findings of the PCT, after exposure of chick embryos to Cd and Cr alone and in combination (430µM and 476µM, respectively) (Venter, 2015). Although the Cd group showed minimal alterations to the glomeruli in this study, a more pronounced effect was expected as seen in our previous study, where contraction of the glomeruli was observed after exposure to Cd alone (Venter, 2015). No changes in UN and creatinine was observed for rats exposed to Cd and Cr alone, although creatinine levels were decreased for rats exposed to Cd and Cr in combination. This again raises the concern that blood markers of tissue damage such as those used to measure liver and kidney damage are poor indicators of tissue damage as a result of exposure to heavy metals.

4.5 <u>Conclusion</u>

In conclusion, Cd and Cr and alone an in combination caused tissue necrosis. In the liver and kidney this was associated with sinusoidal and glomerular dilation respectively. Damage induced by Cd and Cr was not associated with any significant changes in blood levels of markers of liver, pancreatic and kidney damage. Only for Cd and Cr in combination, were associated changes in TP and creatinine levels observed. Poor correlation between histological damage and blood markers of tissue damage is of concern especially related to exposed populations.

Chapter 5

Ultrastructural effects and bio-accumulation of Cd and Cr alone and in combination on Sprague-Dawley rat liver, pancreas and kidney tissue as well as analysis of the coagulation system

5.1 Introduction

In the liver, pancreas and kidney, cadmium (Cd) and chromium (Cr) are metabolized differently, but induce similar effects namely oxidative stress that leads to lipid peroxidation, protein and deoxyribonucleic acid (DNA) damage and apoptosis or necrosis. These effects may lead to ultrastructural changes to the tissue and cellular components of the liver, pancreas and kidney that may lead to functional changes in the tissue (Timbrell, 1999; Venter, 2015; Venter*, et al.*, 2017). Previous studies have shown that Cd and Cr exposure caused similar ultrastructural effects that include irregular chromatin condensation, swelling in between the cristae of the mitochondria, membrane alterations of both the nuclei and mitochondria and dilation of the rough endoplasmic reticulum (rER) (Fu*, et al.*, 2008; Thophon*, et al.*, 2004; Venter*, et al.*, 2017; Venter*, et al.*, 2015). These metals may also have effects on the organ-specific organelles or structures, that includes the glomerular filtration barrier of the kidney and the granules of the Islets of Langerhans (Åkesson*, et al.*, 2014; Kanter*, et al.*, 2003; Prozialeck and Edwards, 2012; Venter*, et al.*, 2017). Therefore, a brief description of the normal ultrastructure and function of the organelles are given, as well as the criteria used to evaluate the alterations caused by the heavy metal toxicity.

The cell membrane surrounds all the organelles of the cell and consists of a phospholipid bilayer that contains proteins which assist in cell-cell recognition and selective transport of molecules and also acts as a protective barrier (Coetzee*, et al.*, 2009c; Kierszenbaum and Tres, 2012). Membranous organelles that include the mitochondria, smooth endoplasmic reticulum (sER) and rER, Golgi complexes and lysosomes are numerous and are widely distributed in the cytoplasm (Kierszenbaum and Tres, 2012; Young*, et al.*, 2006). The plasma and nuclear membrane are specific targets of oxidative damage due to the presence of lipid and proteins.

Nuclei are mostly found in the centre of the cells and consist of a nuclear envelope, chromatin and nucleolus (Coetzee*, et al.*, 2009c; Kierszenbaum and Tres, 2012). The nuclear envelope consists of a double membrane, separated by a perinuclear space. The nuclear envelope is interrupted at random intervals by nuclear pores that allows for metabolic exchange (Coetzee*, et al.*, 2009c; Kierszenbaum and Tres, 2012). The chromatin consists of small, dark granules, called nucleosomes, composed of an histone octamer core,

with about two turns of DNA coiled around it and which plays a crucial role in cell division (Coetzee*, et al.*, 2009c; Kierszenbaum and Tres, 2012). The nucleolus is the site of synthesis, processing, and modification of pre-ribosomal ribonucleic acid (rRNA) and initial pre-ribosomal assembly. The nucleolus also contains several proteins involved in pre-rRNA processing and shuttling between the nucleolus and the nucleoplasm. Structurally the nucleolus consists of three major elements, namely fibrillar centre, dense fibrillar component and granular component (Kierszenbaum and Tres, 2012; Scheer and Hock, 1999). In this study, the nuclear membrane and chromatin condensation were investigated for membrane alterations based on the fact that heavy metals can cause lipid peroxidation and thus causes loss in membrane integrity and DNA damage, respectively (Bertin and Averbeck, 2006).

The main function of the mitochondria is adenosine triphosphate (ATP) synthesis (Kierszenbaum and Tres, 2012). Mitochondria vary significantly in size and shape in all the different types of cells, but overall are elongated and always consist of four compartments, namely the outer and inner membranes, mitochondrial matrix and intermembranous space. The outer membrane plays a role in the transport of small molecules and converts lipid substances into usable molecules for the mitochondria. The inner membrane folds into shelf-like folds called cristae, that project into the mitochondrial matrix (Coetzee*, et al.*, 2009c; Kierszenbaum and Tres, 2012; Young*, et al.*, 2006). The mitochondrial matrix and intermembranous space contains enzymes, calcium, magnesium and even DNA and RNA, which all plays a role in the energy production function of the mitochondria (Coetzee*, et al.*, 2009c; Young*, et al.*, 2006). The mitochondria were evaluated for possible loss in membrane integrity and inner matrix swelling in this study, which might indicate that lipid peroxidation and an increase in fluid in the mitochondria occurred (Bertin and Averbeck, 2006; Thophon*, et al.*, 2004).

The rER consists of stacks of flattened membranous sacs known as cisternae that are interconnected. On the membranes of the rER, ribosomes are attached, giving it a "rough" appearance and assist in the function of the rER: to produce proteins (Coetzee*, et al.*, 2009c; Kierszenbaum and Tres, 2012). In this chapter the dilation of the rER was evaluated, which might indicate an increase of water in the cells due to intoxication with harmful substances like heavy metals (Venter, 2015).

The blood is essential for the distribution of nutrients, metabolites, drugs and toxins to each organ system as well as the removal of waste products including toxic metabolites. Due to the close association between the hepatocytes and blood via sinusoidal endothelium, the urine blood barrier and the contact of the endocrine pancreas via the fenestrated

endothelium, implies that not only does the blood play an essential role in the distribution of Cd and Cr, but may also be a specific target of toxicity. One of the main functions of the coagulation system, to reduce and/or stop excessive blood loss, can thus be altered by the heavy metals. This system needs to be carefully controlled to ensure that it doesn't form clots, which can cause a blockage in the blood vessels (Smith, 2009) and which may move to an organ and cause tissue damage, as seen when a clot enters the brain and causes a stroke (Zhang, *et al.*, 2015). The coagulation pathway includes platelets, fibrin networks and erythrocytes, which all play a major role in clot formation (Pérez-Gómez and Bover, 2007; Smith, 2009; Van Rooy, 2015). Erythrocytes are the most adaptive cells in the body and thus can change shape to fit through the small blood vessels and sinuses (Pretorius, *et al.*, 2016b). In erythrocytes, as with nucleated cells, apoptosis also occurs, but is known as eryptosis. Eryptosis is characterized by cell shrinkage, blebbing and membrane scrambling, that can be caused by oxidative stress, hyperosmotic shock, hyperthermia and energy depletion (Föller, *et al.*, 2008; Lang, *et al.*, 2010; Lang, *et al.*, 2012b; Lang and Qadri, 2012; Mischitelli, *et al.*, 2016; Pretorius, *et al.*, 2016a; Pretorius, *et al.*, 2014). Changes to the erythrocytes morphology, platelet activation and fibrin fiber thickness, due to various substances and illnesses, can cause changes in the coagulation system (Lang and Qadri, 2012; Pretorius, *et al.*, 2016a).

In this chapter the possible ultrastructural changes and bio-accumulation in the liver, pancreas and kidney tissue of male Sprague-Dawley rats after exposure to Cd and Cr alone and in combination, as well as the effects of these metals on the coagulation system, were investigated. As a fundamental component of each organ the effects of Cd and Cr alone and in combination on blood haemostasis was also determined.

5.2 Materials and methods

5.2.1 *Tissue and blood for transmission- and scanning electron microscopy*
Tissue samples and blood were collected for transmission- (TEM) and scanning electron microscopy (SEM), as described in Chapter 3.

5.2.2 *Transmission electron microscopy*
The liver, pancreas and kidney tissue samples were cut into 1mm^3 blocks and fixed in 2.5% glutaraldehyde (GA) and formaldehyde (FA) for 1 hour, rinsed three times in 0.075M sodium potassium phosphate buffer (pH 7.4) for 15 minutes each before the samples were placed in the secondary fixative, a 1% osmium tetroxide (OsO$_4$) solution, for 1 hour. Following fixation, the tissue samples were rinsed again as described above. The tissues were then dehydrated

in 30%, 50%, 70%, 90% and three changes of 100% ethanol. The samples were embedded in epoxy resin and ultra-thin sections (70–100nm) were cut with a diamond knife using an ultramicrotome. Samples were contrasted with uranyl acetate for 5 minutes followed by 2 minutes of contrasting with lead citrate, after which the samples were allowed to dry for a few minutes before being examined with the JEOL JEM 2100F TEM (JEOL Ltd., Tokyo, Japan).

5.2.3 *Analysis of ultrastructural alterations*

Possible ultrastructural alterations of the liver, pancreas and kidney cellular organelles and membranes evaluated included disruption of the nuclear and cellular membrane, condensation of chromatin, disruption of the mitochondrial membrane and swelling of the mitochondrial inner matrix as well as dilation of the rER. Some tissue specific alterations were also evaluated. The degree of damage was graded according to Table 5.1. Summaries of these ultrastructural changes are presented in Tables 5.2–5.4.

Table 5.1: Morphological alterations criteria (Modified from Brzoska, *et al.*, 2003)

Value	Description of damage
-	Normal/No alterations
+	Minor alterations
++	Mild alterations
+++	Severe alterations

5.2.4 *Electron energy-loss spectroscopy*

An FEI Tecnai G^{2}20 high resolution TEM (FEI, Oregon, USA) equipped with the GIF 2001 energy filter (Gatan, Inc., CA, USA) for electron energy-loss spectroscopy (EELS) and energy filtered TEM (EFTEM) analyses were used to evaluate the possible bio-accumulation of Cd and Cr in the liver, pancreas and kidney tissue. EELS spectra [Cd: 403.7eV and Cr: 574eV (Ahn*, et al.*, 1983)] analysis was performed to confirm the presence of the heavy metals in the tissue, together with the EFTEM colour map, to visually express the exact position of the metals in the tissue.

The EELS spectra were collected in normal parallel beam TEM mode, without an objective aperture and employing a GIF entrance aperture of 3mm. This allowed for the use of a large collection semi-angle, β~100mrad, which greatly improved the jump ratio of the spectra. To remove the effects of plural scattering and the contribution from low energy plasmon losses, each spectrum was background-subtracted using a power law line shape. This was followed

by further deconvoluting the ionization edges using a Log-Fourier iterative process, so as to remove all other plural scattering contribution. The EFTEM maps were collected using the Gatan 3 window method with an energy slit width of 20eV. For construction of the Cr map, the pre-edge 1 and pre-edge 2 energy windows were centred at 545eV and 565eV, respectively, whereas the post-edge window was centred at 585eV so as to coincide with the onset of the Cr $L_{2,3}$ ionization edge at 574eV. The positions of the pre-edge 1 and 2 windows were based on the background subtraction model obtained from the EELS analyses when using 2 energy windows. This ensured that only energy loss contributions from the metal under investigation were mapped. Similarly, for mapping of the energy-loss contributions of Cd, the pre-edge 1 and 2 windows were placed at 364eV and 384eV, with a post-edge onset centred at 414eV.

5.2.5 *Scanning electron microscopy*

SEM was used to study the erythrocyte, platelet and fibrin fibre morphology together with the fibrin fibre thickness. The morphology of erythrocytes and fibrin networks were studied by preparing whole blood (WB) and platelet-rich plasma (PRP) respectively (Van Rooy*, et al.*, 2015). Blood was collected in citrate tubes, as described in Chapter 3, and 10µℓ WB, with and without the addition of 5µℓ human thrombin (20U/mℓ; South African National Blood Service), were added to 10mm round glass coverslips (Leica SA). The blood was then centrifuged for 10 minutes at 227xg to obtain the PRP. A 10µℓ volume of the PRP, with and without the addition of 5µℓ human thrombin, was then also placed on 10mm glass coverslips. The glass coverslips were allowed to dry for about 10–20 minutes, before being placed in 24-well plates that contained 0.075M sodium potassium phosphate buffer (pH 7.4). The samples were washed for 20 minutes on a shaker to remove any blood proteins that might interfere with the blood clots (Van Rooy*, et al.*, 2015). The washed samples were then fixed in 2.5% GA/FA solution for 30 minutes. This was followed by rinsing the samples three times in phosphate buffer for 3 minutes before secondary fixation in 1% OsO_4 for 15 minutes. The samples were washed again three times in phosphate buffer for 3 minutes, before being dehydrated in 30%, 50%, 70%, 90% and 3 times in 100% ethanol. The SEM sample preparation was completed by drying the samples in hexamethyldisilazane (HMDS), followed by mounting and coating by carbon evaporation, and was examined by using the Zeiss ULTRA Plus FEG-SEM and Zeiss Crossbeam 540 FEG-SEM (Carl Zeiss Microscopy, Munich, Germany). On the micrographs the thickness of the fibrin fibres was measured to determine if any changes to size of the major thick and minor thin fibre had occurred following exposure to heavy metals (Van Rooy*, et al.*, 2015). Fifty random fibres were measured in the control- and metal-exposed groups SEM micrographs using ImageJ (Version 1.49, Java).

5.3   <u>Results</u>

5.3.1   *Ultrastructural effects of Cd and Cr alone and in combination on the liver*

Control
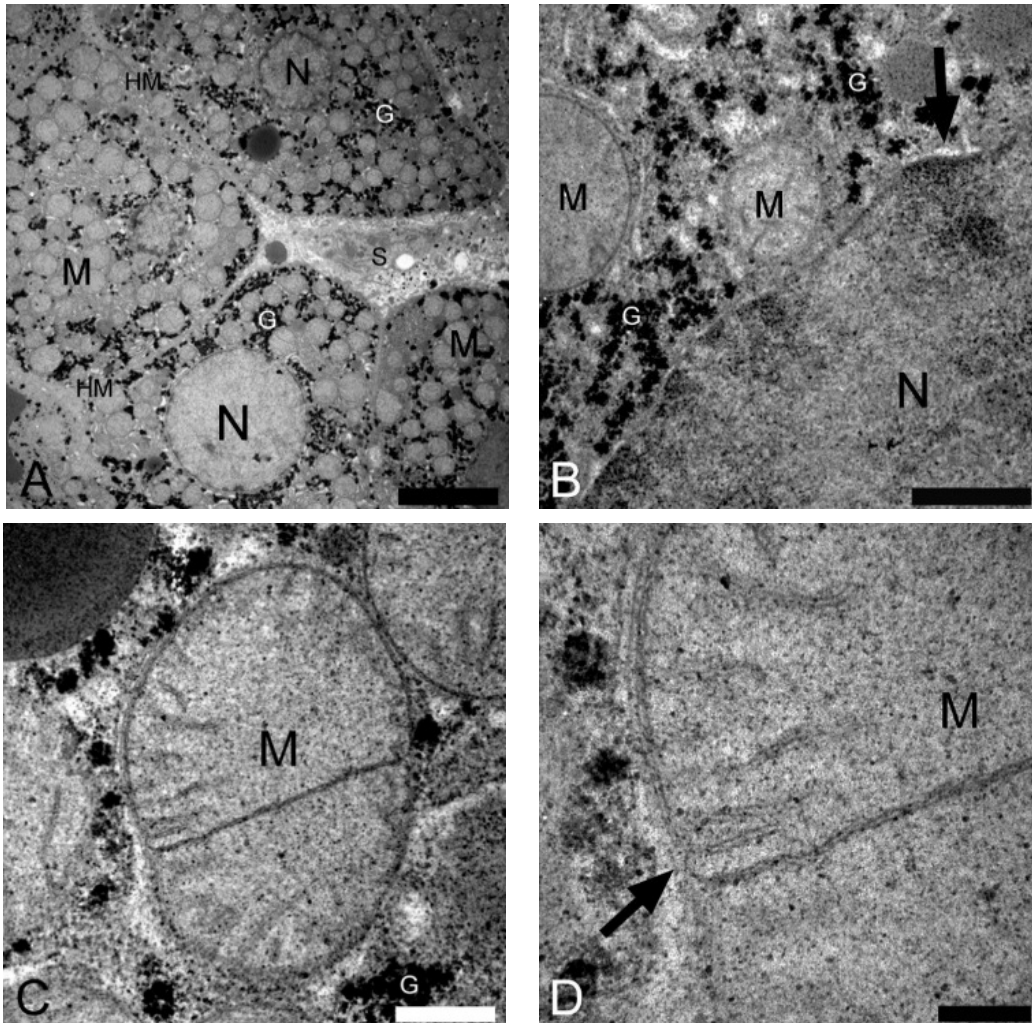
Figure 5.1: TEM micrographs of the control group. Figure A shows the hepatocytes of the liver tissue, with no damage present. Figure B indicates the slight alterations seen in some of the nuclear membranes (arrow). Figures C and D show the minimal alterations to the mitochondrial membrane [Fig. D (arrow)] and intact cristae. **Key:** G: Glycogen granules; HM: Hepatocyte membrane; M: Mitochondria; N: Nucleus membrane (Scale bars: A: 5µm; B: 1µm; C: 500nm; D: 200nm).

Cadmium
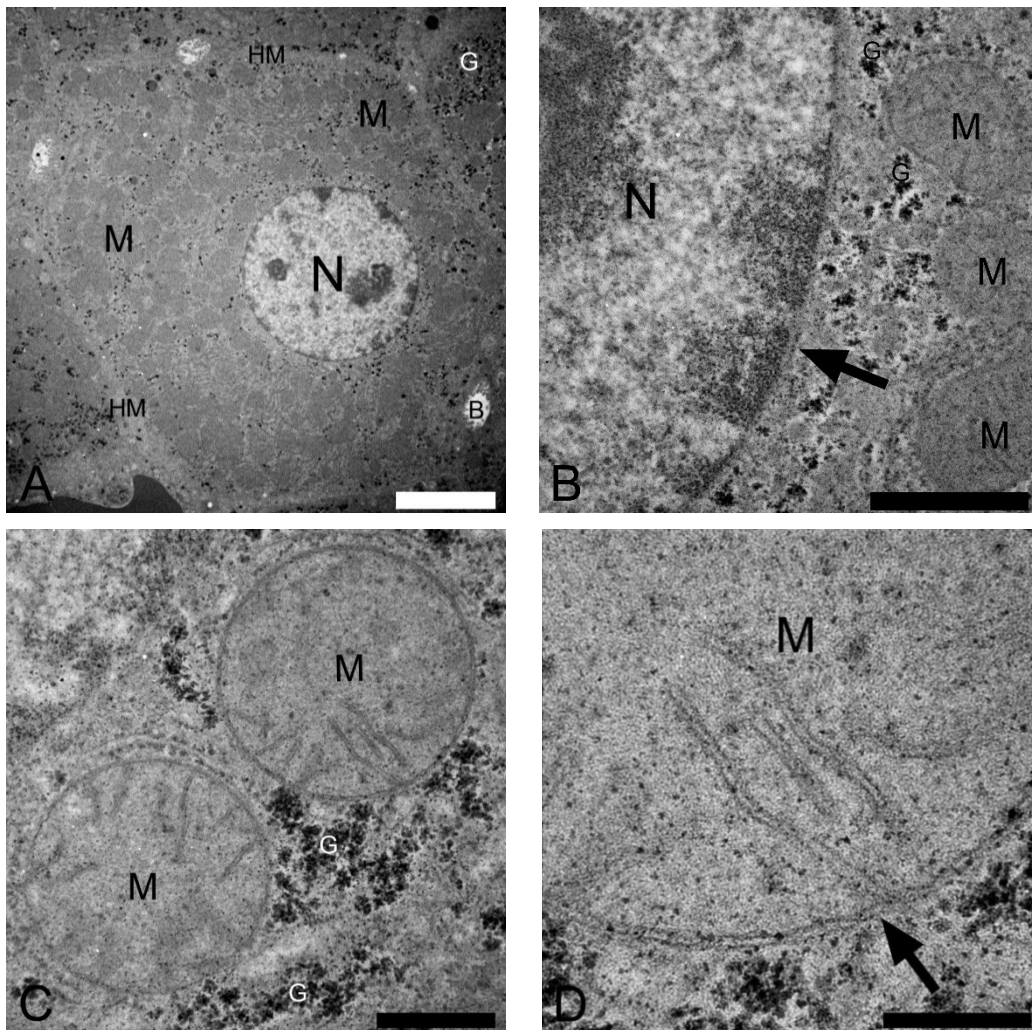
Figure 5.2: TEM micrographs of the Cd experimental group. Figure A is representative of the hepatocytes in the Cd group, with Figure B indicating the alterations seen with the nuclear membranes (arrow). Figures C and D represent the mitochondria present in the liver tissue, with the arrow indicating mitochondrial membrane damage (Fig. D). **Key:** B: Bile canaliculi; G: Glycogen granules; HM: Hepatocyte membrane; M: Mitochondria; N: Nucleus (Scale bars: A: 5µm; B: 1µm; C: 500nm; D: 200nm).

Chromium
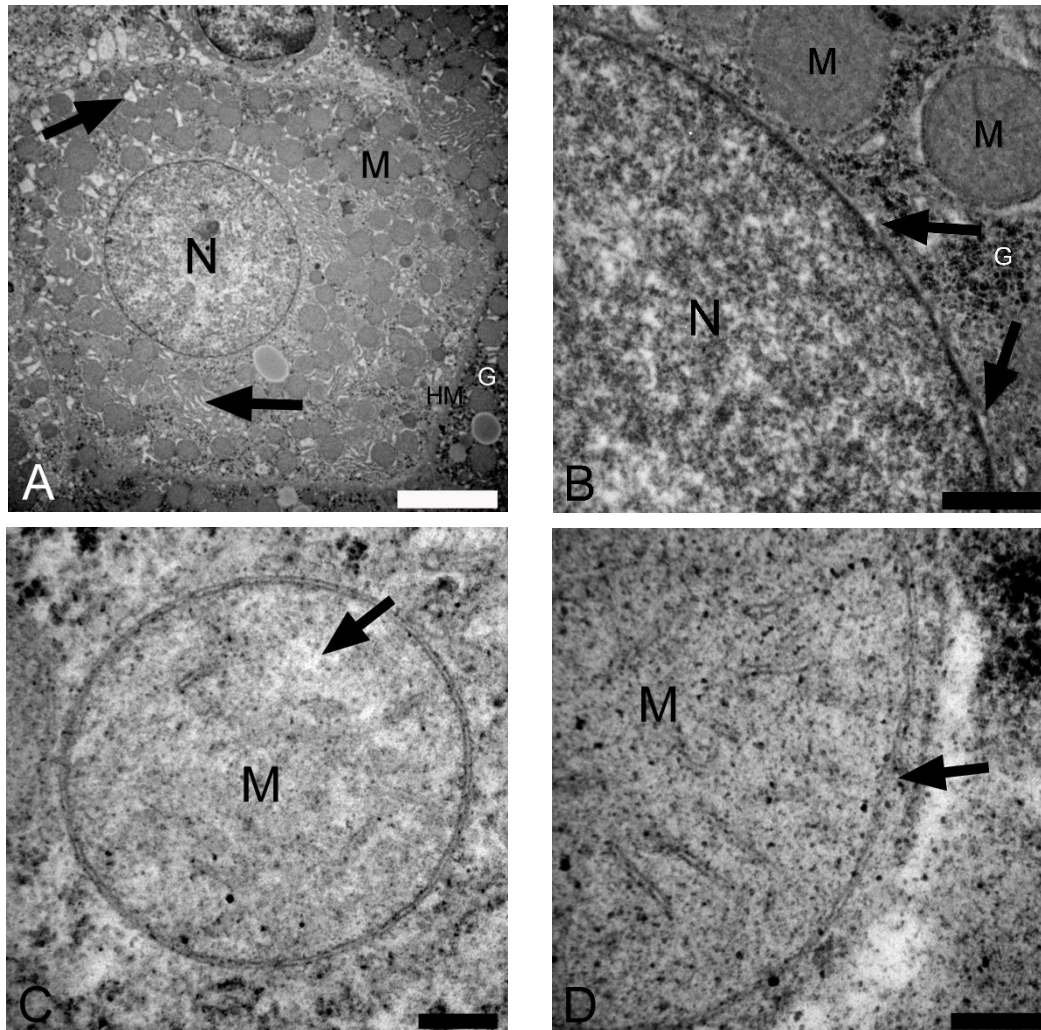
Figure 5.3: TEM micrographs of the Cr experimental groups. Figure A shows the general morphology of the hepatocyte, with the arrows indicating the dilated rER and Golgi apparatus. Figures C and D show the inner matrix swelling and membrane changes of the mitochondria. **Key:** G: Glycogen granules; HM: Hepatocyte membrane; M: Mitochondria; N: Nucleus (Scale bars: A: 5µm; B: 1µm; C and D: 200nm).

Cadmium and chromium
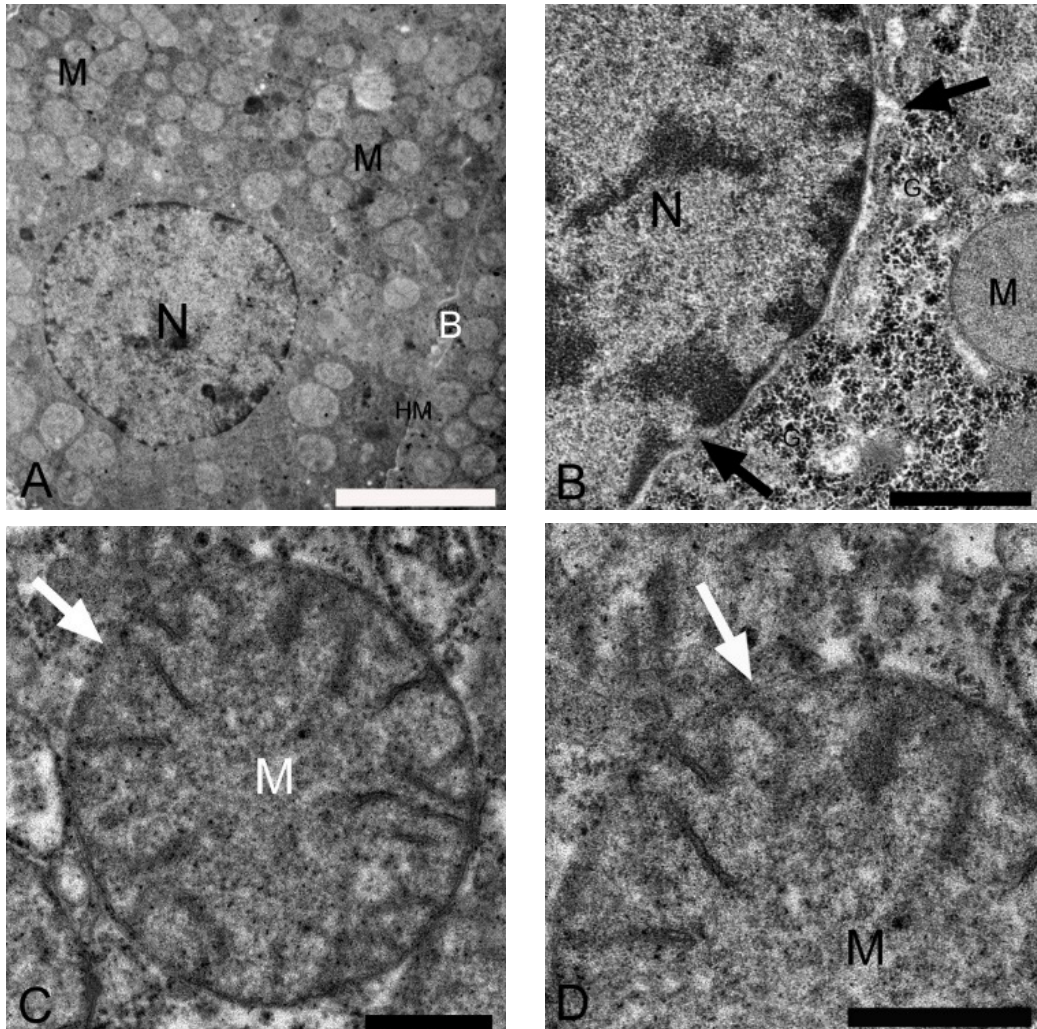
Figure 5.4: TEM micrographs of the liver tissue of the Cd and Cr exposed group. Figure A shows the general hepatocyte structure, with Figures B–D showing the nuclear and mitochondrial alterations (arrows), respectively. **Key:** G: Glycogen granules; HM: Hepatocyte membrane; M: Mitochondria; N: Nucleus (Scale bars: A: 5µm; B: 1µm; C and D: 500nm).

The typical morphology of normal hepatocytes is presented in the control group (Fig. 5.1), with many mitochondria and glycogen granules present in the cytoplasm. Only minor changes to the nuclear and mitochondrial membranes [Fig. 5.1 B and D (arrows), respectively], were observed. No change to the inner matrix of the mitochondria of the control liver tissue was observed. (Fig. 5.1 C). For rat liver exposed to Cd (Figure 5.2), normal hepatocyte structure is still visible although in the cytoplasm some rER dilation is visible (Figure 5.2 A). The incidence of nuclear- and mitochondrial membrane disruptions are more prevalent in the Cd exposed groups [Fig. 5.2 B and D (arrows), respectively]. Irregular chromatin condensation are present in the nuclei (Fig. 5.2 A and B), but no inner matrix swelling is seen in the mitochondria (Fig. 5.2 C).

In the Cr experimental group (Fig. 5.3), there is an increase in the rER dilation [Fig. 5.3 A (arrows)]. Outer membrane alterations in the nuclear [Fig. 5.3 B (arrows)], and mitochondrial membranes were visible in the Cr exposed group [Fig. 5.3 D (arrows)]. The nuclei also presented with irregular chromatin condensation, with inner matrix swelling visible in the cristae of the mitochondria [Fig. 5.3 C (arrow)]. Liver tissue from rats exposed to Cd and Cr showed an increase in nuclear membrane damage and chromatin condensation [Fig. 5.4 A and B (arrows)]. In this group alterations to the mitochondrial membrane and cristae alterations [Fig. 5.4 C and D (arrows)] were also observed. The ultrastructural changes observed in the liver tissue is summarised in Table 5.2.

Table 5.2: Summary of ultrastructural changes in the liver tissue

Group	Cellular membrane disruption	Nuclear membrane disruption	Chromatin condensation	Mitochondrial membrane disruption	Mitochondrial swelling	rER dilation
Control	-	+	-	+	-	-
Cd	+	++	++	+	-	+
Cr	-	++	++	++	++	+++
Cd and Cr	+	+++	+++	++	++	++

-, none; +, minor, ++, mild, +++, severe.

5.3.2 *Ultrastructural effects of Cd and Cr alone and in combination on the pancreas*

Control
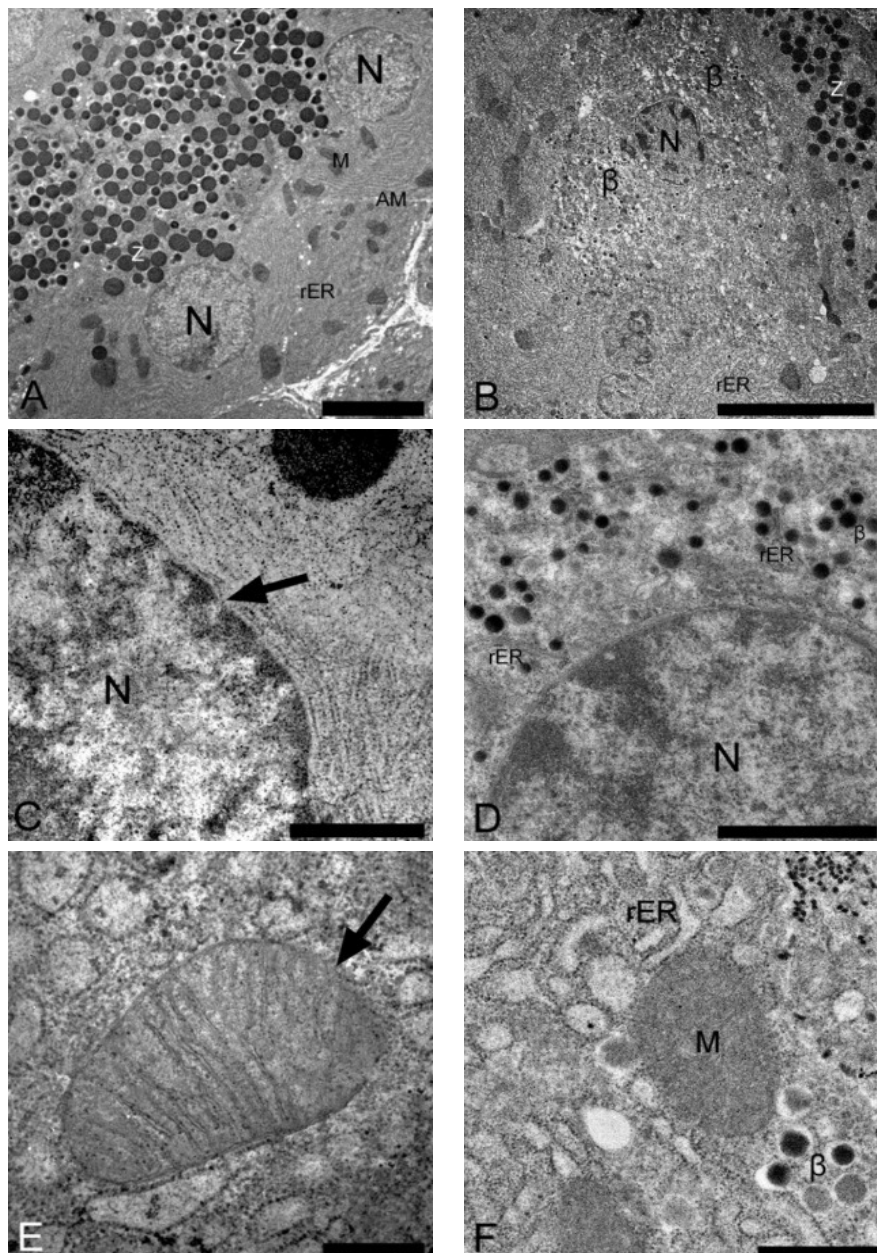
**Figure 5.5:** TEM micrographs of the pancreas tissue from the control group. Figures A, C and E indicate the exocrine pancreas, with the pancreatic acinar cells (Fig. A), nuclear membrane (Fig C) and mitochondria (Fig E). Arrows indicate minimal membrane changes in Figures C and E. Figures B, D and F show the endocrine pancreas, with Figure B indicating the general morphology of the Islets of Langerhans, Figure D shows rER and β-cells and Figure F the mitochondria. **Key:** AM: Acinar membrane; β: β-cells; M: Mitochondria; N: Nucleus; rER: Rough endoplasmic reticulum; Z: Zymogen granules (Scale bars: A: 5µm; B: 10µm; C and F: 1µm; D: 2µm; E: 500nm).

Cadmium
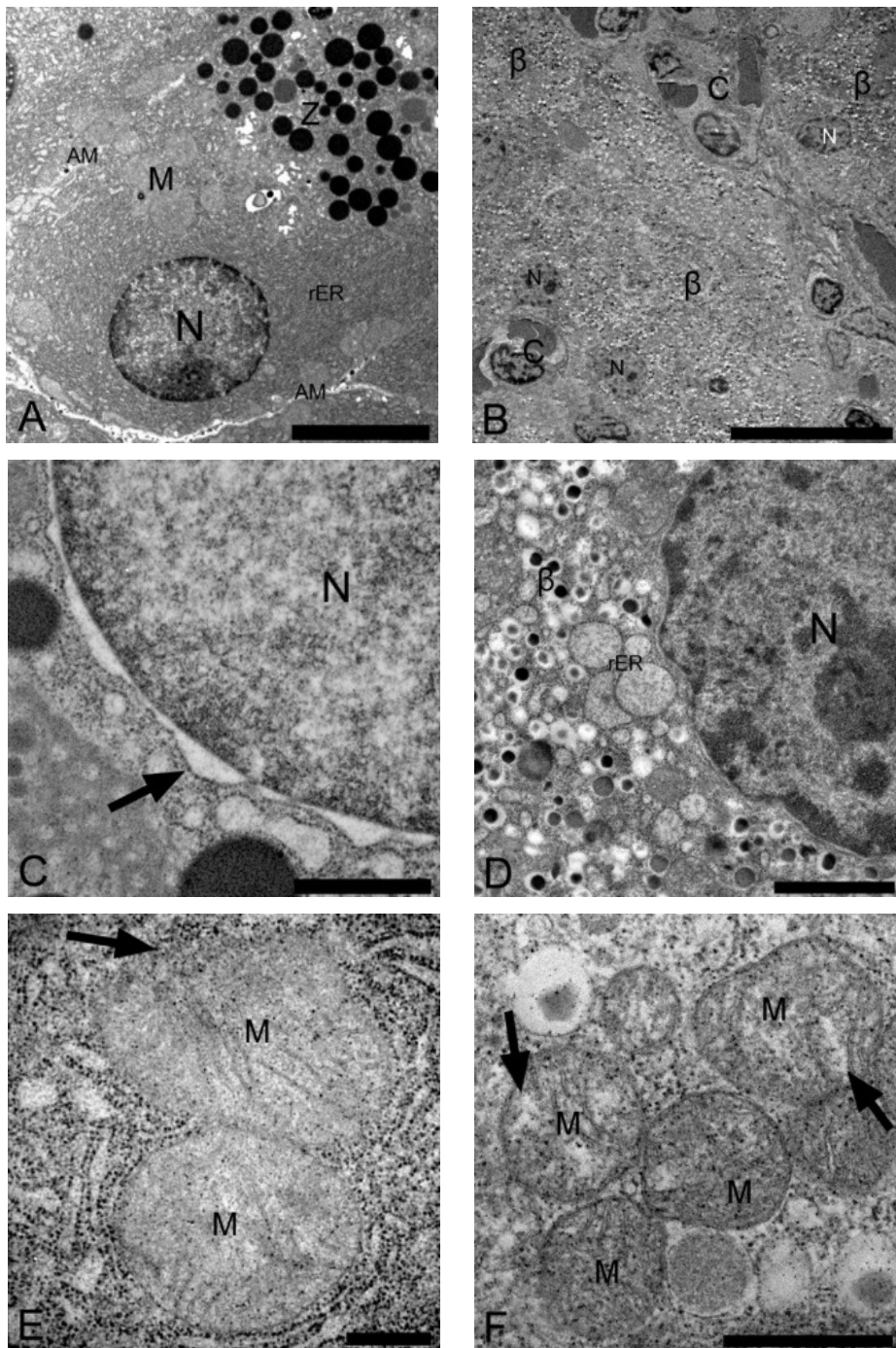
Figure 5.6: TEM micrographs of the Cd experimental group. Figures A, C and E represent the alterations seen in the exocrine pancreas, with Figure A showing a pancreatic acinar cell, Figure C the damaged nuclear membrane (arrow) and damaged mitochondria [Fig. E (arrow)] found in the pancreatic acinar cells. Figures B, D and F are micrographs of the endocrine pancreas, with Figure B mostly indicating the β-cells of the endocrine pancreas, Figures D and F show the rER, nuclear and mitochondrial alterations, respectively. **Key:** AM: Acinar membrane; β: β-cells; C: Capillary; M: Mitochondria; N: Nucleus; rER: Rough endoplasmic reticulum; Z: Zymogen granules (Scale bars: A: 5µm; B: 20µm; C and F: 1µm; D: 2µm; E: 500nm).

Chromium
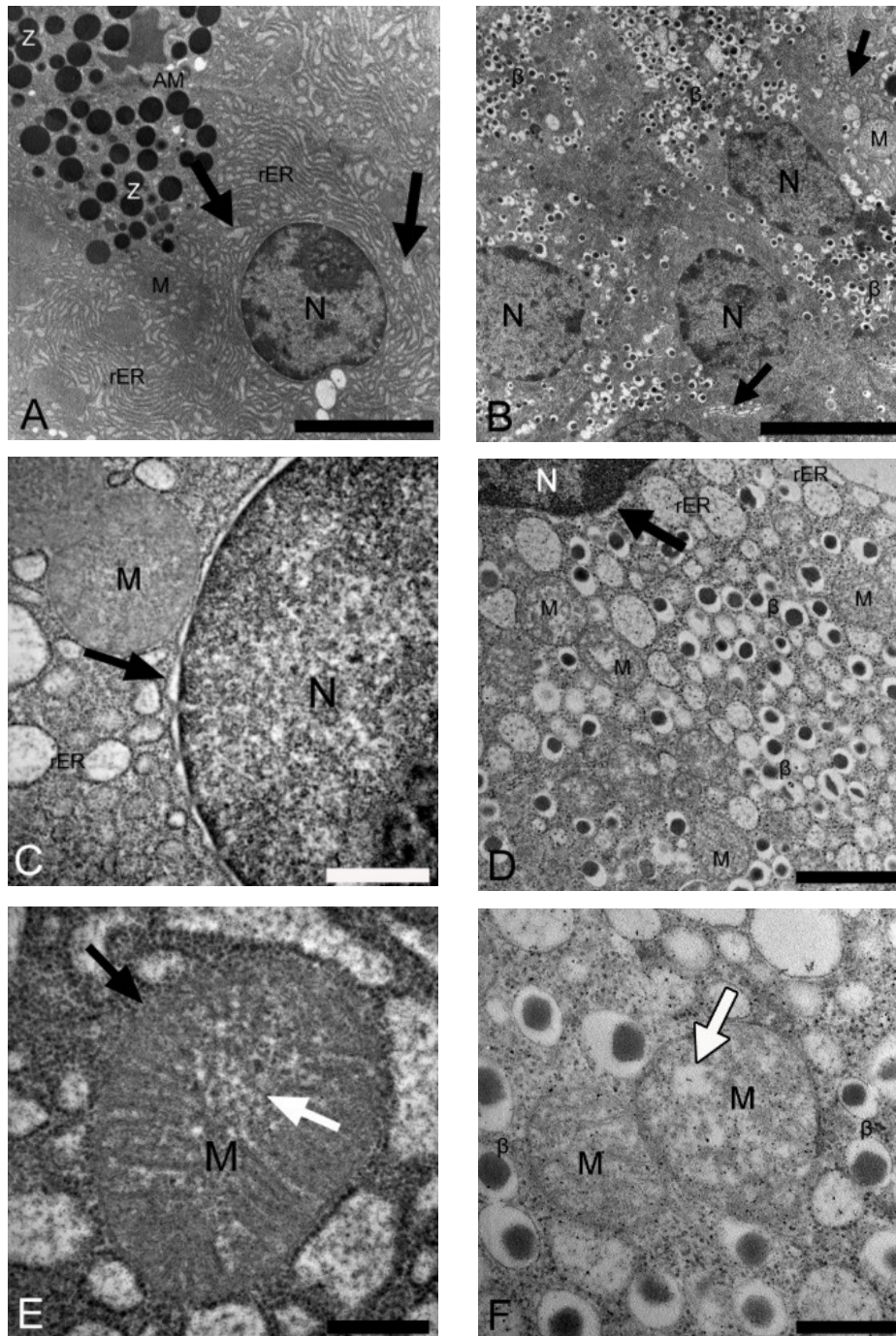
Figure 5.7: TEM micrographs of the Cr experimental group. Figures A, C and E indicate the exocrine cells. Figure A shows the pancreatic acinar cells, with the arrows indicating rER dilation. Figure C shows the nuclear membrane alteration (arrow) and Figure E the mitochondrial alteration (arrow). Figures B, D and F indicate the Islets of Langerhans, with the general morphology shown in Figure B (arrows indicate dilated rER). In Figure D the nuclear membrane alterations (arrow) are shown with Figure F indicating the mitochondrial changes (arrow). **Key:** β: β-cells; C: Capillary: M: Mitochondria**;** N: Nucleus; rER: Rough endoplasmic reticulum; Z: Zymogen granules (Scale bars: A: 10µm; B: 5µm; C, D: 1µm; E, F: 500nm).

Cadmium and chromium
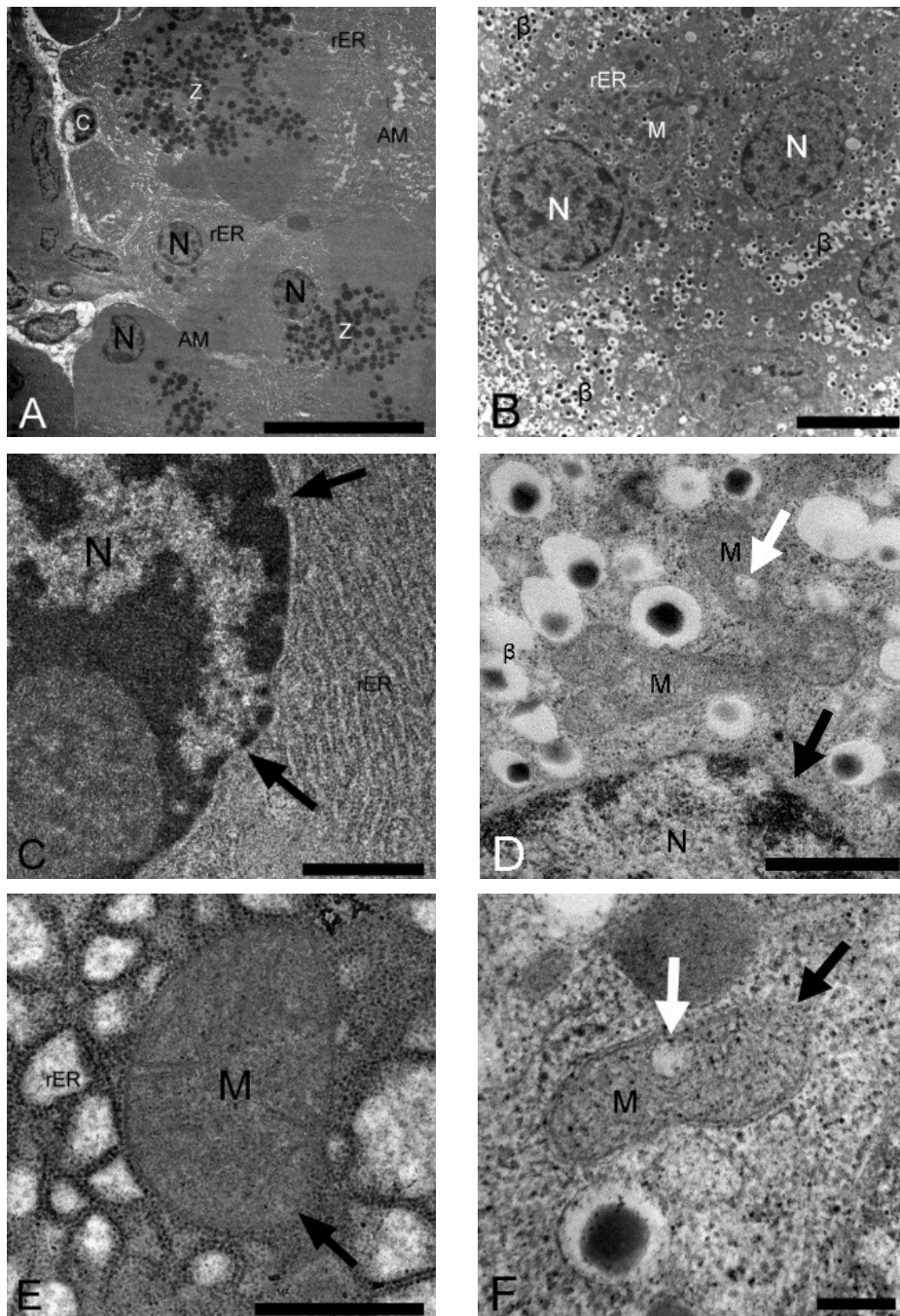
Figure 5.8: TEM micrographs of the Cd and Cr group. Figures A, C and E indicate the exocrine pancreas, with Figure A showing the pancreatic acinar cells, with dilated rER visible in the cytoplasm. Figure C and E indicates the nuclear and mitochondrial alterations (arrows), respectively. In Figures B, D and F the alterations in the endocrine component are shown, with the white arrows indicating inner matrix swelling in the mitochondria and the black arrows indicating membrane changes. **Key:** AM: Acinar membrane; β: β-cells; C: Capillary; M: Mitochondria; N: Nucleus; rER: Rough endoplasmic reticulum; Z: Zymogen granules (Scale bars: A: 20µm; B: 5µm; C–E: 1µm; F: 200nm).

The ultrastructure of the exocrine and endocrine pancreas was evaluated. The exocrine gland contains the pyramidal shaped, pancreatic acinar cells, with the endocrine gland containing the Islets of Langerhans. The normal morphology of these regions is presented in Figure 5.5. Figures 5.5 A, C and E indicate the pancreatic acinar cells, nuclear membrane and mitochondria, respectively, with minimal alterations (arrows) seen in all examined areas. The endocrine pancreas (Figures 5.5 B, D and F) showed minimal changes in the rER, nucleus and mitochondria. In the Cd experimental group (Fig. 5.6), some rER dilation can be seen in the cytoplasm of the pancreatic acinar cells (Fig. 5.6 A). The nucleus displays both membrane disruption, as well as irregular chromatin condensation [Fig. 5.6 A and C (arrow)]. In the mitochondria, some membrane and inner matrix swelling were present in almost all the samples. In terms of the endocrine pancreas, rER cisternae dilation, nuclear membrane alterations (Fig. 5.6 D) and inner matrix swelling [Fig. 5.6 F (arrows)] were also observed.

Analysis of the Cr experimental group revealed an increase in rER, nuclear and mitochondrial alterations, with nuclei outer membrane changes [Fig. 5.7 C (arrow)], irregular chromatin condensation and changes in the mitochondrial membrane [Fig. 5.7 E (black arrow)] and cristae [Fig. 5.7 E (white arrow)]. rER cisternae dilation (Fig. 5.7 C) were also seen in almost all samples. The endocrine pancreas (Fig. 5.7 B, D, and F) shows rER dilation [Fig. 5.7 B (black arrows)] and nuclear membrane alterations seen in Figure 5.7 D (black arrow). Inner matrix swelling was present in the mitochondria [Fig. 5.7 F (white arrow)], with minimal membrane changes seen throughout the group.

A slight decrease in the occurrence of the alterations seen in the exocrine pancreas of the Cd and Cr experimental groups are seen, when compared to the Cr experimental group. All the organelles of the pancreatic acinar cells still showed some changes that include nuclear membrane disruptions [Fig. 5.8 C (arrow)], irregular chromatin condensation, mitochondrial membrane disruption, inner matrix swelling and rER dilation. The endocrine pancreas on the other hand showed an increase in alterations in the metal combination group, in comparison with the other groups. There was an increase in occurrence of nuclear outer membrane changes [Fig. 5.8 D (black arrow)], mitochondrial inner matrix swelling [Fig. 5.8 D and F (white arrows)] and membrane alterations [Fig. 5.8 F (black arrow)]. The observed effects of exposure is summarized in Table 5.3

Table 5.3: Summary of ultrastructural changes in the pancreas tissue

	Exocrine pancreas					
Group	**Cellular membrane disruption**	**Nuclear membrane disruption**	**Chromatin condensation**	**Mitochondrial membrane disruption**	**Mitochondrial swelling**	**rER dilation**
Control	+	+	++	+	+	-
Cd	++	++	++	++	++	+
Cr	++	+++	+++	+++	+++	++
Cd and Cr	++	+++	++	++	+	+

	Endocrine pancreas			
Group	**Nuclear membrane disruptions**	**Mitochondrial alterations**	**rER dilation**	**α-, β-, D- cell alterations**
Control	+	+	+	-
Cd	++	++	++	-
Cr	++	++	++	-
Cd and Cr	+++	+++	++	-

-, none; +, minor, ++, mild, +++, severe.

5.3.3 *Ultrastructural effects of Cd and Cr alone and in combination on the kidney*

Control
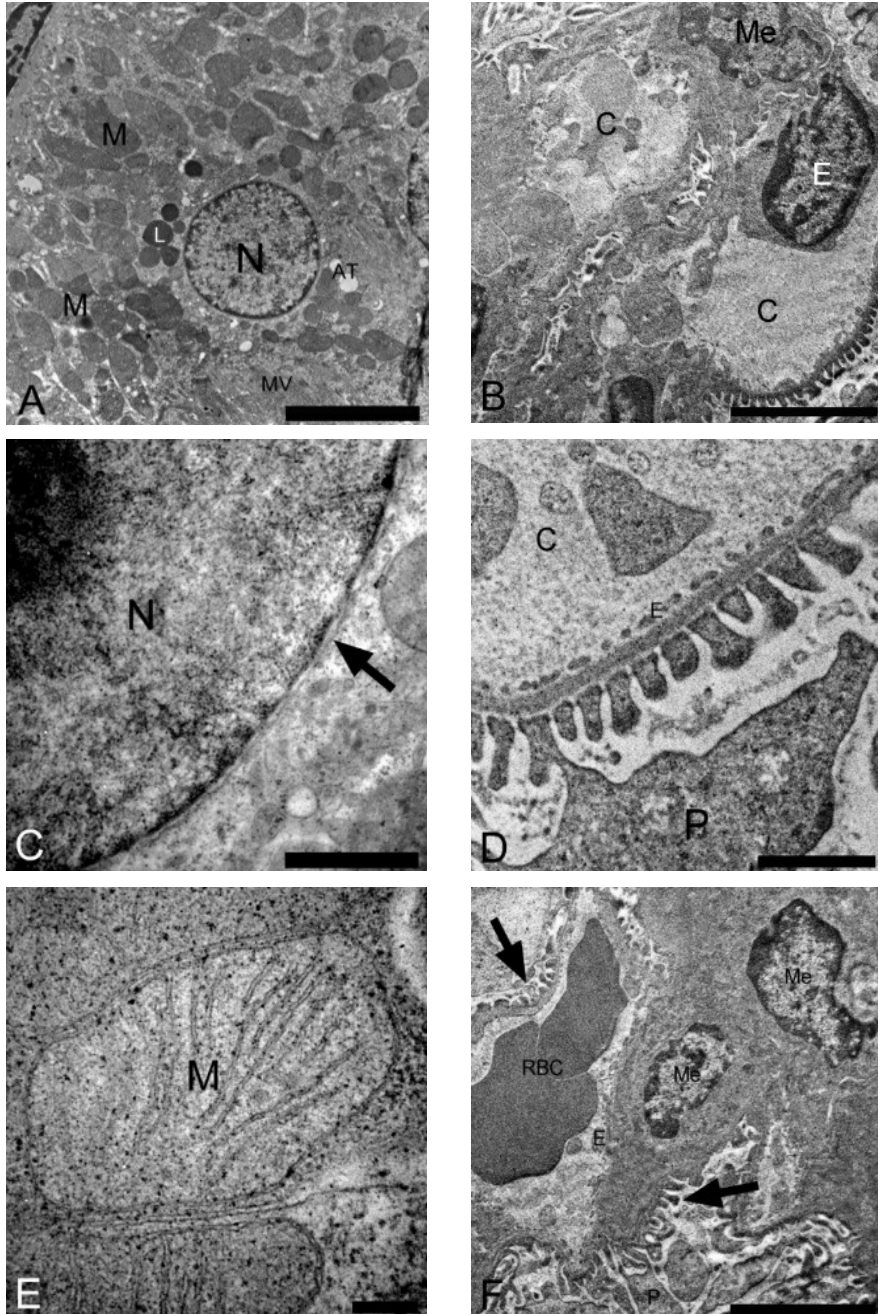
Figure 5.9: TEM micrographs of the kidney tissue from the control animals. Figures A, C and E indicate the proximal convoluted tubule (PCT), nuclear membrane and mitochondria, respectively. The glomerular ultrastructure can be seen in Figures B, D and F that indicate the glomeruli, the cells involved in the filtration system and podocytes and mesangial cells, respectively. **Key:** AT: Apical tubulovesicles C: Capillary; E: Endothelial cell; L: Lysosome; Me: Mesangial cell; MV: Microvilli; M: Mitochondria; N: Nucleus; P: Podocyte; RBC: Red blood cell (Scale bars: A, B and F: 5μm; C and D: 1μm; E: 200nm).

Cadmium
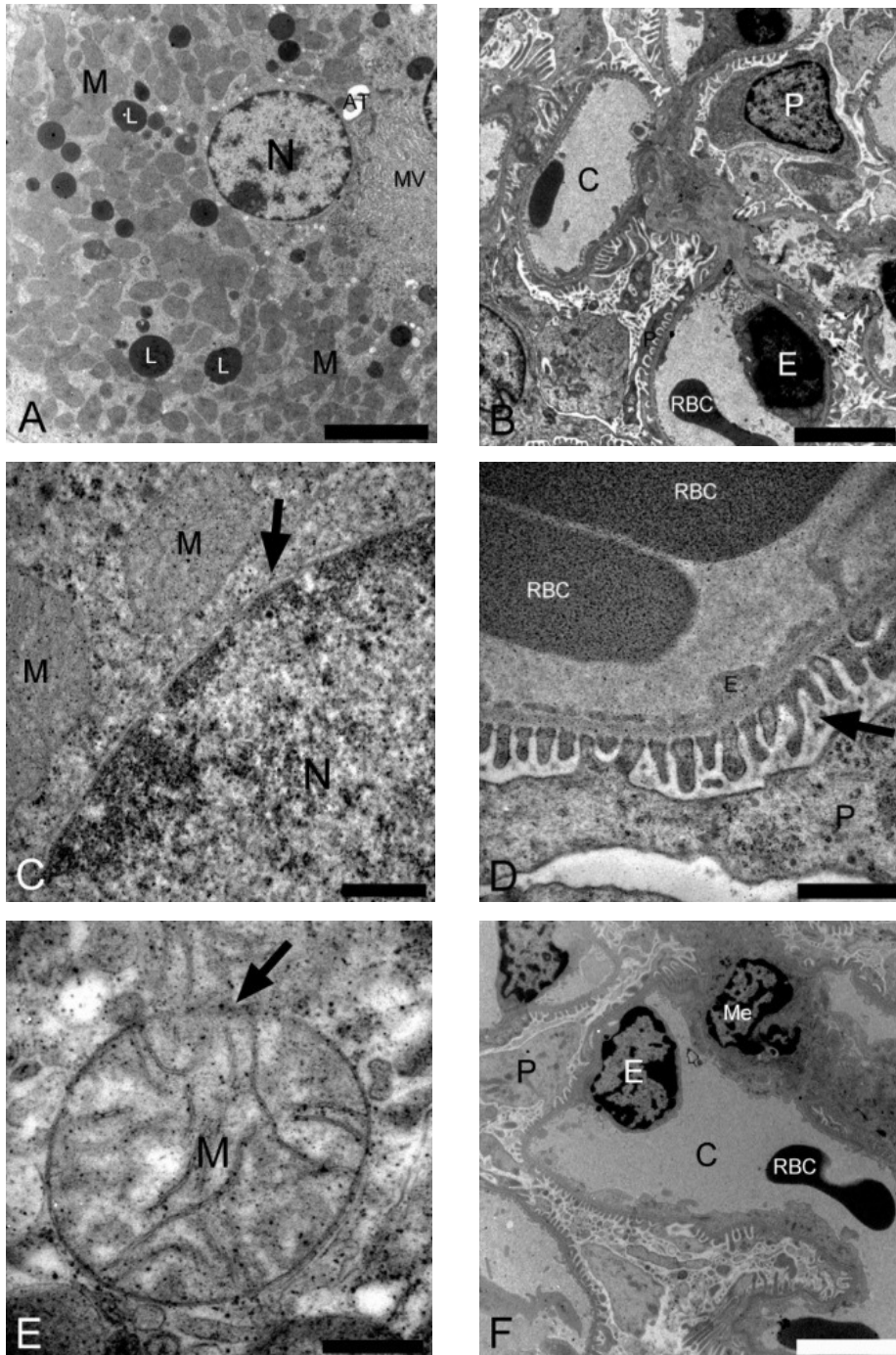
Figure 5.10: TEM micrographs of the Cd experimental group. Figures A, C and E show the cuboidal epithelial cell of the PCT, nucleus and mitochondria, respectively, with the arrows indicating membrane damage (Fig. C and E). Figures B, D and F show the glomeruli and all its components that include the endothelial cells, podocytes, pedicles (Fig. D arrow) and mesangial cell. **Key:** AT: Apical tubulovesicles; C: Capillary; E: Endothelial cell; L: Lysosome; Me: Mesangial cell; MV: Microvilli; M: Mitochondria; N: Nucleus; P: Podocyte; RBC: Red blood cell (Scale bars: A, B and F: 5µm; C and D: 1µm; E: 500nm).

Chromium
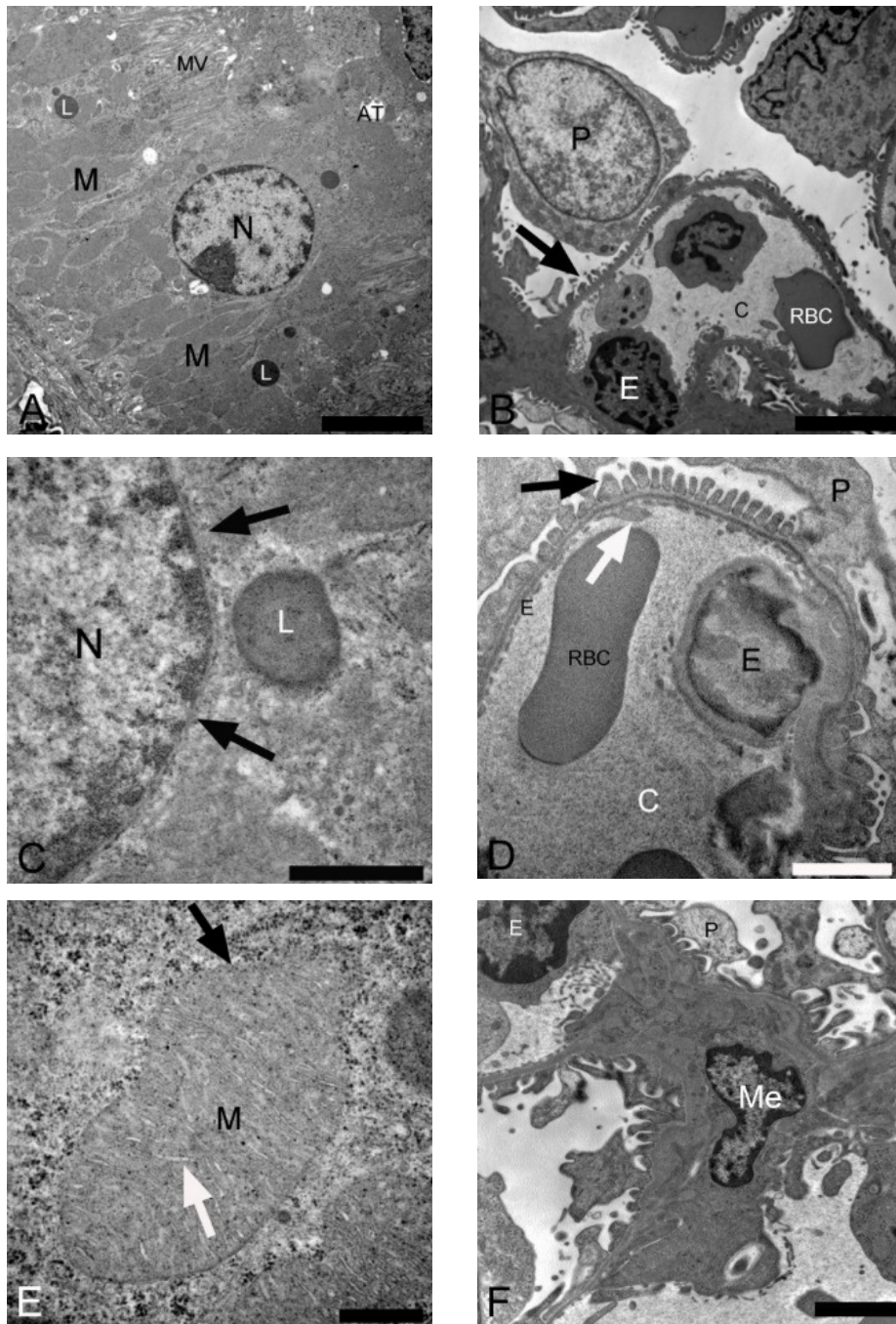
Figure 5.11: TEM micrographs of the kidney tissue of the Cr group. Figures A, C and E represents the alterations seen in the PCT cells, with Figure C (arrows) indicating the nuclear outer membrane damage and Figure E shows the membrane (black arrow) and cristae damage (white arrow) of the mitochondria. Figures B, D and F show the glomeruli, where the endothelial cells, podocytes and mesangial cells alterations are shown. Figures B and D (black arrows) show damage to the pedicles and the white arrow (Fig. D) shows endothelial damage. **Key:** AT: Apical tubulovesicles; C: Capillary; E: Endothelial cell; L: Lysosome; Me: Mesangial cell; MV: Microvilli; M: Mitochondria; N: Nucleus; P: Podocyte; RBC: Red blood cell (Scale bars: A, B and F: 5µm; C and D: 1µm; E: 500nm).

Cadmium and chromium
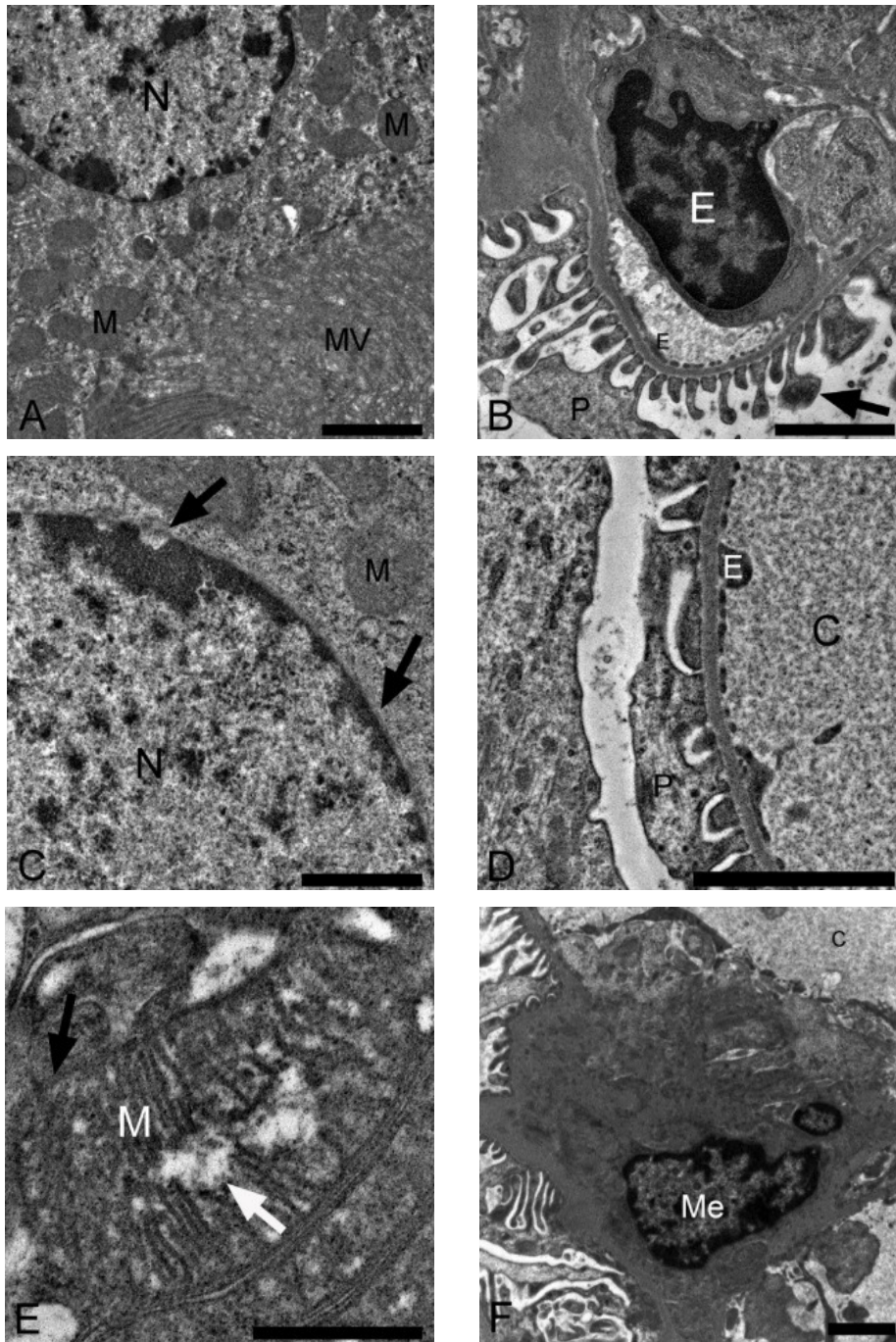
Figure 5.12: TEM micrographs of the kidney tissue from the combination group. Figure A indicates the PCT, with Figures C and E showing the alterations seen in the nucleus and mitochondria (arrows), respectively. Figures B, D and F show the glomeruli and its components, with the altered pedicles and endothelial cells seen in Figures B (arrow) and D, respectively. **Key:** AT: Apical tubulovesicles; C: Capillary; E: Endothelial cell; Me: Mesangial cell; MV: Microvilli; M: Mitochondria; N: Nucleus; P: Podocyte; RBC: Red blood cell (Scale bars: A, B, D and F: 2µm; C and E: 1µm).

Two regions of the kidney were evaluated for cellular damage and these were the PCT and the glomeruli of the kidney (Tavafi, *et al.*, 2016; Venter, 2015). In the kidney samples of the control group, minimal alterations were seen in the ultrastructure the kidney. In a few of the samples evaluated minimal nuclear outer membrane [Fig. 5.9 C (arrow)] and mitochondrial membrane changes (Fig. 5.9 E) were observed. No changes were seen in the PCT cell membrane, rER (Fig. 5.9 A) and mitochondrial cristae (Fig. 5.9 E). The structure of the components of the glomeruli, the endothelial cells, pedicles, mesangial cells and podocytes [Fig. 5.9 F (arrows)], were normal or if any alterations were observed these were minimal (Fig. 5.9 B, D and F). The morphology of the kidney tissue from animals exposed to Cd showed increased alterations to the organelles of the PCT (Fig. 5.10 A, C and E). Increased occurrence of irregular chromatin condensation was observed in the nuclei (Fig. 5.10 A and C). Minimal alterations were also seen in the endothelial cells and pedicles of the glomeruli [Fig. 5.10 B, D (arrow) and F]. No changes were observed in the mesangial cells and podocytes (Fig. 5.10 A and F).

In all rats exposed to Cr noticeable changes were observed and these were visible in the outer membrane [Fig. 5.11 C (arrows)] and mitochondrial membrane [Fig. 5.11 E (black arrow)]. Irregular chromatin condensation was also observed. Minimal alterations were visible in the PCT cell membrane, rER and mitochondrial cristae [Fig. 5.11 E (white arrow)] in almost all kidney tissue evaluated. The endothelial cells and pedicles showed minimal damage in almost all kidney tissue and no changes were seen in the mesangial cells and podocytes. The kidney tissue of the Cd and Cr group also showed altered nuclear and mitochondrial structure. Changes included membrane alterations [Fig. 5.12 C and E (black arrows)], irregular chromatin condensation and inner matrix swelling [Fig. 5.12 E (white arrow)], respectively. Some cellular membrane and rER changes were also seen in the PCT. In all tissue samples, changes in the endothelial cells and pedicles were also observed [Fig. 5.12 B, D and F (arrows)]. The observed effects of exposure are summarized in Table 5.4.

Table 5.4: Summary of ultrastructural changes in the kidney tissue

Proximal convoluted tubule

Group	Cellular membrane disruption	Nuclear membrane disruption	Chromatin condensation	Mitochondrial membrane disruption	Mitochondrial swelling	rER dilation
Control	-	+	++	+	-	-
Cd	+	++	+++	++	++	+
Cr	++	+++	+++	+++	+	+
Cd and Cr	+	++	+++	+++	+++	++

Glomeruli

Group	Endothelial cells disruption	Pedicles disruption	Podocyte cells disruption	Mesangial cells disruption
Control	+	+	-	-
Cd	+	+	-	-
Cr	++	++	-	-
Cd and Cr	++	++	-	-

-, none; +, minor, ++, mild, +++, severe.

5.3.4 *Intracellular localisation of Cd and Cr*

To determine the intracellular localisation of Cd and Cr, EELS was used. Figures 5.13 and 5.14 illustrate how the EELS and EFTEM results were generated when analysing the liver, pancreas and kidney tissue of all the groups for the presence of Cd and Cr. Figures 5.13 and 5.14 A show examples of the Cd and Cr edges that were used in the EELS analysis, respectively, where Figures 5.13 and 5.14 B-D show the Cd and Cr in the organelles of the kidney and liver, respectively, at each specific edge that was analysed, with the final Cd and Cr colour map seen in Figures 5.13 and 5.14 E, with Cd in red and Cr in yellow.
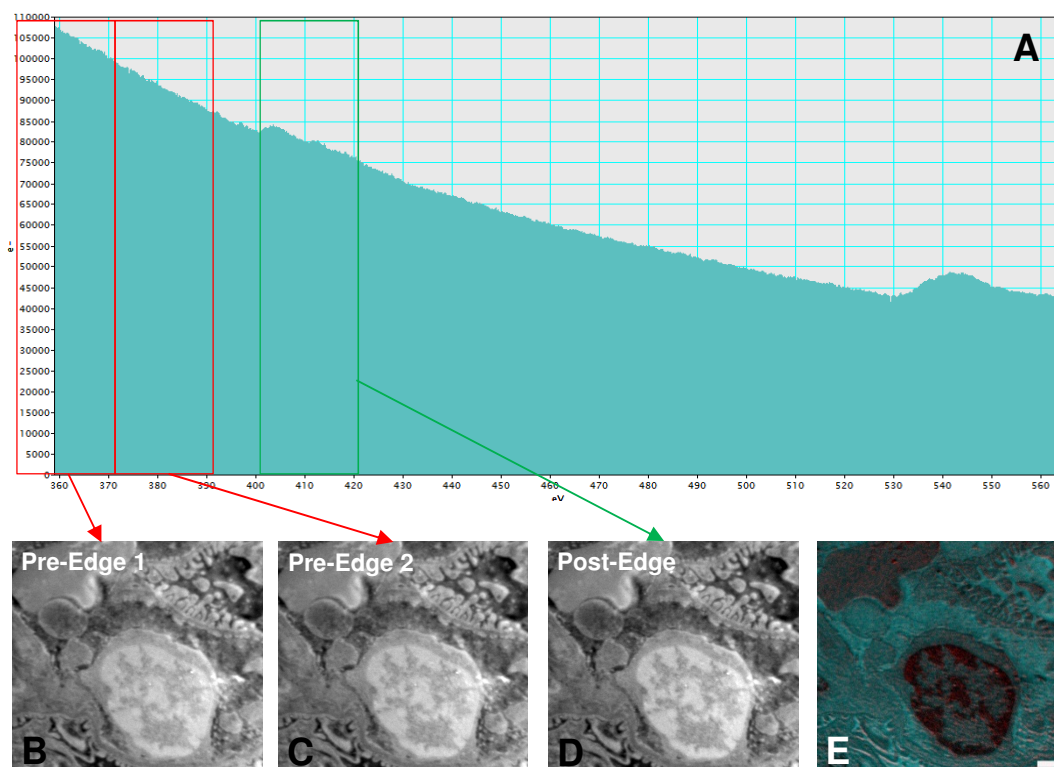
Figure 5.13: EELS and EFTEM micrographs of Cd exposed kidney tissue. Figure A shows the Cd edge that was used in the EELS analysis, with Figures B–D indicating the pre- and post-edge micrographs of Cd in the glomeruli of the kidney at each specific edge that was analysed. Figure E indicates the final Cd map, with the Cd in red (Scale bars: B, C, D and E: 1µm).
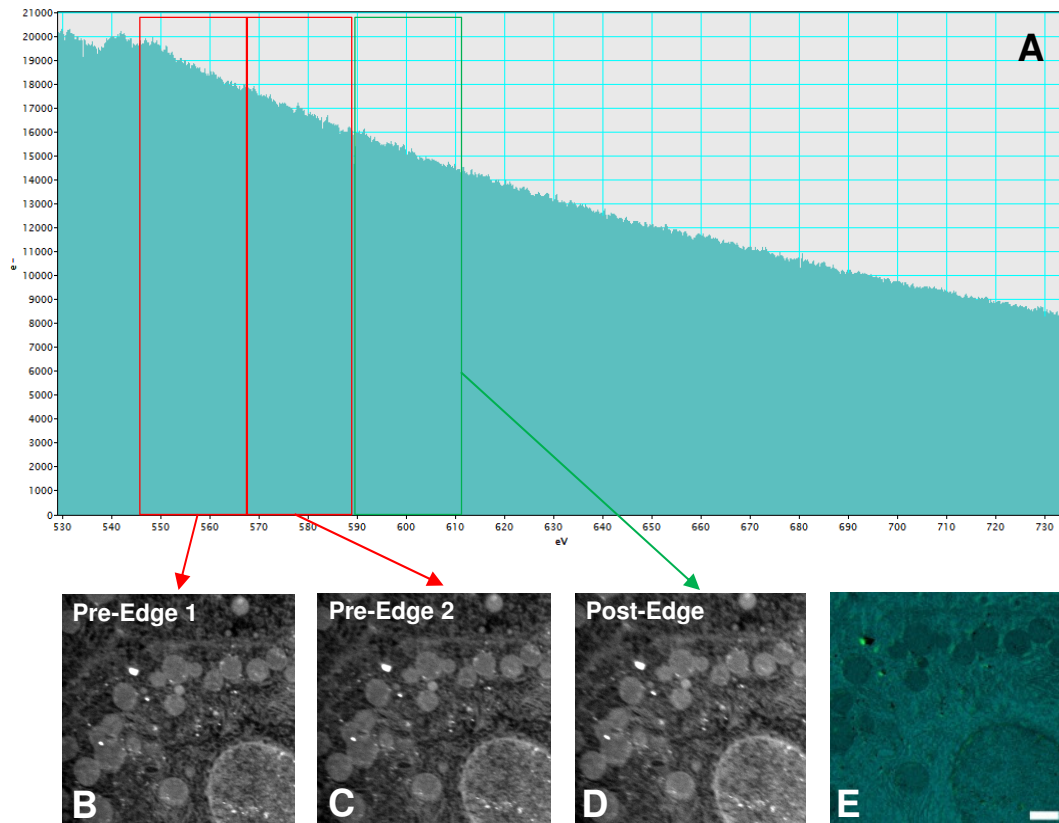
Figure 5.14: EELS and EFTEM micrographs of Cr exposed liver tissue. Figure A shows the Cr edge that was used in the EELS analysis, with Figures B–D indicating the pre- and post-edge micrographs of C of the liver at each specific edge that was analysed. Figure E indicates the final Cr map, with the Cr in yellow (Scale bars: B, C, D and E: 1µm).
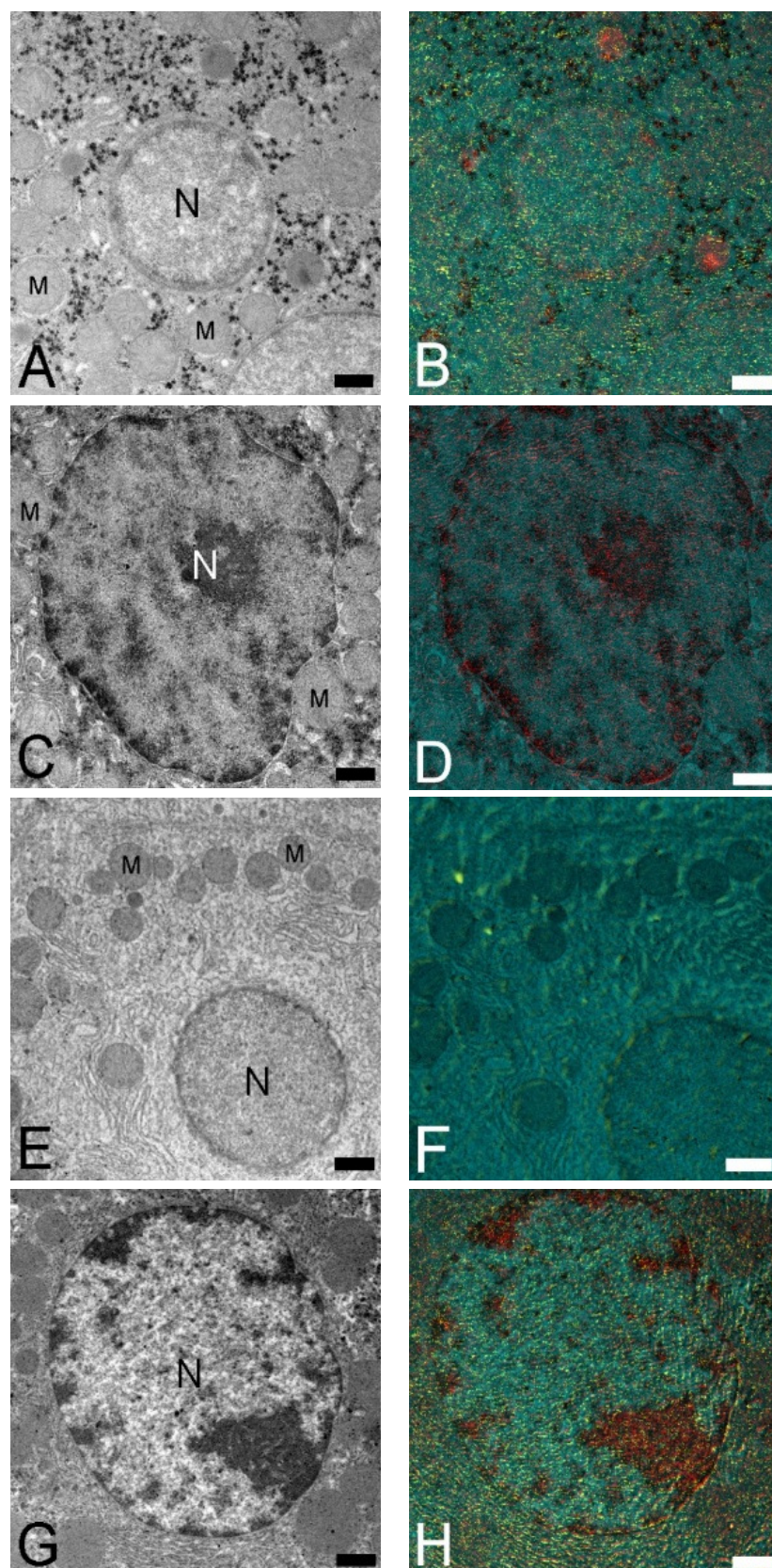
Figure: 5.15: EFTEM micrographs of the liver tissue of the control (A and B), Cd (C and D), Cr (E and F) and Cd and Cr (G and H). Figure A, C, E and G indicates the zero loss images of the colour maps in Figure B, D, F and H, with Cd in red and Cr in yellow. **Key:** N: Nucleus; M: Mitochondria (Scale Bars: A–H: 1μm).
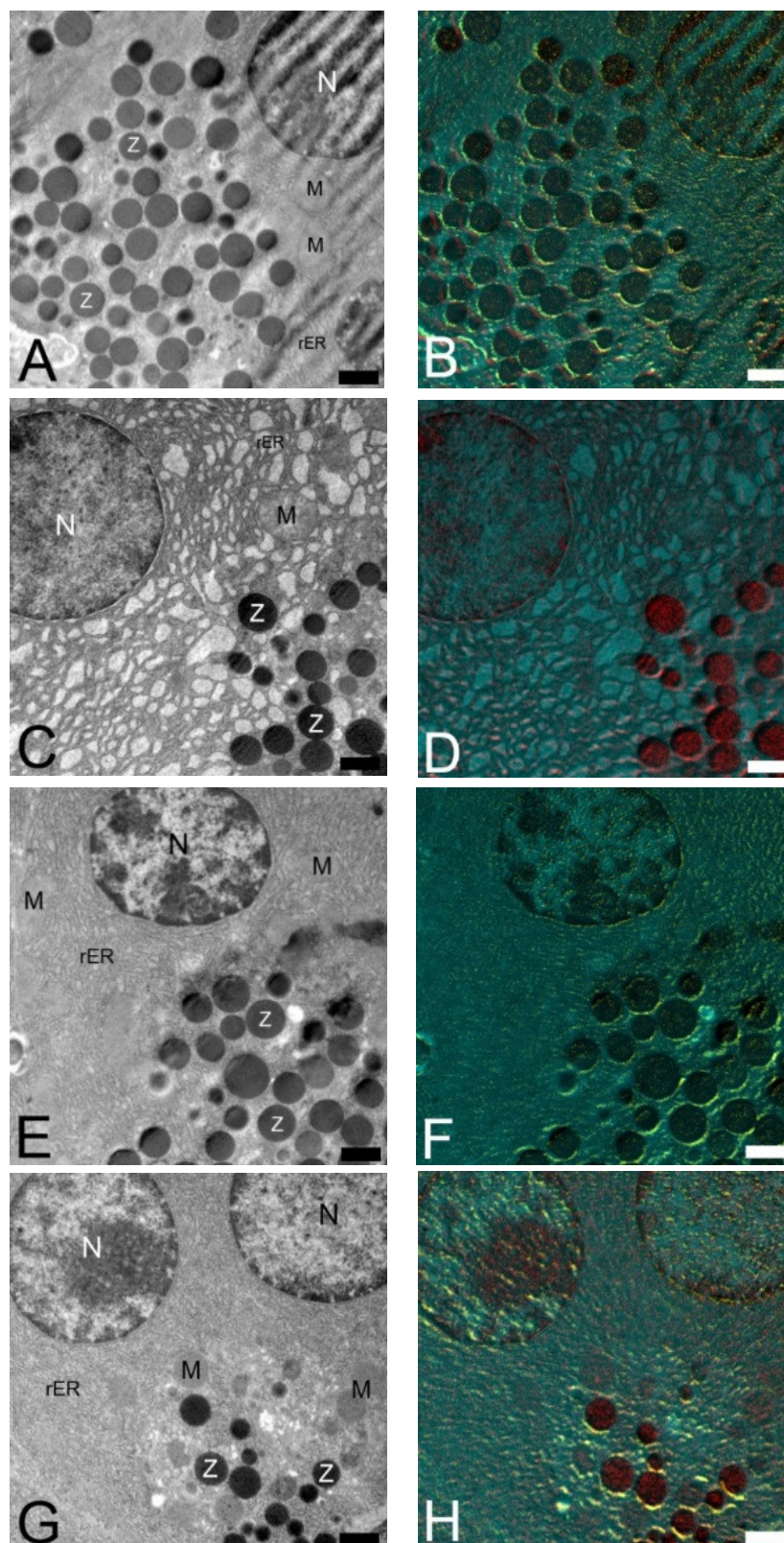
Figure 5.16: EFTEM micrographs of the exocrine pancreas of the control (A and B), Cd (C and D), Cr (E and F) and Cd and Cr (G and H). Figure A, C, E and G indicates the zero loss images of the colour maps in Figure B, D, F and H, with Cd in red and Cr in yellow. **Key:** N: Nucleus; M: Mitochondria; rER: Rough endoplasmic reticulum; Z: Zymogen granules (Scale Bars: A–H: 1μm).
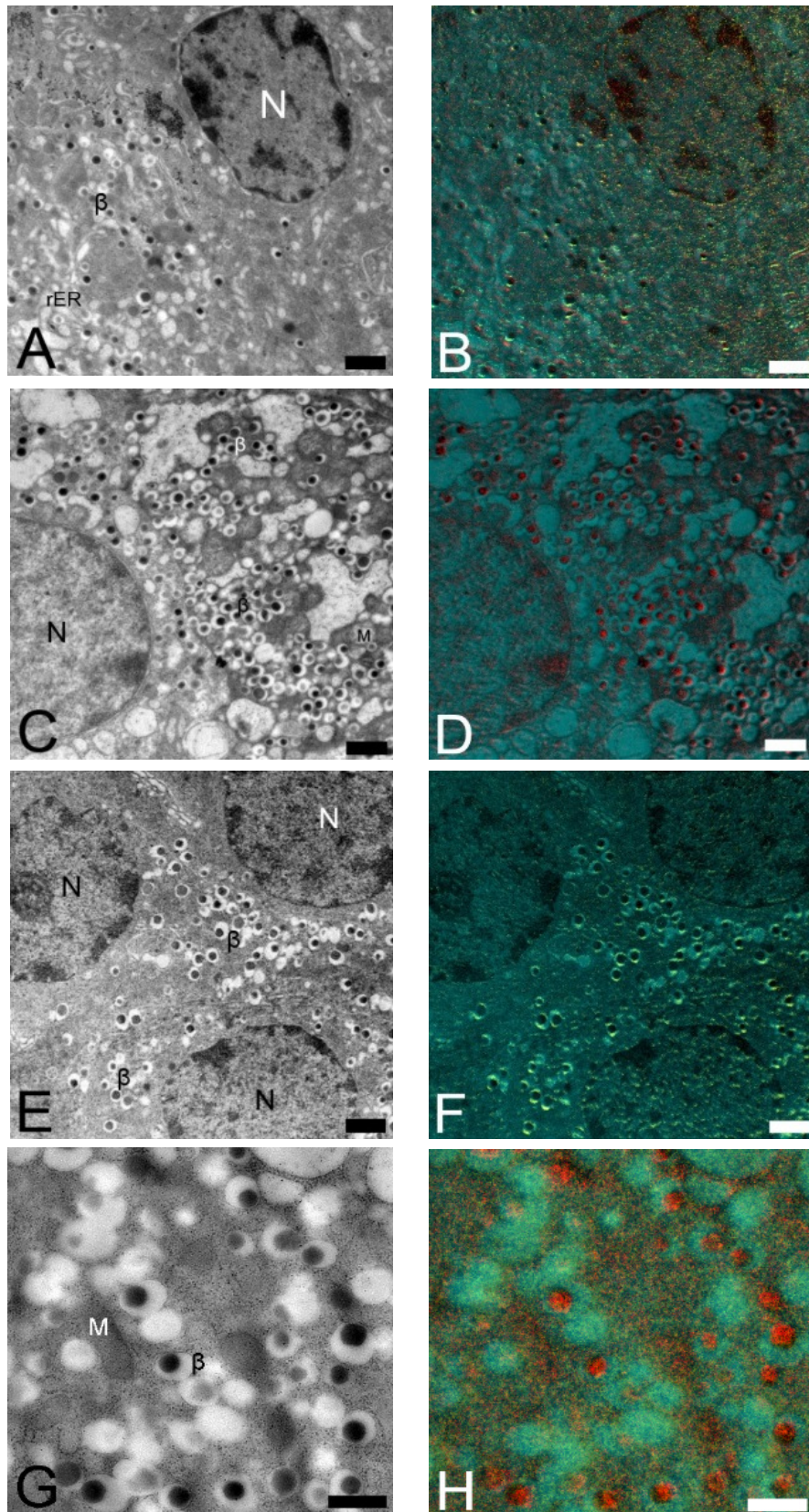
Figure 5.17: EFTEM micrographs of the endocrine pancreas of the control (A and B), Cd (C and D), Cr (E and F) and Cd and Cr (G and H). Figure A, C, E and G indicates the zero loss images of the colour maps in Figure B, D, F and H, with Cd in red and Cr in yellow. **Key:** β: β-cells; N: Nucleus; M: Mitochondria; rER: Rough endoplasmic reticulum (Scale Bars: A–F: 1µm and G and H: 0.5µm).
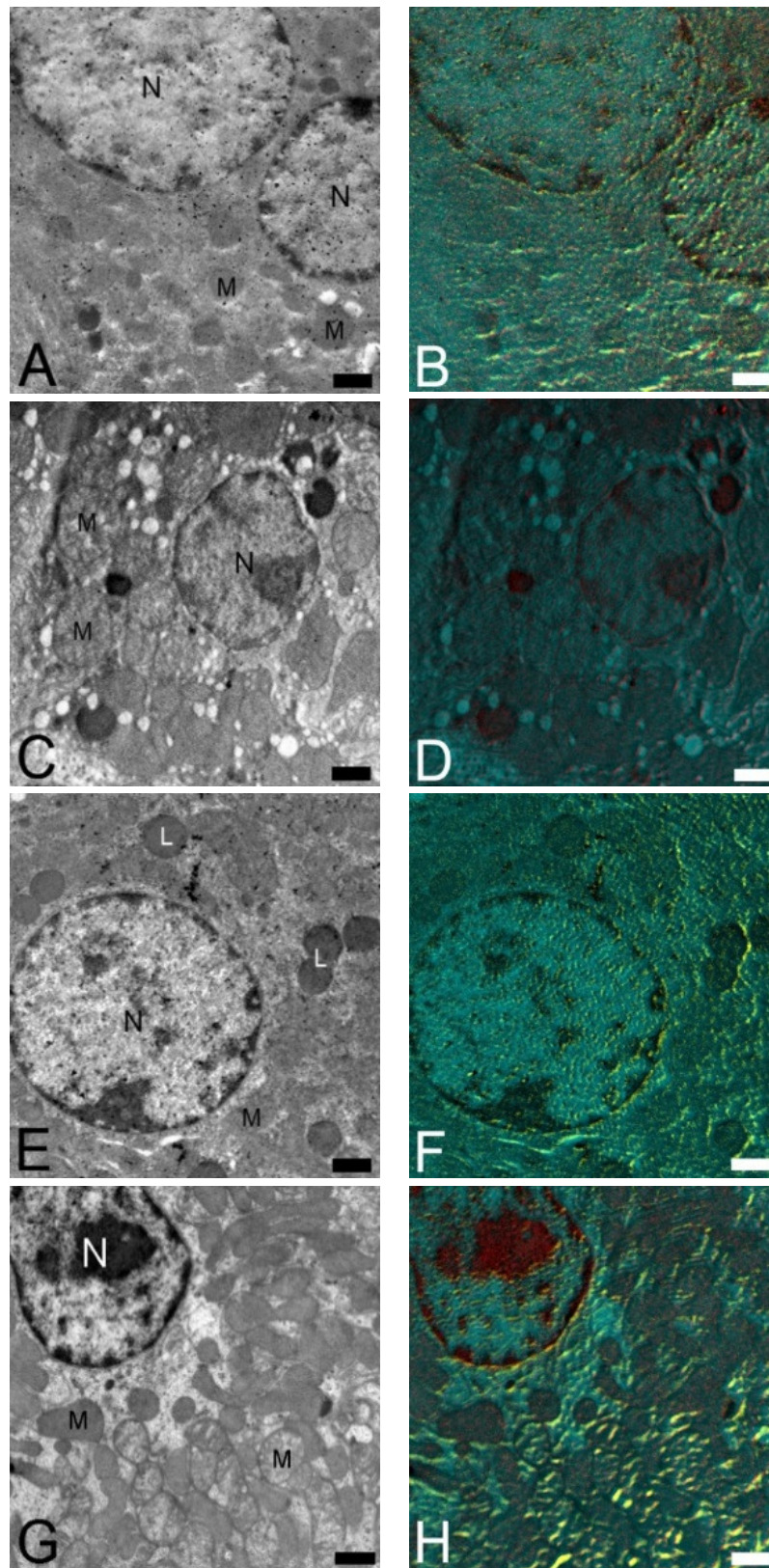
Figure 5.18: EFTEM micrographs of the PCT of the kidney of the control (A and B), Cd (C and D), Cr (E and F) and Cd and Cr (G and H). Figure A, C, E and G indicates the zero loss images of the colour maps in Figure B, D, F and H, with Cd in red and Cr in yellow. **Key:** N: Nucleus; M: Mitochondria; C: Capillary; E: Endothelial cell; Me: Mesangial cell; P: Podocyte; RBC: Red blood cell (Scale Bars: A–H: 1µm).
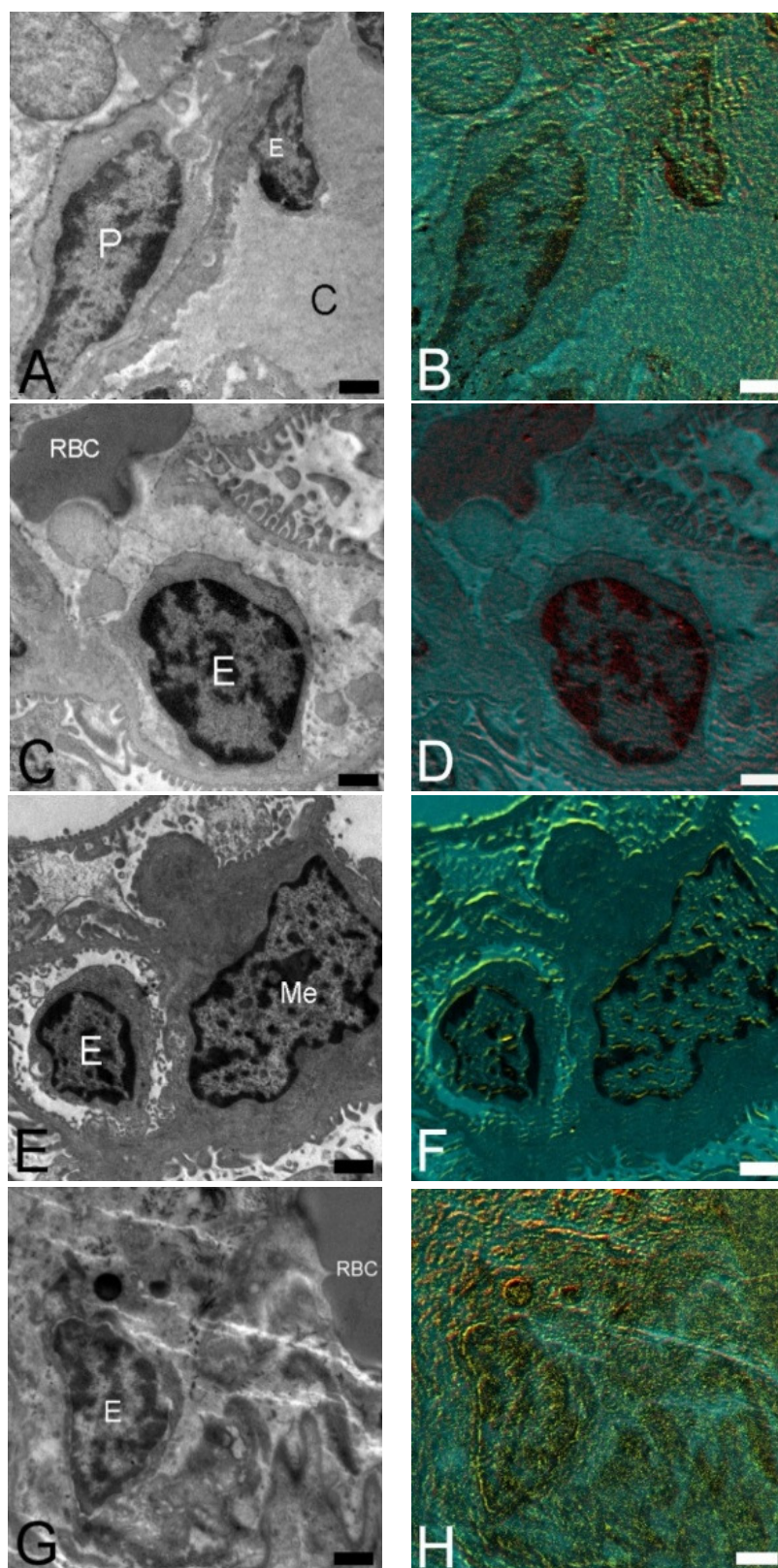
Figure 5.19: EFTEM micrographs of the glomeruli of the kidney of the control (A and B), Cd (C and D), Cr (E and F) and Cd and Cr (G and H). Figure A, C, E and G indicates the zero loss images of the colour maps in Figure B, D, E and H, with Cd in red and Cr in yellow. **Key:** N: Nucleus; M: Mitochondria; C: Capillary; E: Endothelial cell; P: Podocyte; RBC: Red blood cell (Scale Bars: A–H: 1µm).

Evaluation of the tissue with EELS and EFTEM, identified the bio-accumulation of Cd and Cr in the liver, pancreas and kidney, as can be seen in Figures 5.15 – 5.19, even though only minimal energy-loss signals were obtained in both the Cd and Cr groups, alone and in combination. The analysis of the control group showed a noisy signal that does not bio-accumulate specifically in any organelle (Fig. 5.15 – 5.19 B). With the Cd exposed groups, the EFTEM analysis revealed that Cd bio-accumulates not only in the organelles, but also on the membranes of the organelles (Fig. 5.15 – 5.19 D). Cr on the other hand mostly bio-accumulates on the membranes of the organelles (Fig. 5.15 – 5.19 F). This trend is also seen in the Cd and Cr group EFTEM analysis (Fig. 5.15 – 5.19 H).

5.3.5 *Effects of Cd and Cr alone and in combination on blood haemostasis*

Erythrocyte morphology
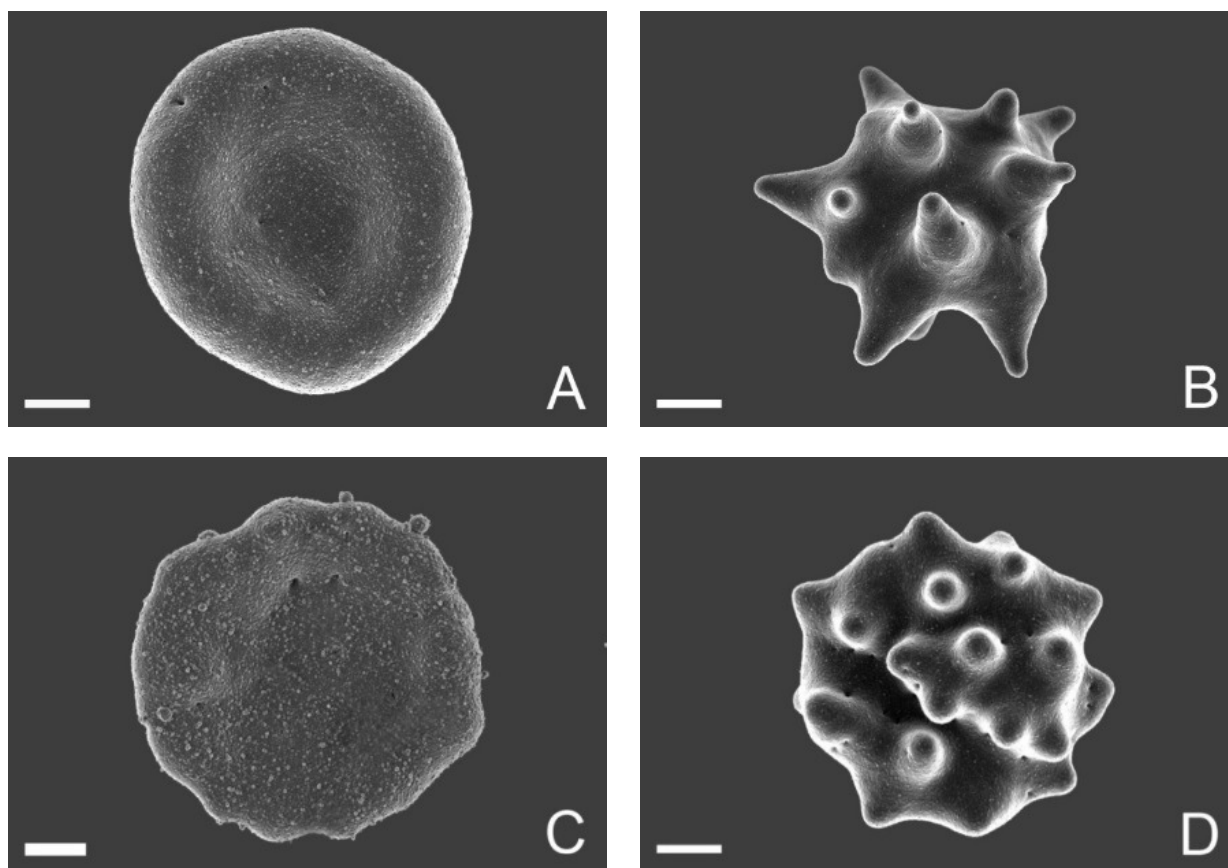
Figure 5.20: SEM micrographs of erythrocytes prepared from WB. In the control group (Fig. A) the normal erythrocyte concave morphology is visible, with leptocytes present in the Cr group (Fig, C) and echinocytes present in the Cd and metal combination groups, respectively (Fig. B and D) (Scale bars: 1µm).
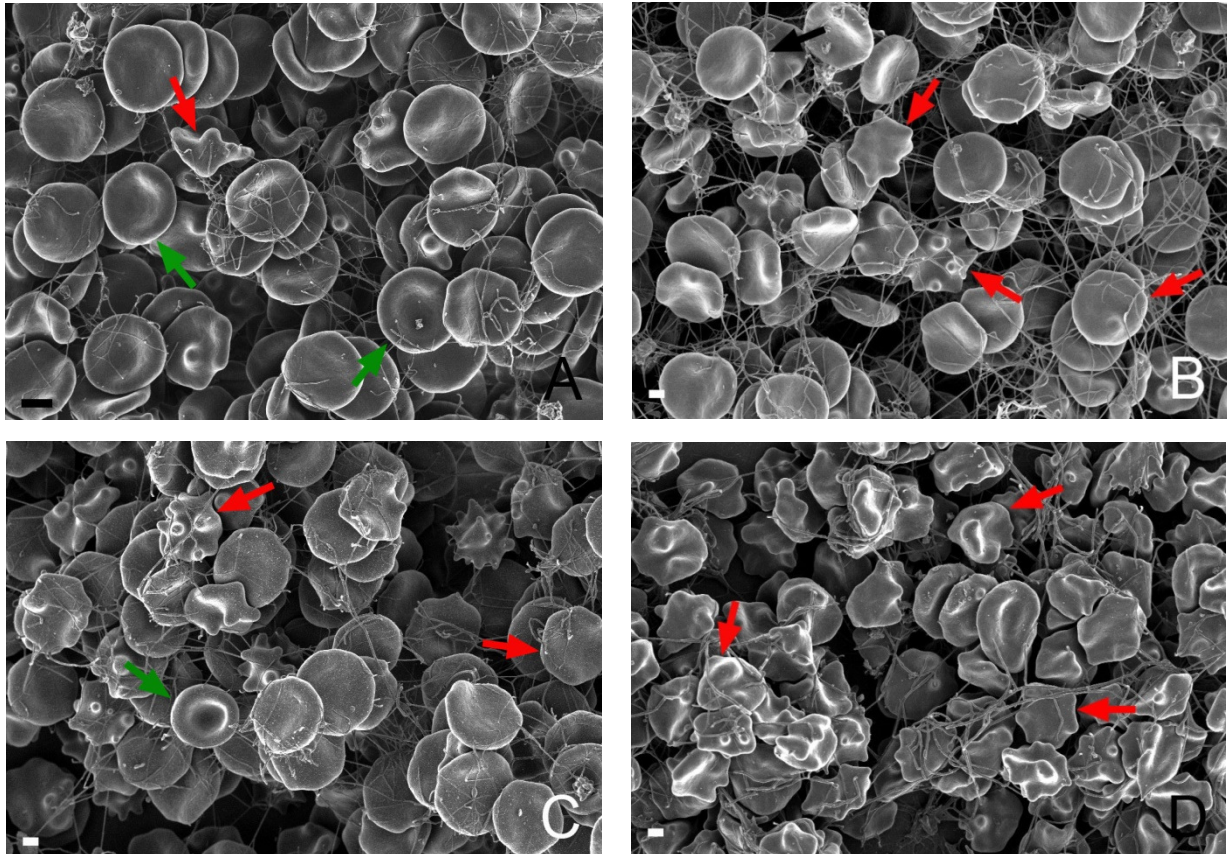
Figure 5.21: SEM micrographs of erythrocytes prepared from WB with added thrombin. Figure A represents the control group, with Figure B-D indicating the Cd, Cr and metal combination groups, respectively. Green arrows: Normal erythrocyte morphology; Red arrows: Variations in erythrocyte morphology (Scale bars: A: 2μm; B, C and D: 1μm).

Platelet morphology
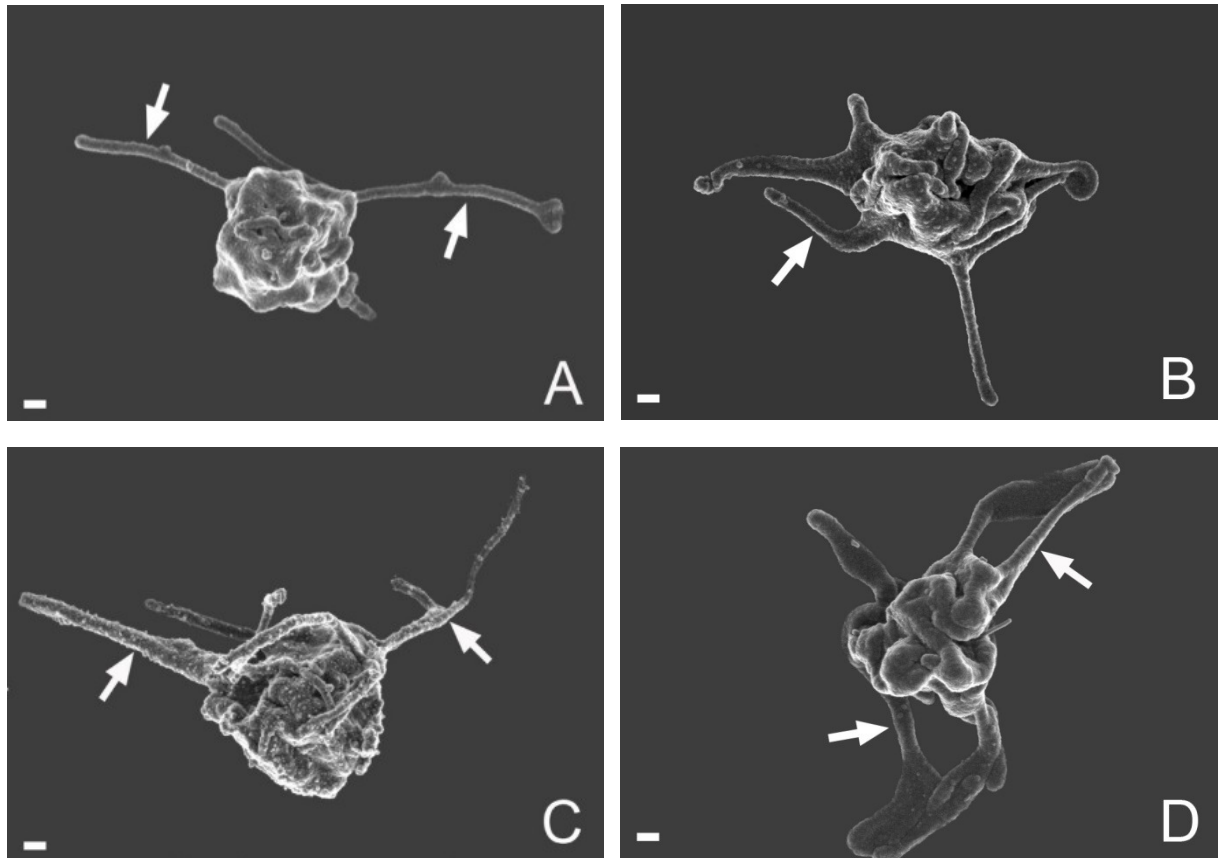
Figure 5.22: SEM micrographs of platelets prepared from PRP. Figure A is representative of the control group with the white arrows indicating pseudopodia. Figures B–D indicate the Cd, Cr and metal combination groups respectively, with the arrows indicating pseudopodia (Scale bars: 200nm).

Fibrin fibre morphology
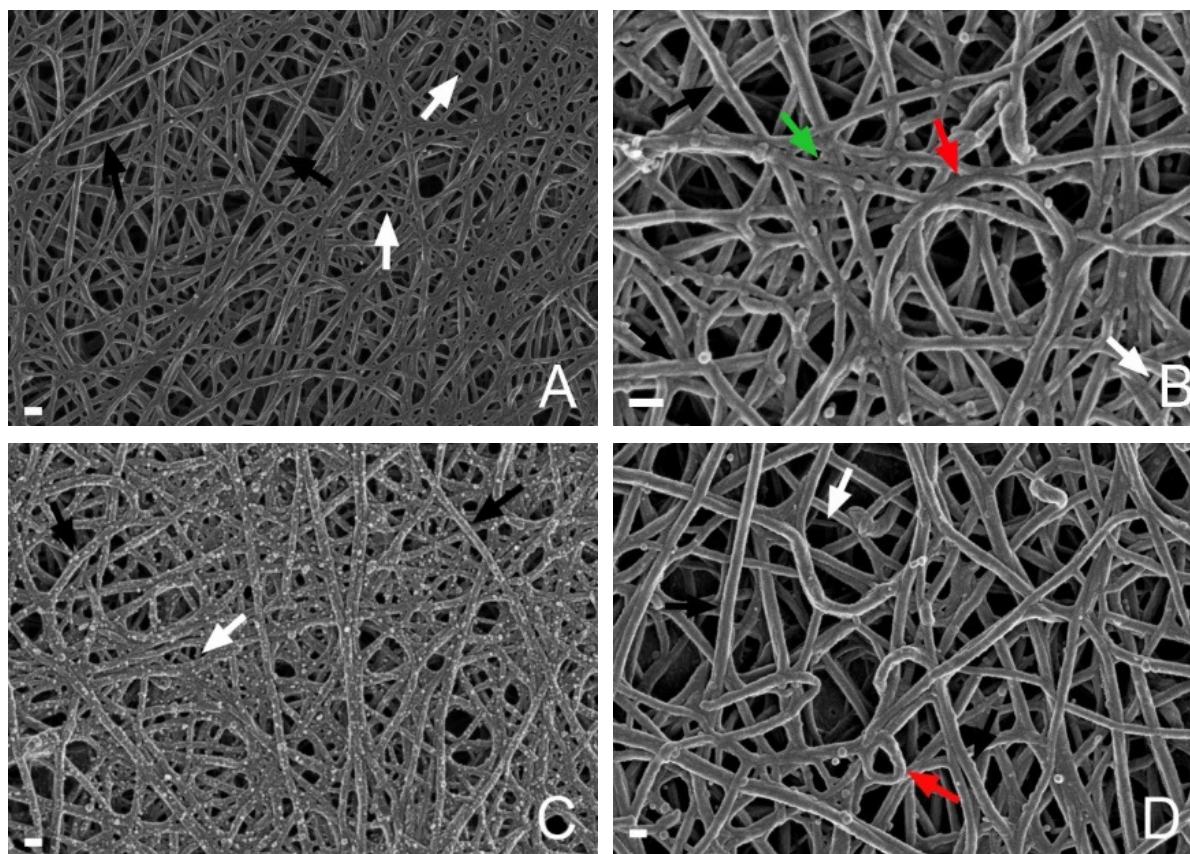
Figure 5.23: SEM of fibrin networks prepared from PRP with added thrombin. Figure A indicates the control group with thick major fibres and thin minor fibers. Figures B–D show the Cd, Cr and Cd and Cr groups, respectively. Black arrows: Thick major fibres. White arrows: Thin minor fibres. Red arrows: Bending, less taut fibres. Green arrow: Sticky mass of fibrin fibres (Scale bars: A–D: 200nm).

Due to unforeseen circumstances on the day of termination, blood was obtained from only one animal in the Cr group for SEM analysis. Therefore, although we commented on the results of the Cr group, these results are not representative of this group. In Figure 5.20 and 5.21 A, normal erythrocyte morphology can be seen, with minimal altered erythrocytes [Fig. 5.21 A (red arrow)] present in the control group. A variety of erythrocyte morphologies were present in the Cd, Cr and combination groups, including leptocytes (Fig. 5.20 and 5.21 C), echinocytes [Fig. 5.20 B and D and Fig. 5.21 B–D (red arrows)] and with the occasional spherocyte present in the blood. These erythrocyte morphologies were also observed in WB to which thrombin was added to induce clot formation. In the control blood the predominant erythrocyte type was the typical normal biconcave erythrocyte morphology with a few echinocytes being present. A thin regularly arranged fibrin network was present. In the blood of rats exposed to Cd the number of echinocytes had increased and the fibrin network is denser. Similar erythrocyte morphologies were observed in the Cr-exposed group although

the fibrin network was less dense. In the Cd and Cr combination group all erythrocytes had abnormal morphology and regions of erythrocyte clumping were observed while the fibrin network appeared sparse, although denser in some areas.

Platelet morphology in PRP was then evaluated. In Figure 5.22 A and C, the control and Cr groups, respectively, minimal changes to platelet shape and pseudopodia (arrows) were observed. Figure 5.22 B and D show an increase in activation in the Cd and metal combination groups (arrows). With the addition of thrombin to PRP, clot formation occurs and the characteristics of the fibrin network can be described and the thickness of the fibres can be measured. Figure 5.23 B and D shows less taut or bent fibres (red arrows) and dense net-like appearance of fibres (green arrow), with Figure 5.23 A and C showing mostly taut fibres, with a variety of thin and thick fibrin fibres (white and black arrows).
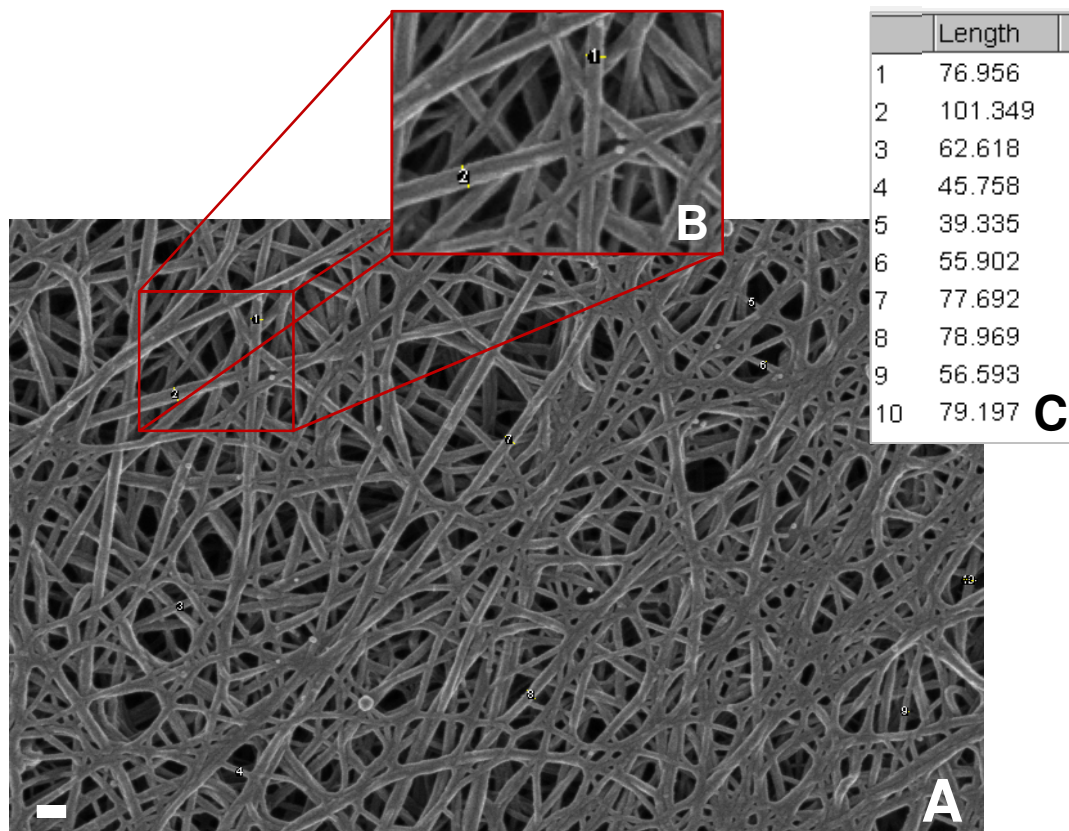
Figure 5.24: The method that was used to obtain the fibrin fibre measurements. Figure A shows a representative micrograph used for measurements, with Figure B an enlargement of an area to show how fiber lengths were measured. Figure C shows tabulated data of the measured fibrin fibres (Scale bar: 200nm).
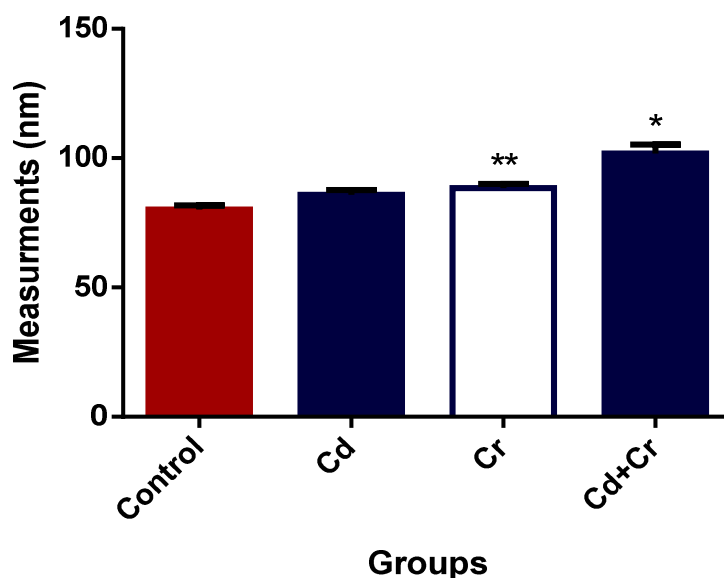
Figure 5.25: Fibrin fibre measurements of the controls and heavy metal groups. *Statistical significant, *p*-value: ≤0.05; **Not representative of entire group.

Figure 5.24 indicates the method used for the measurement of the fibrin networks using the ImageJ software. For the control and each experimental group, five random micrographs were selected and in each ten fibres were measured. Therefore in all groups except the Cr group, a total of 300 measurements per group were taken. Figure 5.25 shows the results obtained from the measurements of the fibrin fibre thickness, with the combination of Cd and Cr was significantly thicker compared to the control, as well as to the single metal groups. In Table 5.5 a summary of the effects of the metals on erythrocyte, platelet and fibrin fibre morphologies are provided.

Table 5.5: Summary of SEM analysis on erythrocytes, platelets and fibrin networks

	Erythrocytes		
	WB	**WB+T**	
Groups	**Altered erythrocyte morphology**	**Altered erythrocyte morphology**	**Changes due to interaction with fibrin fibres**
Control	+	+	+
Cd	++	++	+
Cr	+	++	-
Cd + Cr	++	++	++
	Platelets	**Fibrin network**	
	PRP	**PRP+T**	
Groups	**Altered platelet morphology**	**Altered fibre morphology**	**Dense net-like appearance present**
Control	+	+	+
Cd	++	+	++
Cr	+	+	+
Cd + Cr	++	++	++

-, none; +, minimal; ++, mild; +++, severe.

5.4 <u>Discussion</u>

The increase in heavy metal exposure is of great concern and the effects on the environment, animals and humans should be constantly evaluated (Al-Attar, 2011). Heavy metals, such as Cd and Cr, have the potential to alter cellular functions by catalysing the formation of radicals, inhibition of antioxidant enzymes and binding to antioxidant elements such as glutathione (GSH) that leads to oxidative stress. This results in increased lipid peroxidation, protein and DNA damage and apoptosis, that can lead to associated diseases such as hepatic necroinflammation, non-alcoholic steatohepatitis, fibroplasias, renal fibrosis and failure, and cancer (Bertin and Averbeck, 2006; García-Niño and Pedraza-Chaverrí, 2014; Jin*, et al.*, 2014; Khlifi*, et al.*, 2013; Sarkar*, et al.*, 2013; Thévenod and Lee, 2015; Venter*, et al.*, 2015).

Due to the high lipid content, membranous organelles are specific targets of damage. Therefore in all tissue the presence of cellular and mitochondrial membrane structure disruption was evaluated. Mitochondria act as osmometers in the cells and the mitochondrial swelling seen reflects the entry of solutions and water into the mitochondrial matrix (Thophon*, et al.*, 2004; Venter, 2015). The dilation of the rER can also be caused by the increase of water in the cells (Thophon*, et al.*, 2004; Venter, 2015). These effects may be due to changes in membrane permeability, either as a result of lipid and/or protein damage. Therefore the presence of mitochondrial inner matrix swelling and rER dilation was also evaluated.

In all experimental groups, some ultrastructural changes to the nucleus, mitochondria and rER were observed. In the combination group alterations to these organelles were increased, which indicate that the metals have a synergistic toxic effects where each metals different intracellular targets results in accumulative toxicity. Organ-specific changes were also seen in the components of the glomerular filtration barrier namely the pedicles and endothelial cells. Small amounts of the metals were found in the liver, pancreas and kidney tissue with the EELS and EFTEM analysis. Cd accumulated in the nucleus and mitochondria, where Cr was primarily found at the membranes of the nucleus, mitochondria and rER. Following a similar trend, the organ specific organelles also showed that Cd was found in the granules of the β-cells and zymogen granules of the acinar cells of the pancreas, with Cr accumulating on the membranes of these granules. The ultrastructural and bio-accumulation of the metals further confirms the morphological alterations seen in the histological analysis in Chapter 4.

Reactive oxygen species (ROS) are generated in several organelles including the ER and mitochondria. This occurs during normal cellular metabolism such as oxidative protein folding and mitochondrial respiration and this process is tightly regulated. ROS levels are regulated by the presence of antioxidant enzymes such as catalase, superoxide dismutase and glutathione peroxidase as well as antioxidant elements such as GSH and dietary antioxidants such as vitamins E and C. Cd and Cr toxicity affects certain components of the cellular antioxidant system and when in combination, these effects are accumulative (Venter*, et al.*, 2017).

Cd does not catalyse the Fenton reaction but binds intracellular thiols, like GSH and/or inhibits the activity of antioxidant enzymes such as catalase (Prozialeck and Edwards, 2012). Consequently levels of hydrogen peroxide (H_2O_2), superoxide anion ($O_2\bullet^-$) and hydroxyl radical ($\bullet OH$) are increased (Bertin and Averbeck, 2006; Jomova and Valko, 2011). ROS cause lipid membrane peroxidation as well as protein and DNA damage. Consequences of protein damage and lipid peroxidation are changes in membrane function and stability (Bertin and Averbeck, 2006). This is associated with changes in the morphology of membranous organelles such as the mitochondria as well as plasma and nuclear membranes. Cd was found to accumulate in the mitochondria and nuclei and in these intracellular compartments, Cd can bind membrane and DNA associated proteins thereby altering membrane integrity and function as well as DNA repair mechanisms (Bertin and Averbeck, 2006). This in turn can lead to cell cycle arrest, apoptosis, genome instability, and mutagenesis eventually leading to cancer (Bertin and Averbeck, 2006).

The biochemical pathway of Cr firstly involves the reduction of hexavalent Cr [Cr(VI)] to less toxic trivalent Cr [Cr(III)]. This is mediated by antioxidant elements like ascorbate, one of the most effective biological reductant of Cr(VI), and non-enzymatic reactions with cysteine and GSH. This reduction of Cr(VI) to Cr(III) comes with a price as it generates high levels of Cr-DNA adducts and mutations that leads to DNA damage (Jomova and Valko, 2011). This would affect the structure and function of both genomic and mitochondrial DNA. In addition, a tightly-regulated process of ROS formation occurs in the mitochondria and the ER. The accumulation of Cr, which is a catalyst of the Fenton reaction, will cause ROS homeostasis to be disrupted, resulting in increased lipid membrane peroxidation and altered protein processing, eventually leading to apoptosis. Cr toxicity also affects the mitogen-activated protein kinase (MAPK) signal transduction pathway, where nuclear factor kappa B (NF-κB), activating transcription factor 2 (ATF-2) and *p53* plays a role in regulating cellular processes, including apoptosis (Jomova and Valko, 2011; Venter*, et al.*, 2017).

In a previous *in ovo* study in our laboratory, we found that increasing concentrations of Cd and Cr caused increased organelle damage associated with the accumulation of Cd and Cr in the nuclei and mitochondria of the liver and kidney (Venter, 2015). Madejczyk, *et al.*, undertook a time-based study and found that with a single intraperitoneal injection there was accumulation of Cd and Cr in the liver. With time, metal levels decreased but ROS and cellular damage increased. This was associated with changes in the expression of genes associated with oxidative stress, metabolism, DNA damage, cell cycle and inflammatory responses (Madejczyk*, et al.*, 2015). The present chapter clearly shows that Cd and Cr accumulate in specific compartments such as the mitochondria, rER, nucleus and membranes directly involved with these processes (Venter*, et al.*, 2017).

The blood is an important component of the organs evaluated. Hepatocytes are in direct contact with the blood due to the presence of sinusoidal endothelium; fenestrated endothelium is part of the capillary tuft of the glomeruli as well as the endocrine part of the pancreas. In the coagulation system, the erythrocytes, platelets and fibrin fibres showed some ultrastructural alterations after exposure to Cd and Cr alone and in combination. Alterations in the morphology of erythrocytes were more prevalent in the metal-exposed groups than in the control group. Altered erythrocytes can occur in a variety of different erythrocyte shapes, that include, spherocytes (swollen, spherical erythrocytes), echinocytes (erythrocytes with regularly spaced short projections or spicules), knizocytes (elevated or elongated pinched area in the centre of the erythrocytes) and leptocytes (flattened erythrocytes) (Crosby, 1952; Swanepoel and Pretorius, 2012). The majority of altered erythrocyte morphologies observed in this study were echinocytes and leptocytes. These type of shape changes occur due to oxidative stress, generated by both Cd and Cr as described above (Lupescu*, et al.*, 2012; Sopjani*, et al.*, 2008). The lifespan of an erythrocyte is approximately 120 days, which is partly governed by its ability to maintain its biconcave shape. With altered erythrocyte morphologies, as seen in this study, its lifespan is reduced and these erythrocytes are either removed by phagocytosis or destroyed by haemolysis in the spleen (Kierszenbaum and Tres, 2012; Young*, et al.*, 2006).

The oxidative stress produced by the heavy metals Cd and Cr not only influence the erythrocyte morphology, but also play a role in the activation of the platelets and thus also influence the fibrin fibre morphology. This is due to the fact that platelets are involved in fibrin formation and tautness, thus the bent fibres seen in the fibrin networks of the Cd and metal combination groups might be due to the platelet functional changes or lack of thrombin production as ROS has been shown to induce platelet activation (Van Rooy*, et al.*, 2015). Another possibility might be that due to the functional changes of the liver after exposure to

Cd and Cr alone and in combination, fibrinogen, which is synthesized in the liver, is also affected and thus causes changes in the fibrin production (Tennent, *et al.*, 2007). The significant increase in fibre thickness in the combination group will further contribute to altered erythrocyte morphology and clot formation, as it might cause a reduction in the lysis of the clots (Swanepoel, *et al.*, 2016b).

5.5 <u>Conclusion</u>

Exposure to Cd and Cr alone and in combination causes changes in the ultrastructure of several organelles of the liver, pancreas and kidney tissue of the experimental animals. Metal bio-accumulation was observed in the nucleus, mitochondria and rER of the liver, pancreas and kidney, as well as in the β-cell granules and zymogen granules of the pancreas. The erythrocytes, platelets and fibrin network formation were also adversely affected by Cd and Cr alone and in combination in the blood. The consequence of exposure can be organ dysfunction and possibly the development of diseases such as diabetes, cancer and stroke (Lang, *et al.*, 2012a; Pretorius, *et al.*, 2015; Venter, *et al.*, 2017).

Chapter 6

Effect of Cd and Cr alone and in combination on the human coagulation system using an *ex vivo* blood model

6.1 Introduction

Haemostasis is important to ensure the recovery of injured blood vessels and to prevent excessive blood loss. Furthermore, haemostasis must be carefully controlled to prevent the formation of occlusive thrombi in blood vessels (Smith, 2009) that may lead to, for example, stroke (Zhang*, et al.*, 2015). The classic coagulation pathway excludes the importance of cellular components in the coagulation system and thus a new cell-based model has been introduced that includes platelets and tissue factor expressing cells. The phases of the cell-based coagulation pathway include initiation, amplification and propagation, which contribute to the formation of the clot, with platelets playing a crucial role in this process (Pérez-Gómez and Bover, 2007; Smith, 2009; Van Rooy, 2015). Platelets are involved in the release of certain factors and enzymes that contribute to clot formation and the tautness of the fibrin fibres (Pérez-Gómez and Bover, 2007; Van Rooy, 2015). The formed thrombus consists of platelets, fibrin fibres and erythrocytes that determine the structure and integrity of the clot.

Erythrocytes undergo eryptosis, and characteristic features of this process are cell membrane shrinkage as well as blebbing and membrane scrambling (Föller*, et al.*, 2008; Lang*, et al.*, 2010; Lang*, et al.*, 2012b; Lang and Qadri, 2012; Mischitelli*, et al.*, 2016; Pretorius*, et al.*, 2016a; Pretorius*, et al.*, 2014). During clot formation erythrocytes assist in bringing platelets to the surface of an injured vessel wall and binding inflammatory mediators to surface receptors (Pretorius and Kell, 2014). Other cells that are involved in clot formation are the leukocytes consisting of neutrophils, monocytes, lymphocytes, basophils and eosinophils (Gorbet and Sefton, 2004), of which only the neutrophils and monocytes play a major role in the inflammatory response of the body. The function of leukocytes during coagulation include changes in the expression of membrane receptors, release of inflammatory mediators, releases of oxidants like hydrogen peroxide (H_2O_2) and superoxide anion ($O_2^{\bullet-}$) and when leukocytes associate with platelets it may lead to mutual activation and protection from inhibitors (Gorbet and Sefton, 2004).

Platelets and the fibrin network play an important role in the formation and stability of haemostasis. Platelet activation induces shape changes and aggregation that also leads to fibrin formation. Fibrin formation is the final step in blood coagulation and is necessary for clot stability. Fibrin formation is catalysed by thrombin, as it converts fibrinogen to fibrin

(Swanepoel*, et al.*, 2015; Van Rooy and Pretorius, 2015). Changes to the morphology of erythrocytes, platelet activation and fibrin fibre thickness, caused by exposure to various substances, like smoking, heavy metals, carbon monoxide, sulfur dioxide and certain diseases may alter the haemostatic process leading to the formation of pathological thrombi (Ambrose and Barua, 2004; Hoek*, et al.*, 2001; Lang*, et al.*, 2012a; Pretorius*, et al.*, 2015; Pretorius*, et al.*, 2014; Swanepoel*, et al.*, 2016a; Van Rooy and Pretorius, 2015).

Environmental exposure to heavy metals via water, food and air pollution due to agriculture, mining, transport and related operations as well as cigarette smoking, a major non-occupational source of metals such as cadmium (Cd) and chrome (Cr), are increasing (Langárd and Costa, 2007; Prozialeck and Edwards, 2012). These heavy metals have the potential to adversely affect blood haemostasis especially of people living close to high-risk areas (Venter, 2015). Exposure is usually not to a single metal but as a mixture of metals (Venter, 2015). Therefore, the aim of this chapter was to determine, using an *ex vivo* blood coagulation model, the effects of Cd and Cr alone and in combination on the morphology of erythrocytes, platelet activation and fibrin fibre thickness.

6.2   Materials and methods

6.2.1 *Ex vivo model*

Human blood was collected from six healthy, consenting donors by a trained phlebotomist (Health Sciences Research Ethics Committee number: 111/2016). Healthy male individuals over the age of 18 years, who were non-smokers, not taking chronic medication, and who did not have any inflammatory conditions were permitted to participate in the study.

6.2.2 *Scanning electron microscopy*

Scanning electron microscopy (SEM) was used to study the erythrocyte, platelet and fibrin fibre morphology as described in Chapter 5. The micrographs of fibrin networks were used to analyse fibrin fibre thickness as described in Chapter 5. For morphological analysis whole blood (WB) and platelet-rich plasma (PRP) was used (Van Rooy*, et al.*, 2015). Human blood was collected in citrate tubes and 900µℓ of WB was transferred into an Eppendorf tube and exposed to 100µℓ of 48mg/ℓ cadmium chloride ($CdCl_2$) [Merck (Pty) Ltd, SA] and/or 1450mg/ℓ potassium dichromate ($K_2Cr_2O_7$) [Merck (Pty) Ltd, SA]. The metal concentrations were made up in isotonic phosphate buffered saline (*iso*PBS; pH 7.4). The final osmolality of all solutions were less than 300mOsm to ensure any observed effects were directly due to metal toxicity. The final exposure concentrations were 4.8mg/ℓ for Cd (26µM) and 145mg/ℓ

for (985µM) for Cr(VI) (W.H.O, 2011). These concentrations where chosen based on the World Health Organization (WHO) acceptable water limits (mg/ℓ) for Cd and Cr times 1000 (W.H.O, 2011). Both Cd and Cr are at ratios that are representative of these established limits. By using a 1000 times higher concentration and short exposure times, specific cellular targets can be identified which later can be evaluated in models of chronic exposure. The control blood was exposed to *iso*PBS.

The whole blood was exposed for 10 minutes, before 10µℓ of WB was placed on a 10mm coverslip (Leica SA), with and without the addition of 5µℓ of human thrombin (20U/mℓ; South African National Blood Service). The WB was then centrifuged at 227xg for 10 minutes to obtain PRP; whereafter 10µℓ of the PRP was placed on coverslips, with and without 5µℓ of thrombin. All coverslips were further processed and the blood was analysed as described in Chapter 5.

6.2.3 *Confocal laser scanning microscopy*

The confocal laser scanning microscopy (CLSM) was used to detect phosphatidylserine (PS), a marker of eryptosis, on the erythrocyte membrane. The blood was collected in citrate tubes and exposed to *iso*PBS and the metals, as described above. Melittin (GenScript, New Jersey, USA), an apoptosis-inducing peptide was used as the positive control (Han*, et al.*, 2009; Park and Lee, 2010; Park*, et al.*, 2010). Erythrocytes were exposed to Melittin for four hours. The blood was then centrifuged at 145xg for ten minutes at room temperature to isolate the erythrocytes. The supernatant was removed and the remaining erythrocyte pellet was washed twice with 0.075M PBS (pH 7.4) for 3 minutes. The blood was then washed with the Annexin-V binding buffer (BioLegend, 422201) also for 3 minutes. A volume of 5µℓ of the Annexin-V probe (BioLegend, 640906) was added to the binding buffer and incubated at room temperature, protected from light, for 90 minutes. After incubation the samples were washed again as described with the phosphate and binding buffers, to remove any unbound antibodies. Of the prepared sample, 10µℓ was mounted on a glass slide and mounted with a coverslip (Leica SA). The sample was viewed with the Zeiss LSM 880 confocal laser scanning microscope in Airyscan mode (Carl Zeiss Microscopy, Munich, Germany).

To visualize the erythrocytes, two different lasers were used with different filters and beam splitters, to allow the overlaying of the respective images to show which erythrocytes have a PS flip present on the membrane. For the auto-fluorescence of all the cells present on the slide, the 405nm laser was used to excite naturally occurring fluorescence found in erythrocytes and a red colour was assigned to this fluorescent signal. In an unstained sample, the 405nm laser was used together with the 465nm–505nm band pass (BP) and

525nm long pass (LP) filters and the 488nm/405nm beam splitters. These settings showed that all the erythrocytes present on the slide has auto-fluorescence, and this auto-fluorescence could therefore be used as a contrasting method against the Annexin-V binding, in the case where PS flip is present. To visualize Annexin-V binding (excitation wavelength: 494nm and emission wavelength: 518nm), the 488nm laser was used with the 420nm–480nm/495nm–550nm BP filters and the 488nm/405nm beam splitters, and showed a green fluorescence, indicating the presence of a PS flip on the erythrocyte membranes.

6.2.4 *Viscoelastic analysis*

TEG® is an analytic method by which the viscoelastic changes that occur during coagulation and fibrinolysis are measured. The results from the blood samples are generated by the TEG® through a rotating pin, which constantly measures the resistance of the forming clot on the pin, that indicates a number of characteristics of the coagulation system such as the speed and strength of clot formation (Larsen*, et al.*, 2010; Shin and Kim, 2015; Wiinberg*, et al.*, 2005). The results are displayed as a graph that gives various measurements of the parameters that are listed in Table 6.1. For this part of the study, blood was collected in citrate tubes and exposed, as described above, after which 340µℓ of the WB was placed in a cup of the TEG® (TEG® 5000 computer-controlled device, Haemoscope Crop., Niles, IL, USA), together with 20µℓ of 0.2M calcium chloride ($CaCl_2$) to activate the coagulation process (Van Rooy*, et al.*, 2015). The process was allowed to run until maximal amplitude (MA) was reached, since only the rate and strength of clot formation was relevant to this study.

Table 6.1: TEG® parameters typically generated for whole blood (modified from: Kell and Pretorius, 2016)

Thromboplastic parameters	Description
R: Reaction time	Time of latency from start of test to initial fibrin formation (amplitude of 2mm); i.e. initiation time
K: Kinetics	Time taken to achieve a certain level of clot strength (amplitude of 20mm); i.e. amplification
Angle: Slope between the traces represented by R and K	The angle measures the speed at which fibrin build up and cross linking takes place, hence assesses the rate of clot formation; i.e. thrombin burst
MA: Maximal amplitude	Maximum strength/stiffness of clot. Reflects the ultimate strength of the fibrin clot, i.e. overall stability of the clot
MRTG: Maximum rate of thrombus generation	The maximum velocity of clot growth observed or maximum rate of thrombus generation using G, where G is the elastic modulus strength of the thrombus in dynes per cm^2
TMRTG: Time to maximum rate of thrombus generation	The time interval observed before the maximum speed of the clot growth
TTG: Total thrombus generation	The clot strength: the amount of total resistance (to movement of the cup and pin) generated during clot formation. This is the total area under the velocity curve during clot growth, representing the amount of clot strength generated during clot growth

6.2.5 *Statistical analysis*

Statistical analysis of the SEM fibrin fibre thickness and TEG® parameters were performed on GraphPad Prism Version 6.01 using one-way analysis of variance (ANOVA) and Tukey's multiple comparisons test, where a *p*-value of ≤0.05 was considered to be significant.

6.3 <u>Results</u>

6.3.1 *Effects of Cd and Cr alone and in combination of blood haemostasis: Erythrocyte morphology*
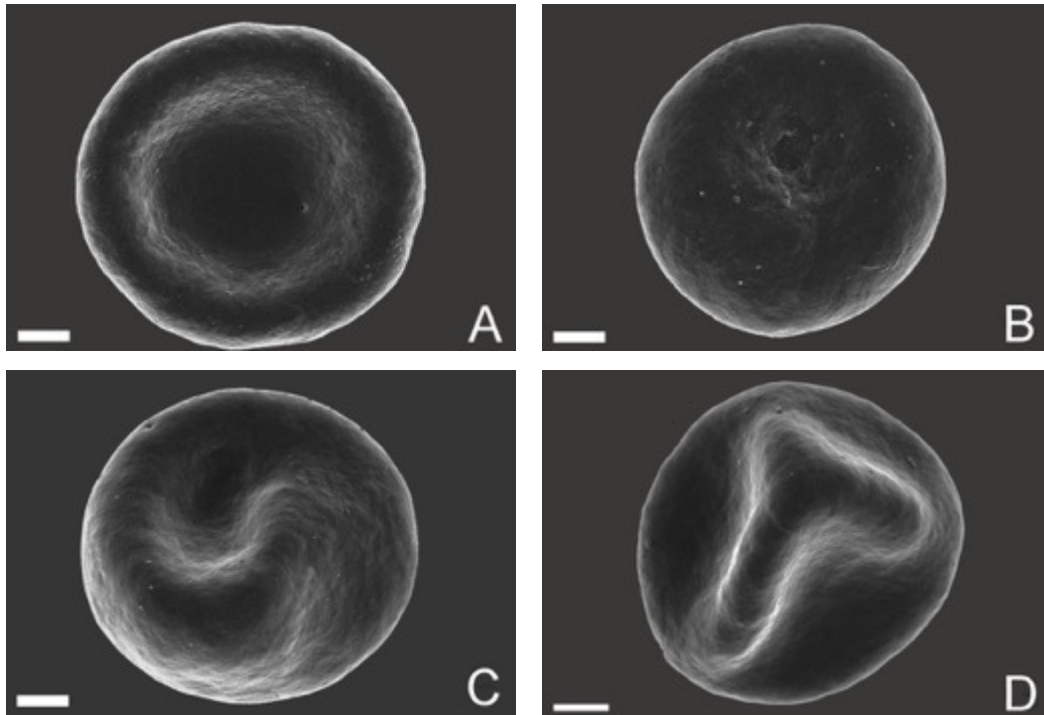
Figure 6.1: Representative SEM micrographs of erythrocytes of the control and metal exposed groups. Figure A (control) shows the normal concaved morphology of an erythrocyte, with Figures B (Cd), C (Cr), and D (Cd and Cr) showing the changes that occurred after metal exposure (Scale bars: 1µm).
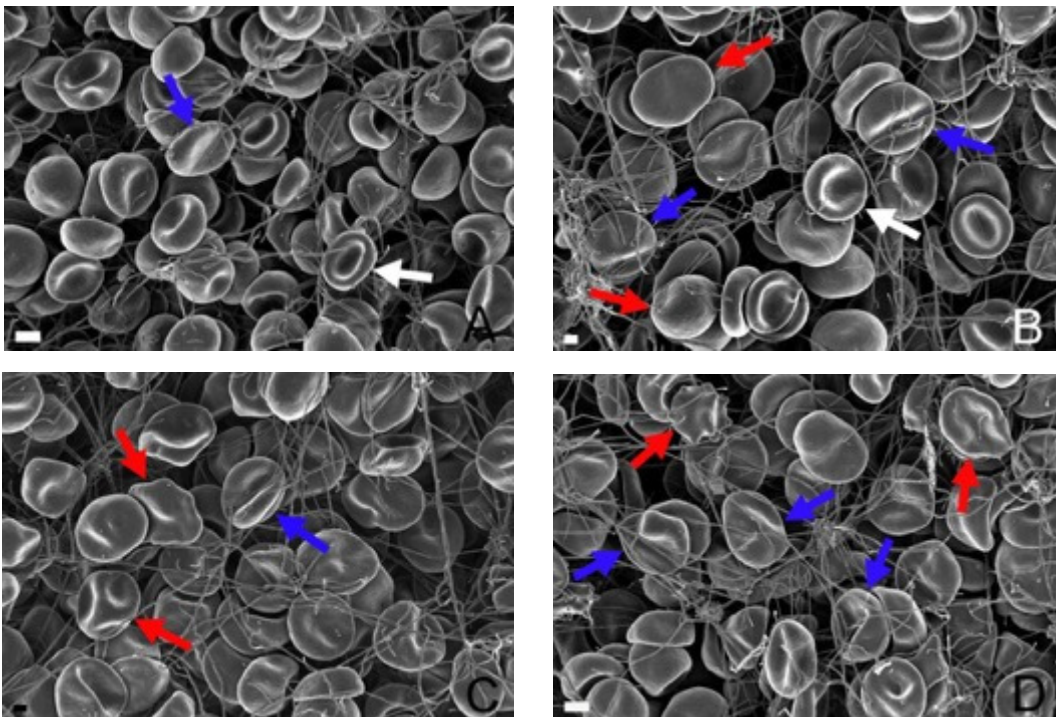
Figure 6.2: Representative SEM micrographs of WB with thrombin of the control and metal exposed groups. Figures A (control), B (Cd), C (Cr) and D (Cd and Cr) indicate the erythrocyte and fibrin fibre interactions. **Key:** White arrow: Normal erythrocytes; Red arrow: Variations in erythrocyte morphology; Blue arrows: Interactions between erythrocytes and fibrin fibres (Scale bars: B and C: 1µm; A and D: 2µm).

6.3.2 *Effects of Cd and Cr alone and in combination of blood haemostasis: Platelet morphology*
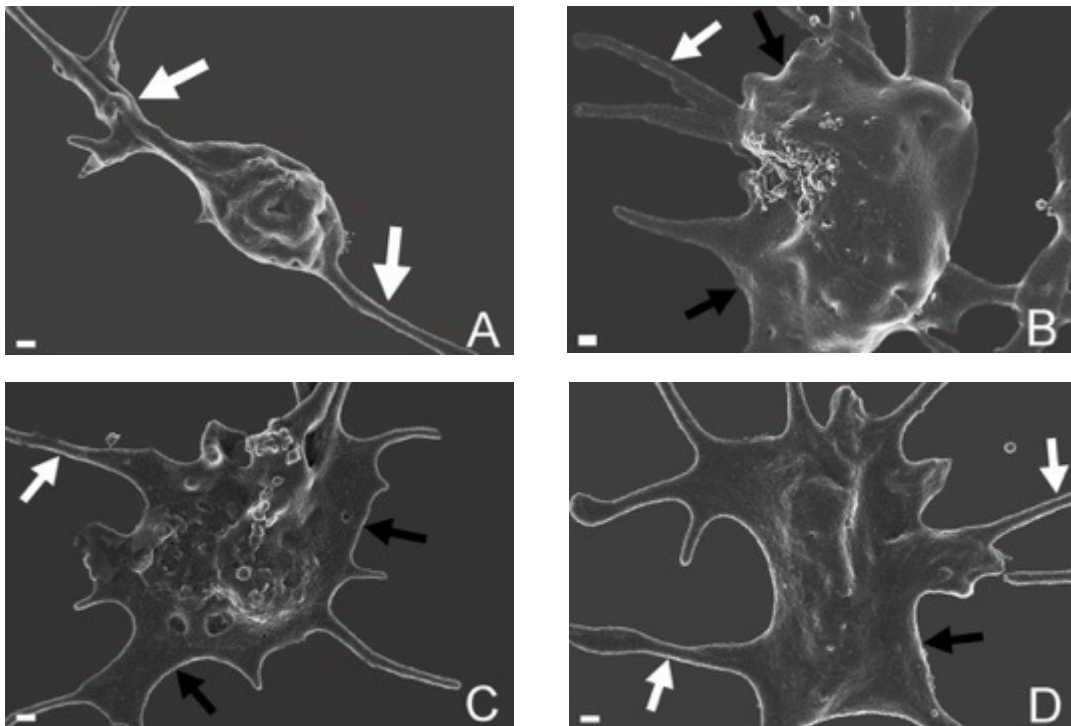
Figure 6.3: Representative SEM micrographs of platelets from the control and metal groups. Figure A shows a typical control platelet with pseudopodia and Figures B (Cd), C (Cr) and D (Cd and Cr), indicating both pseudopodia and membrane spreading. **Key:** White arrows: Pseudopodia; Black arrows: Membrane spreading (Scale bars: 200nm).

6.3.3 *Effects of Cd and Cr alone and in combination of blood haemostasis: Fibrin network morphology*
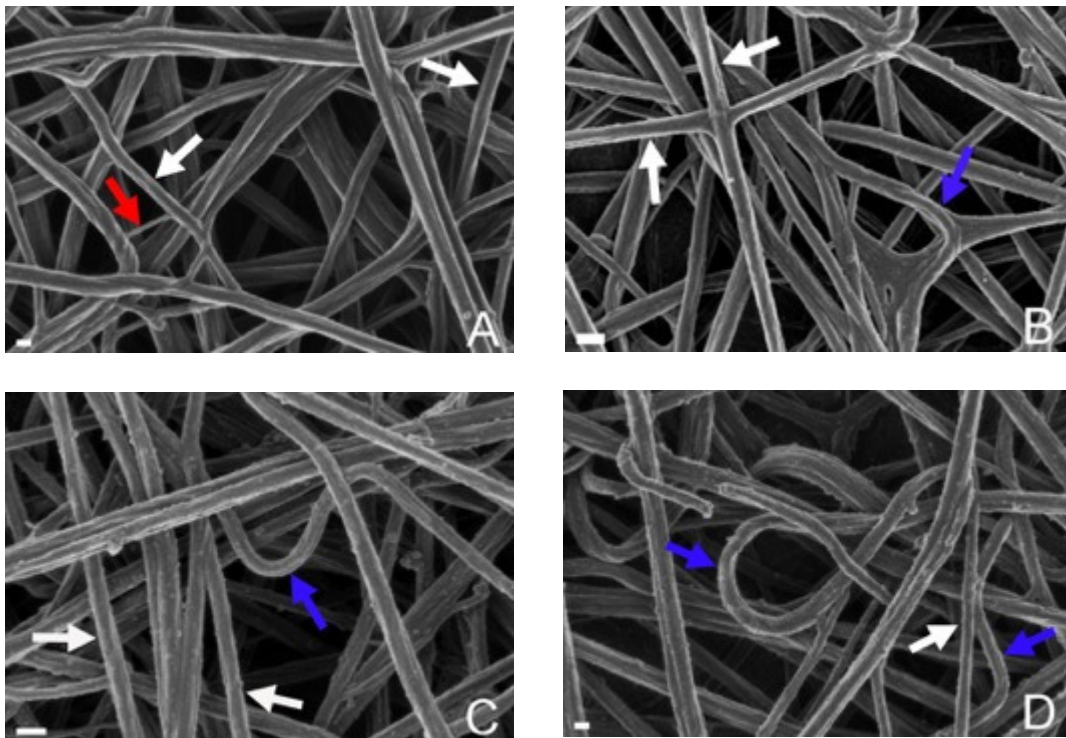
Figure 6.4: Representative SEM micrographs of the fibrin networks of the control and metal groups. Figure A (control) shows a combination of thick and thin fibres, with Figures B (Cd), C (Cr) and D (Cd and Cr) indicating the changes observed after metal exposure. **Key:** White arrow: Major thick fibre; Red arrow: Minor thin fibre; Blue arrow: Bent/loose fibre (Scale bars: A and D: 100nm; B and C: 200nm).

The effects of Cd and Cr alone and in combination as a single, acute exposure were evaluated. The effects on erythrocytes, platelets and fibrin network formation were evaluated. In Figure 6.1 A normal erythrocyte morphology is seen, with minimal eryptotic erythrocytes present in the control group. A variety of erythrocyte morphologies were present in the Cd, Cr, and Cd and Cr groups, including spherocytes (Fig. 6.1 B and C), echinocytes and knizocytes (Fig. 6.1 B, C and D respectively). Figure 6.2 illustrates the effects of the metals on the entire coagulation system, which shows the interactions between the erythrocytes and fibrin fibres. Figure 6.2 A shows the normal erythrocyte morphology with minimal fibre interaction. The erythrocyte morphology of the metal groups shows an increase in changes, e.g. spherocytes, echinocytes and knizocytes, in conjunction with the changes that occurred with the interactions between the erythrocytes and fibrin fibres [Fig. 6.2 B, C and D (blue arrows)].

Figure 6.3 A is representative of the control group, with minimal platelet shape changes and pseudopodia (white arrows). Minor activation is expected as contact activation will occur with the preparation of the sample. Figures 6.3 B (Cd), C (Cr) and D (Cd and Cr) show activated platelets in all the metal exposed groups, with pseudopodia (white arrows) and platelet spreading (black arrows). There also appeared to be an increase in the occurrence of membrane alterations, i.e. granular appearing membranes, visible in the experimental groups. The fibrin networks generated by these platelets were then evaluated. In Figure 6.4 A, mostly taut, straight fibres, with a combination of thin and thick fibrin fibres, typically of a control fibrin network (red and white arrows) were observed. For Cd and Cr alone and in combination (Fig. 6.4 B, C and D) fibres were less taut or bent (blue arrows). Table 6.2 summarises the effects of the metals on the coagulation system.

Table 6.2: Summary of SEM analysis on erythrocytes, platelets and fibrin networks

	Erythrocytes			
	WB		WB+T	
Groups	Altered erythrocyte morphology	Membrane disruption	Altered erythrocyte morphology	Changes due to interaction with fibrin fibres
Control	++	+	++	+
Cd	+++	++	+++	++
Cr	+++	+	+++	++
Cd + Cr	+++	+	+++	++
	Platelets		Fibrin network	
	PRP		PRP+T	
Groups	Altered platelet morphology	Membrane disruption	Altered fibre morphology	Dense net-like appearance present
Control	++	+	+	+
Cd	++++	++	++	+
Cr	++++	++	++	+
Cd + Cr	++++	+++	++	++

+, no or minimal change occurred; ++, some cell or fibre changes were visible; +++, most cells or fibres were altered;

++++, all cells or fibres were altered. WB+T: Whole blood with thrombin; PRP+T: Platelet rich plasma with thrombin.

6.3.4   *Fibrin fibre measurements*
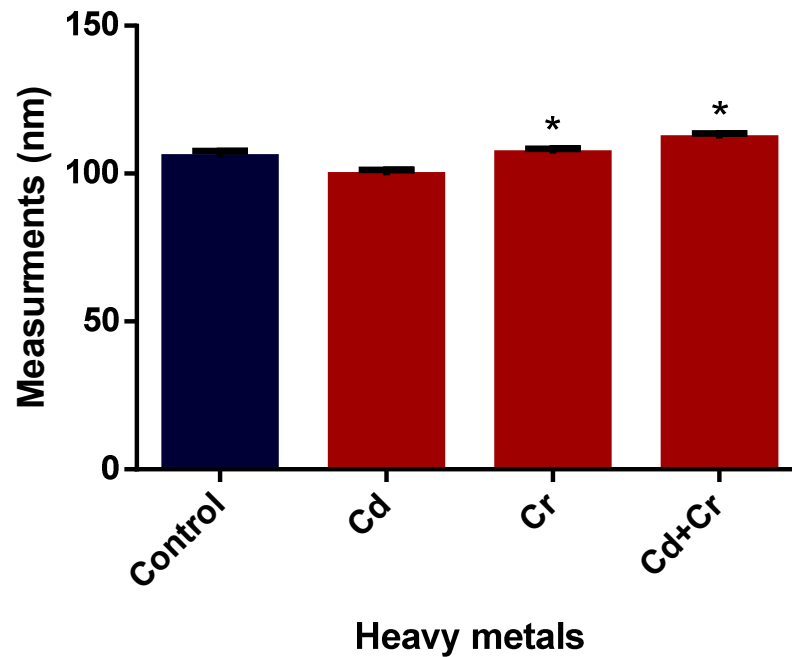
Figure 6.5: Fibrin fibre diameter measurements. *Statistically significant compared to Cd; *p*-value of ≤0.05.

The thickness of the fibres were also quantified (Fig. 6.5). Fibres generated following exposure to Cd were not statically different from the control while the fibres from the Cr as well as the Cd and Cr groups were significantly thicker than the Cd exposed group (Fig. 6.5).

6.3.5 Evaluation of the presence of phosphatidylserine on the erythrocyte membranes
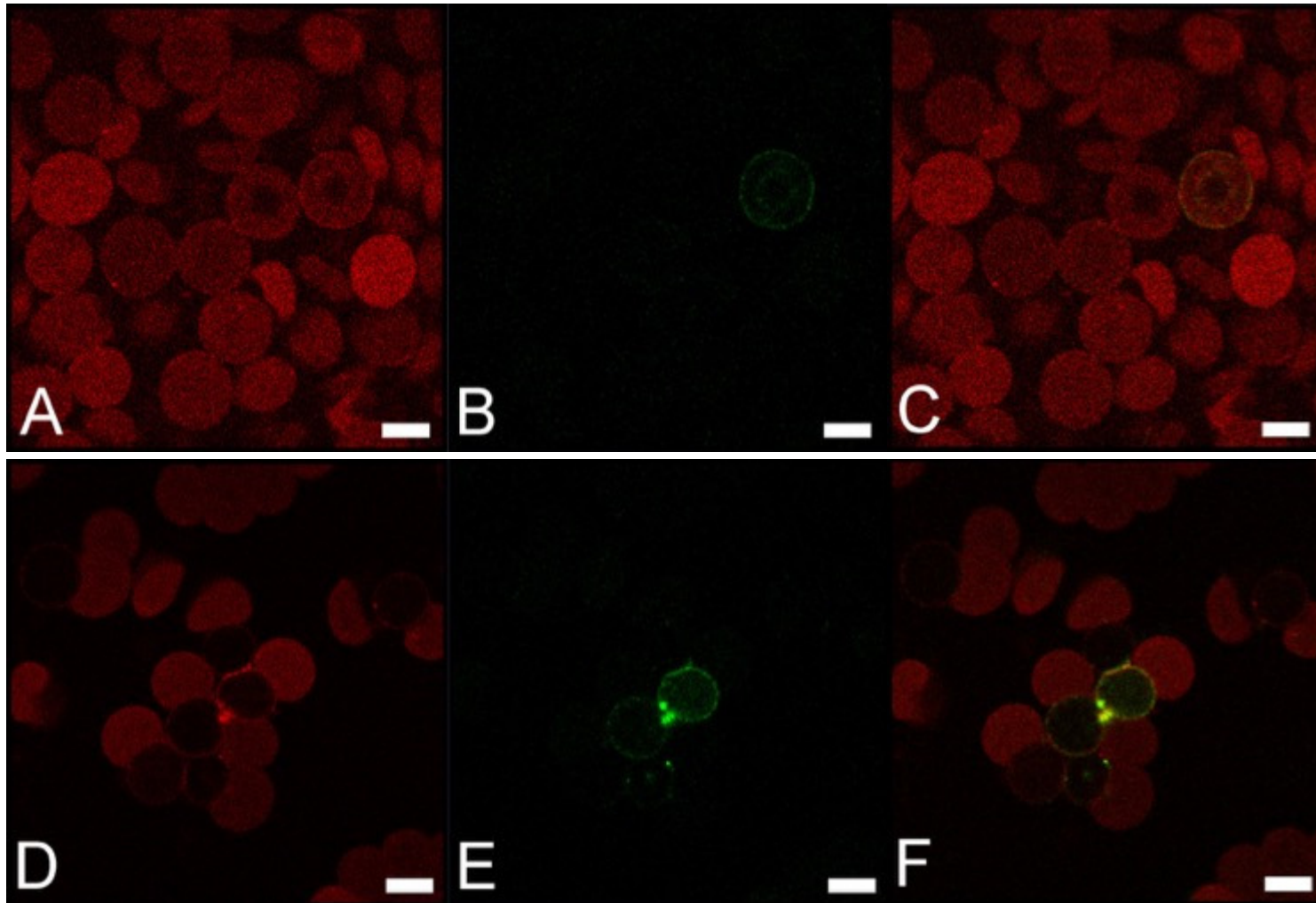
Figure 6.6: CLSM micrographs of the negative control (A–C) and positive control exposed to Melittin (D–F). Figures A and D showing the auto-fluorescence of the erythrocytes, B and E indicating the Annexin-V signal obtained and C and F showing the overlay images (Scale bars: 5µm).
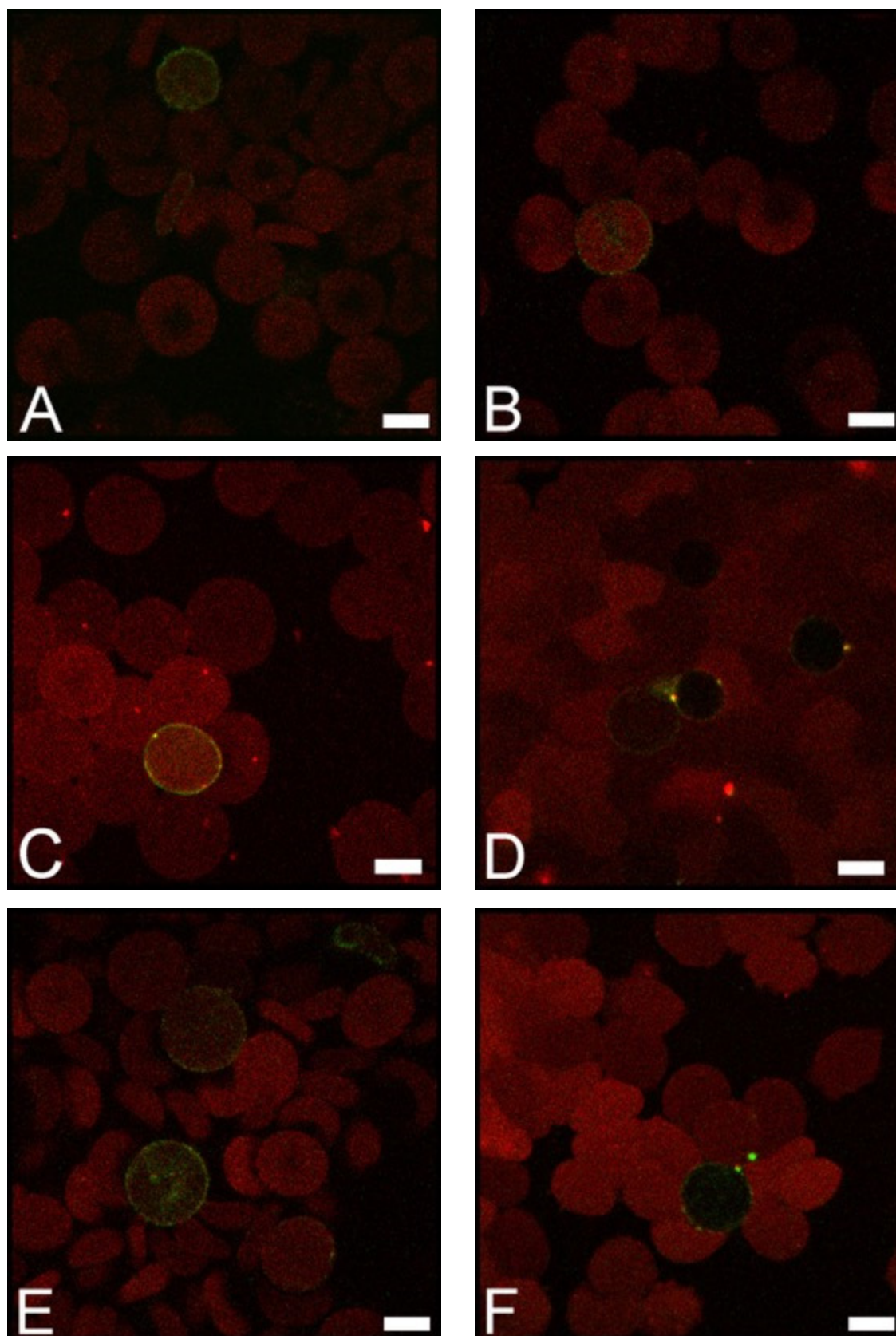
Figure 6.7: PS exposure evaluation of erythrocytes after exposure to the heavy metals Cd and Cr alone and in combination using the CLSM. Figures A–F indicate the Annexin-V positive erythrocytes after exposure to Cd (A and B), Cr (C and D) and Cd and Cr (E and F) (Scale bars: 5µm).

Using Melittin as a positive control, the ability of Cd and Cr alone and in combination was evaluated. In the negative control group, minimal, but expected, positive Annexin-V signal was obtained (Fig. 6.6 A–C). The positive control`s (Fig. 6.6 D–F) Annexin-V positive signal was noticeably higher than the signal that was obtained in the negative control and metal exposed groups. Figures 6.7 A–F are examples of the type of Annexin-V positive signal that was obtained in all the metal exposed groups. PS flip positive cells were scattered throughout the samples. The occurrence of the Annexin-V PS exposure signals seemed to be slightly increased in the metal combination groups, than in the Cd and Cr groups alone. The Annexin-V signal was present mainly in the spherocytes and not the echinocytes (Fig. 6.7 A–F, green fluorescence).

6.3.6 *Evaluation of the viscoelasticity of the blood*
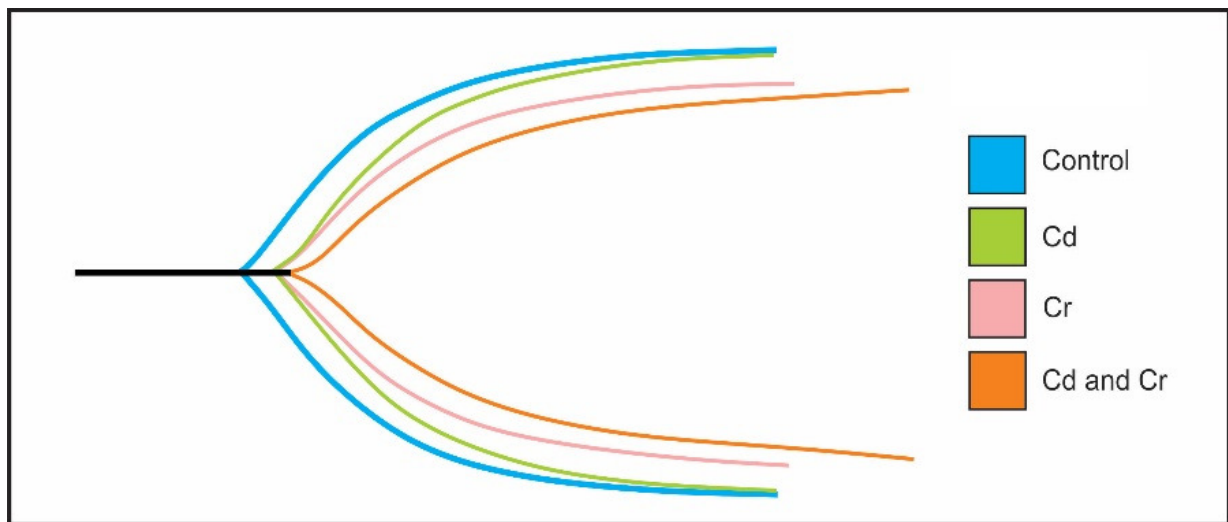
Figure 6.8: Representative viscoelastic traces of the control and metal groups.
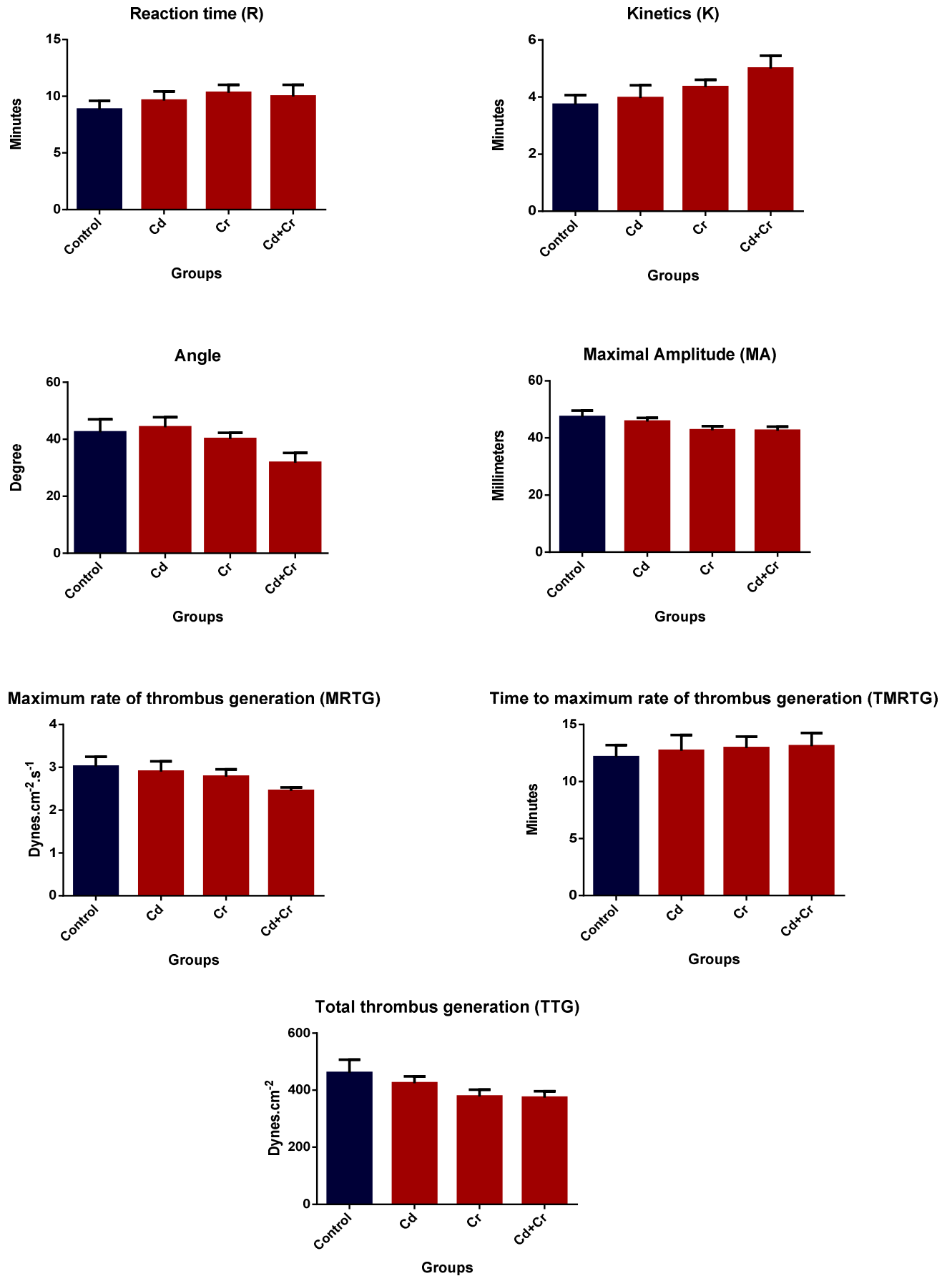
Figure 6.9: The effects of Cd and Cr alone and in combination on the viscoelastic parameters.

Table 6.3: Summary of the effects of Cd and Cr alone and in combination on the viscoelastic parameters

Parameter	Normal ranges	Control		Cd	
		Range	Mean ± SD	Range	Mean ± SD
R (min)	9–27	6.50–11.70	8.83 ± 1.89	7.10-12.30	9.62 ± 1.96
K (min)	2–9	2.60–4.50	3.73 ± 0.82	2.80-5.80	3.97 ± 1.10
Angle (deg)	22–58	27.40–57.00	42.42 ± 11.11	33.50-46.80	4.20 ± 8.61
MA (mm)	44–64	42.30–57.31	47.35 ± 5.46	41.70-51.10	45.72 ± 3.26
MRTG (Dynes/cm^2/s)	0–10	2.56–12.06	4.53 ± 3.72	2.10-7.71	3.61 ± 1.80
TMRTG (min)	5–23	8.08–15.67	12.14 ± 2.58	10.00-18.50	12.71 ± 3.36
TTG (Dynes/s^2)	251–1014	366.56–674.67	460.49 ± 112.92	357.43-524.22	424.43 ± 58.02
Parameter	Normal ranges	Cr		Cd and Cr	
		Range	Mean ± SD	Range	Mean ± SD
R (min)	9–27	8.50–13.20	10.30 ± 1.77	6.40-13.10	9.98 ± 2.49
K (min)	2–9	3.50–4.90	4.35 ± 0.63	4.20-7.10	5.0 ± 1.10
Angle (deg)	22–58	34.70–46.80	40.10 ± 5.34	20.60-42.50	31.70 ± 8.46
MA (mm)	44–64	38.70–48.90	42.72 ± 3.61	37.10-47.50	42.52 ± 3.67
MRTG (Dynes/cm^2/s)	0–10	2.42–3.54	2.78 ± 0.42	2.18-2.75	2.45 ± 0.20
TMRTG (min)	5–23	10.00–16.33	12.93 ± 2.48	9.67-16.75	13.10 ± 2.84
TTG (Dynes/s^2)	251–1014	317.12–481.22	377.76 ± 58.26	296.51-453.38	373.94 ± 55.84

*statistical significance: *p*-value of ≤0.05. SD: Standard deviation

Figure 6.8 shows representative traces of all the groups from which the r-time, k-time, angle and MA was determined. Table 6.3 shows a summary of the control and metal exposed group's viscoelastic profiles after exposure to Cd and Cr alone and in combination (mean ± SD). No statistical significant difference in any of the parameters measured with the TEG® could be detected between the control group and metal exposed groups (Table 6.3) using the one-way ANOVA and Tukey's multiple comparisons test. Although no statistical significance was obtained, there was a visible trend in all the parameters of the metal groups (Fig. 6.9). The R and K values had a slight increase and the angle and MA values decreased with the metal exposed groups. The velocity curve (v-curve) results, namely the MRTG, TMRTG and TTG, further confirms the trend seen with a decrease in the MRTG and TTG, correlating to the angle and MA results and the TMRTG confirming the R value results.

6.4 <u>Discussion</u>

As shown in Chapter 5, exposure of the coagulation system to Cd and Cr alone and in combination causes alterations to the morphology of erythrocyte, platelet morphology as well as fibrin fibres. Findings in animal studies do not always correlate with effects in humans. In the present study the effect of a single exposure to Cd and Cr alone and in combination on human blood was evaluated. The purpose of this was to further investigate the effect of these metals in a relevant cellular model and to identify specific markers that can be used to identify and quantify the effects of exposure. To achieve this, the ultrastructure of erythrocytes, platelets and fibrin networks were evaluated, as well as Annexin-V positive erythrocytes were identified and viscoelastic parameters of clot formation were quantified. Ultrastructural changes were noted in all the metal-exposed groups (Fig. 6.1–6.4), with regards to the different components of the coagulation system evaluated. Some of these changes were also seen in the rat study representing chronic exposure (Chapter 5). The control group showed typical erythrocyte, platelet and fibrin fibre morphology (Fig. 6.1–6.4), with minimal changes as expected.

The variety in erythrocyte morphology, due to eryptosis, might be due to the increase in influx of calcium (Ca^{2+}) into the erythrocytes, activation of the Ca^{2+}/potassium (K^+) channels and adenosine triphosphate (ATP) depletion that are initiated by the oxidative stress and inflammation caused by the Cd and Cr (Lupescu*, et al.*, 2012; Pretorius*, et al.*, 2016b; Pretorius*, et al.*, 2014; Sopjani*, et al.*, 2008). Cd and Cr cause oxidative stress in the cells through different biochemical pathways, but with similar end results. Cd depletes protein-bound sulfhydryl groups and increase the production of reactive oxygen species (ROS) such

as H_2O_2 and $O_2^{\bullet-}$ and hydroxyl radical (Bertin and Averbeck, 2006; Stohs and Bagchi, 1995). In the case of Cr, it enters the redox cycle and also increases the production of ROS. The increase in ROS will cause an increase in oxidative stress that alters erythrocyte membrane fluidity and integrity making erythrocytes more fragile and less osmotic-resistant (Husain and Mahmood, 2017; Stohs and Bagchi, 1995). The increase in cytosolic Ca^{2+} will activate scramblase, in the erythrocytes, which inhibits flippase that in turn causes floppase to translocate PS to the outside, resulting in the PS flip and membrane scrambling (Fig. 6.10). Besides the Ca^{2+} that activates scramblase, it also affects the sensitive Ca^{2+}/K^+ channels which causes K^+ to exit the cells together with water and thus causing cell shrinkage (Fig. 6.10) (Lupescu, *et al.*, 2012; Pretorius, *et al.*, 2016b; Sopjani, *et al.*, 2008). Ca^{2+} entering the cells can also lead to the activation of calpain, a cysteine endopeptidase that degrades membrane proteins, leading to membrane blebbing (Fig. 6.10) (Pretorius, *et al.*, 2014). Energy depletion, also initiated by an increase in cytosolic Ca^{2+}, can also contribute to eryptosis. Interestingly only a few erythrocytes were positive for Annexin-V, which indicates that possibly other cellular mechanisms are involved.
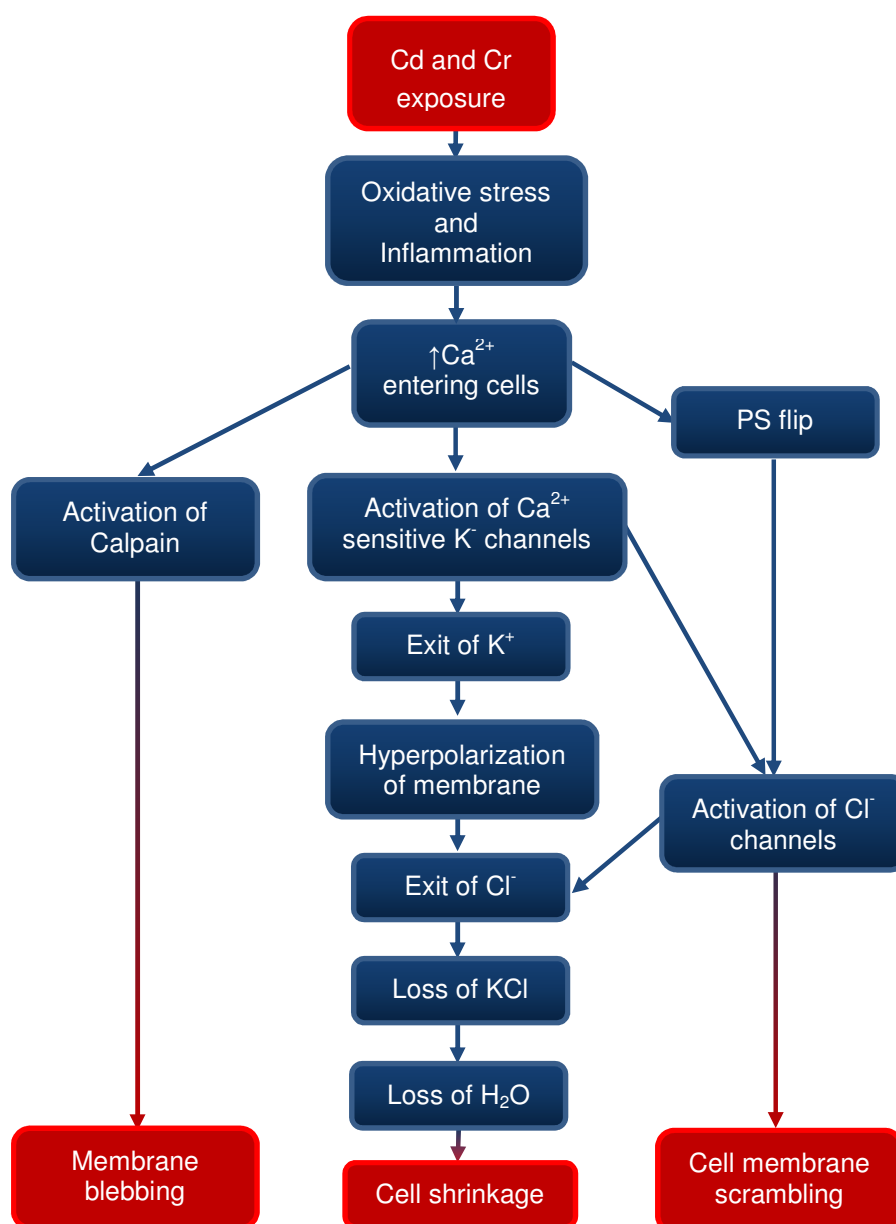
Figure 6.10: Summary of erythrocyte pathology (Modified from: Pretorius E, *et al.,* 2016b).

These alterations to the biochemical pathways of the erythrocyte membrane, account for some of the morphological changes that were visible in all the metal groups. These ultrastructural results, together with the results from the CLSM, that indicated that the Annexin-V positive signals were mainly found on the spherocytic erythrocytes, are contradictory to the results obtained in studies done by Lupescu, *et al.* in 2012 and Sopjani, *et al.* in 2008, where they found that Cd and Cr causes erythrocyte shrinkage (Lupescu*, et al.*, 2012; Sopjani*, et al.*, 2008).

Since Lang and colleagues coined the term "eryptosis" in 2005 (Lang*, et al.*, 2005), a lot of research has been done on only the biochemical aspect of suicide erythrocyte death and from this biochemical research, eryptosis has been characterized by cell membrane

shrinkage, blebbing and scrambling (Föller*, et al.*, 2008; Lang*, et al.*, 2010; Lang*, et al.*, 2012b; Lang and Qadri, 2012; Mischitelli*, et al.*, 2016). It is only recently that a closer look at the erythrocytes ultrastructural morphology has been taken (Pretorius*, et al.*, 2016a; Pretorius*, et al.*, 2016b; Swanepoel and Pretorius, 2012), but still no research has been done on the ultrastructural morphological changes that occur during eryptosis. This was confirmed by a Google Scholar literature search with the keywords, "Eryptosis, ultrastructure, morphology, and confocal", that included articles from 2000 to 2017. Thus, future studies need to focus on both the biochemical and biophysical aspects of eryptosis.

The increase in platelet activation, associated with pseudopodia and membrane spreading, was observed in the metal-exposed groups and that may cause a decrease in taut fibres and thus an increase in loose or bent fibres. Oxidative stress and inflammation is known to cause unnecessary platelet activation that can result in the formation of pathological thrombi (Freedman, 2008; Van Rooy*, et al.*, 2015; Van Rooy and Pretorius, 2015). With the activation of platelets, agonists involved in the formation and stability of clot are released and include adenosine diphosphate (ADP), serotonin, thrombin and thromboxane A_2 (Freedman, 2008; Van Rooy and Pretorius, 2015).

Platelets also play a crucial role in fibrin formation and tautness, thus the bent fibres seen in the fibrin networks of the metal groups might be due to the platelet functional changes or a lack of thrombin production (Van Rooy*, et al.*, 2015). The significant increase in fibre thickness in the metal groups will further contribute to the alterations of the erythrocytes and clot formation, as it might cause a reduction in the lysis of the clots (Swanepoel*, et al.*, 2016b). The alteration in fibre thickness can be due to the transition of the fibres α-helices into β-sheets and protein aggregation, as suggested in the article by Kell and Pretorius (2016). Fibrin fibres consist of a combination of α-helices, β-sheets and turns, loops and random coils which contributes to the normal structure and function of the fibrin fibres (Kell and Pretorius, 2016).

TEG® is widely used in trauma care to evaluate whole blood coagulation (Bolliger*, et al.*, 2012). In a recent analysis of pulmonary emboli by Lehnert*, et al.* (2017) the mean values of TEG® were within normal ranges. Likewise in the present study, acute exposure to Cd and Cr alone and in combination provided TEG® results within the normal range (Table 6.3). However, evaluation of the viscoelastic traces and graphs, Cd and Cr alone and in combination (Figures 6.8 and 6.9) indicated that these heavy metals cause minor, although not statistically significant, changes to the measured parameters. The trend seen in the viscoelastic results indicate that the R value increased slightly, thus resulting in delayed

fibrin formation. Fibrin formation is catalysed by the enzyme thrombin, from fibrinogen and stabilized by thrombin-catalysed factor XIII (FXIII) (Kell and Pretorius, 2016). Both these components depend on the presence of Ca^{2+}, as Ca^{2+} assists in the formation of FXIII and thrombin (Swanepoel*, et al.*, 2015). In the present model Cd and Cr may compete with Ca^{2+} binding and consequently alter blood coagulation. Ca^{2+} depletion is known to occur after heavy metal exposure (Timbrell, 1999). The trend of increased K time indicates that the initial clot formation, after initiation, proceeds quickly. This correlates with the activated platelets seen in SEM analysis (Fig. 6.2). The decrease in both the angle and MA values indicates that the fibrin build up is slower due to the reduction in fibrin cross-linking, which results in a fragile, less-stable clot. The clot strength is also decreased as the platelet-fibrinogen interactions are decreased (Fig. 6.9 and Table 6.3). Again this correlates with the SEM results, as the fibres appear less taut (Fig. 6.3). The v-curve results support the above-mention trends seen in the results. The TMRTG shows that the total clot formation, thus from start to maximum clot formation, will also take longer and correlates with the increased initial clot formation time seen in the R value. The decrease in the thrombus generation (MRTG) and clot strength (TTG) also indicates that the clot will form slower and be weaker. This fragile clot may cause problems in the cardiovascular system, as these weak clots may detach and cause a blockage in an artery or vein, leading to thrombosis.

Cigarette smoking has been shown to increase fibrin fibre thickness and platelet activation and cause erythrocyte alterations (Armani*, et al.*, 2009; Pretorius*, et al.*, 2013; Pretorius*, et al.*, 2010). A complex mixture of more than 4000 components has been identified in mainstream cigarette smoke, this includes heavy metals such as Cd and Cr, and the present study clearly shows that Cd and Cr contributes to this effect (Dallüge*, et al.*, 2002; Fresquez*, et al.*, 2013). Likewise exposure to these metals in water and polluted air can also contribute to increased risk for thrombosis. Although this *ex vivo* study investigated the effect of a 1000 times that of a single acute dosage, this study clearly identifies the blood as a target of toxicity prior to metabolism in the liver and excretion by the kidneys. Furthermore, accumulative effects of low levels of each metal as part of complex mixtures may also adversely affect blood coagulation. Evaluation of the morphology of blood components may be an important technique, although not quantifiable, that can be used to identify early morphological changes prior to the identification of altered coagulation using standard clinical methods. However, lifestyle as well as the presence of existing disease must also be taken into account.

6.5   <u>Conclusion</u>

Exposure of blood to a single acute dosage of 1000 times the WHO water limits of Cd and Cr alone and in combination revealed that these metals altered the morphology of erythrocytes and activated platelets, which resulted in altered clot formation. Altered erythrocyte morphology was associated with eryptosis and some erythrocytes had a positive Annexin-V signal, indicating that the PS flip occurred. Compared to Cd, the fibre thickness was increased for Cr alone and in the combination group. TEG$^{®}$ analysis, although not statistically significant, indicated that the final clot is possibly more fragile and less stable, increasing the risk of associated disease.

Chapter 7

Concluding discussion

The growth in the industrial sector has provided many benefits since its establishment, but has come with some unfavourable environmental effects. Heavy metals have become synonymous with industrial pollution due to their toxicological and physiological effects on the ecosystem (Al-Othman, *et al.*, 2012). This is especially true in South Africa, a country that has a thriving industrial sector and not always the means to correctly dispose of toxic materials, like heavy metals, which then enters the air and water supplies (Venter, *et al.*, 2017). People living in these areas are the most affected and exposure is not limited to a single metal but usually combinations and at different concentrations (Awofolu, *et al.*, 2005; Venter, *et al.*, 2015). Two identified metals that hold potential risk in the South African context is cadmium (Cd) and chromium (Cr) (Venter, *et al.*, 2017) and the effects of these metals alone and in combination were investigated in this study, using an *in vivo* rat and *ex vivo* human blood coagulation model.

The *in vivo* model is widely used for human toxicology, pharmacology, reproduction and behavioural studies (Van Der Schoor, 2014) and thus was an ideal model to use in this study. The *in vivo* model was successfully implemented, in the current study, over a period of 28 days where male Sprague-Dawley rats received daily dosages of Cd and Cr alone and in combination at a 1000 times that of the World Health Organizations (WHO) acceptable water limits for these heavy metals (W.H.O, 2011). This was confirmed with the presence of the heavy metals in the blood plasma. As indicated in Chapter 3, there was no sudden loss in the weight of the rats during the study, but the rats had a steady increase in weight similar to the controls during the experimental period. The blood chemistry analysis revealed that after exposure to Cd and Cr alone and in combination, the levels of certain liver and kidney tests decreased, indicating that the function of these organs were altered but no organ damage had occurred.

In contrast, histological analysis revealed that the liver and kidney tissue showed more severe changes to the tissue structure, with necrosis, sinusoidal and glomerular dilation seen in almost all metal exposed groups. In all the metal groups the pancreas had only minor tissue damage. No tissue fibrosis was present in any of the organs examined. Ultrastructural analysis with transmission electron microscopy (TEM) the liver, pancreas and kidney tissue revealed irregular chromatin condensation, swelling in between the cristae of the mitochondria, membrane alterations of both the nuclei and mitochondria and rough endoplasmic reticulum (rER) dilation. Organ specific damage revealed alterations to the

glomerular filtration barrier of the kidney and in the pancreas the granules of the Islets of Langerhans. The effect of Cd and Cr in combination was increased either due to exposure to higher total metal concentrations or due to a synergistic effect because each metal has different cellular targets. Using electron energy-loss spectroscopy (EELS) and energy filtered TEM (EFTEM) analysis it was found that the Cd accumulated in the nucleus and mitochondria, where Cr was primarily found at the membranes of the nucleus, mitochondria and rER. These sites of accumulation were the same for the liver, pancreas and kidney.

The blood is responsible for the distribution of the absorbed metals but is also an essential functional component of the liver, pancreas and the kidney. The effects of Cd and Cr alone and in combination on erythrocytes, platelets and coagulation were determined using scanning electron microscopy (SEM). Exposure to Cd and Cr alone and in combination altered the structure of erythrocytes and platelets. In addition following coagulation the structure of the formed fibrin network was also altered and changes in the fibre thickness was significantly increased compared to the control.

Using human blood, the above effects were further investigated. The *ex vivo* model was used to analyse the ultrastructural, confocal and viscoelastic characteristics of human whole blood and plasma after exposure to a single dose of Cd and Cr alone and in combination. The ultrastructural analyses were completed by analysing the same components of the coagulation system that were evaluated in the *in vivo* study, with the addition of thromboelastography® (TEG®) that were used to evaluate the effects of Cd and Cr alone and in combination on viscoelastic characteristics of human whole blood and plasma, as well as the presence of PS flip on the membranes of the erythrocytes using confocal laser scanning microscopy (CLSM). The aim of this was to determine if the measurement of these parameters can be used to evaluate risk in an exposed population. Findings were that Cd and Cr alone and in combination caused morphological changes to erythrocytes, platelets and fibrin fibres. In addition eryptosis was associated with Annexin-V positive signal. The TEG® analysis, although not statistically significant, indicated that the final clot will probably result in a fragile, less-stable clot, due to changes mainly to the platelets and fibrin networks.

In conclusion, Cd and Cr alone and in combination adversely affected liver, pancreas and kidney morphology as well as rat and human erythrocyte morphology, platelet activation and the structure of the fibrin networks, indicating organ damage as well as altered viscoelastic characteristics of the blood. The observed effects did not translate into large changes to the blood chemistry parameters. This is of concern as populations exposed to these metals will have tissue damage and the coagulability of their blood will be altered increasing the risk of

associated diseases. Measurement of blood levels of each metal will provide some information on probable risk. However, as an individual is usually exposed to complex mixtures it is difficult to identify the specific metals for which testing will be undertaken. Traditional blood markers are poor indicators of the extent of liver, pancreas and kidney damage observed in the present study. More sensitive methods for identifying tissue damage will be an important area of future research.

The research reported in this thesis, will contribute to the pool of knowledge regarding the adverse effects of heavy metals on the organ structure and function as well as the components of the coagulation system. The exposed erythrocytes and platelets showed altered morphology and the hallmarks of eryptosis, although the number of erythrocytes that were positive for Annexin-V was few. This implies that although changes to the morphology of erythrocytes were observed, Annexin-V quantification using flow cytometry will provide a poor indication of toxicity due to exposure, especially taking into account the high concentrations of Cd and Cr used in this study. Expression of Annexin-V, by erythrocytes may be dependent on exposure time and metal concentration and effect of these parameters need to be evaluated in a population based study. Also, the CLSM analysis revealed that there is a lack of information on the ultrastructural morphological changes that occur during the eryptotic process and more extensive research needs to be conducted on the sequence of erythrocyte cell death.

A limitation of the study was the amount of blood needed from each animal for biochemical analysis as well as for the coagulation studies. In some instances (for the Cr group specifically), it was not possible to obtain enough blood for the coagulation studies, and therefor the results obtained for that part of the *in vivo* model are not representative of that specific experimental group. For future research perspectives, the number of animals per group can be increase to ensure enough samples for all analytic techniques. Also for more accurate conclusions about fibrinolysis, the permeability of the fibrin networks can be evaluated, as done in a study by Leonidakis and colleagues where they combined two techniques namely, confocal microscopy and fiber extraction algorithm and turbidity measurements to evaluate the permeability of a fibrin network (Leonidakis, *et al.*, 2017).

Chapter 8

Reference list

Annual statistics of scientific procedures on living animals great britain. [Online]. UK. Available: www.understandinganimalresearch.org.uk. Accessed: [15 August 2016].

Ahn C, Krivanek O, Burgner R*, et al.,*. 1983. Eels atlas gatan inc. Warrendale, PA: 1-93.

Åkesson A, Barregard L, Bergdahl IA*, et al.,*. 2014. Non-renal effects and the risk assessment of environmental cadmium exposure. Environmental Health Perspectives (Online), 122: 431.

Al-Attar AM. 2011. Antioxidant effect of vitamin E treatment on some heavy metals-induced renal and testicular injuries in male mice. Saudi J Biol Sci, 18: 63-72.

Al-Othman ZA, Ali R and Naushad M. 2012. Hexavalent chromium removal from aqueous medium by activated carbon prepared from peanut shell: Adsorption kinetics, equilibrium and thermodynamic studies. Chem Eng J, 184: 238-247.

Ambrose JA and Barua RS. 2004. The pathophysiology of cigarette smoking and cardiovascular disease: An update. J Am Coll Cardiol, 43: 1731-1737.

Andreyev AY, Kushnareva YE and Starkov A. 2005. Mitochondrial metabolism of reactive oxygen species. Biochemistry (Moscow), 70: 200-214.

Arbi S. 2015. Exploratory descriptive study of the support tissue in keloids. Masters, University of Pretoria, Pretoria, South Africa.

Arbi S, Oberholzer HM, Van Rooy MJ*, et al.,*. 2017. Effects of chronic exposure to mercury and cadmium alone and in combination on the coagulation system of sprague-dawley rats. Ultrastruct Pathol, 41: 275–283.

Armani C, Landini Jr L and Leone A. 2009. Molecular and biochemical changes of the cardiovascular system due to smoking exposure. Curr Pharm Des, 15: 1038-1053.

Asagba S and Obi F. 2004. Effects of oral cadmium exposure on renal glomerular and tubular functions in the rat. J Appl Sci Environ Mgt, 8: 29-32.

Awofolu O, Mbolekwa Z, Mtshemla V*, et al.,*. 2005. Levels of trace metals in water and sediment from Tyume river and its effects on an irrigated farmland. Water SA, 31: 87-94.

Babaknejad N, Moshtaghie AA, Shahanipour K*, et al.,*. 2015. Protective effects of magnesium on cadmium renal toxicity in male Wistar rats. Zahedan J Res Med Sci: 29-32.

Badyal DK and Desai C. 2014. Animal use in pharmacology education and research: The changing scenario. Indian J Pharmacol, 46: 257-265.

Balakrishnan R, Kumar CSS, Rani MU*, et al.,*. 2013. An evaluation of the protective role of α-tocopherol on free radical induced hepatotoxicity and nephrotoxicity due to chromium in rats. Indian J Pharmacol, 45: 490-495.

Bataller R and Brenner DA. 2005. Liver fibrosis. J Clin Invest, 115: 209-218.

Bernhoft RA. 2013. Cadmium toxicity and treatment. Scientific World J, 2013.

Bertin G and Averbeck D. 2006. Cadmium: Cellular effects, modifications of biomolecules, modulation of DNA repair and genotoxic consequences (a review). Biochimie, 88: 1549-1559.

Bester B. 2013. An assessment of the heavy metal status and edibility of fish from three impoundments in the north west province, South Africa. Masters thesis, University of Johannesburg, Johannesburg, South Africa.

Binning K and Baird D. 2001. Survey of heavy metals in the sediments of the swartkops river estuary, Port Elizabeth, South Africa. Water SA, 27: 461-466.

Bolliger D, Seeberger MD and Tanaka KA. 2012. Principles and practice of thromboelastography in clinical coagulation management and transfusion practice. Transfus Med Rev, 26: 1-13.

Brzoska M, Moniuszko-Jakoniuk J, Piłat-Marcinkiewicz B*, et al.,*. 2003. Liver and kidney function and histology in rats exposed to cadmium and ethanol. Alcohol Alcohol, 38: 2-10.

Chang K-C, Hsu C-C, Liu S-H*, et al.,*. 2013. Cadmium induces apoptosis in pancreatic β-cells through a mitochondria-dependent pathway: The role of oxidative stress-mediated c-jun n-terminal kinase activation. PLoS One, 8: e54374.

Chowdhury AR. 2009. Recent advances in heavy metals induced effect on male reproductive function-a retrospective. Al Ameen J Med Sci, 2: 37-42.

Coetzee H, Loots G and Meiring J. 2009a. Blood cells. In: Coetzee H, Loots G and Meiring J (eds.). Human histology. South Africa: Van Schaik Publishers. pp 111-112.

Coetzee H, Loots G and Meiring J. 2009b. Digestive system. In: Coetzee H, Loots G and Meiring J (eds.). Human histology. South Africa: Van Schaik Publishers. pp 271-303.

Coetzee H, Loots G and Meiring J. 2009c. Introduction. In: Coetzee H, Loots G and Meiring J (eds.). Human histology. South Africa: Van Schaik Publishers. pp 3-9.

Coetzee H, Loots G and Meiring J. 2009d. Urinary system. In: Coetzee H, Loots G and Meiring J (eds.). Human histology. South Africa: Van Schaik Publishers. pp 331-349.

Crosby WH. 1952. Analytical review: The pathogenesis of spherocytes and leptocytes (target cells). Blood, 7: 261-274.

Cullinane J, Bannigan J and Thompson J. 2009. Cadmium teratogenesis in the chick: Period of vulnerability using the early chick culture method, and prevention by divalent cations. Reprod Toxicol, 28: 335-341.

Cuypers A, Plusquin M, Remans T, *et al.,*. 2010. Cadmium stress: An oxidative challenge. Biometals, 23: 927-940.

Dallüge J, Van Stee LL, Xu X, *et al.,*. 2002. Unravelling the composition of very complex samples by comprehensive gas chromatography coupled to time-of-flight mass spectrometry: Cigarette smoke. J Chromatogr A, 974: 169-184.

Dayan A and Paine A. 2001. Mechanisms of chromium toxicity, carcinogenicity and allergenicity: Review of the literature from 1985 to 2000. Hum Exp Toxicol, 20: 439-451.

Edwards JR and Prozialeck WC. 2009. Cadmium, diabetes and chronic kidney disease. Toxicol Appl Pharmacol, 238: 289-293.

El-Demerdash F, Yousef M and Elagamy E. 2001. Influence of paraquat, glyphosate, and cadmium on the activity of some serum enzymes and protein electrophoretic behavior (*in vitro*). Journal of Environmental Science and Health, Part B, 36: 29-42.

El-Demerdash FM, Yousef MI, Kedwany FS, *et al.,*. 2004. Cadmium-induced changes in lipid peroxidation, blood hematology, biochemical parameters and semen quality of male rats: Protective role of vitamin e and β-carotene. Food Chem Toxicol, 42: 1563-1571.

El Muayed M, Raja MR, Zhang X, *et al.,*. 2012. Accumulation of cadmium in insulin-producing β cells. Islets, 4: 405-416.

Ernst LM, Ruchelli ED and Huff DS. 2011. Color atlas of fetal and neonatal histology, Springer Science & Business Media. pp

Fatoki O and Awofolu R. 2003. Levels of Cd, Hg and Zn in some surface waters from the eastern cape province, South Africa. Water SA, 29: 375-380.

Föller M, Huber SM and Lang F. 2008. Erythrocyte programmed cell death. IUBMB life, 60: 661-668.

Frantz C, Stewart KM and Weaver VM. 2010. The extracellular matrix at a glance. J Cell Sci, 123: 4195-4200.

Freedman JE. 2008. Oxidative stress and platelets. Arterioscler Thromb Vasc Biol, 28: s11-s16.

Fresquez MR, Pappas RS and Watson CH. 2013. Establishment of toxic metal reference range in tobacco from US cigarettes. J Anal Toxicol, 37: 298-304.

Fu J, Liang X, Chen Y, *et al.,*. 2008. Oxidative stress as a component of chromium-induced cytotoxicity in rat calvarial osteoblasts. Cell Biol Toxicol, 24: 201-212.

García-Niño WR and Pedraza-Chaverrí J. 2014. Protective effect of curcumin against heavy metals-induced liver damage. Food Chem Toxicol, 69: 182-201.

Giannini EG, Testa R and Savarino V. 2005. Liver enzyme alteration: A guide for clinicians. Can Med Assoc J, 172: 367-379.

Gorbet MB and Sefton MV. 2004. Biomaterial-associated thrombosis: Roles of coagulation factors, complement, platelets and leukocytes. Biomaterials, 25: 5681-5703.

Gorden P. 1997. Non-insulin dependent diabetes--the past, present and future. Ann Acad Med Singapore, 26: 326-330.

Ha H and Lee HB. 2003. Reactive oxygen species and matrix remodeling in diabetic kidney. J Am Soc Nephrol, 14: 246-249.

Han SM, Lee KG, Yeo JH*, et al.,*. 2009. Effects of bee venom treatment on growth performance of young pigs. Am J Chin Med, 37: 253-260.

Hoek G, Brunekreef B, Fischer P*, et al.,*. 2001. The association between air pollution and heart failure, arrhythmia, embolism, thrombosis, and other cardiovascular causes of death in a time series study. Epidemiology, 12: 355-357.

Husain N and Mahmood R. 2017. Hexavalent chromium induces reactive oxygen species and impairs the antioxidant power of human erythrocytes and lymphocytes: Decreased metal reducing and free radical quenching ability of the cells. Toxicol Ind Health: 0748233717703892.

Jacobs C, Greyling L and Meiring J. 2006. Embryology for the health science student*,* South Africa, University of Pretoria. pp 74-136.

Jacquillet G, Barbier O, Cougnon M*, et al.,*. 2006. Zinc protects renal function during cadmium intoxication in the rat. Am J Physiol Renal Physiol, 290: F127-F137.

Järup L. 2003. Hazards of heavy metal contamination. Br Med Bull, 68: 167-182.

Jin Y, Zhang S, Tao R*, et al.,*. 2014. Oral exposure of mice to cadmium (ii), chromium (vi) and their mixture induce oxidative-and endoplasmic reticulum-stress mediated apoptosis in the livers. Environ Toxicol, 31: 693-705.

Jomova K and Valko M. 2011. Advances in metal-induced oxidative stress and human disease. Toxicology, 283: 65-87.

Kanter M, Yoruk M, Koc A*, et al.,*. 2003. Effects of cadmium exposure on morphological aspects of pancreas, weights of fetus and placenta in streptozotocin-induced diabetic pregnant rats. Biol Trace Elem Res, 93: 189-200.

Kearney L. 2012. Mining and minerals in South Africa [Online]. Available: www.southafrica.info. Accessed: [May 2013].

Kell DB and Pretorius E. 2015. The simultaneous occurrence of both hypercoagulability and hypofibrinolysis in blood and serum during systemic inflammation, and the roles of iron and fibrin (ogen). Integr Biol, 7: 24-52.

Kell DB and Pretorius E. 2016. Proteins behaving badly. Substoichiometric molecular control and amplification of the initiation and nature of amyloid fibril formation: Lessons from and for blood clotting. Prog Biophys Mol Biol: 1-26.

Khalil S, Awad A and Elewa Y. 2013. Antidotal impact of extra virgin olive oil against genotoxicity, cytotoxicity and immunotoxicity induced by hexavalent chromium in rat. IJVSM, 1: 65-73.

Khlifi R, Olmedo P, Gil F, *et al.,.* 2013. Arsenic, cadmium, chromium and nickel in cancerous and healthy tissues from patients with head and neck cancer. Sci Total Environ, 452: 58-67.

Kierszenbaum AL and Tres LL. 2012. Histology and cell biology : An introduction to pathology, Philadelphia, PA, Elsevier Saunders. pp 438-610.

Koyu A, Gokcimen A, Ozguner F, *et al.,.* 2006. Evaluation of the effects of cadmium on rat liver. Mol Cell Biochem, 284: 81-85.

Kumar A and Kumar A. 2013. Impact of dietary glutathione on hematological indices in rats poisoned with hexavalent chromium. J Appl & Nat Sci, 5: 217-220.

Kumar A, Rana S and Prakash R. 1984. Dysenzymia induced by hexavalent chromium in rat liver. Int J Tissue React, 7: 333-338.

Lakshmi GD, Kumar PR, Bharavi K, *et al.,.* 2012. Protective effect of *tribulus terrestris linn* on liver and kidney in cadmium intoxicated rats. Indian J Exp Biol, 50: 141-146.

Lang E and Lang F. 2015. Triggers, inhibitors, mechanisms, and significance of eryptosis: The suicidal erythrocyte death. BioMed Res Int, 2015.

Lang E, Qadri SM and Lang F. 2012a. Killing me softly–suicidal erythrocyte death. Int J Biochem Cell Biol, 44: 1236-1243.

Lang F, Gulbins E, Lang PA, *et al.,.* 2010. Ceramide in suicidal death of erythrocytes. Cell Physiol Biochem, 26: 21-28.

Lang F, Lang E and Föller M. 2012b. Physiology and pathophysiology of eryptosis. Transfusion Medicine and Hemotherapy, 39: 308-314.

Lang F and Qadri SM. 2012. Mechanisms and significance of eryptosis, the suicidal death of erythrocytes. Blood Purif, 33: 125-130.

Lang KS, Lang PA, Bauer C, *et al.,.* 2005. Mechanisms of suicidal erythrocyte death. Cell Physiol Biochem, 15: 195-202.

Langárd S and Costa M. 2007. Chromium. In: Nordberg GF, Fowler BA and Nordberg M (eds.). Handbook on the toxicology of metals Third Edition ed. Burlington: Academic Press. pp 487-510.

Larsen CC, Hansen-Schwartz J, Nielsen JD, *et al.,*. 2010. Blood coagulation and fibrinolysis after experimental subarachnoid hemorrhage. Acta Neurochir (Wien), 152: 1577-1581.

Lee YK, Park EY, Kim S, *et al.,*. 2014. Evaluation of cadmium-induced nephrotoxicity using urinary metabolomic profiles in sprague-dawley male rats. J Environ Sci Health A Tox Hazard Subst Environ Eng, 77: 1384-1398.

Lehnert P, Johansson PI, Ostrowski SR, *et al.,*. 2017. Coagulopathy in patients with acute pulmonary embolism: A pilot study of whole blood coagulation and markers of endothelial damage. Scand J Clin Lab Invest, 77: 19-26.

Lei L-J, Jin T-Y and Zhou Y-F. 2007. Insulin expression in rats exposed to cadmium. Biomed Environ Sci, 20: 295-301.

Leonidakis KA, Bhattacharya P, Patterson J, *et al.,*. 2017. Fibrin structural and diffusional analysis suggests that fibers are permeable to solute transport. Acta biomaterialia, 47: 25-39.

Liu L, Jin W and Lv J-P. 2010. Oral administration of the high-chromium yeast improve blood plasma variables and pancreatic islet tissue in diabetic mice. Biol Trace Elem Res, 138: 250-264.

Liu Y. 2006. Renal fibrosis: New insights into the pathogenesis and therapeutics. Kidney Int, 69: 213-217.

Lupescu A, Jilani K, Zelenak C, *et al.,*. 2012. Hexavalent chromium-induced erythrocyte membrane phospholipid asymmetry. Biometals, 25: 309-318.

Madejczyk MS, Baer CE, Dennis WE, *et al.,*. 2015. Temporal changes in rat liver gene expression after acute cadmium and chromium exposure. PLoS One, 10: e0127327.

Mischitelli M, Jemaa M, Almasry M, *et al.,*. 2016. Ca^{2+} entry, oxidative stress, ceramide and suicidal erythrocyte death following diosgenin treatment. Cell Physiol Biochem, 39: 1626-1637.

Mishra AK and Mohanty B. 2008. Acute toxicity impacts of hexavalent chromium on behavior and histopathology of gill, kidney and liver of the freshwater fish, *channa punctatus (bloch)*. Environ Toxicol Pharmacol, 26: 136-141.

Mitra E, Ghosh AK, Ghosh D, *et al.,*. 2012. Protective effect of aqueous curry leaf (murraya koenigii) extract against cadmium-induced oxidative stress in rat heart. Food Chem Toxicol, 50: 1340-1353.

Mohandas N and Gallagher PG. 2008. Red cell membrane: Past, present, and future. Blood, 112: 3939-3948.

Moini J. 2016a. Cells. In: Moini J (ed.) Anatomy and physiology for health professionals. USA: Jones & Bartlett Learning. pp 46-66.

Moini J. 2016b. Digestive system. In: Moini J (ed.) Anatomy and physiology for health professionals. USA: Jones & Bartlett Learning. pp 471-492.

Moini J. 2016c. Urinary system. In: Moini J (ed.) Anatomy and physiology for health professionals. USA: Jones & Bartlett Learning. pp 513-550.

Molokwane PE, Meli KC and Nkhalambayausi-Chirwa EM. 2008. Chromium (vi) reduction in activated sludge bacteria exposed to high chromium loading: Brits culture (South Africa). Water Research, 42: 4538-4548.

Myers CR. 2012. The effects of chromium (vi) on the thioredoxin system: Implications for redox regulation. Free Radic Biol Med, 52: 2091-2107.

Nachnani J, Bulchandani D, Nookala A*, et al.,*. 2010. Biochemical and histological effects of exendin-4 (exenatide) on the rat pancreas. Diabetologia, 53: 153–159.

Nordberg GF. 2009. Historical perspectives on cadmium toxicology. Toxicol Appl Pharmacol, 238: 192-200.

Nordberg GF, Fowler BA, Nordberg M*, et al.,*. 2007. Introduction-general considerations and international perspectives. In: Nordberg GF, K N, Nordberg M and Friberg LT (eds.). Handbook of toxicology of metals. Amsterdam and Boston: Academic Press Inc. pp 4-9.

Park C and Lee DG. 2010. Melittin induces apoptotic features in *Candida albicans*. Biochem Biophys Res Commun, 394: 170-172.

Park JH, Jeong Y-J, Park K-K*, et al.,*. 2010. Melittin suppresses PMA-induced tumor cell invasion by inhibiting nf-κb and ap-1-dependent MMP-9 expression. Mol Cells, 29: 209-215.

Park SJ, Lee JR, Jo MJ*, et al.,*. 2013. Protective effects of Korean red ginseng extract on cadmium-induced hepatic toxicity in rats. Apoptosis, 8: 34-44.

Patlolla AK, Barnes C, Hackett D*, et al.,*. 2009. Potassium dichromate induced cytotoxicity, genotoxicity and oxidative stress in human liver carcinoma (HepG2) cells. Int J Environ Res Public Health, 6: 643-653.

Pérez-Gómez F and Bover R. 2007. The new coagulation cascade and its possible influence on the delicate balance between thrombosis and hemorrhage. Rev Esp Cardiol, 60: 1217-1219.

Pretorius E, Bester J, Vermeulen N*, et al.,*. 2015. Poorly controlled type 2 diabetes is accompanied by significant morphological and ultrastructural changes in both erythrocytes and in thrombin-generated fibrin: Implications for diagnostics. Cardiovasc Diabetol, 14: 1-20.

Pretorius E, Du Plooy JN and Bester J. 2016a. A comprehensive review on eryptosis. Cell Physiol Biochem, 39: 1977-2000.

Pretorius E, Du Plooy JN, Soma P*, et al.,*. 2013. Smoking and fluidity of erythrocyte membranes: A high resolution scanning electron and atomic force microscopy investigation. Nitric Oxide, 35: 42-46.

Pretorius E and Kell DB. 2014. Diagnostic morphology: Biophysical indicators for iron-driven inflammatory diseases. Integr Biol, 6: 486-510.

Pretorius E, Oberholzer HM, Van Der Spuy WJ*, et al.,*. 2010. Smoking and coagulation: The sticky fibrin phenomenon. Ultrastruct Pathol, 34: 236-239.

Pretorius E, Oore-Ofe O, Mbotwe S*, et al.,*. 2016b. Erythrocytes and their role as health indicator: Using structure in a patient-orientated precision medicine approach. Blood Rev, 30: 263-274.

Pretorius E, Swanepoel AC, Buys AV*, et al.,*. 2014. Eryptosis as a marker of Parkinson's disease. Aging, 6: 788-819.

Prozialeck WC and Edwards JR. 2012. Mechanisms of cadmium-induced proximal tubule injury: New insights with implications for biomonitoring and therapeutic interventions. J Pharmacol Exp Ther, 343: 2-12.

Quinteros FA, Poliandri AH, Machiavelli LI*, et al.,*. 2007. *In vivo* and *in vitro* effects of chromium VI on anterior pituitary hormone release and cell viability. Toxicol Appl Pharmacol, 218: 79-87.

Rana S. 2014. Perspectives in endocrine toxicity of heavy metals—a review. Biol Trace Elem Res, 160: 1-14.

Rana S, Singh R and Verma S. 1996. Protective effects of few antioxidants on liver function in rats treated with cadmium and mercury. Indian J Exp Biol, 34: 177-179.

Rich L and Whittaker P. 2005. Collagen and picrosirius red staining: A polarized light assessment of fibrillar hue and spatial distribution. Braz J Morphol Sci, 22: 97-104.

Sarkar A, Ravindran G and Krishnamurthy V. 2013. A brief review on the effect of cadmium toxicity: From cellular to organ level. IJBTR, 3: 17-36.

Scheer U and Hock R. 1999. Structure and function of the nucleolus. Curr Opin Cell Biol, 11: 385-390.

Sengupta P. 2013. The laboratory rat: Relating its age with human's. Int J Prev Med, 4: 624-630.

Sharma B, Singh S and Siddiqi NJ. 2014. Biomedical implications of heavy metals induced imbalances in redox systems. BioMed research international, 2014: 1-26.

Shimada H, Funakoshi T and Waalkes MP. 2000. Acute, nontoxic cadmium exposure inhibits pancreatic protease activities in the mouse. Toxicol Sci, 53: 474-480.

Shin K-H and Kim I-S. 2015. Thromboelastographic evaluation of coagulation in patients with liver disease. Blood, 126: 1089-1089.

Singh I. 2011. Textbook of human histology: With colour atlas and practical guide., New Delhi, Jaypee Brothers Medical Publishers. pp 263-289.

Singo NK. 2013. An assessment of heavy metal pollution near an old copper mine dump in Musina, South Africa. MSc, University of South Africa, South Africa.

Smith SA. 2009. The cell-based model of coagulation. J Vet Emerg Crit Car, 19: 3-10.

Solis-Heredia M, Quintanilla-Vega B, Sierra-Santoyo A, et al.,. 2000. Chromium increases pancreatic metallothionein in the rat. Toxicology, 142: 111-117.

Song Y, Zhang J, Yu S, et al.,. 2012. Effects of chronic chromium (VI) exposure on blood element homeostasis: An epidemiological study. Metallomics, 4: 463-472.

Sopjani M, Föller M, Dreischer P, et al.,. 2008. Stimulation of eryptosis by cadmium ions. Cell Physiol Biochem, 22: 245-252.

South Africa national standard. 2008. The care and use of animals for scientific purposes, Pretoria, SABS Standards Division. pp 1-234.

Stohs S and Bagchi D. 1995. Oxidative mechanisms in the toxicity of metal ions. Free Radic Biol Med, 18: 321-336.

Sullivan NJ, Sanchez A, Rollin PE, et al.,. 2000. Development of a preventive vaccine for Ebola virus infection in primates. Nature, 408: 605-609.

Suzuki T, Ishihara K, Migaki H, et al.,. 2005. Zinc transporters, ZNT5 and ZNT7, are required for the activation of alkaline phosphatases, zinc-requiring enzymes that are glycosylphosphatidylinositol-anchored to the cytoplasmic membrane. J Biol Chem, 280: 637-643.

Swanepoel AC, Nielsen VG and Pretorius E. 2015. Viscoelasticity and ultrastructure in coagulation and inflammation: Two diverse techniques, one conclusion. Inflammation, 38: 1707-1726.

Swanepoel AC and Pretorius E. 2012. Scanning electron microscopy analysis of erythrocytes in thromboembolic ischemic stroke. Int J Lab Hematol, 34: 185-191.

Swanepoel AC, Visagie A, De Lange Z, et al.,. 2016a. The clinical relevance of altered fibrinogen packaging in the presence of 17β-estradiol and progesterone. Thromb Res, 146: 23-34.

Swanepoel AC, Visagie A and Pretorius E. 2016b. Synthetic hormones and clot formation. Microsc Microanal, 22: 878-886.

Tavafi M, Hasanvand A and Ashoory H. 2016. Proximal convoluted tubule cells in ischemia and post-injury regeneration. Acta Persica Pathophysiologica, 1: e05.

Tchounwou PB, Yedjou CG, Patlolla AK*, et al.,*. 2012. Heavy metal toxicity and the environment, Springer. pp 133-164.

Tempelhoff E. 2013. Lug bo dié stad vuilste in wêreld [Online]. Available: www.beeld.com. Accessed: [April 2013].

Tennent GA, Brennan SO, Stangou AJ*, et al.,*. 2007. Human plasma fibrinogen is synthesized in the liver. Blood, 109: 1971-1974.

Thévenod F and Lee W-K. 2015. Live and let die: Roles of autophagy in cadmium nephrotoxicity. Toxics, 3: 130-151.

Thophon S, Pokethitiyook P, Chalermwat K*, et al.,*. 2004. Ultrastructural alterations in the liver and kidney of white sea bass, *Lates calcarifer*, in acute and subchronic cadmium exposure. Environ Toxicol, 19: 11-19.

Timbrell J. 1999. Principles of biochemical toxicology, CRC Press. pp 176-211.

Valko M, Rhodes C, Moncol J*, et al.,*. 2006. Free radicals, metals and antioxidants in oxidative stress-induced cancer. Chem Biol Interact, 160: 1-40.

Van Der Schoor C. 2014. An *in vivo* and *in ovo* evaluation of the toxicity of sibutramine. University of Pretoria,

Van Rooy M-J. 2015. Blood coagulation in metabolic syndrome-induced transient ischemic attack. PhD, University of Pretoria, Pretoria, South Africa.

Van Rooy M-J, Duim W, Ehlers R*, et al.,*. 2015. Platelet hyperactivity and fibrin clot structure in transient ischemic attack individuals in the presence of metabolic syndrome: A microscopy and thromboelastography® study. Cardiovasc Diabetol, 14: 1-13.

Van Rooy M-J and Pretorius E. 2015. Metabolic syndrome, platelet activation and the development of transient ischemic attack or thromboembolic stroke. Thromb Res, 135: 434-442.

Venter C. 2015. An *in ovo* investigation of the cellular effects of the heavy metals cadmium and chromium alone and in combination. Masters, University of Pretoria, Pretoria, South Africa.

Venter C, Oberholzer HM, Cummings FR*, et al.,*. 2017. Effects of metals cadmium and chromium alone and in combination on the liver and kidney tissue of male Spraque-Dawley rats: An ultrastructural and electron-energy-loss spectroscopy investigation. Microsc Res Tech, 80: 878–888.

Venter C, Oberholzer HM, Taute H*, et al.,*. 2015. An *in ovo* investigation into the hepatotoxicity of cadmium and chromium evaluated with light-and transmission electron

microscopy and electron energy-loss spectroscopy. J Environ Sci Health A Tox Hazard Subst Environ Eng, 50: 830-838.

Vitale A, Chiarotti F and Alleva E. 2015. The use of animal models in disease research. Rare Dis Orphan Drugs, 2: 1-4.

W.H.O. 2011. Guidelines for drinking-water quality world health organization [Online]. Switzerland. Available: http://www.who.int/water_sanitation_health/publications/dwq-guidelines-4/en/. Accessed: [November 2015].

W.H.O. 2010. Action is needed on chemeicals of major public health concern [Online]. World Health Organization. Available: http://www.who.int/ipcs/assessment/public_health/chemicals_phc/en/. Accessed: [13 February 2017].

Wiinberg B, Jensen AL, Rojkjaer R, et al.,. 2005. Validation of human recombinant tissue factor–activated thromboelastography on citrated whole blood from clinically healthy dogs. Vet Clin Pathol, 34: 389-393.

Wilbur S, Abadin H, Fay M, et al.,. 2011. Toxicological profile for chromium [Online]. Available: http://www.atsdr.cdc.gov. Accessed: [April 2013].

Wynn T. 2008. Cellular and molecular mechanisms of fibrosis. J Pathol, 214: 199-210.

Yoon S, Han S and Rana S. 2007. Molecular markers of heavy metal toxicity-a new paradigm for health risk assessment. J Environ Biol, 29: 1-14.

Young B, Lowe J, Stevens A, et al.,. 2006. Wheater's functional histology: A text and colour atlas, Philadelphia, Churchill Livingstone Elsevier. pp 2-325.

Zhang W, Houb ST and Stanimirovic D. 2015. Blood brain barrier protection in stroke: Taming TPA. In: The blood-brain barrier in health and disease, volume two: Pathophysiology and pathology. pp 226-246.

Appendix A

Published articles

An in ovo investigation into the hepatotoxicity of cadmium and chromium evaluated with light- and transmission electron microscopy and electron energy-loss spectroscopy

Chantelle Venter[a], Hester M. Oberholzer[a], Helena Taute[a], Franscious R. Cummings[b] & Megan J. Bester[a]

[a] Department of Anatomy, Faculty of Health Sciences, University of Pretoria, Pretoria, South Africa

[b] Electron Microscope Unit, University of the Western Cape, Bellville, South Africa
Published online: 01 Jun 2015.

PLEASE SCROLL DOWN FOR ARTICLE

Taylor & Francis
Taylor & Francis Group

An *in ovo* investigation into the hepatotoxicity of cadmium and chromium evaluated with light- and transmission electron microscopy and electron energy-loss spectroscopy

CHANTELLE VENTER[1], HESTER M. OBERHOLZER[1], HELENA TAUTE[1], FRANSCIOUS R. CUMMINGS[2] and MEGAN J. BESTER[1]

[1]*Department of Anatomy, Faculty of Health Sciences, University of Pretoria, Pretoria, South Africa*
[2]*Electron Microscope Unit, University of the Western Cape, Bellville, South Africa*

Excessive agriculture, transport and mining often lead to the contamination of valuable water resources. Communities using this water for drinking, washing, bathing and the irrigation of crops are continuously being exposed to these heavy metals. The most vulnerable is the developing fetus. Cadmium (Cd) and chrome (Cr) were identified as two of the most prevalent heavy metal water contaminants in South Africa. In this study, chicken embryos at the stage of early organogenesis were exposed to a single dosage of 0.430 μM physiological dosage (PD) and 430 μM ($\times$1000 PD) CdCl$_2$, as well as 0.476 μM (PD) and 746 μM ($\times$1000 PD) K$_2$Cr$_2$O$_7$. At day 14, when all organ systems were completely developed, the embryos were terminated and the effect of these metals on liver tissue and cellular morphology was determined with light- and transmission electron microscopy (TEM). The intracellular localization of these metals was determined using electron energy-loss spectroscopy (EELS). With light microscopy, the PD of both Cd and Cr had no effect on liver tissue or cellular morphology. At $\times$1000 PD both Cd and Cr caused sinusoid dilation and tissue necrosis. With TEM analysis, Cd exposed hepatocytes presented with irregular chromatin condensation, ruptured cellular membranes and damaged or absent organelles. In contrast Cr caused only slight mitochondrial damage. EELS revealed the bioaccumulation of Cd and Cr along the cristae of the mitochondria and chromatin of the nuclei.

Keywords: Cadmium, chromium, liver, mitochondria, electron energy-loss spectroscopy.

Introduction

Many heavy metals are essential for human biological functions and occur as structural elements, stabilizers of biological structures, components of control mechanisms like nerves and muscles, as well as components of redox systems.[1] However, some heavy metals, especially at high concentrations, can have toxic, carcinogenic and/or teratogenic effects. The main anthropogenic sources of human exposure to heavy metals are through agriculture, transport, mining and related operations. These activities are also the main sources of increased environmental heavy metal levels.[2]

Communities living in these regions that use contaminated water are the most vulnerable, especially children and pregnant woman, with the developing fetus being at risk. This water is used for drinking, preparing food, and bathing, as well as the irrigation of crops. Heavy metals are absorbed through the skin, by inhalation or orally [3] and the degree of heavy metal toxicity depends on the dose, duration, route of administration and other physiological factors, especially nutrition.[2,4] In the USA there is a lack of international standards for safe threshold levels for cadmium (Cd) especially related to pregnancy.[5] Likewise no information is available for other metals such as chromium (Cr) found in South Africa. The high rate of cellular division and differentiation of embryological cells and tissue makes the fetus highly vulnerable to the toxic effects of heavy metals.[5]

In South Africa the mining sector is estimated to be the fifth largest in the world and the largest reserve of manganese and platinum group metals worldwide is found within the country. South Africa also has one of the largest reserves of gold, diamond, chromium ore and vanadium.[6] When heavy metals from these mines are not correctly disposed of, heavy metal pollution is the consequential result. Several studies have shown that levels of these metals, especially chromium, lead, zinc, titanium, manganese,

strontium, copper and tin, are increased in various water sources.[7,8]

In the current study, two heavy metals, Cd and Cr, were identified based on the risk of exposure in South Africa during pregnancy.[9–11] In addition, both metals cross the placenta and the liver has been found to be a major site of Cd and Cr bio-accumulation.[12–14] The effect of these metals on the embryological cellular structure of the liver was evaluated using an *in ovo* chick model. In conjunction with the histological and ultrastructural evaluation, electron energy-loss spectroscopy (EELS) was used to analyse the possible presence and location of the heavy metals in the liver tissue.

Materials and methods

Obtaining fertilized eggs

Ethical clearance for the use of chicken embryos for experimental purposes was obtained from the Animal Ethics Committee (AEC) of the University of Pretoria (h006-13), South Africa. Fertilized broiler hatching eggs were obtained from a local farmer in the Bronkhorstspruit district in Gauteng, South Africa. A total number of 75 eggs were used (15 eggs per group) and the eggs were incubated at 37°C for two days before exposure.

Exposure

On the third embryonic day, a hole was drilled into the blunt end (air chamber) of the egg under aseptic conditions. The relevant concentrations of the control and experimental groups were injected into the eggs through the air sac onto the chorioallantoic membrane (CAM) using a calibrated micropipette. The four experimental groups were exposed to different concentrations of the two heavy metals used in this study as indicated in Table 1. The heavy metals were administered as $CdCl_2$ [Merck (Pty) Ltd, South Africa] and $K_2Cr_2O_7$ [Merck (Pty) Ltd, South Africa] at physiological dose (PD), ×1000 PD dissolved in sterile water.

The Cd and Cr concentrations were calculated according to the human physiological dose (Cd: 30 μg[15] and Cr: 284.28 μg[16]) and subsequently downscaled to be at the physiologically appropriate concentration for the embryos. After the heavy metal administration, the holes

Table 1. Control and experimental group dosages.

Group	Exposure (μM metal ion)
Control	ddH_2O
Cd PD	0.430 μM
Cd ×1000 PD	430 μM
Cr PD	0.476 μM
Cr ×1000 PD	476 μM

were sealed with paraffin wax and were then returned to the incubator for 11 days.

Termination

On day 14, the embryos were terminated, liver tissue harvested and cut into 1 mm^3 for transmission electron microscopy with the remainder of the sample processed for light microscopy.

Light microscopy tissue processing

The liver samples were fixed in a 2.5% glutaraldehyde (GA)/formaldehyde (FA) in 0.075M sodium phosphate (Na_3PO_4) buffer (pH = 7.4) solution and dehydrated in 30%, 50%, 70%, 90% and three changes of 100% ethanol. The samples were cleared with xylene (Sigma-Aldrich, South Africa), embedded in paraffin wax (Sigma-Aldrich) and 3–5 μm sections were made with a Leica RM 2255 wax microtome (Leica Biosystems GmbH Nussloch, Germany). Tissue sections were stained with haematoxylin and eosin (H&E) to evaluate general tissue morphology with a Nikon Optiphod transmitted light microscope (New York, NY, USA). Three samples were randomly selected from each group for light microscopy analysis.

Transmission electron microscopy tissue processing

The liver samples were fixed in 2.5% GA/FA in 0.075M PO_4 buffer (pH = 7.4), rinsed three times in 0.075M PO_4 buffer before it was placed in the secondary fixative, 1% osmium tetroxide solution for 1 h. Following secondary fixation, the samples were rinsed again as described above. The samples were then dehydrated in 30%, 50%, 70%, 90% and three changes of 100% ethanol. All reagents were obtained from Sigma-Aldrich, South Africa. The samples were embedded in EMbed resin (SPI supplies, West Chester, PA, USA) and ultra-thin sections (70–100 nm) were cut with a diamond knife using an ultramicrotome (Leica Biosystems GmbH). Samples were then contrasted with uranyl acetate and lead citrate, after which they were examined with a JEOL transmission electron microscope (TEM) (JEM 2100F, Tokyo, Japan). Three samples were randomly selected from each group for TEM analysis.

Electron energy-loss spectroscopy measurements

The Tecnai F20 high resolution TEM (200 kV, FEI, Hillsboro, OR, USA) equipped with the GIF 2001 energy filter for electron energy-loss spectroscopy (EELS) and electron spectral imaging (ESI) analyses was used to evaluate ±60 nm thick liver sections. When an unidentified electron-dense granule or cluster of electron-dense granules was observed in the tissue with TEM, the EELS was used to determine if these clusters contained the heavy metals

under investigation. The results were displayed as an EELS spectrum, confirming the presence of the heavy metals in the sample. Together with the ESI color map of the specific area analyzed, the exact position of the metals in the sample was visually expressed.

Due to the low energy-loss signals of the different metals, the EELS spectra were collected in normal parallel beam TEM mode, without an objective aperture and employing a GIF entrance aperture of 3 mm. This allowed for the use of a large collection semi-angle, $\beta \sim 100$ mrad, which greatly improved the signal-to-noise ratio of the spectra. To remove the effects of plural scattering and the contribution from low energy plasmon losses, each spectrum was background subtracted using a power law lineshape. This was followed by further deconvoluting the ionization edges using a Log-Fourier iterative process, as to remove all other plural scattering contribution.

The ESI maps were collected using the Gatan 3 window method with an energy slit width of 20 eV. For construction of the Cr map, the pre-edge 1 and pre-edge 2 energy windows were centered at 515 and 550 eV, respectively, whereas the post-edge window was centered at 583 eV so as to coincide with the onset of the Cr $L_{2,3}$ ionization edge at 573 eV. The positions of the pre-edge 1 and 2 windows were based on the background subtraction model obtained from the EELS analyses when using 2 energy windows. This ensured that only energy loss contributions from the metal under investigation were mapped. Similarly, for mapping of the energy-loss contributions of Cd, the pre-edge 1 and 2 windows were placed at 374 and 394 eV, with a post-edge onset centered at 414 eV.

Results

In Figures 1A and B the normal embryonic histology of the liver can be seen with multi-cellular layered plates of hepatocytes (white arrows), and normally spaced
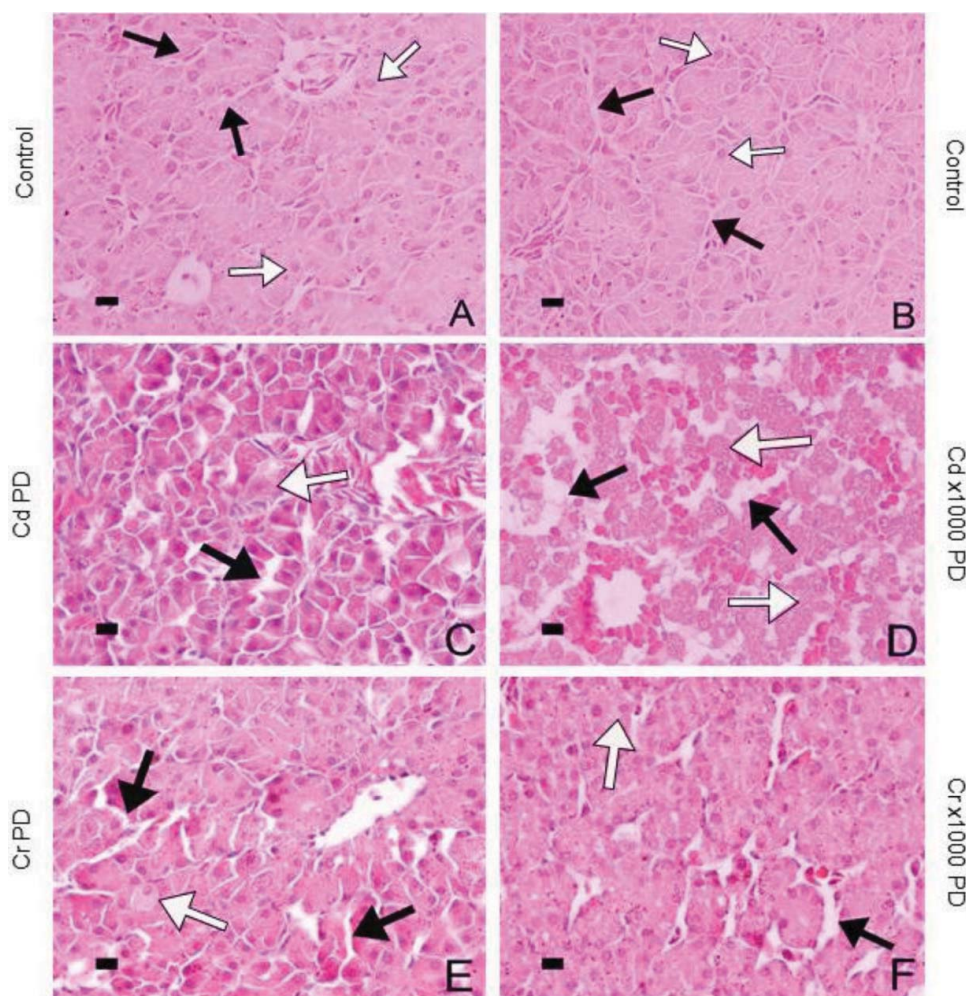
Fig. 1. Light microscopy micrographs of the liver tissue of the different experimental groups. A and B: control group. C and D: Cd PD and Cd ×1000 PD groups, E and F: Cr PD and Cr ×1000 PD groups. Black arrows indicate sinusoid dilation, white arrows in Figure A and B indicate the normal histology of the hepatocytes, whereas in Figures C-F the white arrows indicate cells undergoing necrosis (Scale bars: 10 µm).

sinusoids (black arrows). Figures 1C and D are representative of embryos exposed to the PD of Cd and ×1000 PD respectively. Minimal sinusoidal dilation is visible in the Cd PD group (indicated in Figure 1C), with a noticeable increase in sinusoidal dilation in the Cd ×1000 PD group (Fig. 1D) (black arrows). Some necrosis is also visible in both Cd concentration groups indicated by the white arrows in Figures 1C and 1D. This was not observed in the control group. The same pattern can be seen in the groups exposed to Cr as indicated in Figures 1E and 1F, but with less severity. In both Figures 1E and 1F the black arrows indicate sinusoidal dilation and the white arrows indicate necrosis of the hepatocytes.

Representative TEM micrographs of the liver tissue from the control and Cd experimental groups are shown in Figure 2. A hepatocyte, typical of the control samples, is shown in Figures 2A and 2B with normal cellular [Fig. 2A (black arrows)] and nuclear double membranes and evenly dispersed chromatin [Fig. 2A (white arrow)]. The mitochondria displayed a typical round or oval shape, with a double membrane that surrounds the cristae of the mito-

Fig. 2. Transmission electron micrographs of the hepatocytes and mitochondria of the liver tissue from the control and the different Cd concentration groups. Figure A: control, C: Cd PD and E: Cd ×1000 PD. White arrows indicate the nuclei of the hepatocytes and the black arrows indicate the cellular membranes. Figures B, D and F indicate the mitochondrial morphology (black arrows) of the control (B), Cd PD (D) and Cd ×1000 PD (F) groups (Scale bars: A, C and E = 5 μm; B and D = 2 μm; F = 1 μm).

chondria [Fig. 2B (black arrow)]. In Figures 2C and 2D the hepatocytes of the Cd PD group revealed no significant variations compared to the control (Fig. 2A), with evenly dispersed nuclear chromatin, no mitochondrial damage [Fig. 2D (black arrow)] and intact nuclear [Fig. 2C (white arrows)] and cellular membranes [Fig. 2C (black arrows)]. Figures 2E and 2F are representative of the Cd ×1000 PD group where major alterations can be seen compared to the control group.

Figure 2E reveals major disruption of the typical hepatocyte morphology with irregular chromatin condensation [Fig. 2E (white arrow)], a ruptured cellular membrane [Fig. 2E (black arrow)] and damaged or absent organelles, as seen in Figure 2F that indicates an extensively damaged mitochondria (black arrow). Further evaluation with ESI micrographs identified the bio-accumulation of Cd in the nuclei of the hepatocytes (Fig. 3E). Figure 3A shows the Cd edge that was used in the EELS analysis, with Figures 3B–3D indicating the ESI micrographs of Cd in the nucleus of the hepatocyte at each specific edge that was analyzed. Figure 3E indicates the final Cd map, with the Cd in white.

In Figure 4, liver tissue from the Cr-exposed groups is shown and again compared to the same control micrograph as shown in Figure 2. The hepatocyte [Fig. 4C (black arrow)] and nuclear morphology [Fig. 4C (white arrow)] in the Cr PD group revealed no alterations, but

the mitochondria [Fig. 4D (black arrow)] showed minimal mitochondrial inner matrix swelling. The Cr ×1000 PD group, shown in Figures 4E and 4F, respectively, are comparable to that of the control as little to no damage is observed with evenly spaced chromatin and intact cellular [Fig. 4E (black arrow)] and nuclear [Fig. 4E (white arrow)] membranes. Only slight damage to the mitochondrial membrane was observed [Fig. 4F (black arrows)]. EELS analysis of the mitochondria revealed the presence of Cr associated with the cristae as indicated in Figure 5E. Figure 5A shows the specific edges used in the EELS analysis, with Figures 5B—D indicating the ESI micrographs of Cr in the mitochondria of the hepatocyte at each specific edge that was analyzed. Figure 5E indicates the final Cr map, with the Cr in white.

Discussion

The primary effect of heavy metal toxicity is oxidative stress that causes reactive oxygen species (ROS), which affects essential functions of the membranes through lipid peroxidation, DNA oxidation and formation of protein aggregates.[17] In addition, heavy metals such as Cd and Cr may also have an effect on antioxidant elements such as glutathione reductase, glutathione peroxidase, superoxide dismutase and catalase.[18] Damage and loss of

Fig. 3. EELS and ESI micrographs of liver tissue exposed to Cd ×1000 PD. Figure A shows the Cd edge that was used in the EELS analysis, with Figures B-D indicating the ESI micrographs of Cd in the nucleus of the hepatocyte at each specific edge that was analyzed. Figure E indicates the final Cd map, with the Cd in white (Scale bars: B, C, D and E: 1 μm).
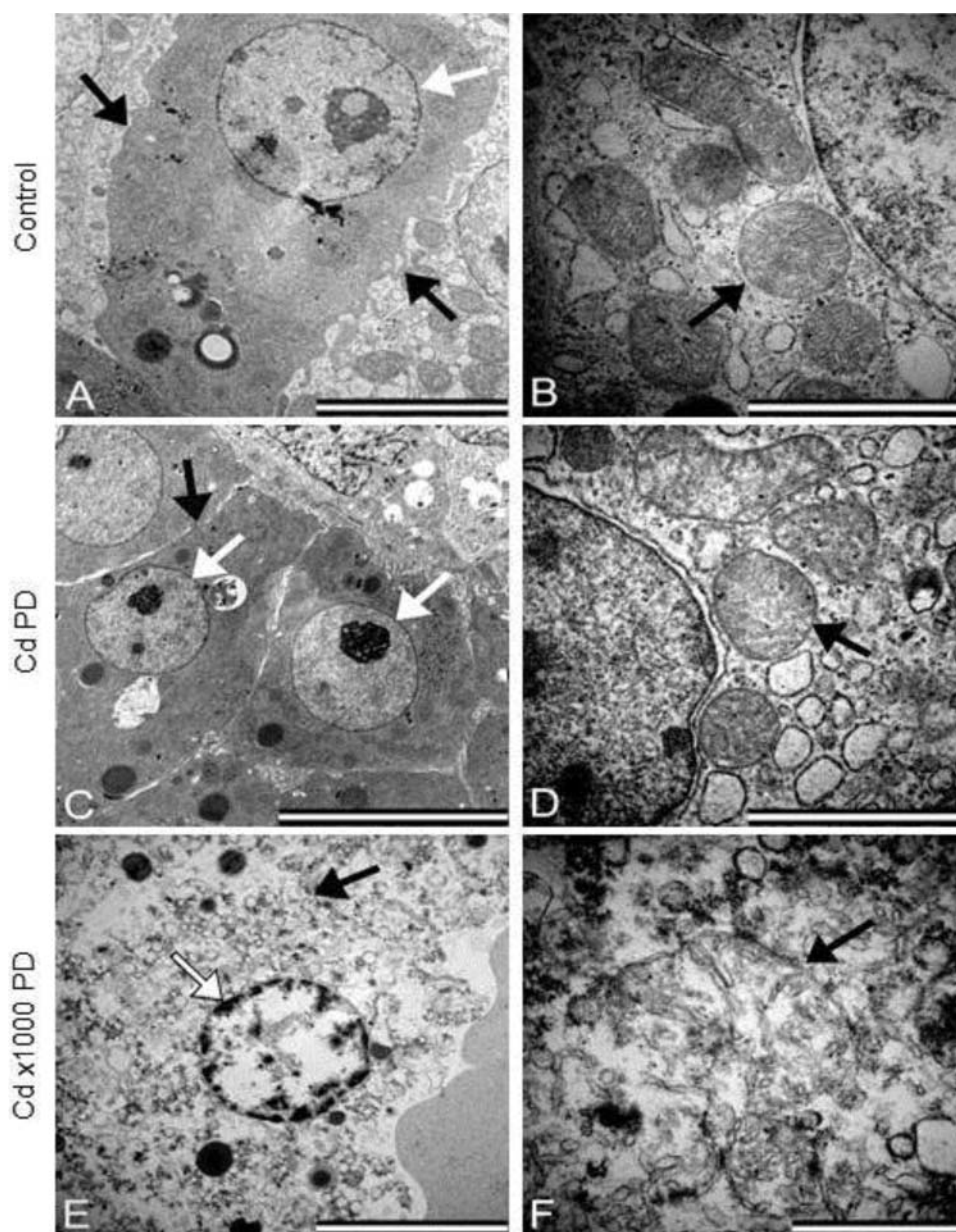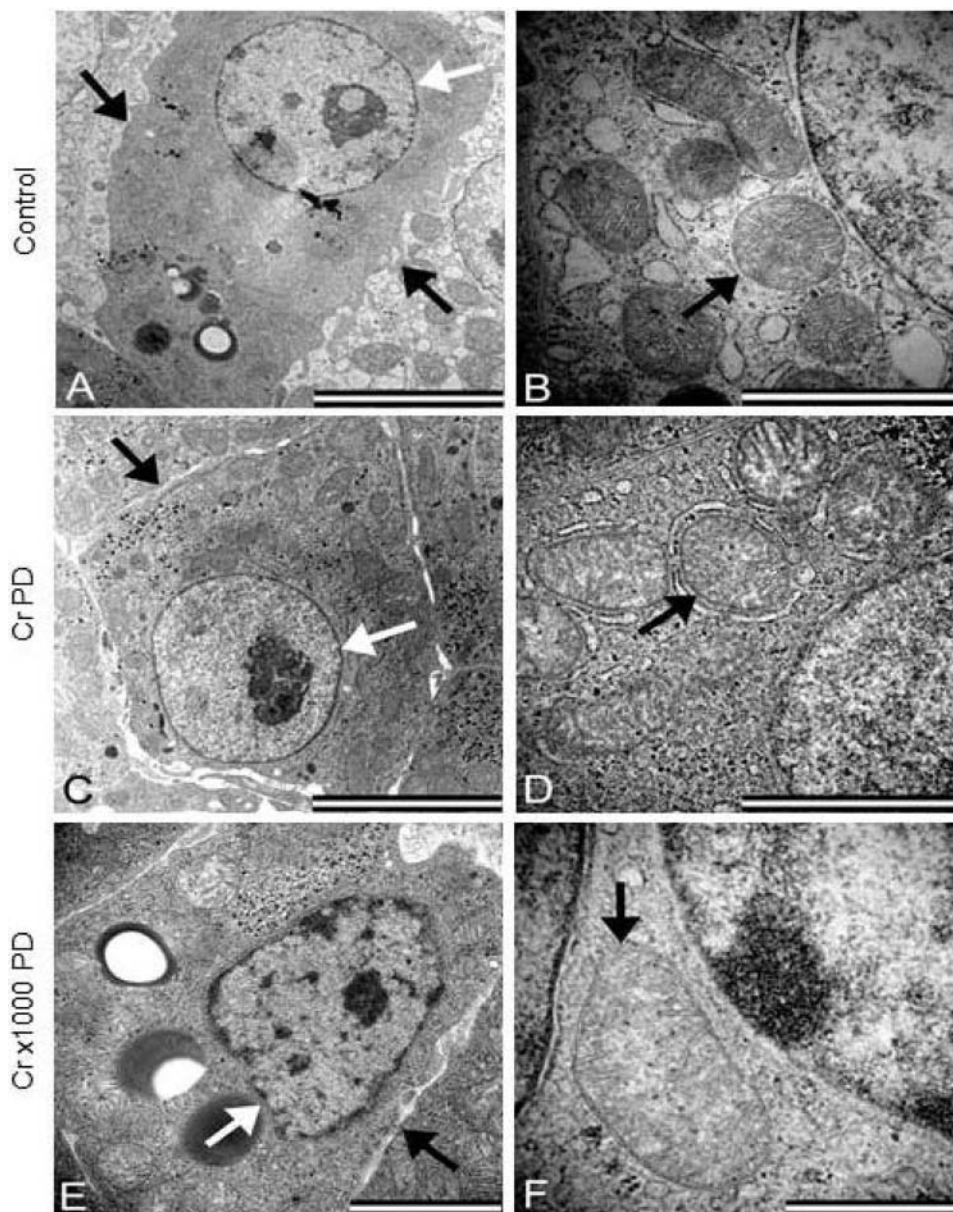
Fig. 4. Transmission electron micrographs of the hepatocytes and mitochondria of the liver tissue of the control and different Cr experimental groups. Figure A: control, C: Cr PD and E: Cr ×1000 PD. The white arrows indicate the nuclei of the hepatocytes and the black arrows indicate cellular membranes. Figures B, D and F indicate the mitochondrial morphology (black arrows) of the control, Cr PD and Cr ×1000 PD groups respectively (Scale bars: A and C = 5 μm; B, D and E = 2 μm; F = 1 μm).

essential function and/or depletion of antioxidant elements can lead to apoptosis and necrosis.[17]

In this study, the effects of Cd and Cr on liver tissue were examined using light microscopy and TEM. Compared to the control, Cd and Cr at PD and ×1000 PD caused sinusoidal dilation and necrosis. Jihen et al. reported sinusoidal dilation and necrosis in rat liver tissue after Cd exposure.[19] Acharya et al. evaluated the effects of Cr on rats and found that Cr caused an increase in sinusoidal space, vacuolation and necrosis in the liver tissue of

these animals.[20] These studies differ in the animal model, dosage and concentrations of the metals used, however it is clear from this study that in the *in ovo* model, Cd and Cr are absorbed and cause significant hepatic damage in the developing embryo.

Evaluation of hepatocyte morphology at an ultrastructural level revealed no observable differences between the PD groups compared to the controls, and hepatocytes in both groups had evenly dispersed chromatin and no nuclear or cellular membrane damage. In contrast, in the
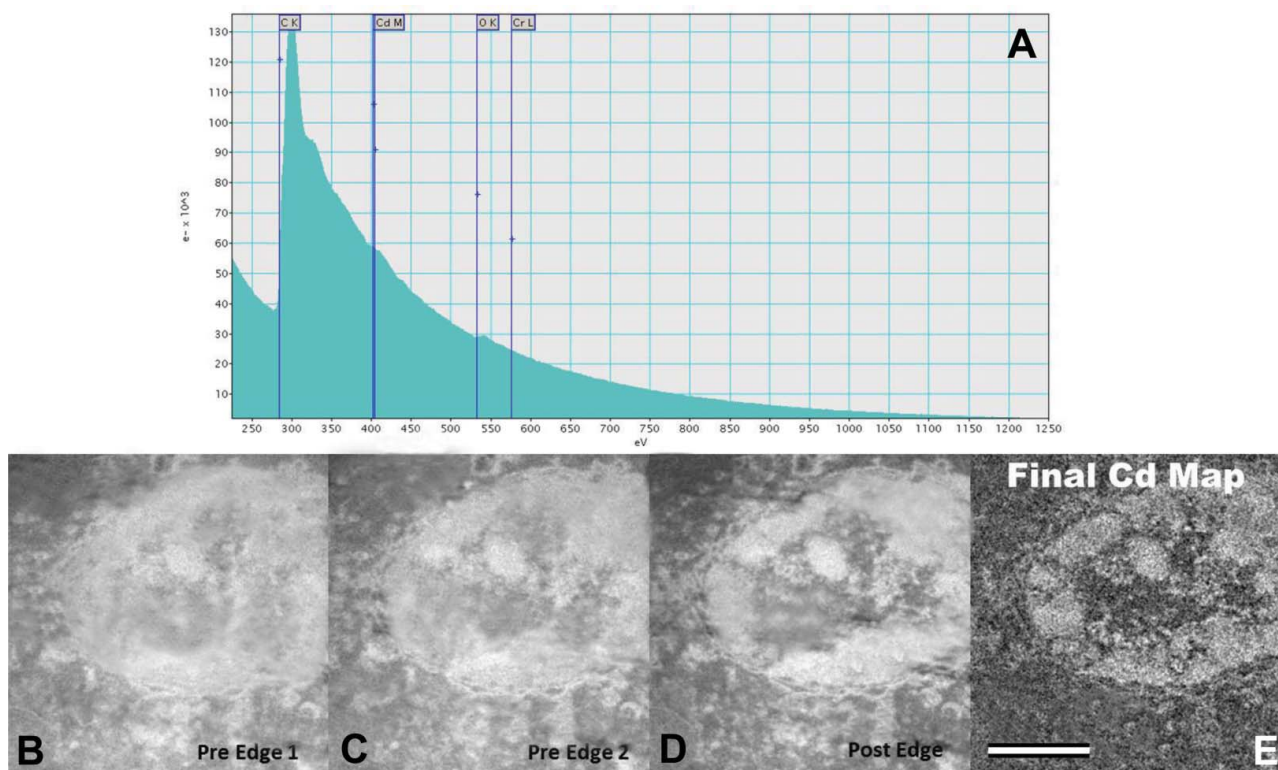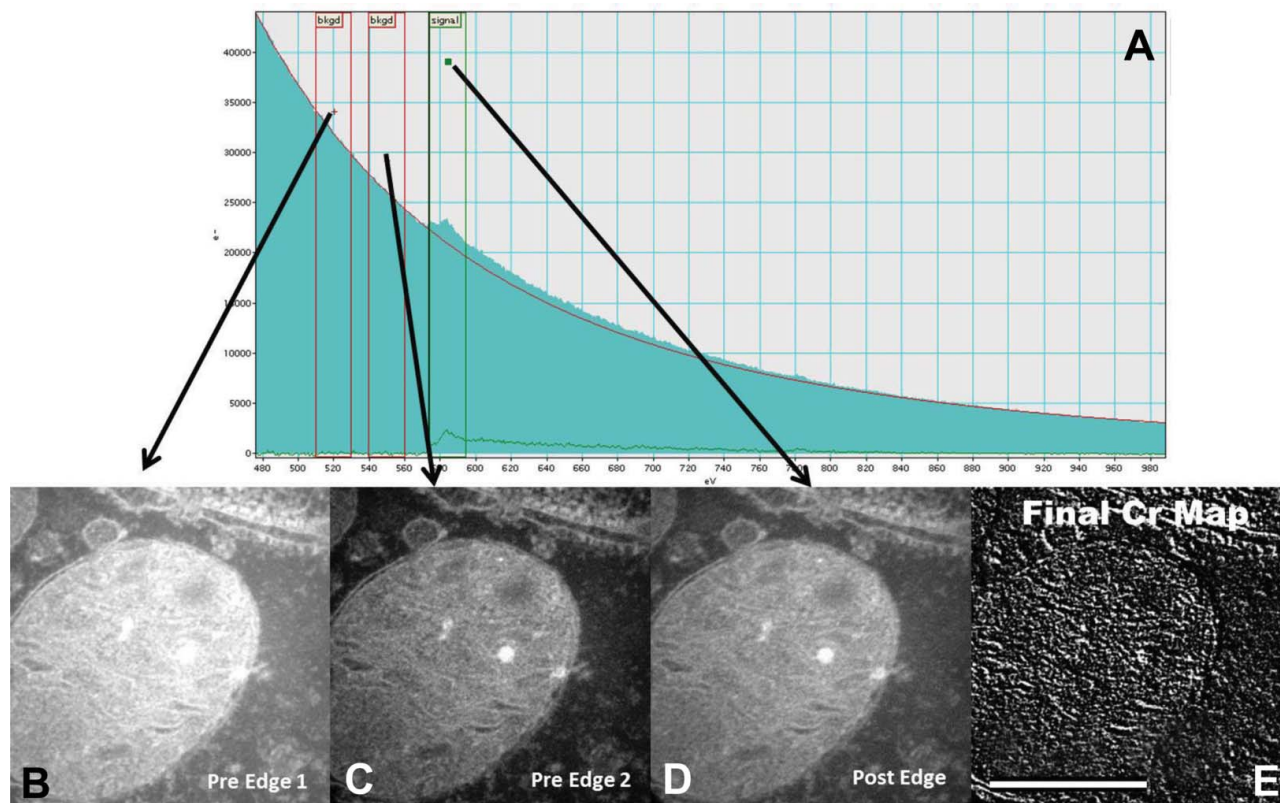
Fig. 5. EELS and ESI micrographs of liver tissue exposed to Cr ×1000 PD. Figure A shows the specific edges used in the EELS analysis, with Figures B-D indicating the ESI micrographs of Cr in the mitochondria of the hepatocyte at each specific edge that was analyzed. Figure E indicates the final Cr map, with the Cr in white (Scale bars: B, C, D and E: 0.5 μm).

×1000 PD groups, especially in the Cd ×1000 PD group, severe cellular damage was observed. Damage to the cell membrane, irregular chromatin condensation and mitochondrial damage was observed.

In 2000, Karmakar et al. investigated the effects of Cd exposure on the liver tissue of male Balb/c mice using light microscopy and TEM. The mice were exposed for 7, 14 and 21 days. At day 21, light microscopy revealed altered tissue morphology of the liver. Further TEM analysis revealed changes in the nuclei and mitochondria of the hepatocytes.[21] Similar structural changes in the morphology of liver tissue were found in mice exposed to Cr. In this study, Wang and colleagues, exposed mice to Cr and found that Cr can induce dose- and time-dependent DNA damage, hepatic oxidative stress and apoptosis in the hepatocytes.[22]

Increased levels of ROS cause lipid peroxidation that results in changes in increased membrane fluidity, which brings about the efflux of cytoplasmic solutes and loss of membrane–protein activity.[17] Extensive lipid peroxidation causes total loss of membrane integrity, as observed in the Cd ×1000 PD group. In addition to oxidative damage, ROS can cause the carboxylation of protein, and ineffective proteosomal degradation can lead to the formation and accumulation of high molecular mass aggregates.[17]

At equimolar concentrations, the ultrastructural effects of Cr were less than that of Cd; where for Cr the cell and nuclear membranes appeared to be intact, although some mitochondrial damage was observed. The reason for the more severe cellular damage observed in the Cd group may be due to the fact that Cr is naturally found in the body and is easily converted to a less toxic form by existing biochemical pathways.[16,23,24] Cd, on the other hand, is not naturally found in the body and thus the body needs to produce metallothionein to restrict the toxicity of Cd. During the production of metallothionein, Cd can damage the tissue, which may lead to altered liver and kidney functions.[15,25,26]

EELS analysis revealed bio-accumulation of the Cd and Cr in the nuclei and mitochondria of the hepatocytes. In two studies done by Lui and Kottke in 2003, the authors also found Cd and Cr present in the deposits of electron-dense granules in the nuclei and cell membranes of root cells after exposure to Cr for 1, 3 and 6 days and to Cd for 9 days.[27,28] Chemical quantification of Cd and Cr has shown that these metals accumulate in cells.[19,29] In contrast, EELS analysis identifies the intracellular sites of bioaccumulation and these specific sites are the nucleus and mitochondria as shown in Figures 3E and 5E for Cd and Cr respectively. Very little Cd is present in the cytoplasm

compared to that present in the nucleus. In the nucleus, Cd is present in the nuclear membrane and is also found with the chromatin. The effect of Cd on nuclear DNA is indirect, and increased oxidative stress is the result of Cd binding DNA amino bases and proteins, which can lead to direct DNA strand breaks and/or epigenetic changes.[30]

Membrane-associated mitochondrial complexes I and III are the major sites of intracellular ROS formation. Within the mitochondrial electron transport chain of complex I are several redox centers that can react with molecular oxygen, leading to the formation of the superoxide anion. This superoxide anion is released into the mitochondrial matrix and transformed into hydrogen peroxide either spontaneously or via manganese superoxide dismutase. The superoxide anion formed by complex III is also converted to hydrogen peroxide by Cu/Zn-dependent superoxide dismutase. The formation of water from hydrogen peroxide is catalyzed by catalase or glutathione peroxidase, or scavenged by mitochondrial thioredoxin, glutaredoxin as well as cytochrome c.[31] In the presence of excess reduced transition metals Fenton transformation occurs, which catalyzes the conversion of hydrogen peroxide to highly reactive hydroxyl ion and causes extensive damage to DNA, proteins and lipids. Both Cd and Cr were found to have accumulated very specifically along the cristae of the mitochondria as shown in Figure 5E for Cr. Associated along this membrane is complex I and III, the site where the superoxide anion is formed. Whether Cd and Cr directly bind to these proteins found in the cristae is unknown and is an important area of further research.

Conclusion

In conclusion Cd and Cr bio-accumulates in the mitochondria and nucleus of hepatocytes. At these sites both metals can cause DNA base modification, changes in cellular homeostasis and increased lipid peroxidation. The consequence of lipid peroxidation and DNA damage namely membrane damage and DNA condensation was observed for Cd while only mitochondria associated damage was observed for Cr.

Acknowledgments

References

[1] Nordberg, G.F.; Fowler, B.A.; Nordberg, M.; Friberg, L.T. Introduction-General Considerations and International Perspectives. In *Handbook of Toxicology of Metal*; Nordberg, G.F.; Nogawa, K.; Nordberg, M.; Friberg, L.T., Eds.; Academic Press: Amsterdam and Boston, 2007a; 4–9.

[2] Al-Attar, A.M. Antioxidant effect of vitamin E treatment on some heavy metals-induced renal and testicular injuries in male mice. Saudi. J. Biol. Sci. **2011**, *18*, 63–72.

[3] Awofolu, O.R.; Mbolekwa, Z.; Mtshemla, V.; Fatoki, O.S. *Levels of trace metals in water and sediment from Tyume River and its effects on an irrigated farmland*, Water SA 31: South Africa, 2005; 87–94.

[4] Chowdhury, A.R. Recent Advances in Heavy Metals Induced Effect on Male Reproductive Function-A Retrospective. Med. Sci. **2009**, *2*(2), 37–42.

[5] Taylor, C.M.; Golding, J.; Emond, A.M. Lead, cadmium and mercury levels in pregnancy: the need for international consensus on levels of concern. Dev. Orig. Health. Dis. **2014**, *5*(1), 16–30.

[6] SouthAfrica.info. Available at http://www.southafrica.info (accessed May 2013).

[7] Binning, K.; Baird, D. *Survey of heavy metals in the sediments of the Swartkops River Estuary, Port Elizabeth South Africa*, Water SA: South Africa, 2001; *27*, 461–466.

[8] Naicker, K.; Cukrowska, E.; McCarthy, T.S. Acid mine drainage arising from gold mining activity in Johannesburg, South Africa and environs. Environ. Pollut. **2003**, *122*(1), 29–40.

[9] Fatoki, O.S.; Awofolu, R. *Levels of Cd, Hg and Zn in some surface waters from the Eastern Cape Province*, Water SA: South Africa, 2003; *29*, 375–380.

[10] Molokwane, P.E.; Meli, K.C.; Nkhalambayausi—Chirwa, E.M. Chromium (VI) reduction in activated sludge bacteria exposed to high chromium loading: Brits culture (South Africa). Water res. **2008**, *42*(17), 4538–4548.

[11] IOL Scitech. Witbank air dirtiest in the world. Available at http://www.iol.co.za/scitech/science/environment/(accessed Apr 2013)

[12] Gonzalez, P.; Baudrimont, M.; Boudou, A.; Bourdineaud, J.P. Comparative effects of direct cadmium contamination on gene expression in gills, liver, skeletal muscles and brain of the zebrafish (*Danio rerio*). BioMetals. **2006**, *19*(3), 225–235.

[13] Kuriwaki, J.I.; Nishijo, M.; Honda, R.; Tawara, K.; Nakagawa, H.; Nishijo H. Effects of cadmium exposure during pregnancy on trace elements in fetal rat liver and kidney. Toxicol. Lett. **2005**, *156*(3), 369–376.

[14] Robinson, J.; Avenant—Oldewage, A. *Chromium, copper, iron and magnesium bioaccumulation in some organs and tissue of Oreochromis mossambicus from the lower Olifants River, inside the Kruger National Park*, Water SA, **2006**; *23*, 387–403.

[15] Nordberg, G.F.; Nogawa, K.; Nordberg, M.; Friberg, L.T. Cadmium. In *Handbook of Toxicology of Metals*; Nordberg, G.F.; Nogawa, K.; Nordberg, M.; Friberg, L.T., Eds.; Academic Press: Amsterdam and Boston, 2007b; 445–486.

[16] Langård, S.; Costa, M. Chromium. In *Handbook on the Toxicology of Metal*; Nordberg, G.F., Fowler, B.A., Nordberg, M., Friberg, L.T., Eds. Academic Press: Amsterdam and Boston, 2007; 487–510.

[17] Avery, S.V. Molecular targets of oxidative stress. Biochem. **2011**, *434*, 201–210.

[18] Kim, S.H.; Jung, M.J.; Lee, Y.M. Effects of heavy metals on the antioxidant enzymes in the marine ciliate Euplotes Crassus. Toxicol. Environ. Health Sci. **2011**, *3*(4), 213–219.

[19] Jihen, E.H.; Imed, M.; Fatima, H.; Abdelhamid, K. Protective effects of selenium (Se) and zinc (Zn) on cadmium (Cd) toxicity in the liver and kidney of rats: Histology and Cd accumulation. Food. Chem. Toxicol. **2008**, *46*(11), 3522–3527.

[20] Acharya, S.; Mehta, K.; Krishnan, S.; Vaman Rao, C. A subtoxic interactive toxicity study of ethanol and chromium in male Wistar rat. Alcohol **2001**, *23*(2), 99–108.

[21] Karmakar, R.; Bhattacharya, R.; Chatterjee, M. Biochemical, haematological and histopathological study in relation to time-related cadmium-induced hepatotoxicity in mice. BioMetals **2000**, *13*(3), 231–239.

[22] Wang, X.F.; Xing, M.L.; Shen, Y.; Zhu, X.; Xu, L.H. Oral administration of Cr(VI) induced oxidative stress, DNA damage and apoptosis cell death in mice. Toxicology **2006**, *228*(1), 16–23.

[23] Dayan, A.D.; Paine, A.J. Mechanisms of chromium toxicity, carcinogenicity and allergenicity: Review of the literature from 1985 to 2000. Hum. Exp. Toxicol. **2001**, *20*(9), 439–451.

[24] Raghunathan, V.K.; Ellis, E.M.; Grant, M.H. Response to chronic exposure to hexavalent chromium in human monocytes. Toxicol. in Vitro **2009**, *23*(4), 647–652.

[25] Prozialeck, W.C.; Edwards, J.R.; Woods, J.M. The vascular endothelium as a target of cadmium toxicity. Life. Sci. **2006**, *79*(16), 1493–1506.

[26] Valko, M.; Rhodes, C.J.; Moncola, J.; Izakovic, M.; Mazura, M. Free radicals, metals and antioxidants in oxidative stress-induced cancer. Chem. Biol. Interact. **2006**, *160*(1), 1–40.

[27] Lui, D.; Kottke, I. Subcellular localization of Cd in the root cells of Allium sativum by electron energy loss spectroscopy. J. Biosci. **2003a**, *28*(4), 471–478.

[28] Lui, D.; Kottke I. Subcellular localization of chromium and nickel in root cells of *Allium cepa* by EELS and ESI. Cell. Biol. Toxicol. **2003b**, *19*(5), 299–311.

[29] Krumschnable, G.; Nawaz, M. Acute toxicity of hexavalent chromium in isolated teleost hepatocytes. Aquat. Toxicol. **2004**, *70*(2), 159–167.

[30] Ray, D.R.; Yonsim, A.; Fry, R.C. Incorporating epigenetic data into the risk assessment progress for the toxic metal arsenic, cadmium, chromium, lead and mercury; strategies and challenges. Front. Genet. **2014**, *5*, 1–26.

[31] Moreira, A.C.; Machando, N.G.; Bernardo, T.C.; Sardão, V. A.; Oliveira, P.J. Mitochondria as a biosensor for drug-induced toxicity – Is really relevant? InTech. **2011**, *4*(1), 411–444.

MICROSCOPY
RESEARCH&TECHNIQUE

RESEARCH ARTICLE

WILEY
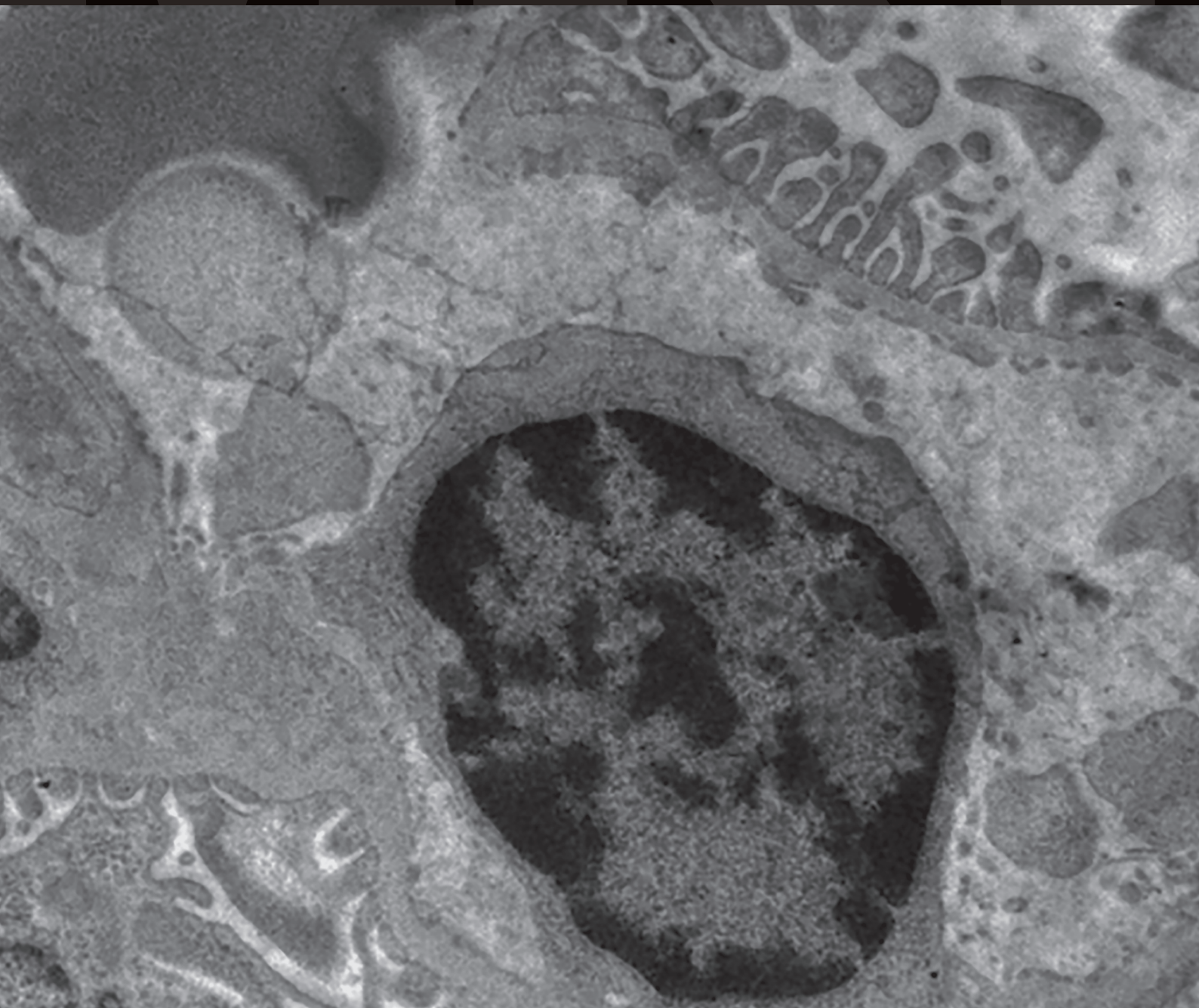
Effects of metals cadmium and chromium alone and in combination on the liver and kidney tissue of male Spraque-Dawley rats: An ultrastructural and electron-energy-loss spectroscopy investigation

Chantelle Venter[1] | Hester Magdalena Oberholzer[1] [iD] |
Franscious Riccardo Cummings[2] | Megan Jean Bester[1]

[1]Department of Anatomy, Faculty of Health Sciences, University of Pretoria, Private Bag x323, Arcadia 0007, South Africa

[2]Electron Microscope Unit, University of the Western Cape, Private Bag X17, Bellville 7535, South Africa

Correspondence
H. M. Oberholzer, Department of Anatomy, Faculty of Health Sciences, University of Pretoria, Private Bag x323, Arcadia 0007, South Africa.
Email: nanette.oberholzer@up.ac.za

Review Editor: Dr. Mingying Yang

Abstract

Heavy metal pollution has increased in the last decades. Water sources are contaminated and human exposure is often long term exposure to variable amounts of different metals. In this study, male Sprague-Dawley rats were exposed via oral gavage for 28 days to cadmium (Cd) and chromium (Cr), alone and in combination at concentrations 1000 times the human World Health Organization's acceptable water limits. Rat equivalent dosages were used. Blood markers of liver and kidney function were measured, changes to cellular morphology was determined with transmission electron microscopy and the intracellular metal localisation was determined with the electron energy-loss spectroscopy and energy filtered transmission electron microscopy analysis. Both Cd and Cr caused changes to the nuclear and mitochondrial membranes and irregular chromatin condensation of hepatocytes. Cr exposure caused dilation of the rough endoplasmic reticulum (rER). The combination caused nuclear and mitochondrial membrane damage as well as irregular chromatin condensation. In the kidney tissue, Cd caused irregular chromatin condensation in the cells of the proximal convoluted tubule (PCT). Cr caused changes to the outer nuclear and mitochondrial membrane and chromatin structure. The combination group caused membrane damage, irregular chromatin condensation and rER changes in the PCT. All the metal groups showed damage to the endothelial cells and pedicles, but not to the mesangial cells. Cd and Cr bioaccumulation was observed in the nucleus, mitochondria and rER of the liver and kidney and therefore are responsible for the cellular observed damage that can cause functional changes to the tissues and organs.

KEYWORDS
chronic effects, environmental toxicity, heavy metals

1 | INTRODUCTION

The growth in the industrial sector has provided many benefits since its establishment, but has come with some unfavourable environmental effects. Heavy metals have become synonymous with industrial pollution due to their toxicological and physiological effects on the ecosystem (Al-Othman, Ali, & Naushad, 2012). Most of the heavy metal pollution can be linked to anthropogenic activities, such as mines, foundries, smelters, and other metal-based industrial operations (Al-Attar,

2011; Tchounwou, Yedjou, Patlolla, & Sutton, 2012), with cigarette smoking being the main nonoccupational source of heavy metal pollution (Langárd & Costa, 2007; Prozialeck & Edwards 2012). The increase in heavy metal levels in the water sources, directly affects the people in the affected areas that are using the water for consumption, preparing food, and bathing, as well as the irrigation of crops. Heavy metals can be absorbed through the skin, orally, or through inhalation (Awofolu, Mbolekwa, Mtshemla, & Fatoki, 2005; Venter, Oberholzer, Taute, Cummings, & Bester, 2015). The degree of heavy metal toxicity

depends on dose, duration, route of administration, and other physiological factors, especially nutrition (Al-Attar, 2011; Chowdhury, 2009). In addition, exposure is not limited to a single heavy metal but a mixture of different types such as a combination of cadmium (Cd), chromium (Cr), Mercury (Hg), and/or Copper (Cu) (Venter & Oberholzer 2015).

In this study, the heavy metals Cd and Cr were focused on based on the likelihood of being exposed to them in South Africa. South Africa is known for its thriving mining sector which include manganese, platinum, gold, diamond, chromium and vanadium mines, of which the waste can cause heavy metal pollution, if not discarded correctly. This is unfortunately seen in areas in the Gauteng and Western Cape provinces in South Africa (Malan, Müller, Cyster, Raitt, & Aalbers, 2015; Venter et al., 2015). Both these metals can, depending on the route of exposure, effect the lungs, liver, kidneys, cardiovascular, and skeletal systems and may lead to cancer (Jomova & Valko, 2011; Langárd & Costa, 2007; Prozialeck & Edwards, 2012). Only the liver and kidneys were focused on in this study, as these organs play a major role in the absorption, distribution, and excretion of toxic compounds, like Cd and Cr (Timbrell, 1999). In the liver and kidney, Cd and Cr are metabolized differently, but induce similar effects namely oxidative stress that leads to lipid peroxidation, protein and DNA damage and apoptosis. These effects may lead to functional and ultrastructural changes to the tissue and cellular components of the liver and kidney (Timbrell, 1999; Venter & Oberholzer, 2015).

The aim of this study was to investigate the possible changes and bio-accumulation in the liver and kidney tissue of male Sprague-Dawley rats after exposure to Cd and Cr alone and in combination.

2 | MATERIALS AND METHODS

2.1 | Spraque-Dawley rat model

Six-week-old male Spraque-Dawley rats (200-250 g) were obtained from the University of Pretoria Biomedical Research Centre (UPBRC). A room temperature of 22°C ($\pm$2°C); relative humidity of 50% ($\pm$20%) and a 12 h light/dark cycle were maintained during the entire study. All experimental protocols complied with the requirements of the University of Pretoria Animal Ethics Committee (Animal ethics number: H009-15). Twenty four rats were randomly divided into four groups, containing 6 rats each. The animals were allowed to acclimatise for 7 days prior to exposure for 28 days.

2.2 | Metal administration

Cadmium chloride ($CdCl_2$) [Merck (Pty), South Africa] and potassium dichromate ($K_2Cr_2O_7$) [Merck (Pty), South Africa] were dissolved in sterile water and was administered to the rats via oral gavage. The control rats only received saline and the daily dosages were as indicated in Table 1. Selected concentrations were 1000 times the World Health Organization's (WHO) acceptable water limits (μg/L) for Cd and Cr (WHO, 2011). The metal dosage (μg/L) for an average person of 60.7 kg, drinking 1.4 L of water per day was calculated and converted

TABLE 1 *In vivo* control and metal dosages

Groups	Dosages	Days
Control	0.5 mL saline	28
Cd	0.854 mg/kg body weight	28
Cr	14.22 mg/kg body weight	28
Cd and Cr	0.854 mg/kg and 14.22 mg/kg body weight	28

using the dose equation of Reagan-Shaw et al. (2008) (Bartram & Howard, 2003; WHO, 2011). The dosages were adjusted weekly according to average weekly weight of the rats. The dosage and duration of exposure represents chronic metal exposure in humans.

2.3 | Termination

The rats were terminated via isoflurane overdose, according to standard methods employed by the UPBRC. The liver and kidneys were harvested and processed for transmission electron microscopy (TEM) and electron energy-loss spectroscopy analysis (EELS).

2.4 | Blood collection

Approximately 5 mL volume of blood was collected on the day of termination (day 28) via cardiac puncture under isoflurane anaesthesia. The blood was then collected in a citrate tube, and the levels of the following were determined: total serum protein (TP), alanine aminotransferase (ALT), alkaline phosphatase (ALP), aspartate aminotransferase (AST), urea nitrogen (UN), creatinine, and total bilirubin (TB).

2.5 | Statistical analysis

Statistical analysis on the blood chemistry analysis were performed on GraphPad Prism Version 6.01 using 1-way ANOVA and Tukey's multiple comparisons test, where a p value of $\leq$.05 was considered significant.

2.6 | Transmission electron microscopy analysis

The liver and kidney tissue samples were cut into 1 mm^3 blocks and fixed in 2.5% glutaraldehyde (GA) and formaldehyde (FA) for 1 h, rinsed three times in 0.075M sodium potassium phosphate buffer (pH = 7.4) for 15 min each before the samples were placed in the secondary fixative, a 1% osmium tetroxide solution, for 1 h. Following fixation, the tissue samples were rinsed again as described above. The tissues were then dehydrated in 30, 50, 70, 90% and three changes of 100% ethanol. The samples were embedded in resin and ultrathin sections (70–100 nm) were cut with a diamond knife using an ultramicrotome. Samples were contrasted with uranyl acetate for 5 min followed by 2 min of contrasting with lead citrate, after which the samples were allowed to dry for a few minutes before being examined with the JEOL TEM (JEM 2100F).

TABLE 2 Organ specific blood chemistry analysis

	TP (g/L)		UN (mmol/L)		Creatinine (µmol/L)	
	Range	Mean ± SD	Range	Mean± SD	Range	Mean ± SD
Control	53.9–62.7	58.30 ± 3.65	7.0–8.0	7.55 ± 0.41	24–30	27.17 ± 2.23
Cd	58.3–61.6	60.18 ± 1.29	5.9–7.9	7.03 ± 0.78	23–26	24.17 ± 1.17
Cr	54.2–58.5	56.28 ± 1.63	6.0–9.1	7.68 ± 1.05	22–28	25.33 ± 2.34
Cd and Cr	52.0–61.3	54.30[b] ± 3.54	6.4–7.6	6.95 ± 0.42	21–25	23.17[a] ± 1.83
	ALT (U/L)		**ALP (U/L)**		**AST (U/L)**	
	Range	Mean ± SD	Range	Mean± SD	Range	Mean ± SD
Control	55–69	61.50 ± 5.58	163–245	201.67 ± 30.43	82–140	94.67 ± 24.90
Cd	50–66	57.17 ± 6.37	156–198	183.33 ± 14.79	73–80	77.60 ± 2.88
Cr	42–64	56.33 ± 9.03	121–223	165.33 ± 38.47	79–245	130.17 ± 58.54
Cd & Cr	52–65	57.67 ± 5.50	122–165	146.33[a] ± 18.45	75–138	110.67 ± 26.69
	TB (µmol/L)					
	Range					Mean ± SD
Control	0.3–1.1					0.70 ± 0.30
Cd	0.6–1.4					0.93 ± 0.28
Cr	0.7–1.6					0.97 ± 0.33
Cd and Cr	0.7–1.3					1.02 ± 0.21

SD: standard deviation.
[a]Statistical significance compared to control.
[b]Statistical significance compared to Cd: *p* value of ≤.05.

2.7 | Electron energy-loss spectroscopy analysis

An FEI Tecnai G^{2}20 high resolution TEM (FEI, Oregon, USA) equipped with the GIF 2001 energy filter (Gatan, Inc., CA, USA) for EELS and energy filtered transmission electron microscopy (EFTEM) analyses were used to evaluate the possible bioaccumulation of Cd and Cr in the liver and kidney tissue. EELS spectra [Cd: 403.7 eV and Cr: 574 eV (Ahn, Krivanek, Burgner, Disko, & Swann, 1983)] analysis was done to confirm the presence of the heavy metals in the tissue, together with the EFTEM colour map, to visually express the exact position of the metals in the tissue.

The EELS spectra were collected in normal parallel beam TEM mode, without an objective aperture and employing a GIF entrance aperture of 3 mm. This allowed for the use of a large collection semi-angle, $\beta \sim 100$ mrad, which greatly improved the jump ratio of the spectra. To remove the effects of plural scattering and the contribution from low energy plasmon losses, each spectrum was background subtracted using a power law line shape. This was followed by further deconvoluting the ionization edges using a Log–Fourier iterative process, as to remove all other plural scattering contribution. The EFTEM maps were collected using the Gatan 3 window method with an energy slit width of 20 eV. For construction of the Cr map, the pre-edge 1 and pre-edge 2 energy windows were centred at 545 and 565 eV, respectively, whereas the post-edge window was centred at 585 eV so as to coincide with the onset of the Cr L$_{2,3}$ ionization edge at 574 eV. The positions of the pre-edge 1 and 2 windows were based on the background subtraction

model obtained from the EELS analyses when using 2 energy windows. This ensured that only energy loss contributions from the metal under investigation were mapped. Similarly, for mapping of the energy-loss contributions of Cd, the pre-edge 1 and 2 windows were placed at 364 and 384 eV, with a post-edge onset centred at 414 eV.

3 | RESULTS

In a rat model representing chronic oral exposure to Cd and Cr alone and in combination at 1000 times the WHO limit the effects of exposure on blood parameters and tissue ultrastructure was evaluated.

3.1 | Blood chemistry test

The TP levels in the combination group were significantly lower than that of the group exposed to Cd alone. The levels of ALP and creatinine in the combination group were significantly lower than the control group. The bilirubin levels, although not statistically significant, showed a slight increase in the exposed groups, compared to the control. Compared to the controls no increases in ALT, AP, or AST were observed (Table 2).

3.2 | Transmission electron microscopy

With TEM, the following ultrastructural features associated with tissue damage were sought and this included cellular, nuclear and
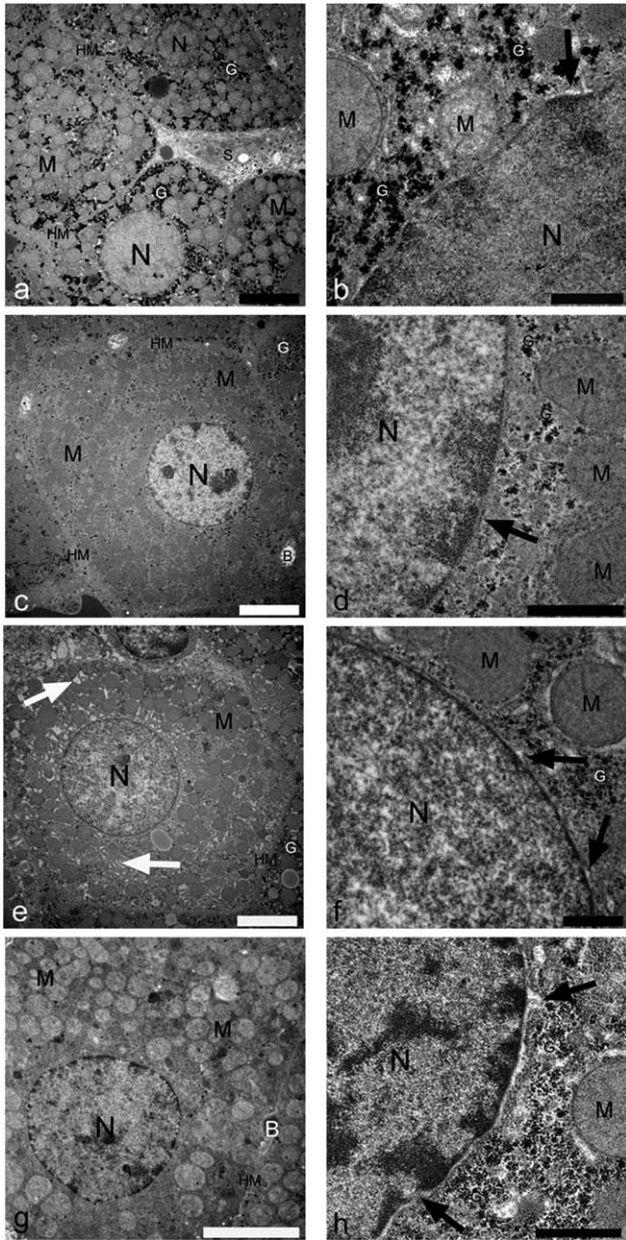
FIGURE 1 TEM micrographs of the hepatocytes of the liver tissue in the control (a and b), Cd (c and d), Cr (e and f), and Cd and Cr (g and h) groups. Black arrows indicate membrane alterations and white arrows indicate rER dilation. Key: B: Bile canaliculi G: Glycogen granules; HM: Hepatocyte membrane; M: Mitochondria; N: Nucleus (scale bars: a c, e, g: 5 μm; b, d, f, h: 1 μm)

hepatocytes of the Cd exposed group showed the presence of nuclear and mitochondrial membrane disruptions that were more prevalent than in the control group [Figure 1D (arrow) and 2D, respectively]. Irregular chromatin condensation is present in the nuclei (Figure 1C), but no inner matrix swelling is seen in the mitochondria (Figure 2C). In the Cr experimental group, nuclear outer membrane [Figure 1F (arrows)] and mitochondrial membrane alterations were visible (Figure 2F), accompanied by irregular chromatin condensation in the nuclei (Figure 1E) and inner matrix swelling present in the cristae of the mitochondria [Figure 2E (arrow)]. There was also a noteworthy increase in
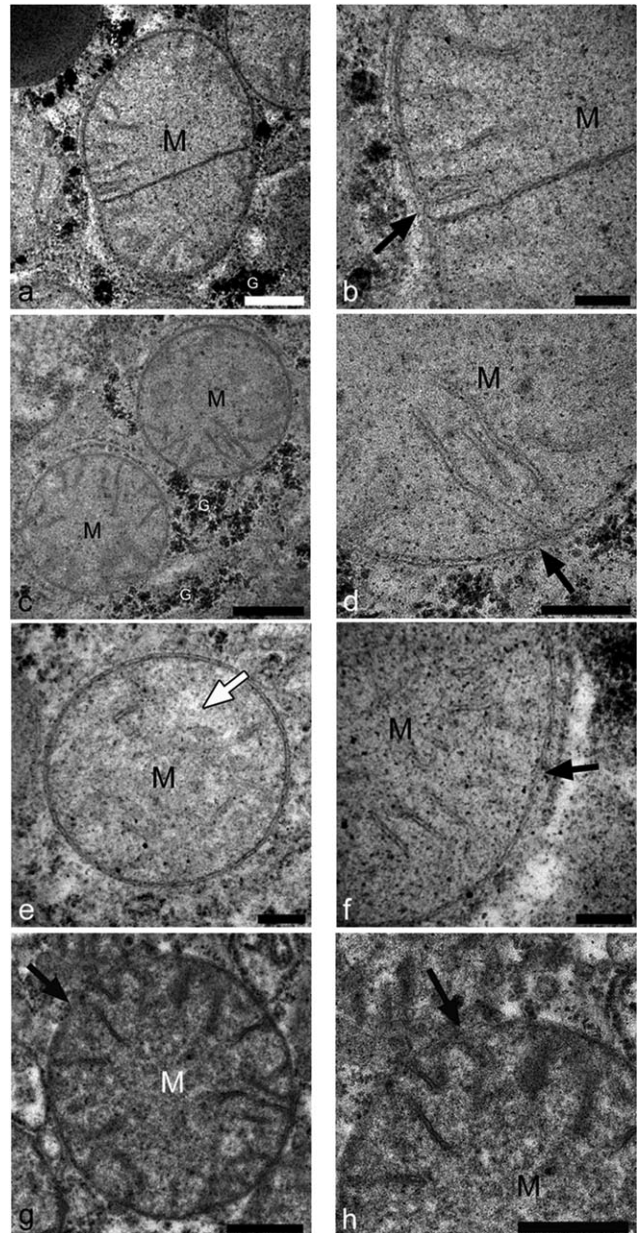
FIGURE 2 TEM micrographs of the mitochondria of the liver tissue of the control (a and b), Cd (c and d), Cr (e and f), and Cd and Cr (g and h) groups. Black arrows indicate membrane alterations, with the white arrow that indicates inner matrix swelling. Key: G: Glycogen granules; M: Mitochondria; N: Nucleus (scale bars: a, c, g, h: 500 nm; b, d, e, f: 200 nm)

mitochondrial membrane disruption, irregular chromatin condensation, mitochondrial inner membrane swelling, and rough endoplasmic reticulum (rER) dilation. For the kidney this included the ultrastructural of the endothelial cells, pedicles, podocytes and mesangial cells.

In Figure 1, the hepatocytes and nuclear ultrastructure of these cells are presented. Normal hepatocyte morphology was observed in all control samples (Figure 1A). Only minimal alterations to the nuclear [Figure 1B (arrow)] and mitochondrial membranes [Figure 2B (arrow)], were observed in all the control rats. No inner matrix alterations were seen in the mitochondria of the control liver tissue (Figure 2A). The

FIGURE 3 TEM micrographs of the kidney tissue of the control group. (a, c and e) indicate the PCT, nuclear membrane and mitochondria, respectively. The glomeruli ultrastructure can be seen in (b, d), and f. Key: AT: Apical tubulovesicles C: Capillary; E: Endothelial cell; L: Lysosome; Me: Mesangial cell; MV: Microvilli; M: Mitochondria; N: Nucleus; P: Podocyte; RBC: Red blood cell (scale bars: a, b, and f: 5 μm; c and d: 1 μm; e: 500 nm)

the dilation of the rER [Figure 1E (arrows)]. In the combination group an increase in both nuclear membrane [Figure 1H (arrows)] and chromatin condensation alterations were noted (Figure 1G). The metal combination group also revealed changes to the mitochondrial membranes and cristae [Figure 2G and H (arrows)].

The two main areas of the kidney involved in toxicity and filtration were evaluated. Firstly the proximal convoluted tubule (PCT) was analysed, as it is the part of the kidney most likely to show any changes that occurred in the kidney tubules (Tavafi et al., 2016). The second area of the kidney analysed was the glomeruli. The glomeruli will show any changes in the filtration system of the kidney. In the control group, minimal changes were seen in a few of the rats analysed, with negligible nuclear outer membrane alterations [Figure 3C (arrow)] as well as mitochondrial membrane changes (Figure 3E). No changes were seen in the PCT cell membrane, rER (Figure 3A) and mitochondrial cristae (Figure 3E) as would be expected for the control samples. The components of the glomeruli: endothelial cells (involved in the filtration system), pedicles, mesangial cells, and podocytes, all showed minimal to

no alterations in the control group (Figure 3B, D, and F). Changes in the organelles of the PCT of the Cd exposed group (Figure 4C, E) were more prevalent than in the control group, with a noteworthy increase in the occurrence of irregular chromatin condensation seen in the nucleus (Figure 4A). Minimal alterations were also seen in the endothelial cells and pedicles of the glomeruli [Figure 4B and D (arrow)]. No changes were noted in the mesangial cells and podocytes (Figure 4F).

In the Cr experimental group, changes were seen in the outer membrane [Figure 5C (arrows)] and chromatin of the nucleus (Figure 5A), as well as in the mitochondrial membranes [Figure 5E (black arrow)]. Minimal alterations were visible in the PCT cell membrane, rER (Figure 5A) and mitochondrial cristae [Figure 5E (white arrow)] in almost all the animals in this group. The endothelial cells [Figure 5D (white arrows)] and pedicles [Figure 3B and D (black arrows)] showed minimal damage in almost all the rats, with no changes seen in the mesangial cells (Figure 5F) and podocytes. The kidney tissue of the
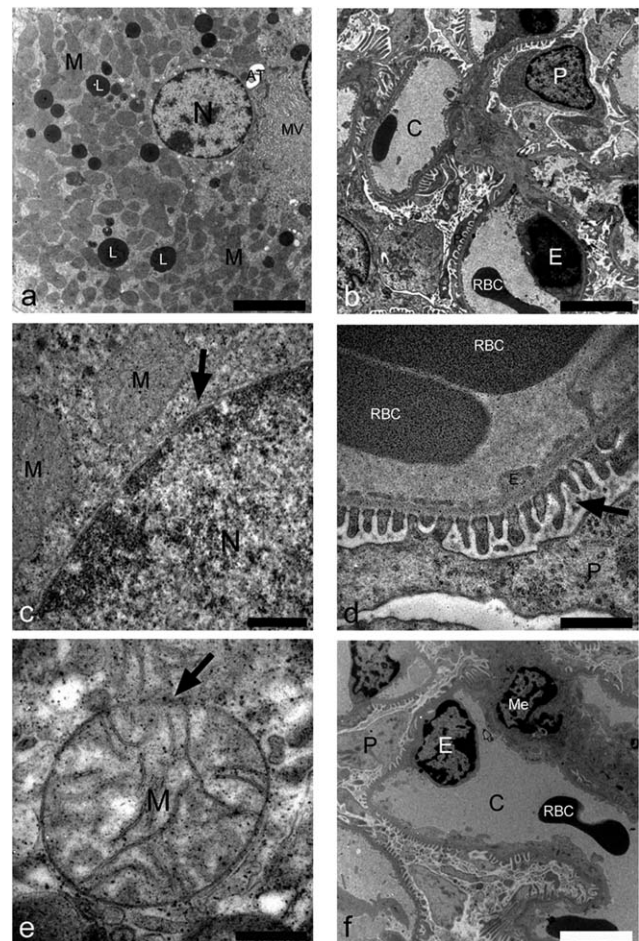
FIGURE 4 TEM micrographs of the kidney tissue of the Cd experimental group. (a, c, and e) indicate the PCT cuboidal epithelial cell, nucleus, and mitochondria, respectively, with the arrows indicating membrane changes. (b, d, and f) shows the glomeruli and all its components, with the arrow in d indicating the pedicles. Key: AT: Apical tubulovesicles; C: Capillary; E: Endothelial cell; L: Lysosome; Me: Mesangial cell; MV: Microvilli; M: Mitochondria; N: Nucleus; P: Podocyte; RBC: Red blood cell (scale bars: a, b, and f: 5 μm; c and d: 1 μm; e: 500 nm)
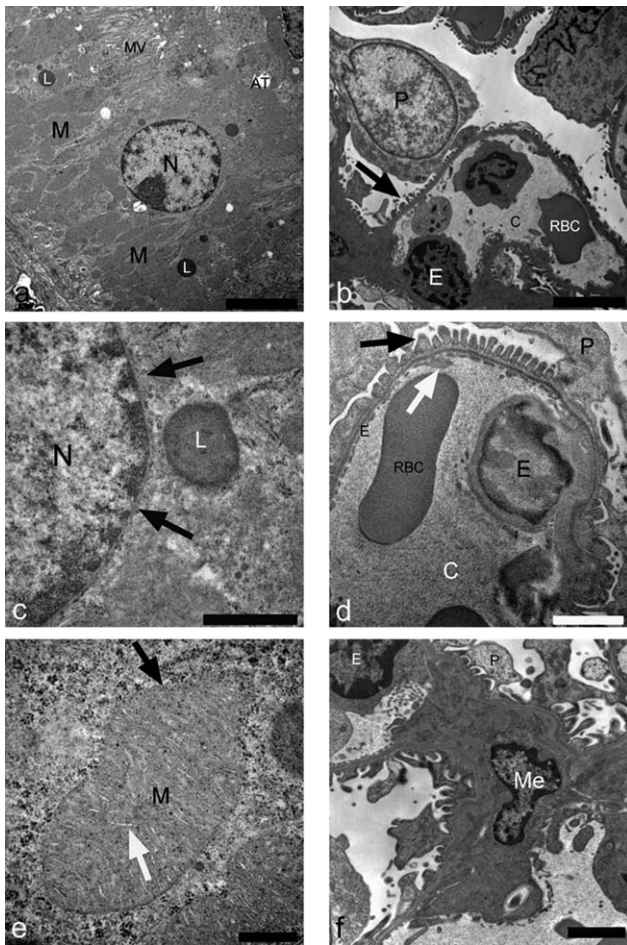
FIGURE 5 TEM micrographs of the kidney tissue of the Cr group. (a, c, and e) represents the alterations seen in the PCT cells, with c (arrows) indicating changes in the outer membrane of the nucleus and (e) shows changes in the membrane (black arrow) and cristae (white arrow). (b, d and f) show the glomeruli, where endothelial cells, podocytes and mesangial cells alterations are shown. In (b and d) the black arrows show damage to the pedicels and the white arrow (d) indicates endothelial cell damage. **Key**: AT: Apical tubulovesicles; C: Capillary; E: Endothelial cell; L: Lysosome; Me: Mesangial cell; MV: Microvilli; M: Mitochondria; N: Nucleus; P: Podocyte; RBC: Red blood cell (scale bars: a, b and F: 5μm; c and d: 1μm; E: 500nm)

combination of Cd and Cr group also showed changes in the nucleus and mitochondria, with membrane alterations [Figure 6C and E (black arrows)] and irregular chromatin condensation (Figure 6A) and inner matrix swelling [Figure 6E (white arrow)]. Some cellular membrane and rER changes were also seen in the PCT (Figure 6A). The endothelial cells and pedicles also showed alterations in almost all the experimental rats [Figure 6B (arrow) and D], with no changes seen in the mesangial cells (Figure 6F).

3.3 | Electron energy-loss spectroscopy

Figures 7 and 8 are examples of how the EELS and EFTEM results were generated when analyzing the liver and kidney samples of all the experimental groups.

3.4 | Energy filtered transmission electron microscopy

Further evaluation of the tissue with EELS and EFTEM, identified that Cd and Cr bio-accumulates in the liver and kidney, as can be seen in Figures 9 and 10, even though only minimal energy-loss signals were obtained in both the Cd and Cr groups, alone and in combination.

Figures 7 and 8 A show examples of the Cd and Cr edges that were used in the EELS analysis, respectively, where Figures 7 and 8 B–D show the Cd and Cr in the organelles of the kidney and liver, respectively, at each specific edge that was analysed, with the final Cd and Cr colour map seen in Figures 7 and 8E, with Cd in red and Cr in yellow.

In Figures 9 and 10, the EFTEM micrographs are shown of the liver and kidney tissue, respectively. The analysis of the control group showed a noisy signal that does not bio-accumulate specifically in any organelle (Figures 9 and 10A,B). With the Cd exposed groups, the EFTEM analysis revealed that Cd bioaccumulates not only in the organelles, but also on the membranes of the organelles (Figures 9 and 10C, D, respectively). Cr on the other hand mostly bio-accumulates on the
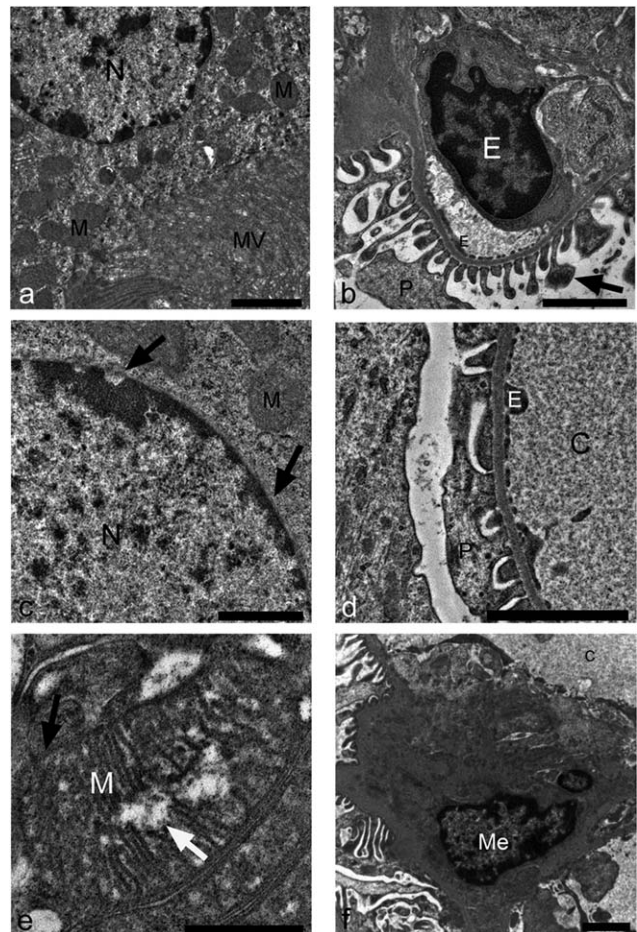
FIGURE 6 TEM micrographs of kidney tissue of the Cd and Cr group. (a) indicates the PCT, with (c) and (e) showing the alterations seen in the nucleus and mitochondria (arrows), respectively. (b, d, and f) show the glomeruli and components. Key: C: Capillary; E: Endothelial cell; Me: Mesangial cell; MV: Microvilli; M: Mitochondria; N: Nucleus; P: Podocyte (scale bars: a, b, d, and f: 2 μm; c and e: 1 μm)
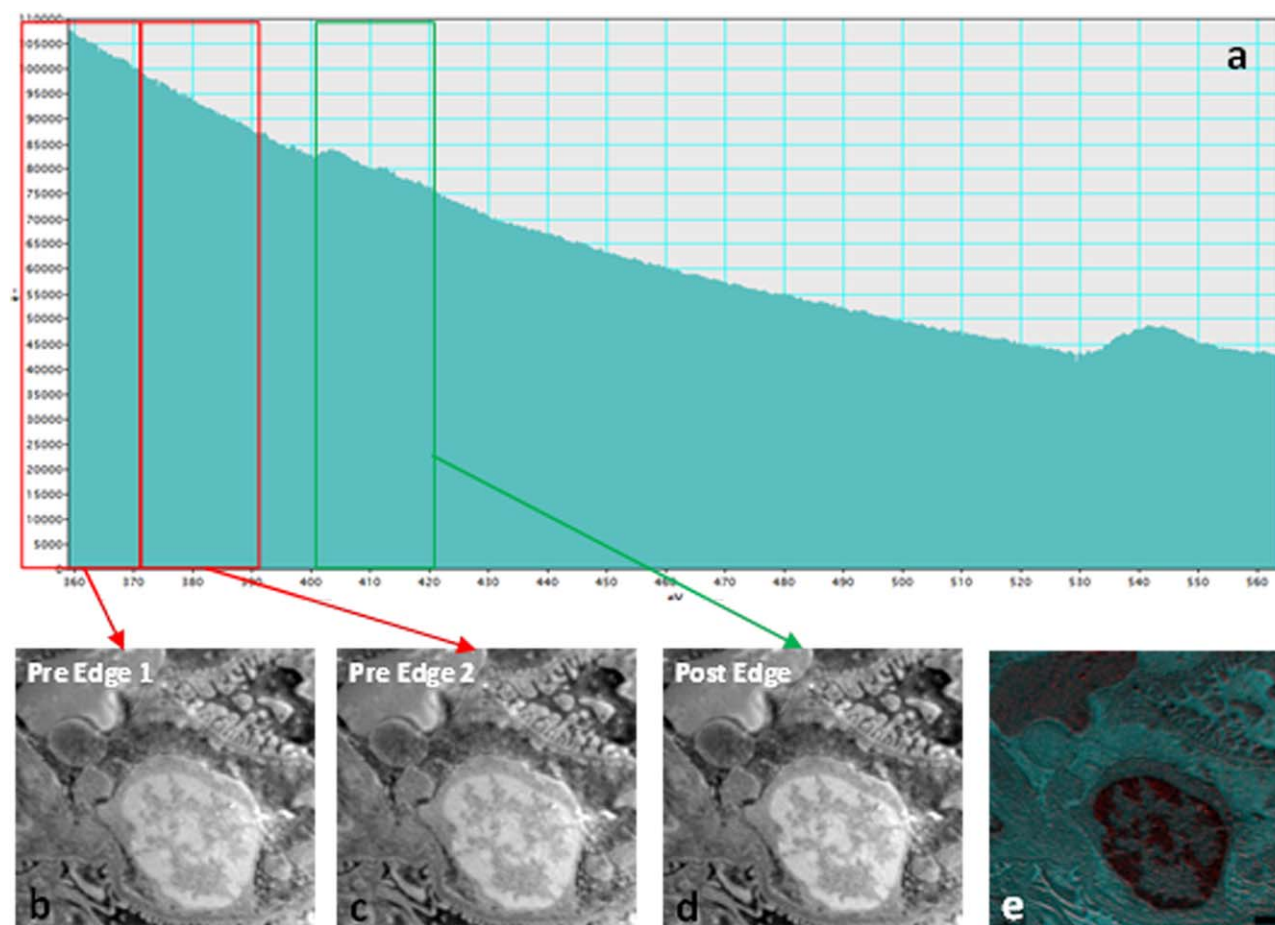
FIGURE 7 EELS and EFTEM micrographs of Cd exposed kidney tissue. (a) shows the Cd edge that was used in the EELS analysis, with (b–d) indicating the pre- and post-edge micrographs of Cd in the glomeruli of the kidney at each specific edge that was analyzed. (e) indicates the final Cd map, with the Cd in red (scale bars: b, c, d, and e: 1 μm) [Color figure can be viewed at wileyonlinelibrary.com]

membranes of the organelles (Figures 9 and 10E, F). This trend of specific localisation was also seen in the Cd and Cr group with EFTEM analysis (Figures 9 and 10G, H).

4 | DISCUSSION

The increase in heavy metal exposure is of great concern and the effects on the environment, animals and humans should be constantly evaluated (Al-Attar, 2011). Heavy metals, such as Cd and Cr, have the potential to alter cellular functions by catalyzing the formation of radicals, inhibition of antioxidant enzymes and binding to antioxidant elements such as glutathione (GSH) this leads to oxidative stress. This results in increased lipid peroxidation, protein, and DNA damage and apoptosis, that can lead to associated diseases such as hepatic necroinflammation, nonalcoholic steatohepatitis, fibroplasias, renal fibrosis and failure, and cancer (Bertin & Averbeck, 2006; García-Niño & Pedraza-Chaverrí 2014; Jin et al., 2014; Khlifi et al., 2013; Sarkar, Ravindran, & Krishnamurthy, 2013; Thévenod & Lee 2015; Timbrell, 1999; Venter & Oberholzer, 2015).

Many studies have investigated the effect of Cd or Cr administered either as a single dosage or as several smaller dosages over a period of several days. Although these studies identify the toxicity of these metals, the relevance of dosage related to actual human exposure is unknown. In the present study, metal dosages were selected to identify the effect of a 1,000 times human exposure limit on liver and kidney function and structure using a rat model. Very rarely is exposure to a single metal but rather complex mixtures of metals in varying concentrations and therefore this is a first of a series of studies we wish to undertake to evaluate the toxicity of metal combinations.

Blood markers of liver and kidney damage were not raised, indicating normal liver and kidney function. TP, ALP, and creatinine levels were reduced but were only significant for the Cd and Cr combination group compared to the control. A reduction in ALP levels have been reported for rats treated with CdCl₂ (El-Demerdash, Yousef, & Elagamy, 2001; El-Demerdash, Yousef, Kedwany, & Baghdadi, 2004; Rana, Singh, & Verma, 1996). Cd can influence zinc either through replacing membrane associated zinc or inhibiting apoptosis and necrosis prevention properties of zinc (El-Demerdash et al., 2004; Jacquillet et al., 2006). Zinc is a cofactor essential for ALP function and with zinc displacement ALP synthesis and function is compromised (Suzuki et al., 2005). Compared to the control, creatinine levels were significantly lower in the metal combination group and may indicate renal tubular
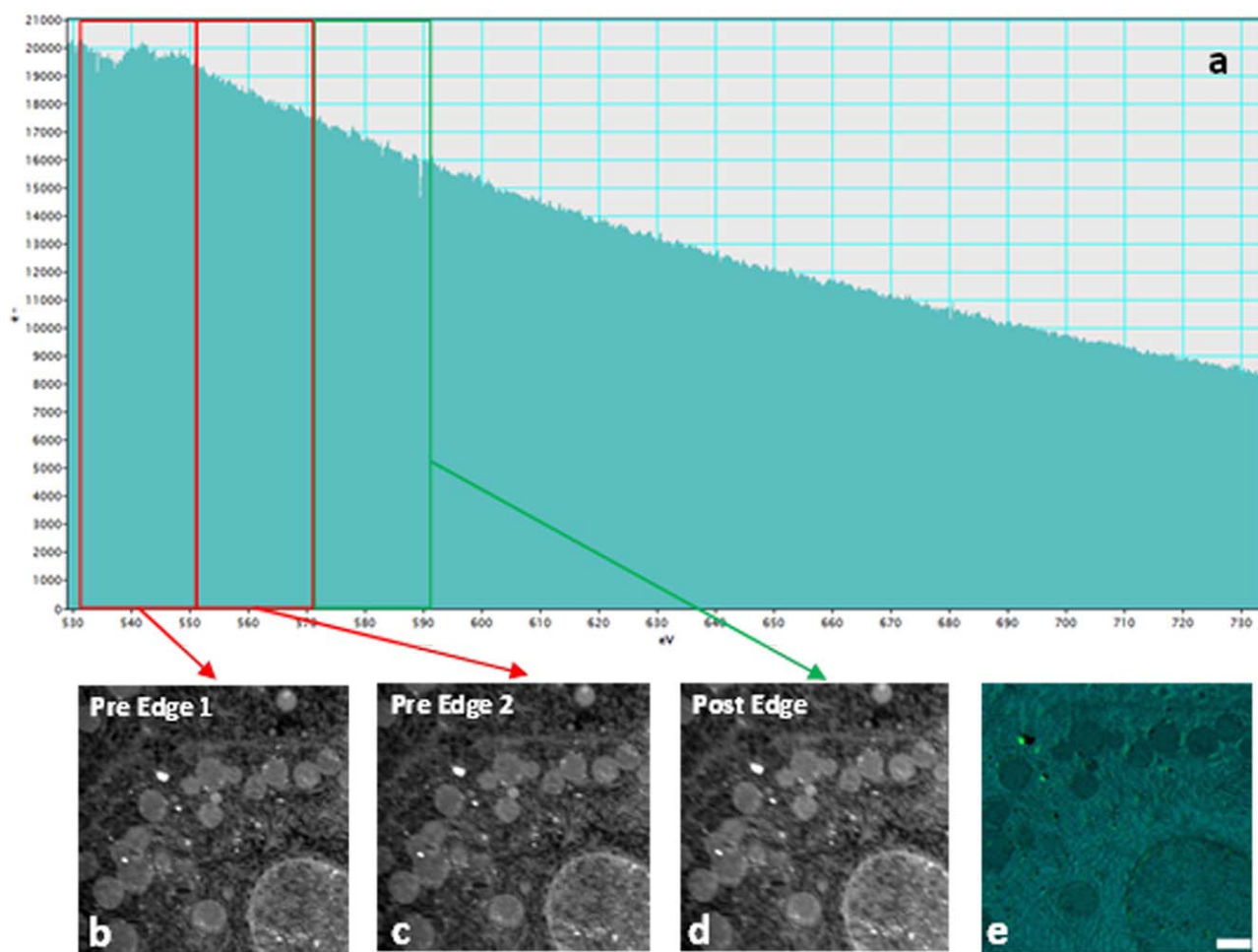
FIGURE 8 EELS and EFTEM micrographs of Cr exposed liver tissue. (a) shows the Cr edge that was used in the EELS analysis, with (Cd in the glomeruli of the kidney at each) indicating the pre- and postedge micrographs of (c) of the liver at each specific edge that was analyzed. (r) indicates the final Cr map, with the Cr in yellow (scale bars: b, c, d, and e 1 μm) [Color figure can be viewed at wileyonlinelibrary.com]

dysfunction (Asagba & Obi 2004; Babaknejad, Moshtaghie, Shahanipour, & Bahrami, 2015). Several researchers have also reported lower ALP and creatinine levels after exposed to Cr (Kumar & Kumar, 2013; Kumar, Rana, & Prakash, 1984). The TP and bilirubin levels (although the latter was not significant) were altered and may suggest early changes in liver and kidney function. Similar results were obtained in the studies of Lakshimi et al., and Kumar et al., where after exposure to Cd and Cr, the TP and bilirubin levels were decreased and increased, respectively (Kumar, Rani, Reddy, & Reddy, 2013; Lakshmi et al., 2012). The blood chemistry results show no major damage to the liver or kidneys. However, small reductions in TP, creatinine and ALP indicates that some changes in the tissue biochemical functioning has occurred.

The morphological changes and bio-accumulation of Cd and Cr alone and in combination in the liver and kidneys of male Sprague-Dawley rats was then analysed. Minor ultrastructural changes were found in nucleus, mitochondria and rER of all the experimental groups. Organ specific changes were also seen in the components of the glomerular filtration barrier namely the pedicles and endothelial cells. Small amounts of the metals were found in the liver and kidney tissue

with the EELS and EFTEM analysis. The Cd accumulated in the nucleus and mitochondria, where Cr was primarily found at the membranes of the nucleus, mitochondria, and rER.

Reactive oxygen species (ROS) is generated in several organelles including the endoplasmic reticulum and mitochondria. This occurs during normal cellular metabolism such as oxidative protein folding and mitochondrial respiration and this process is tightly regulated. ROS levels are regulated by the presence of antioxidant enzymes such as catalase, superoxide dismutase and glutathione peroxidase as well as antioxidant elements such as GSH and dietary antioxidants such as vitamins E and C. Cd and Cr toxicity affects certain components of the cellular antioxidant system and when in combination these effects are accumulative.

Cd does not catalyse the Fenton reaction but binds intracellular thiols, like GSH and/or inhibits the activity of antioxidant enzymes such as catalase (Prozialeck & Edwards, 2012). Consequently levels of hydrogen peroxide (H_2O_2), superoxide anion ($O_2{}^\bullet$) and hydroxyl radical ($^\bullet OH$) are increased (Bertin & Averbeck, 2006; Jomova & Valko, 2011). These ROS cause lipid membrane peroxidation as well as protein and

This in turn can lead to cell cycle arrest, apoptosis, genome instability, mutagenesis eventually leading to cancer.

The biochemical pathway of Cr firstly involves the reduction of hexavalent Cr [Cr(VI)] to less toxic trivalent Cr [Cr(III)]. This is mediated by antioxidant elements like ascorbate, one of the most effective biological reductant of Cr(VI), and nonenzymatic reactions with cysteine and GSH. This reduction of Cr(VI) to Cr(III) comes with a price as it generates high levels of Cr-DNA adducts and mutations that leads to DNA

FIGURE 9 EFTEM micrographs of the liver tissue of the control (a and b), Cd (c and d), Cr (e and f) and Cd and Cr (g and h). (a, c, e, and g) indicates the zero loss images of the colour maps in (b, d, e, and h), with Cd in red and Cr in yellow. Key: N: Nucleus; M: Mitochondria (scale bars: a–h: 1 μm) [Color figure can be viewed at wileyonlinelibrary.com]

DNA damage. A consequence of protein damage and lipid peroxidation are changes in membrane function and stability (Bertin & Averbeck, 2006). This is associated with changes in the morphology of membranous organelles such as the mitochondria as well as plasma and nuclear membranes. Cd was found to accumulate in the mitochondria and nuclei and in these intracellular compartments, Cd can bind membrane and DNA associated proteins thereby altering membrane integrity and function as well as DNA repair mechanisms (Bertin & Averbeck, 2006).

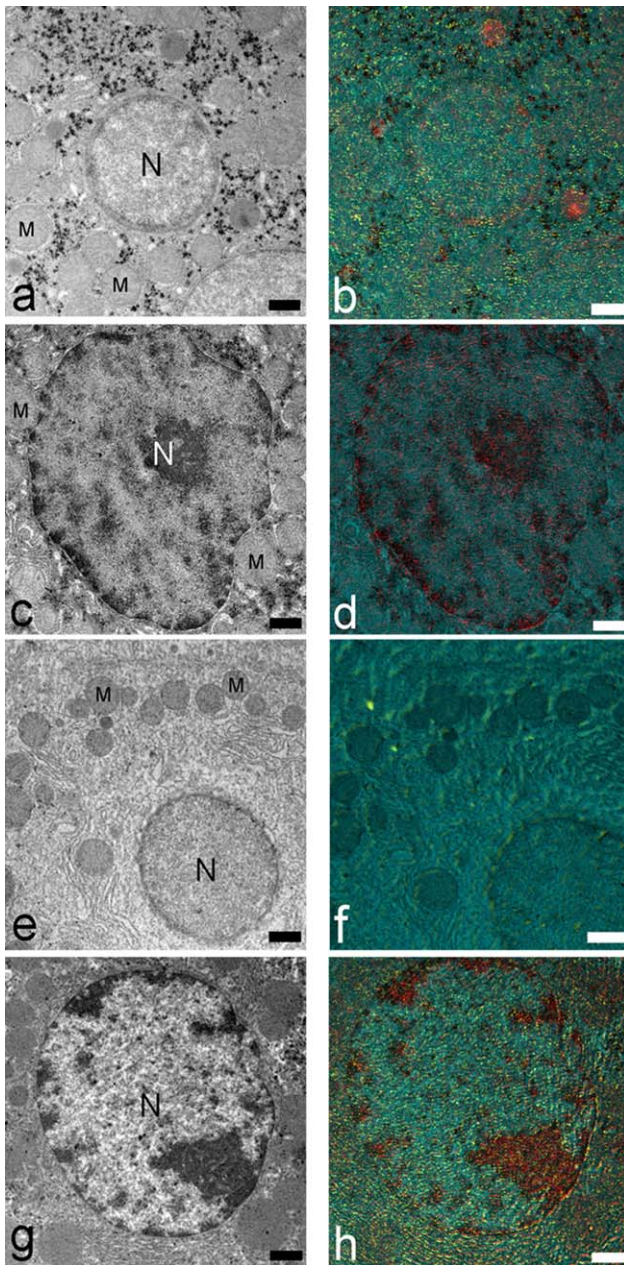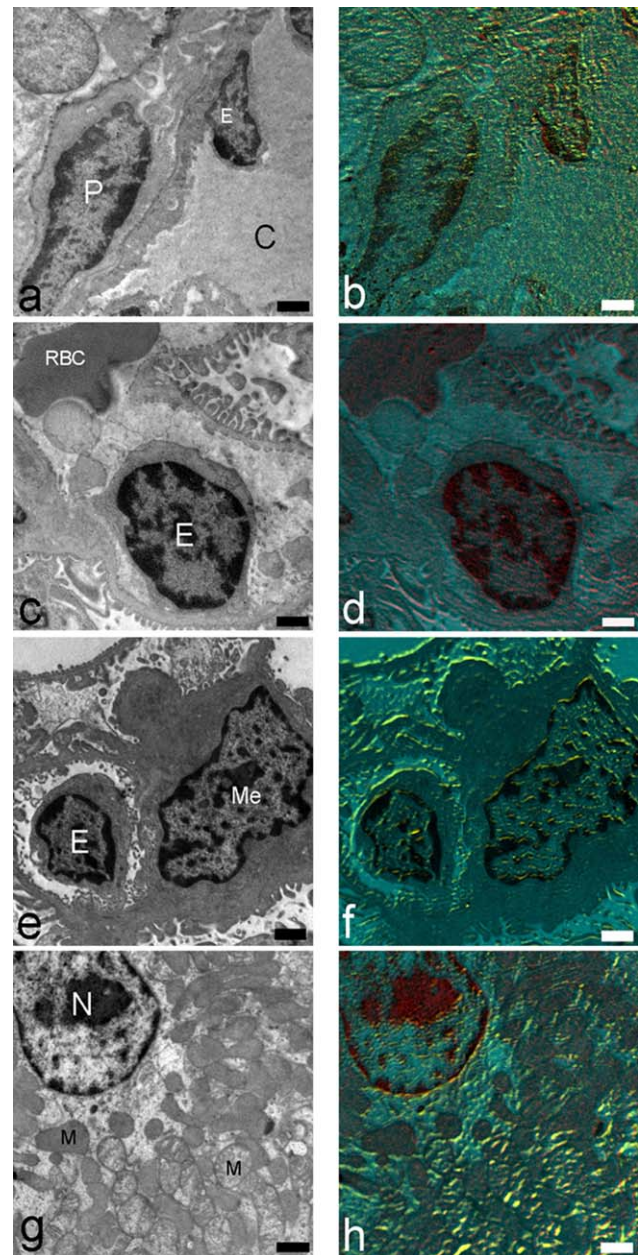**FIGURE 10** EFTEM micrographs of the kidney tissue of the control (a and b), Cd (c and d), Cr (e and f), and Cd and Cr (g and h). (a, c, e, and g) indicates the zero loss images of the colour maps in (b, d, e, and h), with Cd in red and Cr in yellow. Key: N: Nucleus; M: Mitochondria; C: Capillary; E: Endothelial cell; P: Podocyte; RBC: Red blood cell (scale bars: a–h: 1 μm) [Color figure can be viewed at wileyonlinelibrary.com]

damage (Jomova & Valko, 2011). This would affect the structure and function of both genomic and mitochondrial DNA. In addition a tightly regulated process of ROS formation occurs in the mitochondria and the endoplasmic reticulum. The accumulation of Cr which is catalyst of the Fenton reaction with cause ROS homeostasis to be disrupted, resulting in increased lipid membrane peroxidation, altered protein processing eventually leading to apoptosis. Cr toxicity also affects the mitogen-activated protein kinases (MAPK) signal transduction pathway, where nuclear factor kappa B (NF-κB), activating transcription factor 2 (ATF-2) and p53 plays a role in regulating cellular processes, including apoptosis (Jomova & Valko, 2011).

In a previous *in ovo* study by the authors, we found that increasing concentrations of Cd and Cr caused increased organelle damage associated with the accumulation of Cd and Cr in the nuclei and mitochondria of the liver and kidney (Venter & Oberholzer, 2015). Madejczyk et al., undertook a time based study and found that with a single intraperitoneal injection there was accumulation of Cd and Cr in the liver. With time metal levels decreased but ROS and cellular damage increased. This was associated with changes in the expression of genes associated with oxidative stress, metabolism, DNA damage, cell cycle and inflammatory responses (Madejczyk et al., 2015). The present study clearly shows that Cd and Cr accumulate in specific compartments such as the mitochondria, rER, nucleus and membranes directly involved with these processes.

5 | CONCLUSION

In conclusion, exposure to Cd and Cr alone and in combination at levels that do not increase markers of liver or kidney damage however these metals were found to cause changes in the ultrastructure of several organelles of the liver and kidney. Metal bioaccumulation was observed in the nucleus, mitochondria and rER of the liver and kidney. At these sites the metals can induce DNA- and protein damage and lipid peroxidation which can cause functional changes in tissue and organ function.

REFERENCES

Ahn, C., Krivanek, O., Burgner, R., Disko, M., & Swann, P. (1983). EELS Atlas Gatan Inc. (pp. 1–93). Warrendale, PA.

Al-Attar, A. M. (2011). Antioxidant effect of vitamin E treatment on some heavy metals-induced renal and testicular injuries in male mice. *Saudi Journal of Biological Sciences*, *18*(1), 63–72.

Al-Othman, Z. A., Ali, R., & Naushad, M. (2012). Hexavalent chromium removal from aqueous medium by activated carbon prepared from peanut shell: adsorption kinetics, equilibrium and thermodynamic studies. *Chemical Engineering Journal*, *184*, 238–247.

Asagba, S., & Obi, F. (2004). Effects of oral cadmium exposure on renal glomerular and tubular functions in the rat. *Journal of Applied Sciences and Environmental Management*, *8*(1), 29–32.

Awofolu, O., Mbolekwa, Z., Mtshemla, V., & Fatoki, O. (2005). Levels of trace metals in water and sediment from Tyume River and its effects on an irrigated farmland. *Water SASa*, *31*(1), 87–94.

Babaknejad, N., Moshtaghie, A. A., Shahanipour, K., & Bahrami, S. (2015). Protective Effects of Magnesium on Cadmium Renal Toxicity in Male Wistar Rats. *Zahedan Journal of Research in Medical Sciences*, 29–32.

Bartram, H. G., & Howard, G. (2003). *Domestic water quantity: Service level and health*. Geneva: World Health Organization.

Bertin, G., & Averbeck, D. (2006). Cadmium: Cellular effects, modifications of biomolecules, modulation of DNA repair and genotoxic consequences (a review). *Biochimie*, *88*(11), 1549–1559.

Chowdhury, A. R. (2009). Recent advances in heavy metals induced effect on male reproductive function-A retrospective. *Al Ameen Journal of Medical Sciences*, *2*(2), 37–42.

El-Demerdash, F., Yousef, M., & Elagamy, E. (2001). Influence of paraquat, glyphosate, and cadmium on the activity of some serum enzymes and protein electrophoretic behavior (*in vitro*). *Journal of Environmental Science and Health, Part B*, *36*(1), 29–42.

El-Demerdash, F. M., Yousef, M. I., Kedwany, F. S., & Baghdadi, H. H. (2004). Cadmium-induced changes in lipid peroxidation, blood hematology, biochemical parameters and semen quality of male rats: protective role of vitamin E and β-carotene. *Food and Chemical Toxicology*, *42*(10), 1563–1571.

García-Niño, W. R., & Pedraza-Chaverrí, J. (2014). Protective effect of curcumin against heavy metals-induced liver damage. *Food and Chemical Toxicology : An International Journal Published for the British Industrial Biological Research Association Toxicology*, *69*, 182–201.

Jacquillet, G., Barbier, O., Cougnon, M., Tauc, M., Namorado, M., Martin, D., Reyes, J., et al. (2006). Zinc protects renal function during cadmium intoxication in the rat. *American Journal of Physiology. Renal Physiology*, *290*(1), F127–F137.

Jin, Y., Zhang, S., Tao, R., Huang, J., He, X., Qu, L., & Fu, Z. (2014). Oral exposure of mice to cadmium (II), chromium (VI) and their mixture induce oxidative-and endoplasmic reticulum-stress mediated apoptosis in the livers. *Environmental Toxicology*, *31*, 693–705.

Jomova, K., & Valko, M. (2011). Advances in metal-induced oxidative stress and human disease. *Toxicology*, *283*(2), 65–87.

Khlifi, R., Olmedo, P., Gil, F., Hammami, B., Chakroun, A., Rebai, A., & Hamza-Chaffai, A. (2013). Arsenic, cadmium, chromium and nickel in cancerous and healthy tissues from patients with head and neck cancer. *Science of the Total Environment*, *452*, 58–67.

Kumar, A., & Kumar, A. (2013). Impact of dietary glutathione on hematological indices in rats poisoned with hexavalent chromium. *Journal of Applied and Natural Science*, *5*(1), 217–220.

Kumar, A., Rana, S., & Prakash, R. (1984). Dysenzymia induced by hexavalent chromium in rat liver. *International Journal of Tissue Reactions*, *7*(4), 333–338.

Kumar, C., Rani, M. U., Reddy, K. K., & Reddy, A. G. (2013). Effect of probiotic strain Lactobacillus casei strain 17 against toxicity induced by chromium in female reproductive system of rats. *Journal of Natural Science, Biology and Medicine*, *4*(1), 1119–1130.

Lakshmi, G. D., Kumar, P. R., Bharavi, K., Annapurna, P., Rajendar, B., Patel, P.T., Kumar, C., et al. (2012). Protective effect of *Tribulus terrestris* linn on liver and kidney in cadmium intoxicated rats. *Indian Journal of Experimental Biology*, *50*, 141–146.

Langárd, S., & Costa, M. A. X. (2007). Chromium. In G.F. Nordberg, B.A. Fowler, & M. Nordberg (Eds.), *Handbook on the toxicology of metals* (3rd ed.) (pp. 487–510). Burlington: Academic Press.

Madejczyk, M. S., Baer, C. E., Dennis, W. E., Minarchick, V.C., Leonard, S. S., Jackson, D.A., Stallings, J.D., et al. (2015). Temporal changes in rat liver gene expression after acute cadmium and chromium exposure. *PloS One*, *10*(5), e0127327.

Malan, M., Müller, F., Cyster, L., Raitt, L., & Aalbers, J. (2015). Heavy metals in the irrigation water, soils and vegetables in the Philippi horticultural area in the Western Cape Province of South Africa. *Environmental Monitoring and Assessment*, *187*(1), 1–8.

Prozialeck, W. C., & Edwards, J. R. (2012). Mechanisms of cadmium-induced proximal tubule injury: New insights with implications for biomonitoring and therapeutic interventions. *Journal of Pharmacology and Experimental Therapeutics*, *343*(1), 2–12.

Rana, S., Singh, R., & Verma, S. (1996). Protective effects of few antioxidants on liver function in rats treated with cadmium and mercury. *Indian Journal of Experimental Biology*, *34*(2), 177–179.

Reagan-Shaw, S., Nihal, M., & Ahmad, N. (2008). Dose translation from animal to human studies revisited. *Faseb Journal: Official Publication of the Federation of American Societies for Experimental Biology Journal*, *22*(3), 659–661.

Sarkar, A., Ravindran, G., & Krishnamurthy, V. (2013). A brief review on the effect of cadmium toxicity: From cellular to organ level. *International Journal of Bio-Technology and Research*, *3*(1), 17–36.

Suzuki, T., Ishihara, K., Migaki, H., Matsuura, W., Kohda, A., Okumura, K., Nagao, M., et al. (2005). Zinc transporters, ZnT5 and ZnT7, are required for the activation of alkaline phosphatases, zinc-requiring enzymes that are glycosylphosphatidylinositol-anchored to the cytoplasmic membrane. *Journal of Biological Chemistry*, *280*(1), 637–643.

Tavafi, M., Hasanvand, A., & Ashoory, H. (2016). Proximal convoluted tubule cells in ischemia and post-injury regeneration. *Acta Persica Pathophysiologica*, *1*(1), e05.

Tchounwou, P. B., Yedjou, C. G., Patlolla, A. K., & Sutton, D. J. (2012). *Heavy metal toxicity and the environment*. New York: Springer.

Thévenod, F., & Lee, W.-K. (2015). Live and let die: roles of autophagy in cadmium nephrotoxicity. *Toxics*, *3*(2), 130–151.

Timbrell, J. (1999). *Principles of biochemical toxicology* (404 p.). Boca Raton: CRC Press.

Venter, C., & Oberholzer, H. M. (2015). An *in ovo* investigation of the cellular effects of the heavy metals cadmium and chromium alone and in combination. University of Pretoria. Pretoria, South Africa.

Venter, C., Oberholzer, H. M., Taute, H., Cummings, F. R., & Bester, M. J. (2015). An *in ovo* investigation into the hepatotoxicity of cadmium and chromium evaluated with light-and transmission electron microscopy and electron energy-loss spectroscopy. *Journal of Environmental Science and Health. Part A: Toxic/Hazardous Substances & Environmental Engineering*, *50*(8), 830–838.

WHO. (2011). *Guidelines for drinking-water quality*. Geneva, Switzerland: World Health Organization.

Original Paper

Ultrastructural, Confocal and Viscoelastic Characteristics of Whole Blood and Plasma After Exposure to Cadmium and Chromium Alone and in Combination: An *Ex Vivo* Study

Chantelle Venter[a]   Hester Magdalena Oberholzer[a]   Janette Bester[b]
Mia-Jeanne van Rooy[b]   Megan Jean Bester[a]

[a]Department of Anatomy, Faculty of Health Sciences, University of Pretoria, Pretoria [b]Department of Physiology, Faculty of Health Sciences, University of Pretoria, Pretoria, South Africa

Key Words

Heavy metals • Cadmium • Chromium • Erythrocytes • Fibrin fibres • Platelets • Thromboelastography • Scanning electron microscopy • Confocal microscopy

Abstract

Background/Aims: Heavy metal pollution is increasing in the environment, contaminating water, food and air supplies. This can be linked to many anthropogenic activities. Heavy metals are absorbed through the skin, inhalation and/or orally. Irrespective of the manner of heavy metal entry in the body, the blood circulatory system is potentially the first to be affected following exposure and adverse effects on blood coagulation can lead to associated thrombotic disease. Although the plasma levels and the effects of cadmium (Cd) and chromium (Cr) on erythrocytes and lymphocytes have been described, the environmental exposure to heavy metals are not limited to a single metal and often involves metal mixtures, with each metal having different rates of absorption, different cellular, tissue, and organ targets. Therefore the aim of this study is to investigate the effects of the heavy metals Cd and Cr alone and whether Cr synergistically increases the effect of Cd on physiological important processes such as blood coagulation. *Methods:* Human blood was exposed to the heavy metals *ex vivo*, and thereafter morphological analysis was performed with scanning electron- and confocal laser scanning microscopy (CLSM) in conjunction with thromboelastography®. *Results:* The erythrocytes, platelets and fibrin networks presented with ultrastructural changes, including varied erythrocytes morphologies, activated platelets and significantly thicker fibrin fibres in the metal-exposed groups. CLSM analysis revealed the presence of phosphatidylserine on the outer surface of the membranes of the spherocytic erythrocytes exposed to Cd and Cr alone and in combination. The viscoelastic analysis revealed only a trend that indicates that clots that will form after heavy metal exposure, will likely be fragile and unstable especially for Cd and Cr in combination. *Conclusion:* This study identified the blood as an important target system of Cd and Cr toxicity.

© 2017 The Author(s)
Published by S. Karger AG, Basel

H.M. Oberholzer

Department of Anatomy, Faculty of Health Sciences, University of Pretoria
Private Bag x323, Arcadia 0007, (South Africa)
E-Mail nanette.oberholzer@up.ac.za

KARGER

Introduction

Haemostasis is important to ensure the recovery of injured blood vessels and to prevent excessive blood loss and this process is tightly regulated to prevent the formation of occlusive thrombi in blood vessels [1], that may lead to for example stroke [2]. The classic coagulation pathway introduced in 1964 focused on the role of the coagulation factors in thrombus formation, and ignored the role of cellular elements in the activation of the coagulation system and for this reason a new model that includes platelets and tissue factor expressing cells known as the cell-based model of coagulation was introduced. The phases of the cell-based coagulation pathway include initiation, amplification and propagation, which contribute to the formation of the clot, with platelets playing a crucial role in this process [1, 3, 4]. Platelets are involved in the release of certain factors and enzymes that contribute to clot formation and the tautness of the fibrin fibres [3, 4]. The formed thrombus consists of platelets, fibrin fibres and erythrocytes that determine the structure and integrity of the clot.

Apoptosis is well described for nucleated cells, but recently this process of programmed cell death has also been described for enucleate cells such as erythrocytes and platelets. In erythrocytes this process is known as eryptosis [5-11]. Characteristic features of this process are cell membrane shrinkage as well as blebbing and membrane scrambling [11]. During clot formation erythrocytes assist in bringing platelets to the surface of an injured vessel wall and binding inflammatory mediators to surface receptors [12]. Other cells that are involved in clot formation are the leukocytes that comprise of neutrophils, monocytes, lymphocytes, basophils and eosinophils [13], of which only the neutrophils and monocytes play a major role in the inflammatory response of the body. Leukocytes functions during coagulation include: changes in the expression of membrane receptors, release inflammatory mediators, releases oxidants like hydrogen peroxide (H_2O_2) and superoxide anion ($O_2\bullet$) and when leucocytes associate with platelets it may lead to mutual activation and protection form inhibitors [13].

Platelets and the fibrin network play an important role in the formation and stability of haemostasis. Platelet activation induces shape changes and aggregation that also leads to fibrin formation. Fibrin formation is the final step in blood coagulation and is necessary for clot stability. Fibrin formation is catalysed by thrombin, as it converts fibrinogen to fibrin [14, 15]. Changes to the morphology of erythrocytes, platelet activation and fibrin fibre thickness, caused by exposure to various substances, like smoking, heavy metals, carbon monoxide, sulfur dioxide and the presence of certain disease conditions, may alter the haemostatic process leading to the formation of pathological thrombi [11, 14, 16-20].

Environmental exposure to heavy metals via water, food and air pollution due to agriculture, mining, transport and related operations as well as cigarette smoking, a major non-occupational source of metals such as cadmium (Cd) and chromium, (Cr), are increasing [21-23]. These heavy metals have the potential to adversely affect blood homeostasis especially of those living close to high-risk areas [24]. Exposure is usually not to a single metal but as a mixture of metals [24]. Therefore the aim of this study was to determine, using and *ex vivo* blood model, the effects of Cd and Cr alone and in combination on the morphology of erythrocytes, platelet activation and fibrin fibre thickness, by using scanning electron microscopy (SEM), confocal laser scanning microscopy (CLSM) and thromboelastography® (TEG®).

Materials and Methods

Ex vivo model

Human blood was collected from six healthy consenting donors by a trained phlebotomist (Health Sciences Research Ethics Committee number: 111/2016). The inclusion criteria were: Healthy male individuals over the age of 18 years, non-smokers, that are not taking chronic medication and do not have inflammatory conditions.

Cellular Physiology and Biochemistry

Cell Physiol Biochem 2017;43:1288-1300

DOI: 10.1159/000481841
Published online: October 09, 2017

© 2017 The Author(s). Published by S. Karger AG, Basel
www.karger.com/cpb

1290

Venter et al.: Effect of Cadmium and Chromium on the Coagulation System

Scanning electron microscopy

SEM was used to study the erythrocyte, platelet and fibrin fibre morphology. The micrographs of fibrin networks were used to analyse fibrin fibre thickness. For morphological analysis whole blood (WB) and platelet-rich plasma (PRP) was used [25]. Human blood was collected in citrate tubes and 900µℓ of WB was placed in an Eppendorf tube and exposed to 100µℓ of 48mg/ℓ cadmium chloride (CdCl$_2$) [Merck (Pty) Ltd, South Africa] and/or 1450mg/ℓ potassium dichromate (K$_2$Cr$_2$O$_7$) [Merck (Pty) Ltd, South Africa]. The metal concentrations were made up in isotonic phosphate buffered saline (pH=7.4) (*iso*PBS). The final osmolality of all solutions were less than 300mOsm to ensure any observed effects were directly due to metal toxicity. The final exposure concentrations were 4.8mg/ℓ for Cd (26µM) and 145mg/ℓ for (985µM) for Cr(VI) [26]. These concentrations where chosen based on the World Health Organization (WHO) acceptable water limits (mg/ℓ) for Cd and Cr times 1000 [26]. Both Cd and Cr are at ratios that are representative of these established limits. By using a 1000x higher concentration and short exposure times, specific cellular targets can be identified which later can be evaluated in models of chronic exposure. The control blood was exposed to *iso*PBS.

The WB was exposed for 10 minutes, before 10µℓ of WB was placed on a 10mm coverslip (LeicaSA), with and without the addition of 5µℓ of human thrombin (20U/mℓ; South African National Blood Service). The WB was then centrifuged at 227xg for 10 minutes to obtain PRP; where after 10µℓ of the PRP was placed on coverslips, with and without 5µℓ of thrombin. The cover slips were placed in 24-well plates that contained 0.075M sodium potassium phosphate buffer solution (PBS) (pH=7.4). The samples were washed for 20 minutes on a shaker to remove any blood proteins that might be trapped within the blood clots [25]. The washed samples were fixed in 2.5% glutaraldehyde and formaldehyde for 30 minutes. This was followed by rinsing of the samples, three times in PBS for 3 minutes, before secondary fixation in 1% osmium tetroxide (OsO$_4$) for 15 minutes. The samples were washed again as described above, where after it was serially dehydrated in 30%, 50%, 70%, 90% and 3 times in 100% ethanol. The SEM sample preparation was completed by drying the samples in hexamethyldisilazane (HMDS), followed by mounting and coating with carbon, and examining using the Zeiss Crossbeam 540 FEG-SEM and Zeiss Ultra Plus FEG-SEM (Carl Zeiss Microscopy, Munich, Germany). The thickness of the fibrin fibres was measured on the micrographs using ImageJ (Version 1.49, Java) [25]. Fifty random fibres were measured per volunteer in the control- and metal exposed groups.

Confocal laser scanning microscopy

The CLSM was used to detect phosphatidylserine (PS) on the erythrocyte membrane indicating that eryptosis is taking place. Annexin V was used to mark PS on the surface of the membrane. The blood was collected in citrate tubes and the control were ones again only exposed to *iso*PBS and for the metal groups were exposed to the metals dissolved in *iso*PBS, as described above. The positive control was Melittin (GenScript, New Jersey, USA), an apoptosis inducing peptide [27-29], to which the blood was exposed for four hours. The blood was then centrifuged at 145xg`s for ten minutes at room temperature to collect the erythrocytes. The supernatant was removed and the remaining erythrocyte pellet was washed twice with PBS for 3 minutes. The blood was then washed with the Annexin V binding buffer (BioLegend, 422201) also for 3 minutes. 5µℓ of the Annexin V probe (BioLegend, 640906) was added to the binding buffer and incubated at room temperature, protected from light, for 90 minutes. After incubation the samples were washed again as described with the phosphate- and binding buffers, to remove any unbound antibodies. 10µℓ of the prepared sample was mounted on a glass slide and covered with a coverslip (LeicaSA). The sample was viewed with the Zeiss LSM 880 confocal laser scanning microscope in Airyscan mode (Carl Zeiss Microscopy, Munich, Germany).

To visualize the erythrocytes, two different lasers were used with different filters and beam splitters, to allow the overlaying of the respective images to show which erythrocytes have a PS flip present on the membrane. For the auto-fluorescence of all the cells present on the slide, the 405nm laser was used to excite naturally occurring fluorescence found in erythrocytes and a red colour was assigned to this fluorescent signal. In an unstained sample, the 405nm laser was used together with the 465nm-505nm band pass (BP) and 525nm long pass (LP) filters and the 488nm/405nm beam splitters. These settings showed that all the erythrocytes present on the slide has auto-fluorescence, and this auto-fluorescence could therefore be used as a contrasting method against the Annexin-V binding, in the case where PS flip is present. To visualize Annexin-V binding (excitation wavelength: 494nm and emission wavelength: 518nm), the 488nm laser was

KARGER

Cellular Physiology and Biochemistry

Cell Physiol Biochem 2017;43:1288-1300

DOI: 10.1159/000481841
Published online: October 09, 2017

© 2017 The Author(s). Published by S. Karger AG, Basel
www.karger.com/cpb

1291

Venter et al.: Effect of Cadmium and Chromium on the Coagulation System

used with the 420nm-480nm/495nm-550nm BP filters and the 488nm/405nm beam splitters, and showed a green fluorescence, indicating the presence of a PS flip on the erythrocyte membranes.

Viscoelastic analysis

TEG® is an analytic method by which the viscoelastic changes that occur during coagulation and fibrinolysis are measured. The results from the blood samples are generated by the TEG® through a rotating pin, which constantly measures the resistance of the forming clot on the pin, that indicates a number of characteristics of the coagulation system such as the speed and strength of clot formation [30-32]. The results are displayed as a graph that gives various measurements of the parameters that are listed in Table 1. For this study, blood was collected in citrate tubes and exposed, as described above, where after $340\mu\ell$ of the WB was placed in a cup of the TEG® (TEG® 5000 computer-controlled device, Haemoscope Crop., Niles, IL, USA), together with $20\mu\ell$ of 0.2M calcium chloride ($CaCl_2$) to activate the coagulation process [25]. The process was allowed to run until MA was reached, since only the rate and strength of clot formation was relevant to this study.

Table 1. TEG parameters typically generated for whole blood (modified from: [33])

Thromboplastic parameters	Description
R: Reaction time	Time of latency from start of test to initial fibrin formation (amplitude of 2 mm); i.e. initiation time
K: Kinetics	Time taken to achieve a certain level of clot strength (amplitude of 20 mm); i.e. amplification
α angle: Alpha angle (slope between the traces represented by R and K)	The angle measures the speed at which fibrin build up and cross linking takes place, hence assesses the rate of clot formation; i.e. thrombin burst
MA: Maximal amplitude	Maximum strength/stiffness of clot. Reflects the ultimate strength of the fibrin clot, i.e. overall stability of the clot
MRTG: Maximum rate of thrombus generation	The maximum velocity of clot growth observed or maximum rate of thrombus generation using G, where G is the elastic modulus strength of the thrombus in dynes per cm^{-2}
TMRTG: Time to maximum rate of thrombus generation	The time interval observed before the maximum speed of the clot growth
TTG: Total thrombus generation	The clot strength: the amount of total resistance (to movement of the cup and pin) generated during clot formation. This is the total area under the velocity curve during clot growth, representing the amount of clot strength generated during clot growth

Statistical analysis

Statistical analysis of the SEM fibrin fibre thickness and TEG® parameters were performed on GraphPad Prism Version 6.01 using one-way ANOVA and Tukey's multiple comparisons test, where a *p*-value of ≤ 0.05 was considered to be significant.

Results

Scanning electron microscopy

Fig. 1 represents the erythrocytes identified in the various groups. In Fig. 1A normal erythrocyte morphology is seen, with minimal eryptotic erythrocytes, the predominant morphology observed in the control group. A variety of erythrocyte morphologies were present in the Cd, Cr and Cd and Cr groups, including spherocytes (Fig. 1B), echinocytes and knizocytes (Fig. 1C and D respectively). Fig. 2 represents the platelets seen in the various groups included in this study. Fig. 2A shows normal platelets with minimal changes

Cellular Physiology and Biochemistry

Cell Physiol Biochem 2017;43:1288-1300

DOI: 10.1159/000481841
Published online: October 09, 2017

© 2017 The Author(s). Published by S. Karger AG, Basel
www.karger.com/cpb

1292

Venter et al.: Effect of Cadmium and Chromium on the Coagulation System

Fig. 1. Representative scanning electron micrographs of erythrocytes of the control and metal exposed groups. Fig.s A (control) shows the normal concaved morphology of an erythrocyte, with Fig.s B (Cd), C (Cr), and D (Cd and Cr) showing the changes that occurred after metal exposure (Scale bars: 1μm).
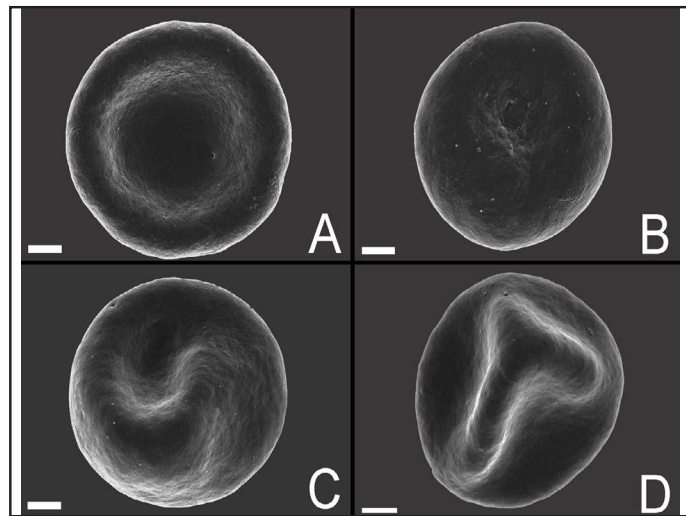
Fig. 2. Representative scanning electron micrographs of platelets from the control and metal groups. Fig. A shows a typical control platelet with pseudopodia and Fig.s B (Cd), C (Cr) and D (Cd and Cr), indicating both pseudopodia and membrane spreading. White arrows: Pseudopodia; Black arrows: Membrane spreading (Scale bars: 200nm).
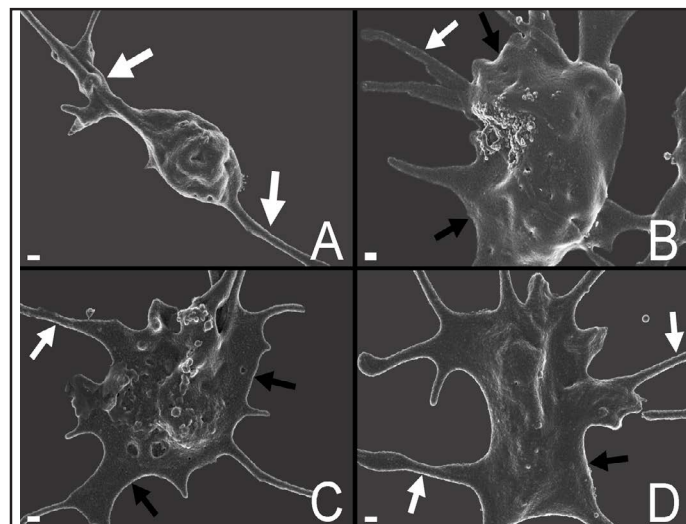
to platelet shape and pseudopodia (white arrows). Minor activation is expected as contact activation will occur during sample preparation. Fig. 2B (Cd), C (Cr) and D (Cd and Cr) show activated platelets in all the metal exposed groups, with pseudopodia (white arrows) and platelet spreading (black arrows). There also appears to be an increase in the occurrence of membrane alterations, i.e. granular appearing membranes, visible in the experimental groups. Fig. 3 shows representative fibrin networks obtained in each group. In Fig. 3A a typical control fibrin network can be seen, with mostly taut, straight fibres and a combination of thin and thick fibrin fibres (red and white arrows). Figures 3B, C and D show abnormal fibrin networks that are less taut or bent fibres (blue arrows). Fig. 4 illustrates the effects of the metals on the entire coagulation system, which shows the interactions between the erythrocytes and fibrin fibres. Fig. 4A shows the normal erythrocyte morphology with minimal fibre interaction. With exposure to metals, erythrocyte morphology is altered with increased formation of spherocytes, echinocytes and knizocytes and associated interaction between the erythrocytes and fibrin fibres [Fig. 4B, C and D (blue arrows)]. Table 2 summarises the effects of the metals on the coagulation system.

Fig. 5 shows the results obtained from the measurement of the fibrin fibre thickness. The fibres in the group exposed to Cr alone and Cd and Cr in combination are statistically thicker than the Cd fibrin fibres, but are similar in thickness compared to the control group.

KARGER

Venter et al.: Effect of Cadmium and Chromium on the Coagulation System

Fig. 3. Representative scanning electron micrograph of the fibrin networks of the control and metal groups. Fig. A (control) shows a combination of thick and thin fibres, with Fig.s B (Cd), C (Cr) and D (Cd and Cr) indicating the changes observed after metal exposure. White arrow: Major thick fibre; Red arrow: minor thin fibre; Blue arrow: Bend/loose fibre (Scale bars: A and D: 100nm; B and C: 200nm).
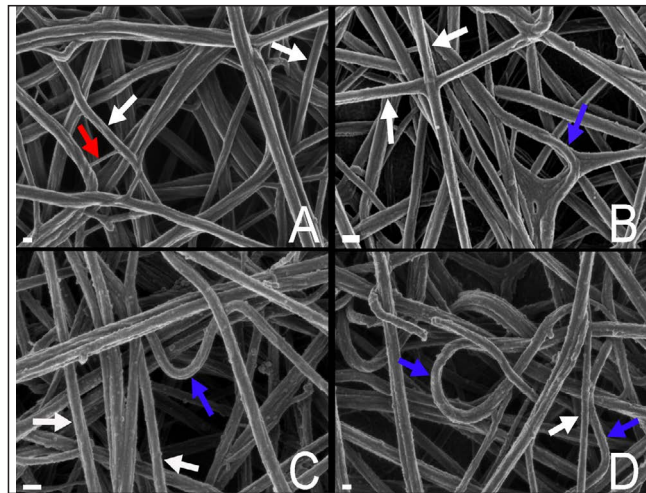
Fig. 4. Representative scanning electron micrographs of WB with thrombin of the control and metal exposed groups. Fig.s A (control), B (Cd), C (Cr) and D (Cd and Cr) indicate the erythrocyte and fibrin fibre interactions. White arrow: Normal erythrocytes; Red arrow: Variations in erythrocyte morphology; Blue arrows: Interactions between erythrocytes and fibrin fibres (Scale bars: B and C: 1µm; A and D: 2µm).
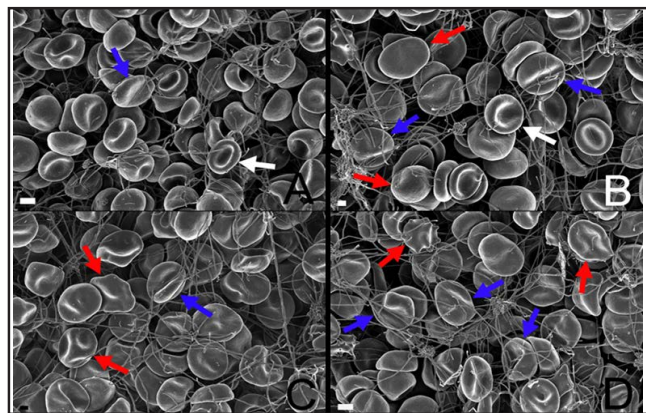
Table 2. Summary of SEM analysis on erythrocytes, platelets and fibrin networks; +, no or minimal change occurred; ++, some cell or fibre changes were visible; +++, most cells or fibres were altered; ++++, all cells or fibres were altered. WB+T: Whole blood with thrombin; PRP+T: Platelet rich plasma with thrombin

	Erythrocytes				Platelets		Fibrin network	
	WB		WB+T		PRP		PRP+T	
Groups	Altered erythrocyte morphology	Membrane disruption	Altered erythrocyte morphology	Changes due to interaction with fibrin fibres	Altered platelet morphology	Membrane disruption	Altered fibre morphology	Dense net-like appearance present
Control	++	+	++	+	++	+	+	+
Cd	+++	++	+++	++	++++	++	++	+
Cr	+++	+	+++	++	++++	++	++	+
Cd + Cr	+++	+	+++	++	++++	+++	++	++

Confocal laser scanning microscopy

In the negative control group, minimal positive Annexin V signal was obtained (Fig. 6 A-C). In the positive control, containing erythrocytes exposed to Mellitin (Fig. 6 D-F), an Annexin V positive signal was observed. Figures 7 A-F are examples of the type of Annexin V positive signal that was obtained in all the metal exposed groups. PS flip positive cells were scattered throughout the samples. The occurrence of the Annexin V PS flip positive cells

KARGER

Fig. 5. Fibrin fibre diameter measurements. *Statistically significant compared to Cd; p-value of ≤0.05.
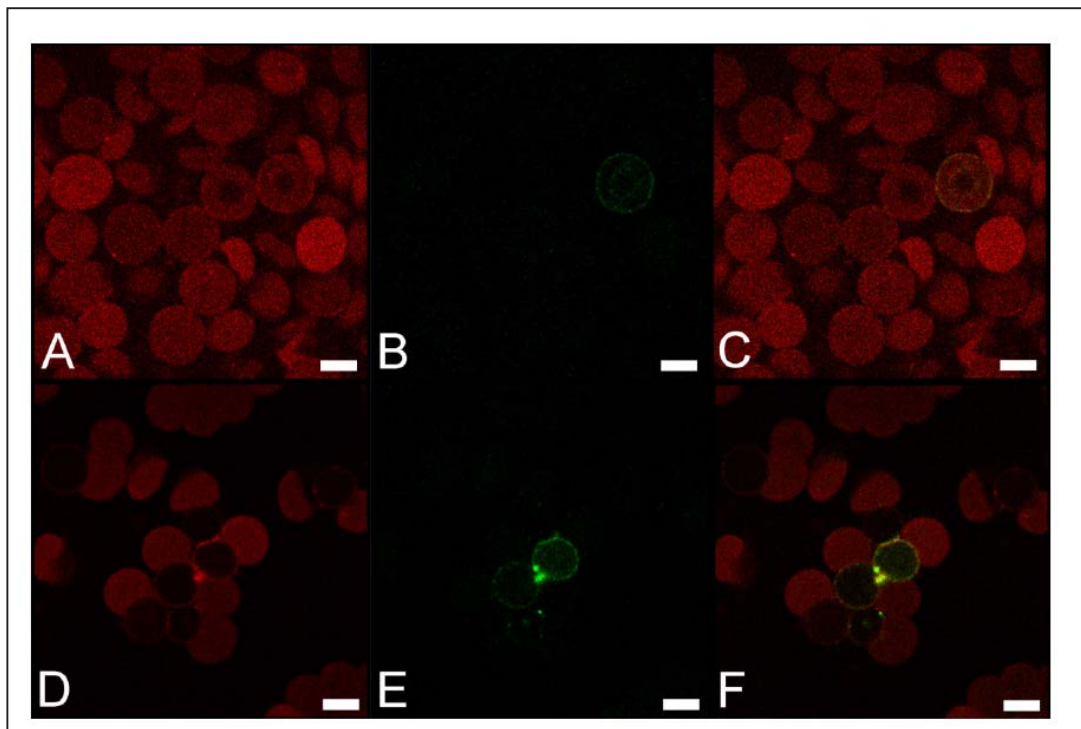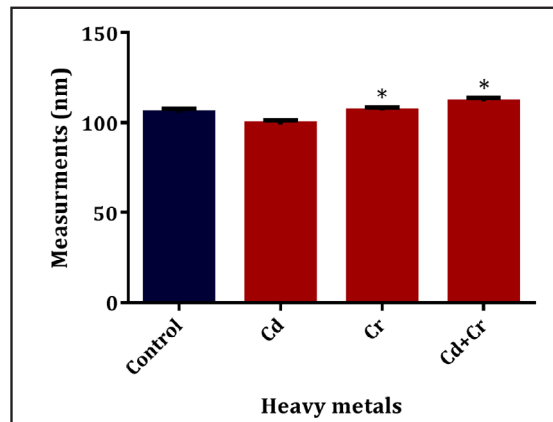
Fig. 6. Confocal laser scanning micrographs of the negative control (A-C) and positive control (D-F). Fig.s A and D showing the auto-fluorescence of the erythrocytes, B and D indicating the Annexin V signal obtained and C and F showing the overlay images (Scale bars: 5μm).

appears to be slightly increased in the metal combination groups, compared to the Cd and Cr groups. The Annexin V positive erythrocytes are mainly present in the spherocytes and not echinocytes (Fig. 7 A-F, green fluorescence).

Viscoelasticity

Fig. 8 shows representative traces of all the groups from which the r-time, k-time, α angle and MA was determined. Table 3 is a summary of the control and metal exposed group's viscoelastic profiles after exposure to Cd and Cr alone and in combination (mean ± standard deviation). No statistical significant difference in any of the parameters measured with TEG® could be found between the control group and metal exposed groups (Table 3) using the one-way ANOVA and Tukey's multiple comparisons test. Although no statistical significates

KARGER

Cellular Physiology and Biochemistry

Cell Physiol Biochem 2017;43:1288-1300

DOI: 10.1159/000481841
Published online: October 09, 2017

© 2017 The Author(s). Published by S. Karger AG, Basel
www.karger.com/cpb

1295

Venter et al.: Effect of Cadmium and Chromium on the Coagulation System

Fig. 7. PS exposure evaluation of erythrocytes after exposure to the heavy metals Cd and Cr alone and in combination using the confocal laser scanning microscope. Fig.s A - F indicate the Annexin V positive erythrocytes after exposure to Cd (A and B), Cr (C and D) and Cd and Cr (E and F) (Scale bars: 5µm).

were obtained, there was a visible trend in all the parameters of the metal groups.

The R and K values had a slight increase and the α angle and MA values decreased with the metal exposed groups. The velocity curve (v-curve) results, namely the MRTG, TMRTG and TTG, further confirms the trend seen with a decrease in the MRTG and TTG, correlating to the α angle and MA results and the TMRTG confirming the R value results.

Discussion

Blood is an important component involved in the distribution of heavy metals like Cd and Cr to organs such as the liver and kidneys which are common sites of damage [24]. During this process of distribution these metals can adversely affect blood homeostasis, altering the structure and functioning of the cellular component of blood that includes the erythrocytes, platelets and the fibrin networks. In this study, an *ex vivo* model was used to evaluate the effects of Cd and Cr alone and in combination. Exposure concentrations of Cd was similar to that used by Sopjani

Fig. 8. Representative viscoelastic traces of the control and metal groups.

et al. where exposure of a packed erythrocyte volume to 27.3µM for 48 hours caused 25% erythrocyte PS exposure and 5% haemolysis [34]. In the present study, WB was exposed to 26µM Cd for 10 minutes. Lupescu et al. exposed 0.4% haematocrit erythrocytes to 20µM Cr(VI) for 48hrs [35]. Erythrocyte haemolysis was 1% and PS exposure was 15%. WB haematocrit for healthy males is 42% [36] and therefore using WB, exposure to 200µM Cr(VI) would theoretically provide the same results. In the present study erythrocytes in WB were exposed to 5 fold higher Cr(VI) concentration's for only 10 minutes. PS exposure and associated changes in Ca^{2+} and erythrocyte morphology, after exposure to Cd and Cr alone and in combination, may adversely affect blood coagulation parameters. The focus of this a study is to determine the effect of blood coagulation providing an indication of possible thrombotic risk following exposure.

Cd and Cr alone and in combination caused ultrastructural changes (Fig. 1-4), to erythrocyte, platelet and fibrin fibre morphology (Fig. 1-4) compared to the controls. The increase in platelet activation, seen with the presence of pseudopodia and membrane
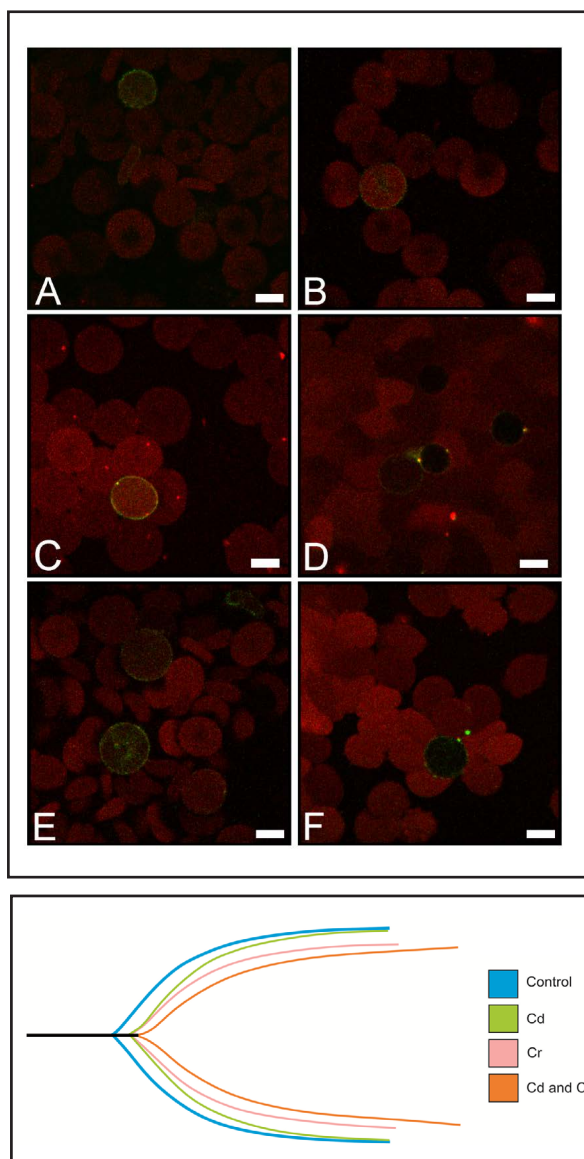
KARGER

Table 3. Summary of the effects of Cd and Cr alone and in combination on the viscoelastic parameters; *statistical significance: p-value of ≤0.05. SD: Standard deviation

Parameter	Normal ranges	Control		Cd		Cr		Cd and Cr	
		Range	Mean ± SD	Range	Mean ± SD	Range	Mean ± SD	Range	Mean ± SD
R (min)	9-27	6.50-11.70	8.83 ± 1.89	7.10-12.30	9.62 ± 1.96	8.50-13.20	10.30 ± 1.77	6.40-13.10	9.98 ± 2.49
K (min)	2-9	2.60-4.50	3.73 ± 0.82	2.80-5.80	3.97 ± 1.10	3.50-4.90	4.35 ± 0.63	4.20-7.10	5.0 ± 1.10
α angle (deg)	22-58	27.40-57.00	42.42 ± 11.11	33.50-46.80	44.20 ± 8.61	34.70-46.80	40.10 ± 5.34	20.60-42.50	31.70 ± 8.46
MA (mm)	44-64	42.30-57.31	47.35 ± 5.46	41.70-51.10	45.72 ± 3.26	38.70-48.90	42.72 ± 3.61	37.10-47.50	42.52 ± 3.67
MRTG (Dynes/cm^2/s)	0-10	2.56-12.06	4.53 ± 3.72	2.10-7.71	3.61 ± 1.80	2.42-3.54	2.78 ± 0.42	2.18-2.75	2.45 ± 0.20
TMRTG (min)	5-23	8.08-15.67	12.14 ± 2.58	10.00-18.50	12.71 ± 3.36	10.00-16.33	12.93 ± 2.48	9.67-16.75	13.10 ± 2.84
TTG (Dynes/s^2)	251-1014	366.56-674.67	460.49 ± 112.92	357.43-524.22	424.43 ± 58.02	317.12-481.22	377.76 ± 58.26	296.51-453.38	373.94 ± 55.84

spreading, were seen in the metal exposed groups that may cause a decrease in taut fibres and thus an increase in loose or bended fibres. Oxidative stress and inflammation is known to cause platelet activation that can cause pathological thrombi [14, 25, 37]. With the activation of platelets, agonists involved in the formation and stability of clot are released and include adenosine diphosphate (ADP), serotonin, thrombin and thromboxane A$_2$ [14, 37]. Platelets also play a crucial role in fibrin formation and tautness, thus the bent fibres seen in the fibrin networks of the metal groups might be due to the platelet functional changes or lack of thrombin production [25]. The significant increase in fibre thickness in the metal groups will further contribute to the alterations of the erythrocytes and clot formation, as it might cause a reduction in the lysis of the clots [38]. The alteration in fiber thickness can be due to the transition of the fibers α-helices into β-sheets and protein aggregation [33]. Fibrin fibres consist of an combination of α-helices, β-sheets and turns, loops and random coils which contributes to the normal structure and function of the fibrin fibres [33].

Cd and Cr alone and in combination caused changes in erythrocyte morphology and this was associated with increased expression of Annexin V. Cd and Cr cause oxidative stress in the cells via different biochemical pathways. Cd binds sulfhydryl groups of proteins and glutathione (GSH) and especially GSH depletion results in increased production of reactive oxygen species (ROS) such as hydrogen peroxide, superoxide anion and hydroxyl radical [39-42]. Cr in contrast enters the redox cycle and acts as a catalyst of the Fenton reaction involving H$_2$O$_2$, leading to an increase in ROS production and alters erythrocyte membrane fluidity and integrity making erythrocytes more fragile and less osmotic resistant [40, 43]. Gao et al. observed following exposure of erythrocytes to increasing concentration of betulinic acid, erythrocyte morphology changed from normal, to a mixture of normal, early discocyte-echinocytes (biconcave disk to star-shape), discocyte-stomatocytes (biconcave disk to cup-shape), echinocytes, echinocytes with vesicles, spherocytes and a few stomatocytes [44]. Likewise, a mixture of erythrocyte morphologies was observed in the present study. Low Annexin-V binding was associated with echinocytes (erythrocytes with regularly spaced short projections or spicules) and knizocytes (elevated or elongated pinched area in the centre of the erythrocytes), with regular peripheral Annexin V signal associated with the spherocytes (swollen, spherical erythrocytes). Ultrastructural results, together with the results from CLSM, that indicated that the Annexin V positive signals were mainly found on the spherocytic erythrocytes exposed to Cd and Cr in combination. Lupescu et al. reported that erythrocytes exposed to 54.5μM for 48 hours observed that only 40% erythrocytes bound Annexin

KARGER

Cellular Physiology and Biochemistry

Cell Physiol Biochem 2017;43:1288-1300

DOI: 10.1159/000481841
Published online: October 09, 2017

© 2017 The Author(s). Published by S. Karger AG, Basel
www.karger.com/cpb

1297

Venter et al.: Effect of Cadmium and Chromium on the Coagulation System

V. Likewise, Sopjani et al. 20µM Cr(VI) for 48 hours resulted in positive in 12% erythrocytes staining positive for Annexin V [34, 35].

The Annexin V signals seen in this study might be due to the increase in influx of Ca^{2+} into the erythrocytes, activation of the Ca^{2+}/K^+ channels and ATP depletion that are initiated by oxidative stress caused by the Cr and to lessor degree Cd [11, 34, 35, 45]. The increase in cytosolic Ca^{2+} will activate scramblase in the erythrocytes, which inhibits flippase that in turn causes floppase to translocate PS to the outside, resulting in the PS flip and membrane scrambling (Fig. 9). Besides the Ca^{2+} that activates scramblase, it also affects the sensitive Ca^{2+}/K^+ channels which causes KCl exiting the cells together with water and thus causing cell shrinkage (Fig. 9) [34, 35, 45]. Ca^{2+} entering the cells can

Fig. 9. Summary of erythrocyte pathology (Modified from: [46]).

also lead to the activation of Calpain, a cysteine endopeptidase that degrades membrane proteins, leading to membrane blebbing (Fig. 9) [11]. Energy depletion also initiated by an increase in cytosolic Ca^{2+} and can also contribute to eryptosis. Although both Cd and Cr both have different mechanisms of toxicity, the consequence thereof is similar resulting in eryptosis, which is increased due to a concentration effect when erythrocytes are exposed to Cd and Cr in combination.

TEG® is widely used in trauma care to evaluate whole blood coagulation [47]. In a recent study by Lehnert et al. [48], analysis of acute pulmonary embolisms, the mean values of TEG® were within normal ranges. Likewise in the present study acute exposure to Cd and Cr alone and in combination provides TEG® results within the normal range (Table 3). However evaluation of the viscoelastic traces Cd and Cr alone and in combination (Fig. 8) indicates that these heavy metals cause minor although no statistically significant changes to the measured parameters. The trend seen in the viscoelastic results indicate that the R value slightly increased, thus resulting in a delayed fibrin formation. Fibrin formation is catalysed by the enzyme thrombin from fibrinogen and stabilized by thrombin-catalysed factor XIII (FXIII) [33]. Both these components depend on the presence of calcium, as calcium is a co-factor in the formation of FXIII and thrombin and it is known that heavy metals deplete calcium levels [15, 49]. The increased trend seen in K time indicates that the initial clot formation, after it starts forming is rapid. This correlates with the activated platelets seen with SEM analysis (Fig. 2). The decrease in both the α angle and MA values indicates that the fibrin build up is slower due to the reduction in fibrin cross-linking, which results in a fragile, less-stable clot. The clot strength is also decreased as the platelet-fibrinogen interactions are decreased (Table 3) which also correlates with the SEM results, as the fibres appear to be less taut (Fig. 3). This is further supported by the v-curve data. The TMRTG shows that the total clot formation, from start to maximum clot formation takes longer and correlates with
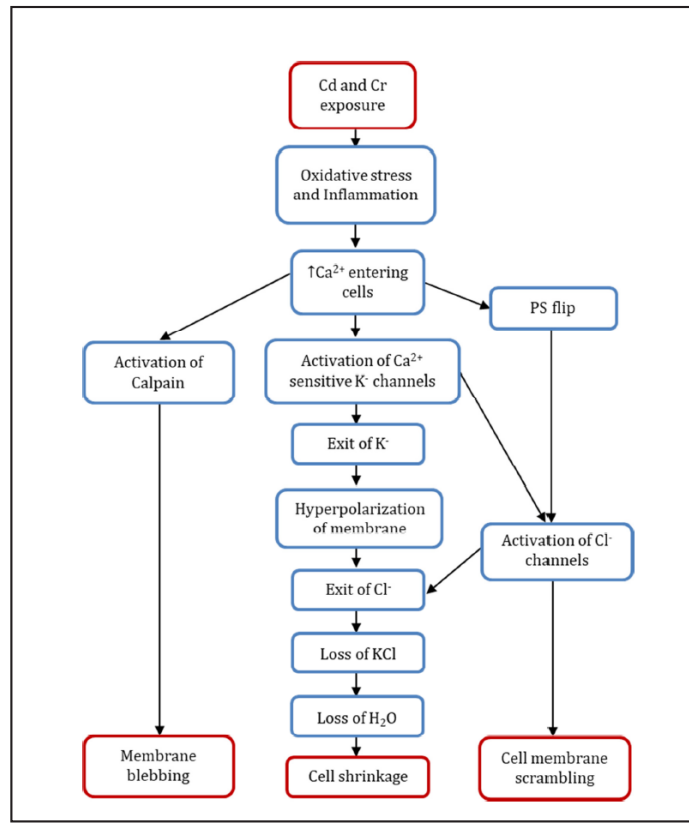
Cellular Physiology and Biochemistry

Cell Physiol Biochem 2017;43:1288-1300

DOI: 10.1159/000481841
Published online: October 09, 2017

© 2017 The Author(s). Published by S. Karger AG, Basel
www.karger.com/cpb

1298

Venter et al.: Effect of Cadmium and Chromium on the Coagulation System

the longer time for initial clot formation as observed with increased R value. The decrease in MRTG and TTG also indicates that clot formation will be slower and weaker. This fragile clot may cause problems in the cardiovascular system, as these weak clots may detach and cause a blockage in an artery or vein leading to thrombosis.

Cigarette smoking has been shown to increase fibrin fibre thickness and platelet activation and cause erythrocyte alterations [50-52]. Cigarette smoke is a complex mixture of more than 4000 components that has been identified in mainstream cigarette smoke, this includes heavy metals such as Cd and Cr and the present study clearly shows that Cd and Cr contributes to this effect [53, 54]. Likewise exposure to these metals in water and polluted air can also contribute to increased risk for thrombosis. Although this *ex vivo* study investigated the effect of a 1000 times of a single acute dosage, this study clearly identifies the blood as a target of toxicity prior to metabolism in the liver and excretion by the kidneys. Furthermore, accumulative effects of low levels of each metal as part of complex mixtures may also adversely affect blood coagulation. Evaluation of the morphology of blood components may be an important technique that can be used to identify early morphological changes prior to the identification of altered coagulation using standard clinical methods.

Conclusion

Cd and Cr alone and in combination causes increased platelet activation, abnormal fibrin network formation and Annexin V positive signal. The TEG® analysis, although not statistically significant, indicated that the final clot will probably result in a fragile and less stable clot. This study identifies the blood as an important target system of Cd and Cr toxicity.

Acknowledgements

Disclosure Statement

The authors declare no conflict of interest.

References

1   Smith SA: The cell-based model of coagulation. J Vet Emerg Crit Car 2009;19:3-10.
2   Zhang W, Houb ST, Stanimirovic D: Blood Brain Barrier Protection in Stroke: Taming tPA; The Blood-Brain Barrier in Health and Disease, Volume Two: Pathophysiology and Pathology, 2015, pp 226-246.
3   Van Rooy M-J: Blood coagulation in metabolic syndrome-induced transient ischemic attack: Department of Physiology. Pretoria, South Africa, University of Pretoria, 2015, PhD,
4   Pérez-Gómez F, Bover R: The new coagulation cascade and its possible influence on the delicate balance between thrombosis and hemorrhage. Rev Esp Cardiol 2007;60:1217-1219.
5   Föller M, Huber SM, Lang F: Erythrocyte programmed cell death. IUBMB life 2008;60:661-668.
6   Lang F, Gulbins E, Lang PA, Zappulla D, Föller M: Ceramide in suicidal death of erythrocytes. Cell Physiol Biochem 2010;26:21-28.
7   Lang F, Lang E, Föller M: Physiology and pathophysiology of eryptosis. Transfusion Medicine and Hemotherapy 2012;39:308-314.

Cellular Physiology and Biochemistry

Cell Physiol Biochem 2017;43:1288-1300

DOI: 10.1159/000481841
Published online: October 09, 2017

© 2017 The Author(s). Published by S. Karger AG, Basel
www.karger.com/cpb

1299

Venter et al.: Effect of Cadmium and Chromium on the Coagulation System

8   Lang F, Qadri SM: Mechanisms and significance of eryptosis, the suicidal death of erythrocytes. Blood Purif 2012;33:125-130.

9   Mischitelli M, Jemaa M, Almasry M, Faggio C, Lang F: Ca2+ Entry, Oxidative Stress, Ceramide and Suicidal Erythrocyte Death Following Diosgenin Treatment. Cell Physiol Biochem 2016;39:1626-1637.

10 Pretorius E, du Plooy JN, Bester J: A Comprehensive Review on Eryptosis. Cell Physiol Biochem 2016;39:1977-2000.

11 Pretorius E, Swanepoel AC, Buys AV, Vermeulen N, Duim W, Kell DB: Eryptosis as a marker of Parkinson's disease. Aging 2014;6:788-819.

12 Pretorius E, Kell DB: Diagnostic morphology: biophysical indicators for iron-driven inflammatory diseases. Integrative Biology 2014;6:486-510.

13 Gorbet MB, Sefton MV: Biomaterial-associated thrombosis: roles of coagulation factors, complement, platelets and leukocytes. Biomaterials 2004;25:5681-5703.

14 van Rooy M-J, Pretorius E: Metabolic syndrome, platelet activation and the development of transient ischemic attack or thromboembolic stroke. Thromb Res 2015;135:434-442.

15 Swanepoel AC, Nielsen VG, Pretorius E: Viscoelasticity and ultrastructure in coagulation and inflammation: two diverse techniques, one conclusion. Inflammation 2015;38:1707-1726.

16 Lang E, Qadri SM, Lang F: Killing me softly–suicidal erythrocyte death. Int J Biochem Cell Biol 2012;44:1236-1243.

17 Pretorius E, Bester J, Vermeulen N, Alummoottil S, Soma P, Buys AV, Kell DB: Poorly controlled type 2 diabetes is accompanied by significant morphological and ultrastructural changes in both erythrocytes and in thrombin-generated fibrin: implications for diagnostics. Cardiovasc Diabetol 2015;14:1.

18 Ambrose JA, Barua RS: The pathophysiology of cigarette smoking and cardiovascular disease: an update. J Am Coll Cardiol 2004;43:1731-1737.

19 Hoek G, Brunekreef B, Fischer P, van Wijnen J: The association between air pollution and heart failure, arrhythmia, embolism, thrombosis, and other cardiovascular causes of death in a time series study. Epidemiology 2001;12:355-357.

20 Swanepoel AC, Visagie A, de Lange Z, Emmerson O, Nielsen VG, Pretorius E: The clinical relevance of altered fibrinogen packaging in the presence of 17β-estradiol and progesterone. Thromb Res 2016;146:23-34.

21 Prozialeck WC, Edwards JR: Mechanisms of cadmium-induced proximal tubule injury: new insights with implications for biomonitoring and therapeutic interventions. J Pharmacol Exp Ther 2012;343:2-12.

22 Langárd S, Costa MAX: Chromium; in Nordberg GF, Fowler BA, Nordberg M (eds): Handbook on the Toxicology of Metals Burlington, Academic Press, 2007, pp 487-510.

23 Zhou Z, Lu Y-h, Pi H-f, Gao P, Li M, Zhang L, Pei L-p, Mei X, Liu L, Zhao Q: Cadmium Exposure is Associated with the Prevalence of Dyslipidemia. Cell Physiol Biochem 2016;40:633-643.

24 Venter C, Oberholzer HM: An *in ovo* investigation of the cellular effects of the heavy metals cadmium and chromium alone and in combination: Anatomy. Pretoria, South Africa, University of Pretoria, 2015, Masters,

25 van Rooy M-J, Duim W, Ehlers R, Buys AV, Pretorius E: Platelet hyperactivity and fibrin clot structure in transient ischemic attack individuals in the presence of metabolic syndrome: a microscopy and thromboelastography® study. Cardiovasc Diabetol 2015;14:86.

26 W.H.O: Guidelines for drinking-water quality World Health Organization: World Health Organization. Switzerland, 2011, 2015,

27 Han SM, Lee KG, Yeo JH, Hwang SJ, Jang CH, Chenoweth PJ, Pak SC: Effects of bee venom treatment on growth performance of young pigs. The American journal of Chinese medicine 2009;37:253-260.

28 Park C, Lee DG: Melittin induces apoptotic features in Candida albicans. Biochem Biophys Res Commun 2010;394:170-172.

29 Park JH, Jeong Y-J, Park K-K, Cho H-J, Chung I-K, Min K-S, Kim M, Lee K-G, Yeo J-H, Park K-K: Melittin suppresses PMA-induced tumor cell invasion by inhibiting NF-κB and AP-1-dependent MMP-9 expression. Mol Cells 2010;29:209-215.

30 Larsen CC, Hansen-Schwartz J, Nielsen JD, Astrup J: Blood coagulation and fibrinolysis after experimental subarachnoid hemorrhage. Acta Neurochir (Wien) 2010;152:1577-1581.

31 Shin K-H, Kim I-S: Thromboelastographic Evaluation of Coagulation in Patients with Liver Disease. Blood 2015;126:1089-1089.

KARGER

Cellular Physiology and Biochemistry

Cell Physiol Biochem 2017;43:1288-1300

DOI: 10.1159/000481841
Published online: October 09, 2017

© 2017 The Author(s). Published by S. Karger AG, Basel
www.karger.com/cpb

1300

Venter et al.: Effect of Cadmium and Chromium on the Coagulation System

32   Wiinberg B, Jensen AL, Rojkjaer R, Johansson P, Kjelgaard Hansen M, Kristensen AT: Validation of human recombinant tissue factor–activated thromboelastography on citrated whole blood from clinically healthy dogs. Vet Clin Pathol 2005;34:389-393.

33   Kell DB, Pretorius E: Proteins behaving badly. Substoichiometric molecular control and amplification of the initiation and nature of amyloid fibril formation: lessons from and for blood clotting. Prog Biophys Mol Biol 2016:1-26.

34   Sopjani M, Föller M, Dreischer P, Lang F: Stimulation of eryptosis by cadmium ions. Cell Physiol Biochem 2008;22:245-252.

35   Lupescu A, Jilani K, Zelenak C, Zbidah M, Qadri SM, Lang F: Hexavalent chromium-induced erythrocyte membrane phospholipid asymmetry. Biometals 2012;25:309-318.

36   Brun J, Bouchahda C, Chaze D, Aïssa Benhaddad A, Micallef J, Mercier J: The paradox of hematocrit in exercise physiology: which is the "normal" range from an hemorheologist's viewpoint? Clin Hemorheol Microcirc 2000;22:287-303.

37   Freedman JE: Oxidative stress and platelets. Arterioscler Thromb Vasc Biol 2008;28:s11-s16.

38   Swanepoel AC, Visagie A, Pretorius E: Synthetic Hormones and Clot Formation. Microsc Microanal 2016;22:878-886.

39   Bertin G, Averbeck D: Cadmium: cellular effects, modifications of biomolecules, modulation of DNA repair and genotoxic consequences (a review). Biochimie 2006;88:1549-1559.

40   Stohs S, Bagchi D: Oxidative mechanisms in the toxicity of metal ions. Free Radic Biol Med 1995;18:321-336.

41   Hu K-H, Li W-X, Sun M-Y, Zhang S-B, Fan C-X, Wu Q, Zhu W, Xu X: Cadmium induced apoptosis in MG63 cells by increasing ROS, activation of p38 MAPK and inhibition of ERK 1/2 pathways. Cell Physiol Biochem 2015;36:642-654.

42   Chen Z-Y, Liu C, Lu Y-h, Yang L-L, Li M, He M-D, Chen C-H, Zhang L, Yu Z-P, Zhou Z: Cadmium exposure enhances bisphenol A-induced genotoxicity through 8-oxoguanine-DNA glycosylase-1 OGG1 inhibition in NIH3T3 fibroblast cells. Cell Physiol Biochem 2016;39:961-974.

43   Husain N, Mahmood R: Hexavalent chromium induces reactive oxygen species and impairs the antioxidant power of human erythrocytes and lymphocytes: Decreased metal reducing and free radical quenching ability of the cells. Toxicol Ind Health 2017:0748233717703892.

44   Gao M, Lau P, Kong S: Mitochondrial toxin betulinic acid induces *in vitro* eryptosis in human red blood cells through membrane permeabilization. Arch Toxicol 2014;88:755-768.

45   Pretorius E, Oore-ofe O, Mbotwe S, Bester J: Erythrocytes and their role as health indicator: Using structure in a patient-orientated precision medicine approach. Blood Rev 2016

46   Pretorius E, Oore-ofe O, Mbotwe S, Bester J: Erythrocytes and their role as health indicator: Using structure in a patient-orientated precision medicine approach. Blood Rev 2016;30:263-274.

47   Bolliger D, Seeberger MD, Tanaka KA: Principles and practice of thromboelastography in clinical coagulation management and transfusion practice. Transfus Med Rev 2012;26:1-13.

48   Lehnert P, Johansson PI, Ostrowski SR, Møller CH, Bang LE, Olsen PS, Carlsen J: Coagulopathy in patients with acute pulmonary embolism: a pilot study of whole blood coagulation and markers of endothelial damage. Scand J Clin Lab Invest 2017;77:19-26.

49   Timbrell J: Principles of Biochemical Toxicology, ed 3. CRC Press, 1999.

50   Pretorius E, Oberholzer HM, van der Spuy WJ, Meiring JH: Smoking and coagulation: the sticky fibrin phenomenon. Ultrastruct Pathol 2010;34:236-239.

51   Armani C, Landini Jr L, Leone A: Molecular and biochemical changes of the cardiovascular system due to smoking exposure. Curr Pharm Des 2009;15:1038-1053.

52   Pretorius E, du Plooy JN, Soma P, Keyser I, Buys AV: Smoking and fluidity of erythrocyte membranes: A high resolution scanning electron and atomic force microscopy investigation. Nitric Oxide 2013;35:42-46.

53   Fresquez MR, Pappas RS, Watson CH: Establishment of toxic metal reference range in tobacco from US cigarettes. J Anal Toxicol 2013;37:298-304.

54   Dallüge J, Van Stee LL, Xu X, Williams J, Beens J, Vreuls RJ, Udo A: Unravelling the composition of very complex samples by comprehensive gas chromatography coupled to time-of-flight mass spectrometry: Cigarette smoke. J Chromatogr A 2002;974:169-184.
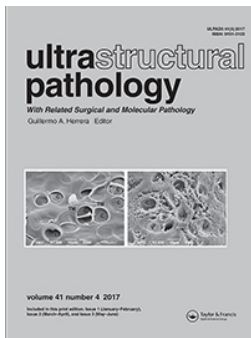
KARGER

Effects of chronic exposure to mercury and cadmium alone and in combination on the coagulation system of Sprague-Dawley rats

Sandra Arbi, Hester Magdalena Oberholzer, Mia Jeanne Van Rooy, Chantelle Venter & Megan Jean Bester

Published online: 15 Jun 2017.

Submit your article to this journal ⤤

View related articles ⤤

View Crossmark data ⤤

Taylor & Francis
Taylor & Francis Group

BASIC RESEARCH

Check for updates

Effects of chronic exposure to mercury and cadmium alone and in combination on the coagulation system of Sprague-Dawley rats

Sandra Arbi[a], Hester Magdalena Oberholzer[a], Mia Jeanne Van Rooy[b], Chantelle Venter[a], and Megan Jean Bester[a]

[a]Department of Anatomy, Faculty of Health Sciences, University of Pretoria, Pretoria, South Africa; [b]Department of Physiology, Faculty of Health Sciences, University of Pretoria, Pretoria, South Africa

ABSTRACT

Water contamination with heavy metals may adversely affect our health. High metal levels lead to changes in blood coagulation processes, increasing the risk for cardiovascular disease. Exposure is not limited to a single metal but usually involves a mixture of metals. In this study 24 male Sprague-Dawley rats were exposed to cadmium (Cd) and mercury (Hg), alone and in combination, for 28 days at dosages equivalent to 1000 times the World Health Organization water limits. Scanning electron microscopy analysis revealed that both metals caused platelet activation. Cd significantly increased fibrin fibers thickness and caused aggregation and formation of dense matted deposits (DMDs). Hg reduced fibrin network formation. In the combination group, Hg appeared to augment the effect of Cd, and the presence of extensive DMDs or aggregates between the fibers, with no changes to the actual fibrin thickness, was observed.

Introduction

Increasing contamination of water, food, and air with metals due to increased industrialization, mining, transport, and other related activities has a negative impact on the health of those living in highly industrialized areas. Most susceptible populations include those working in or living close to mines and those using water from these areas for drinking, washing, and agricultural purposes. Heavy metals are absorbed through the skin by inhalation and/or orally and can have toxic, carcinogenic, mutagenic, and/or teratogenic effects [1,2].

The World Health Organization (WHO) has identified 10 chemicals of major public health concern and these include cadmium (Cd) and mercury (Hg) [3]. The contribution of these metals to the development of noncommunicable diseases such as cardiovascular disease (CVD) is unknown. Although dietary factors play an important role, metals found in pollution and cigarette smoke that induce the formation of reactive oxygen species (ROS) may increase the risk for the development of disease. Little is known about how exposure to heavy metals, especially as part of mixtures in contaminated water, contributes to the development of CVD.

Environmental exposure usually involves a mixture of different metals at different concentrations, as levels of heavy metals in the environment often fluctuate and total exposure time differs between individuals. In addition, possible synergism between metals can enhance toxicity. The concentration of metals administered in animal studies is based on previously reported dosages and subsequently the observed effects are difficult to extrapolate to the possible consequence of human environmental exposure. In the present study, Sprague-Dawley rats were exposed to metal concentrations 1000 times the WHO limits for each metal, alone and in combination. A concentration of 1000 times the WHO limits was selected in order to identify specific targets and possible risk markers associated with the development of CVD. A 28-day, daily exposure period was selected as epidemiological studies have shown that long-term exposure to heavy metals is required to observe adverse health effects. Considering that every day in a rat would be approximately 34.8 human days [4], the exposure period is therefore approximately equivalent to a 3-year chronic human exposure.

Several individual metals such as iron (Fe) and zinc (Zn) have been shown to have procoagulative effects [5] and Fe has been shown to alter the structure of fibrin networks [6]. The oxidation of Fe has been shown to inhibit Fe-induced blood coagulation [7], which implies that metal pollutants, as found in the environment, may have an adverse effect on cardiovascular health.

Studies on fibrin and thrombus formation provide physiologically relevant information about the possible risk for thrombosis-associated diseases and a correlation has been found between *in vitro* and clinical studies [8,9]. Fibrin formed from patients with different diseases has been shown to have a wide variety of morphologies and diameters, and an idea has recently been developed on the contribution of fibrin to amyloidogenesis – the process of amyloid formation in which proteins change their conformation and aggregate to form fibrils, playing an important role in disease pathogenesis [10].

Therefore, the aim of this study was to investigate the effect of chronic exposure to Cd and Hg on the coagulation system of Sprague-Dawley rats at dosages of 1000 times the WHO limits for each metal, alone and in combination.

Materials and methods

Implementation of the Sprague-Dawley rat model

Twenty-four male Sprague-Dawley rats (250–300 g) were used in this study and maintained at the University of Pretoria's Biomedical Research Centre (UPBRC). These rats were provided with irradiated commercial Epol rat pellets and municipal water *ad libitum*. All experimental protocols complied with the requirements of the University of Pretoria's Animal Ethics Committee (ethical clearance number: H007-15). The animals were housed in conventional cages complying with the sizes laid out in the SANS 10386:2008 recommendations. A room temperature of 22°C (±2°C), relative humidity of 50% (±20%), and a 12-hour light–dark cycle were maintained during the entire study. Animals were allowed to acclimatize for 7 days prior to the project commencement, which was conducted over the following 28 days and the animals were therefore housed for a total period of 35 days.

Administration of test compounds

Cadmium chloride (CdCl$_2$) [Merck (Pty) Ltd., South Africa] and mercury chloride (HgCl$_2$) [Merck (Pty) Ltd., South Africa] were dissolved in sterile water and administered daily to the rats via oral gavage. The control group received saline via the same route. Weekly dosages were adjusted based on the changes in the mass of the rats. The dosage given to the rats was calculated from the WHO water limits for consumption by a-60 kg human consuming 1.4 L water per day [11]. The conversion of human dosages to rat dosages was calculated according to the method of Reagan-Shaw et al. in 2008 [12] and represented a concentration ±1000 times WHO levels (Table 1).

Termination

The rats were terminated via isoflurane overdose, according to standard methods employed by the UPBRC.

Blood collection

On the day of termination (day 28), approximately 5 ml blood was collected in citrate tubes via cardiac puncture under isoflurane anesthesia for ultrastructural analysis. Another 3–5 ml (maximum volume) was collected in heparin tubes for measurement of plasma levels of Cd and Hg in all of the experimental groups. The Cd and Hg levels in the blood samples were quantified with inductively coupled plasma mass spectrometry (ICP-MS).

Scanning electron microscopy

Scanning electron microscopy (SEM) analysis was performed to study the morphology of platelets and fibrin networks as well as fibrin fiber thickness. Blood was centrifuged for 10 minutes at 300×g to obtain platelet-rich plasma (PRP). A volume of 10 μl of the PRP, with and without the addition of 5 μl of human thrombin, was placed on a 10-mm round glass coverslip. The glass coverslips were left to dry for 10 minutes and placed in 24 well plates to which 0.075 M phosphate buffer solution (pH 7.4) was added. The samples were washed for 20 minutes on a shaker to remove any blood proteins. The washed samples were then fixed in

a 2.5% glutaraldehyde/formaldehyde solution for 30 minutes. This was followed by rinsing the samples three times in buffer for 3 minutes before secondary fixation in 1% osmium tetroxide (OsO_4) for 15 minutes. The samples were washed again three times as described above. The samples were then dehydrated in 30%, 50%, 70%, 90%, and 3 times in 100% ethanol. The SEM sample preparation was completed by drying the samples in hexamethyldisilazane, followed by mounting and coating with carbon and viewing using a ZEISS Crossbeam 540 FEG-SEM.

The thickness of the fibrin fibers was measured to determine any alterations to the normal major (thick) and minor (thin) fiber arrangement of the network [12]. Fifty fibers were randomly chosen and measured on the SEM micrographs using ImageJ (Version 1.49, Java).

Statistical analysis

Statistical analysis on both the plasma levels of heavy metals and fibrin fiber thickness was performed on GraphPad Prism Version 6.01 using one-way analysis of variance (ANOVA) and Tukey's multiple comparisons test, where a p-value of ≤ 0.05 was considered significant.

Results

Both Hg and Cd were absorbed into the blood of the rat, and plasma levels of the metals on the day of termination are presented in Table 2. The molar concentrations of Hg were 10-fold higher than that of Cd, administered alone or in combination. Total metal concentration was equivalent to the sum of the metal concentrations of the Hg and Cd groups.

Scanning electron microscopy

Figure 1a–d is a representative of platelets in the control and exposed groups. In the control group (Figure 1a), round/oval platelets with some pseudopodia were visible as indicated by arrows. Pseudopodia, change in platelet shape, and spreading indicate platelet activation, but is not expected in the control groups and is merely an artifact of contact activation during sample preparation [13]. Platelet activation can be seen in all the metal-exposed groups (arrows in Figure 1b–d), with an increase in activation; relevant to the amount of pseudopodia and platelet spreading, seen in the Cd (Figure 1b) and Hg (Figure 1c) and Cd and Hg groups (Figure 1d). Platelet–platelet interactions (Figure 1c) and spontaneous fibrin fiber formation (Figure 1d) are also indicative of increased activation and consequently thrombotic potential of the exposed groups.

Evaluation of the fibrin network in the control group (Figure 2a) revealed a typical fibrin network structure, with individual fibers of varying thickness in some cases overlapping to form a meshwork. As expected the fibrin fibers of the control group consisted of both thick, major fibers and thin, minor fibers [14]. Fibrin fibers in the Cd group (Figure 2b) appear denser as compared to the control and formed areas of fused fibers as indicated by the arrows. The Hg group had little or no fiber formation, the most in samples being shown in Figure 2c, where thick fibers (thick arrow) and thin fibers (thin arrow) are seen in a sparse network. The combination group (Figure 2d–f) revealed denser and more aggregated fibers as compared to the control and has areas where the fibers appear fused (Figure 2d, dashed arrow). A low magnification image is included to show the dense matted deposits (DMDs) present between the fibrin fibers of the combination group (Figure 2e, arrow head), and a higher magnification of the deposits (Figure 2f) shows a more detailed structure. The fibrin fiber thickness measurements for all the groups revealed that only the Cd group fibrin fibers had a statistically significant increase in fiber thickness as

Table 1. Rat dosage, groups and exposure time.

Groups	WHO limit (mg/L) (WHO, 2011)	Dosages (mg/kg rat weight)	Rats per group	Days
Control	–	0.5 mL saline	6	28
Cd	0.003	0.696	6	28
Hg	0.006	1.148	6	28
Cd and Hg	–	0.696 and 1.148	6	28

Table 2. Administered dosages and blood levels of metals.

Group	Administered dose (µg/kg)	Plasma concentrations (µg/l) ± SD	Plasma concentrations (µM)
Cd	696.01	1.872 ± 0.15	0.017 ± 0.0034
Hg	1147.50	35.41 ± 2.60	0.177 ± 0.0032
Cd* + Hg	696.01	11.75 ± 6.05	0.025 ± 0.0055
Cd + Hg*	1147.50	33.20 ± 3.57	0.166 ± 0.044

*Indicates individual metal concentration as measured in the combination group.

compared to the control and the other two experimental groups (p-value ≤0.05). These results are presented in Figure 3.

Discussion

In this study rats were exposed to Cd and Hg alone and in combination to levels ±1000 times the WHO safety guidelines for drinking water. Many studies have been undertaken to determine the tissue and organ toxicity of a single dosage of Cd and Hg [15–18]. These models represent acute exposure and provide very little information on longer exposure times to Cd and Hg alone or in combination.

Limited information is available in literature on the plasma levels of rats after exposure to these metals and how these levels correlate to human populations. Rat plasma levels of Cd following exposure to 1000 times

the WHO safety limits for Cd were 1.872 ± 0.37 µg/L (Table 2). Smokers are a population that are exposed to chronic levels of Cd. In the Egyptian population, blood Cd levels were 1.37 ± 0.45 µg/L for nonsmokers and increased to 2.67 ± 1.21 µg/L in smokers [19]. Likewise in a Canadian population, a level of 0.21 µg/L for nonsmokers was increased to 1.64 µg/L in smokers [20]. Therefore, in the present study, the blood results represent chronic exposure to Cd.

Raised Cd blood levels are associated with an increase in CVD and associated mortality such as atherosclerosis and consequent thrombosis [21,22]. Hecht et al. in 2016 reported a positive association between Cd biomarkers and CVD [23]. Cd alone was found to have similar effects to cigarette smoke, primarily targeting the endothelium of the vascular system, causing inflammation, impaired nitric oxide production, decreased endothelium migration, as
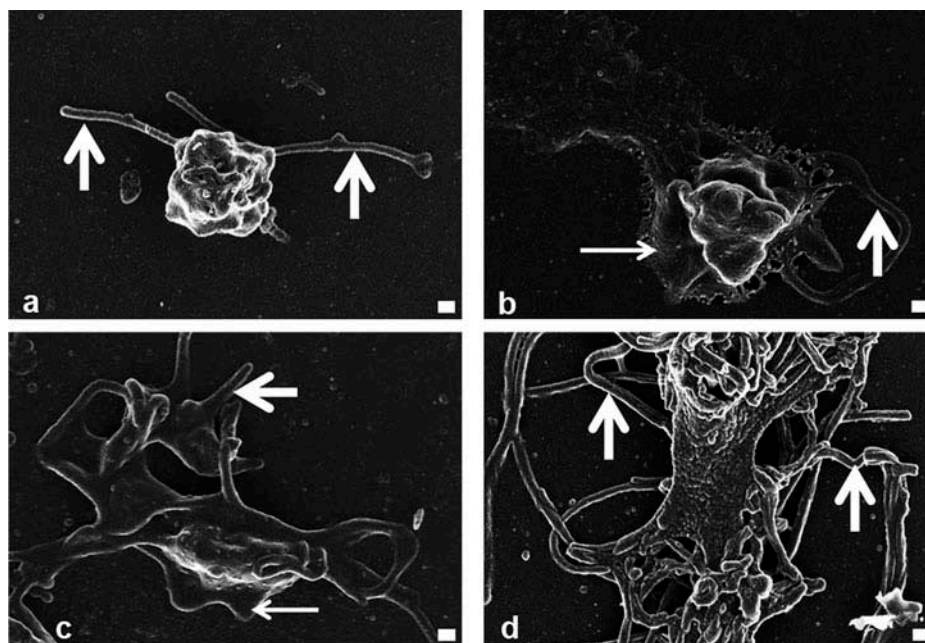

Figure 1. SEM micrographs of platelets prepared from PRP. A representative of the (a) control group with the arrows indicating pseudopodia, (b) Cd group with pseudopodia and platelet spreading indicated by the thick and thin arrows, respectively, (c) platelets from the Hg exposed group where pseudopodia (thick arrow) and platelet spreading (thin arrow) are also present, and (d) combination group where the presence of many pseudopodia can be seen (thick arrows). (Scale bars: 200 nm).
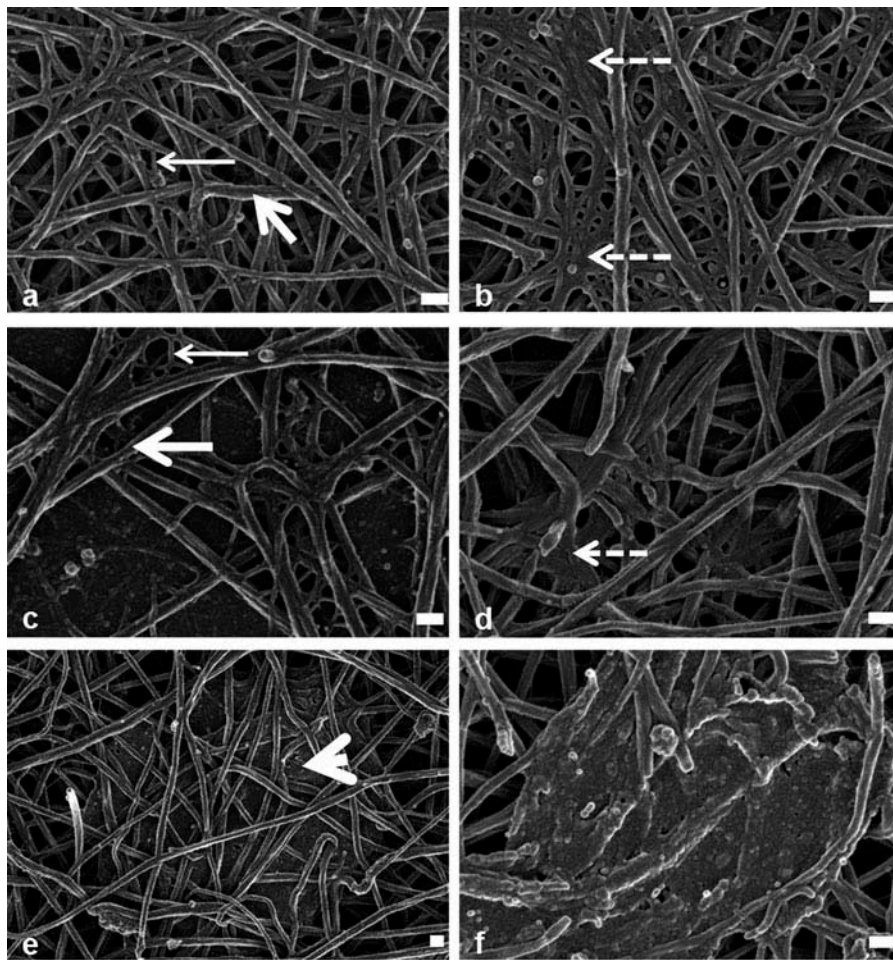
Figure 2. SEM micrographs of fibrin networks prepared from PRP with added thrombin from the control (a), Cd (b), Hg (c), and combination (d–f) groups. A regular network of fibrin fibers representative of the control group (a, large arrow indicating thick, major fibers and thin arrow indicating thin, minor fibers). In Cd (b) the fibers are aggregated to form dense fused areas (dashed arrows). The Hg group (c) had fewer fibrin fibers formed, with both thick (thick arrow) and thin (thin arrow) fibers present. In the combination group (d), the fibers formed dense aggregated areas (dashed arrow) and dense matted deposits (DMDs) were observed and indicated in (e) (arrow head) at low magnification and a different area on higher magnification in (f). (Scale bars = 200 nm).
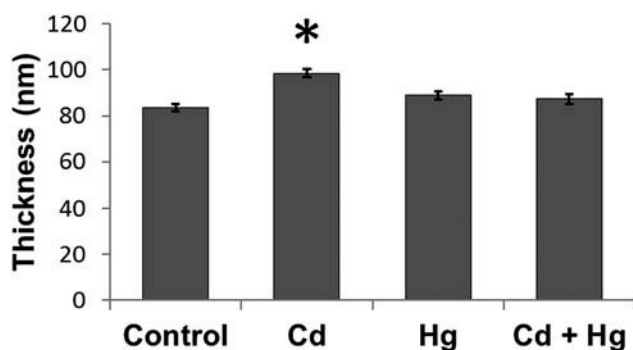

Figure 3. Average fibrin thickness (nm) of the control and metal exposed groups. Fibrin thickness was measured for at least 30 different fibers in each metal group and represented as an average ± SEM. *Represents significant differences compared to control, *p*-value ≤0.05.

well as cell death. Key to this effect was the formation of ROS that caused changes to endothelial structure and function; platelet activation triggers the activation of the coagulation cascade. Smooth muscle cell proliferation, migration, or death can also occur further exacerbating the activation of the coagulation cascade [24]. All these factors contribute to the development of pathological thrombi that, according to the Society of Thrombosis and Hemostasis, are responsible for the 25% of deaths that occur worldwide every year [25].

Plasma Hg levels differ between populations, and an average of 3.08 ± 1.55 μg/L for a Korean male college population (*n* = 43) [26] and 4.6 ± 3.0

μg/L for a large population of Korean males (*n* = 4283) [27] was reported. In an Egyptian population, Hg levels were 4.4–12.1 μg/L [19], and in a South African population 0.1–8.82 μg/L [28]. In a study by Röllin et al. (2009), levels in South African rural women were 0.18–0.82 μg/L and for women living in mining areas the levels were 0.28–1.25 μg/L [28]. In contrast, in regions of the world where small-scale gold mining occurs, blood Hg levels were raised and increased from 16.6 ± 10.7 μg/L to 102.0 ± 55.8 μg/L for different mining areas in Ghana. Biomonitoring levels reported by Baeuml et al. in 2011 [29] found that the highest median Hg blood levels were found in Indonesia-Sulawesi and Zimbabwe and reported median levels were 11.1 μg/L and 10.2 μg/L, respectively, while the maximum Hg blood levels were 429 and 186 μg/L and were reported for Indonesia-Kalimantan and Indonesia-Saluwesi, respectively. In South Africa, informal small-scale gold mining occurs and no reported data could be found regarding Hg levels in this population. An increase in cardiovascular events has been reported in people exposed to 0.05 μM Hg, equivalent to 10.29 μg/L Hg. In the present study rat blood levels of 35.41 ± 2.60 μg/L represent the upper range of Hg exposure which is associated with cardiovascular risk.

Gómez et al. (2007) have reported an increased mortality among miners from the Almadén region of Spain exposed to Hg due to circulatory disease, specifically hypertension and CVD [30]. Sources of Hg contamination within these communities include water contamination due to gold mining and Hg leaching due to deforestation as well as the consumption of fish in which Hg has bioaccumulated.

Platelet changes consistent with activation were observed in this study [13,31]. The degree of activation was evaluated based on the amount of pseudopodia stemming from the platelet body, platelet–platelet interactions, as well as the amount of platelet spreading, relative to the control. These changes in platelet shape and membrane characteristics affect the formed thrombus, and have also been linked to inflammation [13]. Lateral aggregation as observed in the Cd exposed group results in denser fiber networks which are often associated with a reduction of clot permeability to fibrinolytic factors and subsequently inhibits or prolongs clot lysis [32–34].

Cd is also a major component in cigarette smoke. Pretorius et al. (2010) showed that the fibrin fiber networks prepared from the plasma of smokers had a net-like appearance in some areas, as well as areas where thick matted masses (DMDs) were present, and that these changes occurred immediately and not only over an extended period of time [35]. The authors describe DMD formation to be most likely due to the generation of oxidative stress, specifically free radicals such as ROS. Oxidation has been shown to alter fibrin formation and degradation [36–38].

A study by Roitman et al. (2004) showed that 10% oxidized fibrinogen is able to moderately activate the intrinsic pathway while inhibiting the extrinsic pathway of coagulation, and a 20% oxidation would inhibit both, resulting in a decrease of thrombin formation and a decrease in the clotting rate [39].

Fibrinogen has been identified as the primary oxidized protein in the plasma of smokers. The most common alteration is the formation of two 3-nitrotyrosine, which increases fibrin polymerization and turbidity while fibrin clot lysis is reduced. The identified viscoelastic properties that occur as a result of this oxidation are increased stiffness and viscosity with the formation of increased fiber clusters [40]. The findings of this study were therefore similar to previous literature, in that compared to the control, the thickness of the Cd fibrin fibers was increased suggesting that Cd, which is also a major component of cigarette smoke, has a pro-fibrotic effect on the coagulation system.

Little is known about the effect of Hg on fibrin network formation. S-nitrosoglutathione (GSNO) plays an important role in vascular homeostasis by inhibiting platelet activation and aggregation and fibrinogen binding to platelets. Akhter et al. (2002) reported that GSNO reduced the initial rate of polymerization [41]. Bateman et al. (2012) observed that GSNO alters the secondary structure of fibrinogen where low dosages generate coarse networks with thicker fibers while higher dosages induce abnormal fibrin networks with the formation of fibrin aggregates [42].

Hg can cleave the S–NO bond of GSNO resulting in increased NO levels. Vadseth et al. (2004) reported that exposure of fibrinogen to

nitrating oxidants caused rapid clot formation and cross-linking, while in contrast exposure to non-nitrating oxidants reduced rate of clot formation and increased permeation [43]. Shacter et al. (1995) showed that oxidative modification by Hg inhibits thrombin catalyzed clot formation [44]. *In vitro* HgCl oxidization of fibrinogen results in the formation of methionine sulfoxide residues with decreased fibrin polymerization and reduced final turbidity. The clot that forms has decreased stiffness and viscosity although there is an increase in fiber density, decreased fiber diameter and pore size. Becatti et al. (2014) reported that carbonylation of purified human fibrinogen by 2,2'-azobis(2-amidinopropane) dihydrochloride (AAPH) that generates physiologically relevant hydroxyl radicals is responsible for a decrease in thrombin-induced clot formation due to an increase in protein carbonylation with the most susceptible amino acids being methionine and cysteine [45].

In the present study the Hg group had little or no fiber formation and a sparse fibrin network had formed. An extensive review of the literature leads to the conclusion that Hg-mediated depletion of GSNO did not lead to the formation of a denser fibrin network but the observed effect is rather as a direct result of ROS accumulation either due to direct Hg binding to GSH and/or Hg-mediated inhibition of the antioxidant pathways. Inflammatory sources of ROS can also contribute to this effect.

The structure and function of fibrin are important in the fibrinolytic process [46]. Cd and Hg have different effects where Cd forms a dense, more rigid fibrin network with thicker fibrin fibers while that of Hg appears more fragile. During fibrinolysis fibrin plays a double role acting as a cofactor and a substrate to plasmin. As a result, altered fibrin structure has an altered susceptibility to fibrinolysis [46–48] and these alterations can have significant physiological implications. Clots that are resistant to fibrinolysis are prone to thrombosis whereas fragile clots are more susceptible to fibrinolysis and consequent bleeding [49–51]. Thinner fibers would therefore have a slower rate of tissue plasminogen activator (t-PA)-mediated plasmin generation than thicker fibers, resulting in a reduced fibrinolytic activity of the system and therefore a greater resistance to fibrinolysis. For a given amount of fibrinogen, clots produced by thicker fibers are loosely woven, with fewer fibers while clots composed of thinner fibers have more fibers that are more closely packed [46,47]. An initial fibrin scaffold is formed followed by further branching and elongation of the fibrin fibers, as well as the addition of new fibers over time, resulting in different fibrin thickness throughout the sample [46]. Therefore, the overall structure of the clot, rather than the thickness of individual fibers, determines the fibrinolytic activity on the clot system [47,52].

For Cd and Hg in combination the sum of the two effects is expected. Instead in the combination group the fibrin network was denser with more aggregated fibers and areas of fiber fusion. It appears that Hg enhances via the possible oxidation of methionine residues Met[78], Met[367], and Met[476] and the nitration of Tyr[292] and Tyr[422]. A possible mechanism is that Hg causes the oxidation of methionine residues, which alters the tertiary structure of fibrinogen, and consequently the tyrosine residues become more susceptible to Cd-induced nitration [53]. In addition, increased NO levels due to Hg cleave of the S–NO bond of GSNO increase levels of NO causing further nitration of the Tyr residues, resulting in the formation of a denser more thrombotic clot phenotype with increased risk for CVD.

Conclusion

The heavy metals Cd and Hg alone and in combination caused platelet activation. Exposure to Cd results in a fibrin network with a more thrombotic morphology. In contrast, Hg appeared to inhibit fibrin network formation. In the combination group, Hg appeared to enhance the effect of Cd, and the presence of extensive DMDs or aggregates between the fibers, with no changes to the actual fibrin thickness, was observed. In conclusion, chronic exposure to metals at relevant dosages especially as part of mixtures has profound effects on the fibrin fiber network formation and consequently has serious health implications, especially related to the development of CVD.

Declaration of interest

References

1. García-Niño WR, Pedraza-Chaverrí J. Protective effect of curcumin against heavy metals-induced liver damage. *Food Chem Toxicol*. 2014;69:182–201.
2. Venter C, Oberholzer HM, Taute H, Cummings FR, Bester MJ. An *in ovo* investigation into the hepatotoxicity of cadmium and chromium evaluated with light- and transmission electron microscopy and electron energy-loss spectroscopy. *J Environ Sci Health A Tox Hazard Subst Environ Eng*. 2015;50:830–838.
3. The World Health Organization. Ten chemicals of major public health concern. Geneva: WHO. 2015. www.who.int/ipcs/assessment/public_health/chemicals_phc/en/. Accessed November 22, 2016.
4. Sengupta P. The laboratory rat: Relating its age with human's. *Int J Prev Med*. 2013;4(6):624–630.
5. Sangani RG, Soukup JM, Ghio AJ. Metals in air pollution particles decrease whole-blood coagulation time. *Inhal Toxicol*. 2010;22(8):621–626.
6. Lipinski B, Pretorius E. Iron-induced fibrin in cardiovascular disease. *Curr Neurovasc Res*. 2013;10:269–274.
7. Pretorius E, Bester J, Vermeulen N, Lipinski B. Oxidation inhibits iron-induced blood coagulation. *Curr Drug Targets*. 2013;14:13–19.
8. Undas A, Ariens RA. Fibrin clot structure and function: A role in the pathophysiology of arterial and venous thromboembolic diseases. *Arterioscler Thromb Vasc Biol*. 2011;31(12):e88–e99.
9. Weisel JW, Litinov RI. Mechanisms of fibrin polymerization and clinical implications. *Blood*. 2013;121 (10):1712–1719.
10. Kell DB, Pretorius E. Proteins behaving badly. Substoichiometric molecular control and amplification of the initiation and nature of amyloid fibril formation: Lessons from and for blood clotting. *Prog Biophys Mol Biol*. 2017;123:16–41.
11. The World Health Organization. Guidelines for drinking water quality. Geneva: WHO. 2011.www.who.int/water_sanitation_health/.../2011/9789241548151_annex.pdf. Accessed November 22, 2016.
12. Reagan-Shaw S, Nihal M, Ahmad N. Dose translation from animal to human studies revisited. *Faseb J*. 2008;22 (3):659–661.
13. Van Rooy MJ, Duim W, Ehlers R, Av B, Pretorius E. Platelet hyperactivity and fibrin clot structure in transient ischemic attack individuals in the presence of metabolic syndrome: A microscopy and thromboelastography* study. *Cardiovasc Diabetol*. 2015;14:86.
14. Pretorius E, Steyn H, Engelbrecht M. Swanepoel AC and Oberholzer HM. Differences in fibrin fiber diameters in healthy individuals and thromboembolic ischemic stroke patients. *Blood Coagul Fibrinolysis*. 2011;22(8):696–700.
15. Schumacher L, Abbott LC. Effects of methyl mercury exposure on pancreatic beta cell development and function. *J Appl Toxicol*. 2017;37(1):4–12.
16. Celikoglu E, Aslanturk A, Kalender Y. Vitamin E and sodium selenite against mercuric chloride-induced lung toxicity in the rats. *Braz Arch Biol Technol*. 2015;58 (4):587–594.
17. Agrawal S, Flora G, Bhatnagar P, Flora SJ. Comparative oxidative stress, metallothionein induction and organ toxicity following chronic exposure to arsenic, lead and mercury in rats. *Cel Mol Biol (Noisy-Le-Grand)*. 2014;60 (2):13–21.
18. Bernhoft RA. Cadmium toxicity and treatment. *Scientific World J*. 2013. https://doi.org/10.1155/2013/394652
19. Mortada WI, Sobh MA, El-Defrawy MM, Farahat SE. Reference intervals of cadmium, lead, and mercury in blood, urine, hair, and nails among residents in Mansoura city, Nile delta, Egypt. *Environ Res*. 2002;90 (2):104–110.
20. Garner R, Levallois P. Cadmium levels and sources of exposure among Canadian adults. *Health Rep*. 2016;27 (2):10.
21. Barregard L, Sallsten G, Fagerberg B, et al. Blood cadmium levels and incident cardiovascular events during follow-up in a population-based cohort of Swedish adults: The Malmö Diet and Cancer Study. *Environ Health Perspec*. 2016;124(5):594.
22. Tellez-Plaza M, Jones MR, Dominguez-Lucas A, Guallar E, Navas-Acien A. Cadmium exposure and clinical cardiovascular disease: A systematic review. *Curr Atheroscler Rep*. 2013;15(10):1–15.
23. Hecht EM, Arheart KL, Lee DJ, Hennekens CH, HlainG WM. Interrelation of cadmium, smoking, and cardiovascular disease (from the National Health and Nutrition Examination Survey). *Am J Cardiol*. 2016;118(2):204–209.
24. Messner B, Knoflach M, Seubert A, et al. Cadmium is a novel and independent risk factor for early atherosclerosis mechanisms and in vivo relevance. *Arterioscler Thromb Vasc Bio*. 2009;29(9):1392–1398.
25. Raskob GE, Angchaisuksiri P, Blanco AN, et al. Committee for World Thrombosis Day. *Semin Thromb Hemost*. 2014;40:724.
26. Jung E, Hyun W, Ro Y, Lee H, Song K. A study on blood lipid profiles, aluminum and mercury levels in college students. *Nutr Res Pract*. 2016;10(4):442–447.
27. Lee S, Yoon JH, Won JU, et al. The association between blood mercury levels and risk for overweight in a general adult population: Results from the Korean National Health and Nutrition Examination **Survey**. *Biol Trace Elem Res*. 2016;171(2):251–261.

28. Röllin HB, Rudge CV, Thomassen Y, Mathee A, Odland JØ. Levels of toxic and essential metals in maternal and umbilical cord blood from selected areas of South Africa: Results of a pilot study. *J Environ Monit*. 2009;11(3):618–627.

29. Baeuml J, Bose-O'Reilly S, Gothe RM, et al. Human biomonitoring data from mercury exposed miners in six artisanal small-scale gold mining areas in Asia and Africa. *Minerals*. 2011;1(1):122–143.

30. Gómez MG, Klink JDC, Boffetta P, Espanol S, Sallsten G, Jg Q. Exposure to mercury in the mine of Almaden. *Occup Environ Med*. 2007;64:389–395.

31. Kuwahara M, Sugimoto M, Tsuji S, et al. Platelet shape changes and adhesion under high shear flow. *Arterioscler Thromb Vasc Bio*. 2002;22(2):329–334.

32. Undas A, Zawilska K, Mariola Ciesla-Dul M, et al. Altered fibrin clot structure/function in patients with idiopathic venous thromboembolism and in their relatives. *Blood*. 2009;114(19):4272–4278.

33. Undas A, Slowik A, Wolkow P, Szczudlik A, Tracz W. Fibrin clot properties in acute ischemic stroke: Relation to neurologic deficit. *Thromb Res*. 2010;125(4):357–361.

34. Stanford SN, Sabra A, D'Silva L, et al. The changes in clot microstructure in patients with ischaemic stroke and the effects of therapeutic intervention: A prospective observational study. *BMC Neurol*. 2015;15(1):1.

35. Pretorius E, Oberholzer HM, Van Der Spuy WJ, Meiring JH. Smoking and coagulation: The sticky fibrin phenomenon. *Ultrastruct Pathol*. 2010;34 (4):236–239.

36. Undas A, Szułdrzynski K, Stepien E, et al. Reduced clot permeability and susceptibility to lysis in patients with acute coronary syndrome: Effects of inflammation and oxidative stress. *Atherosclerosis*. 2008;196:551–557.

37. Undas A, Zeglin M. Fibrin clot structure and cardiovascular disease. *Vasc Dis Prev*. 2006;3:99–106.

38. De Maat M, Verschuur M. Fibrinogen heterogeneity: Inherited and noninherited. *Curr Opin Hematol*. 2005;12:377–383.

39. Roitman EV, Azizova OA, Morozov YA, Aseichev AV. Effect of oxidized fibrinogens on blood coagulation. *Bull* Exp *Biol Med*. 2004;138(9):245–247.

40. Martinez M, Weisel JW, Ischiropoulos H. Functional impact of oxidative posttranslational modifications on fibrinogen and fibrin clots. *Free Radic Biol Med*. 2014;65:411–418.

41. Akhter S, Vignini A, Wen Z, English A, Wang PG, Mutus B. Evidence for S-nitrosothiol-dependent changes in fibrinogen that do not involve transnitrosation or thiolation. *Proc Natl Acad Sci USA*. 2002;99:9172–9177.

42. Bateman RM, Ellis CG, Suematsu M, Kr W. S-Nitrosoglutathionine acts as a small molecule modulator of human fibrin clot architecture. *Plos One*. 2012;7(8):e43660,1–13.

43. Vadseth C, Souza JM, Thomson L, et al. Pro-thrombotic state induced by post-translational modification of fibrinogen by reactive nitrogen species. *J Biol Chem*. 2004;279(10):8820–8826.

44. Shacter E, Wiliams JA, Levine R. Oxidative modification of fibrinogen inhibits thrombin catalysed clot formation. *Free Radic Biol Med*. 1995;15(4):815–821.

45. Becatti M, Maruci R, Bruschi G, et al. Fiorillo. Oxidative modification of fibrinogen is associated with altered function and structure in the subacute phase of myocardial infarction. *Arterioscler Thromb Vasc Bio*. 2014;34(7):1355–1361.

46. Wolberg AS. Thrombin generation and fibrin clot structure. *Blood Rev*. 2007;21:131–142.

47. Collet JP, Park D, Lesty C, et al. Influence of fibrin network conformation and fibrin fiber diameter on fibrinolysis speed dynamic and structural approaches by confocal microscopy. *Arterioscler Thromb Vasc Biol*. 2000;20(5):1354–1361.

48. Marchi R, Lundberg U, Grimbergen J, et al. An abnormal fibrinogen with an Aα Ser-> Cys substitution associated with thrombosis. *Thromb Haemost*. 2000;84(2):263–270.

49. Sugo T, Nakamikawa C, Yoshida N, et al. End-linked homodimers in fibrinogen Osaka VI with a Bβ-chain extension lead to fragile clot structure. *Blood*. 2000;96 (12):3779–3785.

50. Dunn EJ, Ariens RA, Grant PJ. The influence of type 2 diabetes on fibrin structure and function. *Diabetologia*. 2005;48:1198–1206.

51. Dunn EJ, Philippou H, Ariens RA, Grant PJ. Molecular mechanisms involved in the resistance of fibrin to clot lysis by plasmin in subjects with type 2 diabetes mellitus. *Diabetologia*. 2006;49:1071–1080.

52. Bhattacharjee P, Bhattacharyya D. An insight into the abnormal fibrin clots: Its pathophysiological roles. In: Kolev K, Ed. *Fibrinolysis and Thrombolysis*. Croatia: InTech, Croatia University Press; 2014. p. 3–29.

53. Ji YL, Wang H, Meng C, et al. Melatonin alleviates cadmium-induced cellular stress and germ cell apoptosis in testes. *J Pineal Res*. 2012;52(1):71–79.